



University of Bradford eThesis

This thesis is hosted in [Bradford Scholars](#) – The University of Bradford Open Access repository. Visit the repository for full metadata or to contact the repository team



© University of Bradford. This work is licenced for reuse under a [Creative Commons Licence](#).

**POLYETHYLENE TEREPHTHALATE / CLAY
NANOCOMPOSITES**

A.M. AL-FOUZAN

PhD

Supervisors:

Dr. T. Gough

Prof. P. Coates

University of Bradford

2011

POLYETHYLENE TEREPHTHALATE / CLAY NANOCOMPOSITES

Compounding, fabrication and characterisation of the thermal, rheological, barrier and mechanical properties of Polyethylene Terephthalate / clay nanocomposites

Abdulrahman M AL-FOUZAN

B.Sc. (Chem. Eng.). MSc. (Poly. Tech.)

Submitted for the degree of

Doctor of Philosophy

Supervisors:

Dr. Tim Gough

Prof. Phil Coates

School of Engineering, Design and Technology

University of Bradford

2011

Polyethylene Terephthalate / clay nanocomposites

Abdulrahman M AL-FOUZAN

Keywords: Polyethylene Terephthalate, PET, nanocomposites, rheological, crystallisation, mechanical, thermal, permeability, degradation, nanoclays

Abstract

Polyethylene Terephthalate (PET) is one of the most important polymers in use today for packaging due to its outstanding properties. The usage of PET has grown at the highest rate compared with other plastic packaging over the last 20 years, and it is anticipated that the increase in global demand will be around 6% in the 2010 – 2015 period.

The rheological behaviour, thermal properties, tensile modulus, permeability properties and degradation phenomena of PET/clay nanocomposites have been investigated in this project. An overall, important finding is that incorporation of nanoclays in PET gives rise to improvements in several key process and product parameters together – processability/ reduced process energy, thermal properties, barrier properties and stiffness. The PET pellets have been compounded with carefully selected nanoclays (Somasif MAE, Somasif MTE and Cloisite 25A) via twin screw extrusion to produce PET/clay nanocomposites at various weight fractions of nanoclay (1, 3, 5, 20 wt.%). The nanoclays vary in the aspect ratio of the platelets, surfactant and/or gallery spacing so different effects are to be expected. The materials were carefully prepared prior to processing in terms of sufficient drying and re-crystallisation of the amorphous pellets as well as the use of dual motor feeders for feeding the materials to the extruder.

The rheological properties of PET melts have been found to be enhanced by decreasing the viscosity of the PET i.e. increasing the ‘flowability’ of the PET melt during the injection or/and extrusion processes. The apparent shear viscosity of PETNCs is shown to be significantly lower than un-filled PET at high shear rates. The viscosity exhibits shear thinning behaviour which can be explained by two mechanisms which can occur simultaneously. The first mechanism proposed is that some polymer has entangled and few oriented molecular chains at rest and when applying high shear rates, the level of entanglements is reduced and the molecular chains tend to orient with the flow direction. The other mechanism is that the nanoparticles align with the flow direction at high shear rates. At low shear rate, the magnitudes of the shear viscosity are dependent on the nanoclay concentrations and processing shear rate. Increasing nanoclay concentration leads to increases in shear viscosity. The viscosity was observed to deviate from Newtonian behaviour and exhibited shear thinning at a 3 wt.% concentration. It is possible that the formation of aggregates of clay is responsible for an increase in shear viscosity. Reducing the shear viscosity has positive benefits for downstream manufacturers by reducing power consumption. It was observed that all

three nanoclays used in this project act as nucleation agents for crystallisation by increasing the crystallisation temperature from the melt and decreasing the crystallisation temperature from the solid and increasing the crystallisation rate, while retaining the melt temperature and glass transition temperatures without significant change. This enhancement in the thermal properties leads to a decrease in the required cycle time for manufacturing processes thus potentially reducing operational costs and increasing production output.

It was observed that the nanoclay significantly enhanced the barrier properties of the PET film by up to 50% this potentially allows new PET packaging applications for longer shelf lives or high gas pressures.

PET final products require high stiffness whether for carbonated soft drinks or rough handling during distribution. The PET/Somasif nanocomposites exhibit an increase in the tensile modulus of PET nanocomposite films by up to 125% which can be attributed to many reasons including the good dispersion of these clays within the PET matrix as shown by TEM images as well as the good compatibility between the PET chains and the Somasif clays. The tensile test results for the PET/clay nanocomposites micro-moulded samples shows that the injection speed is crucial factor affecting the mechanical properties of polymer injection moulded products.

Conferences and papers

Alfouzan, A., Gough, T. and Coates, P., “Rheological, Thermal and Mechanical Properties of PET Nanocomposites”, PPS26, Banff, Canada, (2010).

Posters in IRC Show Cases at Bradford, Durham and York universities.

Chamberlain, P., Drewello, R., Korn, K., Bauer, W., Gough, T., Al-Fouzan, A., Collins, M., Doorn, N., Craig, O. and Heron, C., “Construction of the Khoja Zaynuddin Mosque: Use of Animal Glue Modified with Urine”, University of Oxford, Archaeometry, (2011)

Gough, T., Alfouzan, A. and Coates, P., “Thermal, rheological, barrier and mechanical properties of polymer nanocomposites”, IRC Showcase at Sheffield University, (2011)

Contents

Abstract	i
List of Figures	ix
List of Tables	xvii
Acknowledgements	xix
1 Introduction	1
1.1 Introduction	1
1.2 Polyethylene Terephthalate (PET) preparation and chemistry	4
1.3 Solid State Polymerisation (SSP)	8
1.4 Safety and application of PET	12
1.5 Objectives and writing tactic	16
2 Polymer Nanocomposites	19
2.1 Introduction	19
2.2 Nanocomposites	20
2.3 Nanoparticles	24
2.4 Structure and properties of Montmorillonite organoclay (MMT) and synthetic mica clay	26
2.5 Nanoclay modification	28
2.6 Previous studies of polymer nanocomposites	30
2.7 Nanoclay selection	37
2.8 Nanocomposites processing	40
2.8.1 Solution method	41
2.8.2 In-situ polymerisation method	41
2.8.3 Melt intercalation	41
3 Experimental work	43
3.1 Introduction	43
3.2 Raw materials	43
3.2.1 Polyethylene Terephthalate (PET) pellets	43
3.2.2 Nanoclay additives	44
3.3 Drying process	46

3.4	Extrusion and injection processes	48
3.4.1	Compounding of Polyethylene Terephthalate (PET) nanocomposites	49
3.4.2	PET cast film	53
3.4.3	Micro-moulding process	56
3.5	Analytical techniques methods	59
3.5.1	Density measurements	59
3.5.2	ThermoGravimetric Analysis (TGA)	60
3.5.3	Differential Scanning Calorimetry (DSC)	61
3.5.4	Intrinsic viscosity (I.V.)	64
3.5.5	Rheometry	65
3.5.6	Permeability tests	74
3.5.7	Tensile tests	75
3.5.8	Transmission Electron Microscopy (TEM)	77
3.5.9	X-ray diffraction	80
4	Rheological behaviour of PET nanocomposites	82
4.1	Literature review	82
4.2	Experimental work	89
4.2.1	Rheological behaviour	89
4.2.2	Intrinsic viscosity	90
4.3	Results and discussion	92
4.3.1	Capillary rheometer (high shear rates)	92
4.3.2	Oscillatory rheometer (low shear rate)	102
4.3.3	The Cox-Merz rule	121
4.3.4	Shear viscosity behaviour at fixed shear rates and varying clay concentrations	125
4.3.5	The intrinsic viscosity (I.V.) of PET nanocomposites	126
4.4	Conclusions	131
5	Thermal properties	134
5.1	Introduction	134
5.1.1	Amorphous phase	134

5.1.2	Melting phase	136
5.1.3	Semi-crystalline polymers	136
5.2	Literature review	145
5.3	Experimental work	151
5.4	Results and discussion	153
5.4.1	Introduction	154
5.4.2	PET/MAE nanocomposites	157
5.4.3	PET/MTE nanocomposites	162
5.4.4	PET/Cloisite 25A nanocomposites	165
5.4.5	Comparative study of PET nanocomposites with different clay types and the same loading concentrations	170
5.4.6	Thermal properties of PET/MTE films (un-oriented and equal-biaxial stretch)	174
5.4.7	Double melting endotherm behaviour of PET	179
5.5	Conclusions	186
6	Mechanical properties	188
6.1	Introduction	189
6.2	Literature review	190
6.3	Experimental work	198
6.4	Results and discussion	199
6.4.1	Tensile testing for un-filled PET and PET nanocomposite films	199
6.4.2	The interplay of injection speed and nanoclay levels on the mechanical properties of PET nanocomposites	205
6.5	Conclusions	209
7	The permeability of PET nanocomposites	212
7.1	Introduction	212
7.2	Experimental work	220
7.3	Results and discussion	221
7.4	Conclusions	226

8 Degradation of PET nanocomposites	228
8.1 PET degradation	228
8.1.1 Introduction	228
8.1.2 Degradation processes	230
8.2 PET nanocomposite degradation (literature review)	234
8.3 Experimental work	237
8.4 Results and discussion	238
8.4.1 Thermogravimetric analysis (TGA) results for the nanoclays	238
8.4.2 Re-processing of pellets	240
8.4.3 Effect of time on viscosity	246
8.5 Conclusions	248
9 General conclusion and future work	249
9.1 General conclusions	249
9.2 Future work	257
REFERENCES	259
APPENDICES	
x3 The appendix of chapter 3	274
x3.1 Raw material data sheets	274
x3.2 Density results	282
x3.3 XRD results for all nanoclays used in this project	283
x4 The appendix of chapter 4	284
x4.1 Cox-Merz rule	284
x4.2 Loss modulus vs. shear rate for different PETNCs at various concentrations	285
x4.3 Storage modulus as a function of shear rate for different nano-fillers at certain loading %.	287
x4.4 Shear rate (s^{-1}) vs. complex viscosity (Pa.s) for different types of PET nanocomposites with the same nano-filler content	289

x5 The appendix of chapter 5	290
x5.1 Additional results for sections 5.4.2, 5.4.3 and 5.4.4	290
x5.2 Additional results for section 5.4.6	294
x5.3 Additional results for section 5.4.5	296
x5.4 Preliminary study	299
x5.4.1 Introduction	299
x5.4.2 PET nanocomposite sheets	299
x5.4.3 Differential scanning calorimetry (DSC) results and discussion	300
x5.4.4 Comparison of the samples analysed in the preliminary and main studies	311
x6 The appendix of chapter 6	313
x6.1 Tensile modulus of PET nanocomposites films vs. clay content at tensile test speed of 5 and 50 mm/min	313
x6.2 TEM micrographs for PET nanocomposites films	314
x6.3 Stress-strain curve for PET nanocomposites micro size sample prepared at different injection speeds	319
x8 The appendix of chapter 8	322
x8.1 Sample description	322
x8.2 Viscosity vs. shear rate of PET nanocomposites re-extruded a number of times and the photographs.	323

List of Figures

Figure 1.1	European plastics demand by resin type 2009	2
Figure 1.2	World demand of Polyethylene Terephthalate (PET) (actual demand 2005 – 2009 and forecast demand 2010 – 2015)	2
Figure 1.3	Preparing the reaction for ethylene glycol	5
Figure 1.4	Preparation of DMT from Para-xylene	5
Figure 1.5	Chemical structure of bis (B-hydroxyethyl) terephthalate (BHET)	6
Figure 1.6	Chemical structure of PET	6
Figure 1.7	Polycondensation reaction	9
Figure 1.8	Vinyl ester group interacting with hydroxyl end group	9
Figure 1.9	Esterification reaction	9
Figure 1.10	Schematic of PET manufacturer	11
Figure 2.1	Schematic showing polymer-clay nanocomposite classifications	22
Figure 2.2	The chemical structure of dry phyllosilicates: a) Montmorillonite clay, b) synthetic mica clay	27
Figure 2.3	Attraction energy vs. the separation distance between two plates between two phyllosilicate layers	29
Figure 2.4	The chemical structure of all Cloisite additives	38
Figure 3.1	Pictures of the driers, A) Motan Drier (Luxor) and B) Vacuum dryer	47
Figure 3.2	The twin screw extruder (APV).	51
Figure 3.3	Screw design	51
Figure 3.4	The rotating angle of the mixing zones	52
Figure 3.5	(A) the Prism pelletizer and (B) Extruded nanocomposites exit from the die and are then quenched by cold water bath	52
Figure 3.6	Cast film single screw extruder (Betol 2525)	54
Figure 3.7	Vertical die (A) and chilled rolls (B)	54
Figure 3.8	Schematic representation of the PET cast film process, showing the single screw extruder and the chill rolls	55
Figure 3.9	Micro-moulding specimen picture and diagram	57
Figure 3.10	Microsystem 50 (A), Plastication unit (B) and the used screw (C).	58

Figure 3.11	AccuPyc™ 1330 Pycnometer	60
Figure 3.12	Simple diagram for TGA	61
Figure 3.13	TGA TA instruments Q5000	61
Figure 3.14	DSC TA Instruments Q2000	62
Figure 3.15	Schematic of Heat Flux DSC	63
Figure 3.16	Schematic of capillary viscometer	65
Figure 3.17	Rosand RH10 (A), front view (B) and rods and reservoirs (C)	66
Figure 3.18	The elements of the capillary rheometer	67
Figure 3.19	Bagley correction curve	68
Figure 3.20	The Physica MCR rheometer	69
Figure 3.21	The modulus curve	70
Figure 3.22	The basic elements of the concentric cylinder rotary rheometer	71
Figure 3.23	The cone-and-plate rheometer	72
Figure 3.24	The Physica MCR 501 rheometer. Front view for the equipment (A), the equipment located inside the cabinet (B) and the parallel plates (C)	73
Figure 3.25	The parallel-plate rheometer	73
Figure 3.26	Cross section of OTR test cell	74
Figure 3.27	Bose ElectroForce 3220	75
Figure 3.28	Instron 5564 (A), sample dimensions and schematic of the clamp (C)	76
Figure 3.29	Biaxial grips of stretching machine	77
Figure 3.30	Schematic structure of Transmission Electron Microscopy (TEM)	78
Figure 3.31	Transmission Electron Microscopy (TEM) apparatus	79
Figure 3.32	Leica microtome	80
Figure 3.33	Schematic of the Leica microtome	80
Figure 3.34	Bruker D8 advance model	81
Figure 4.1	Shear rate vs. shear viscosity for neat PET (vPET) and extruded PET (re-crystallised and amorphous)	93
Figure 4.2	Sketch map exhibiting the different types of PET-nanoclay interactions	95
Figure 4.3	Shear viscosity variation of PET/MAE nanocomposites at different MAE concentration with shear rate	96

Figure 4.4	Shear viscosity variations of PET/MTE nanocomposites at different MTE concentration with shear rate	97
Figure 4.5	Shear viscosity variations of PET/Cloisite 25A nanocomposites at different Cloisite 25A concentration with shear rate	97
Figure 4.6	Shear viscosity variation of PET NC with different nanofillers (MTE, MAE and Cloisite 25A) with 1 wt.% clay concentration	99
Figure 4.7	Shear viscosity variation of PET NC with different nanofillers (MTE, MAE and Cloisite 25A) with 3 wt.% clay concentration	100
Figure 4.8	Shear viscosity variation of PET NC with different nanofillers (MTE, MAE and Cloisite 25A) with 5wt.% clay concentration	100
Figure 4.9	Shear viscosity variation of PET NC with different nanofillers (MTE, MAE and Cloisite 25A) with 20 wt.% clay concentration	101
Figure 4.10	Strain amplitude sweep of vPET and PET/MTE (5 wt.%) nanocomposites at 260°C, $\omega= 10\text{rad/sec}$	102
Figure 4.11	Complex viscosity of vPET tested under shear rates from 0.1 to 100 s^{-1} and 100 to 0.1 s^{-1}	103
Figure 4.12	Shear rate vs. complex viscosity for Ext. vPET (amorphous and re-crystallised)	104
Figure 4.13	Complex viscosity variation of PET/MAE nanocomposites at different MAE concentrations with low shear rate	105
Figure 4.14	Complex viscosity variation of PET/MTE nanocomposites at different MTE concentrations with low shear rate	106
Figure 4.15	Complex viscosity variation of PET/Cloisite 25A nanocomposites at different Cloisite 25A concentrations with low shear rate	106
Figure 4.16	Complex viscosity variation of PET nanocomposites at the same concentration (3 wt.%) with low shear rate	108
Figure 4.17	Complex viscosity variation of PET nanocomposites at the same concentration (5 wt.%) with low shear rate	108
Figure 4.18	Complex viscosity variation of PET nanocomposites at the same concentration (20 wt.%) with low shear rate	109
Figure 4.19	Storage modulus behaviour for PET/MAE NC at different clay concentrations	111

	with low shear rate	
Figure 4.20	Storage modulus behaviour for PET/MTE NC at different clay concentrations with low shear rate	111
Figure 4.21	Storage modulus behaviour for PET/Cloisite 25A NC at different clay concentrations with low shear rate	112
Figure 4.22	Storage modulus behaviour for PETNCs at 3 wt.% loading with low shear rate	112
Figure 4.23	Cole-Cole plot for vPET, ext. vPET and PET/MAE nanocomposites at different clay concentrations	114
Figure 4.24	Cole-Cole plot for vPET, ext. vPET and PET/MTE nanocomposites at different clay concentrations	114
Figure 4.25	Cole-Cole plot for vPET, ext. vPET and PET/Cloisite 25A nanocomposites at different clay concentrations	115
Figure 4.26	Storage and loss modulus behaviour on increasing the shear rate for PET/MAE nanocomposites	116
Figure 4.27	Storage and loss modulus behaviour on increasing the shear rate for PET/MTE nanocomposites	117
Figure 4.28	Storage and loss modulus behaviour on increasing the shear rate for PET/Cloisite 25A nanocomposites	117
Figure 4.29	Relaxation time of PET/MAE nanocomposites at different composite loadings over several shear rates	120
Figure 4.30	Relaxation time of PET/MTE nanocomposites with different composite loadings over several shear rates	120
Figure 4.31	Relaxation time of PET/Cloisite 25A nanocomposites with different composite loadings over several shear rates	121
Figure 4.32	Shear viscosity of high density PP at 200 °C [from Kelly et al. (2009)]	122
Figure 4.33	Plot of $\log \eta$ vs. $\log \dot{\gamma}$ for homopolymer PS [from Han et al. (1995)].	123
Figure 4.34	Plots of shear rate vs. shear viscosity for PET nanocomposites at 5 wt.% nano- filler concentrations	124
Figure 4.35	Shear viscosity as a function of nano-filler concentration at two constant shear rates (100 and 2000s ⁻¹).	125

Figure 4.36	Absolute values of intrinsic viscosities (I.V.) of PET nanocomposites (pellets) at different clay concentrations.	129
Figure 4.37	Absolute values of intrinsic viscosities (I.V.) of PET nanocomposites (amorphous films) at different clay concentrations	129
Figure 5.1	Schematic representation of the different types of amorphous chain	135
Figure 5.2	The change in free energy for the nucleation process during polymer crystallisation	140
Figure 5.3	The triclinic crystal structure of PET	141
Figure 5.4	Structural organization within spherulites in melt-crystallized polymers [O'dian 2004]	142
Figure 5.5	Schematic development of a spherulite from a chain-folded precursor crystal. Rows (a) and (b) represent, respectively, edge-on and flat-on views of the evolution of the spherulite [Sperling (2006)]	143
Figure 5.6	Spherulitic growth as a function of temperature [Brink (2003)]	143
Figure 5.7	Illustration of a spherulite growing into a melt [Culbert and & Christel (2003)]	144
Figure 5.8	Typical DSC curve for PET amorphous	154
Figure 5.9	DSC curve for crystallised PET pellets (Tergal F9)	155
Figure 5.10	DSC curve for amorphous PET film	156
Figure 5.11	DSC results for 6 samples from the same run to produce PET/MAE (1 wt.%)	157
Figure 5.12	Average of thermal analysis results of PET nanocomposites (MAE) for various MAE contents	158
Figure 5.13	Tmc curves obtained from the DSC for all NC (PET/MAE)	160
Figure 5.14	Crystallisation half-time for crystallisation from melt states for PET/MAE	161
Figure 5.15	DSC results for 5 samples from the same run to produce PET/MTE (20 wt.%)	162
Figure 5.16	Average of thermal analysis results of PET/MTE nanocomposites for various MTE contents	163
Figure 5.17	Tmc curves obtained from the DSC for all NC (PET/MTE)	164
Figure 5.18	Crystallisation half-time for crystallisation from melt states for PET/MTE	165
Figure 5.19	DSC results for 5 samples from the same run to produce PET/Cloisite 25A (3 wt.%)	165

Figure 5.20	The average of thermal analysis results of PET/Cloisite 25A nanocomposites for various Cloisite 25A contents	166
Figure 5.21	Tmc curves obtained from the DSC for all NC (PET/Cloisite 25A)	167
Figure 5.22	Crystallisation half-time for crystallisation from melt states for PET/Cloisite 25A	168
Figure 5.23	DSC results of PET nanocomposites at 1 wt.% for all nanoclay types	170
Figure 5.24	Tmc curves obtained from the DSC for all clays at 1 wt.%	171
Figure 5.25	DSC results of PET nanocomposites at 20 wt.% for all nanoclay types	172
Figure 5.26	Tmc curves obtained from the DSC for all clays at 20 wt.%	172
Figure 5.27	Part of the DSC curves for extruded vPET film (un-oriented and equal biaxial stretch) showing the Tg and Tgc curves	175
Figure 5.28	Part of the DSC curves for extruded PET/MTE 1 wt.% film (un-oriented and equal biaxial stretch) showing the Tg and Tgc curves	175
Figure 5.29	Part of the DSC curves for extruded PET/MTE 3 wt.% film (un-oriented and equal biaxial stretch) showing the Tg and Tgc curves	176
Figure 5.30	Part of DSC curves for extruded PET/MTE (5 wt.%) film (un-oriented and equal biaxial stretch) showing the Tg and Tgc curves	177
Figure 5.31	Schematic of DSC diagram for PET pellets during SSP process	181
Figure 5.32	Double melting endotherm behaviour with different heating rates	183
Figure 5.33	Shape of double melting endotherms for heating rates of 20°C/min and 0.5°C/min, in sequence	184
Figure 5.34	MDSC curves for the [F] scenario	184
Figure 6.1	Tensile strength vs. DK2 content. [Wang and Gao et al. (2006)]	191
Figure 6.3	Tensile modulus vs. ionic content for nanocomposites made with different types of nanoclays [Barber (2005)]	192
Figure 6.3	Tensile modulus of rPET/clay nanocomposites [Bizarria et al. (2007)]	193
Figure 6.4	Schematic of nanoplatelets orientation from skin to core for specimens moulded at 50°C	197
Figure 6.5	Schematic of nanoplatelets orientation from skin to core for specimens moulded at 130°C	197

Figure 6.6	Typical stress-strain curve for cold drawing of PET film	199
Figure 6.7	Tensile modulus of PETNCs films vs. clay contents at tensile test speed of 5 mm/min	200
Figure 6.8	Tensile modulus of PETNCs films vs. clay contents at tensile test speed of 50 mm/min	202
Figure 6.9	TEM micrographs for PET/MAE nanocomposites films at various clay concentrations	203
Figure 6.10	TEM micrographs for PET/MTE nanocomposites films at various clay concentrations	203
Figure 6.11	TEM micrographs for PET/Cloisite 25A nanocomposites films at various clay concentrations	203
Figure 6.12	Stress-strain curve for extruded vPET micro size sample prepared at different injection speeds	205
Figure 6.13	Stress-strain curve for PET/MTE (1 wt.%) micro size sample prepared at different injection speeds	206
Figure 6.14	Stress-strain curve for PET/Cloisite 25A (3 wt.%) micro size sample prepared at different injection speeds	207
Figure 6.15	Stress-strain curve for PET/MAE (5 wt.%) micro size sample prepared at different injection speeds	207
Figure 7.1	Schematic of 5-layer bottle	213
Figure 7.2	Plasma coating method	215
Figure 7.3	The regular arrangement of platelets in a parallel array	217
Figure 7.4	Reductions in PET film permeability on adding nanoclay	222
Figure 7.5	Reduction in the permeability of unfilled PET and PETNC films over a long period	223
Figure 7.6	Transparency level of each film	225
Figure 8.1	The chemical structures for some end groups [Jabarin (1996)]	230
Figure 8.2	Hydrolytic degradation mechanism [Jabarin (1996)]	231
Figure 8.3	Thermal degradation reactions [Mark (2007)]	231
Figure 8.4	Thermal-oxidative degradation mechanisms [Jabarin (1996)]	233

Figure 8.5	TGA curves for different nanoclays	239
Figure 8.6	Viscosity of un-filled PET re-extruded up to four times	241
Figure 8.7	Colour of the amorphous vPET after re-pass stages	241
Figure 8.8	Viscosity vs. shear rate of PET/MAE (3 wt.%) nanocomposites re-extruded up to four times	242
Figure 8.9	Colour of amorphous PET/MAE (3 wt.%) after re-pass stages	243
Figure 8.10	Viscosity vs. shear rate of PET/MAE (5 wt. %) nanocomposites re-extruded up to four times	244
Figure 8.11	Colour of the amorphous PET/ MAE (5 wt.%) after re-pass stages	245
Figure 8.12	Viscosity behaviour of vPET and PET/MTE (1, 3 and 5 wt.%) over a long period (10 hrs)	246

List of Tables

Table 1.1	Barrier properties of rigid containers	3
Table 1.2	Some PET applications	14
Table 1.3	PET applications by intrinsic viscosity	14
Table 2.1	Surfactant content and basal spacing between layers for all Cloisite clays studied [Kracalik and Puffr et al. (2007)]	39
Table 3.1	Some properties of the chosen nanoclays	49
Table 3.2	Processing parameters for the compounding process in the APV twin screw extruder	50
Table 3.3	PET (un-filled) and PET nanocomposite sample descriptions	53
Table 3.4	PET nanocomposite film processing parameters	55
Table 3.5	Micro-moulding processing parameters	67
Table 3.6	Density of the raw materials	60
Table 4.1	Description of the samples used in the rheological study	89
Table 4.2	Description of the film samples used in intrinsic viscosity (I.V.) analysis	90
Table 5.1	Crystallinity degree of PET nanocomposites	169
Table 5.2	The enthalpy of crystallinity in heating stage for un-oriented and oriented of un-unfilled PET and PET/MTE films at various concentrations	174
Table 5.3	First and second melting endotherms under various SSP processes	182
Table 7.1	Permeability results for PET nanocomposite films	221
Table 8.1	Weight loss from each clay at 260 and 280°C and degradation onset temperature for different clays from TGA	238
Table 8.2	Description of the re-passed samples	240



In the name of Allah, the Beneficent, the Merciful

قال الله تعالى :

Allah said:

[وفوق كل ذي علم عليم]

[and over every lord of knowledge there is one more knowing]

This thesis is dedicated to my parents

Acknowledgements

I am heartily thankful to my supervisor Dr. Tim Gough for his support, encouragement and guidance from the initial to the final stage which enabled me to create a good understanding of this subject. It is an honour to work under his supervision with his high standards of output and creative ideas. I would like to express my thanks to my supervisor Prof. Phil Coates for all his valuable discussion, suggestions and support during my study.

I would like also to take this opportunity to thank many people who worked and helped me throughout this project in different stages:

I would like to thank Dr. Adrian Kelly and Dr. John Sweeney for their constant support and co-operation and especially for their valuable guidance during the MPhil exam which helped me to complete this project. Thanks to Dr. Emma Burton, Dr. Leigh Johnson, Dr. Fin Caton-Rose, Dr. Ben Whiteside and Dr. Robert Spares for their assistance and encouragement. Many thanks to Mr. John Wyborn for his wonderful co-operation and assistance during the compounding process and also thanks go to Mr. Stephen Brook who helped me with professional assistance to produce PET nanocomposite films. Many thanks also to Mr. Keith Norris who helped me in the micromoulding stage based on his great experience in this field. Thanks also to Mr. Glen Thompson for his support in film the tensile test and Mr. Ken Howell for assistance in electronic issues.

It is also my pleasure to thank those who helped me from external sites. Thanks to Prof. Eileen Harkin-Jones from Queens University, Belfast for providing me with some raw materials. Thanks to Mr. Mohammed Isreb and Mr. Richard Telford from the IPI laboratories for their assistance in the thermal tests. Thanks to Mr. Abdullah Alotaibi and Dr. Ashok Menon from the SABIC Company for their support to conduct TEM, Barrier and Intrinsic viscosity tests. Many thanks to my colleagues at IRC Bradford. I greatly appreciate the financial support from the SABIC company.

I owe my deepest gratitude to my parents and lovely family; my wife (Reem) and my daughters (Haifa, Layan and Jory) for their wonderful support and patience. Their encouragement and continuous prayer are countless gifts. Thanks to my brothers, sisters and friends for their support. I thank the almighty God 'Allah' for providing me with the means to complete this thesis.

Chapter One

1. PolyEthylene Terephthalate (PET)

1.1 Introduction

Polyethylene Terephthalate (PET) exhibits excellent chemical and mechanical properties such as optical haze, chemical resistance, low weight, excellent electrical insulation, high stiffness and strength as well as good thermal resistance. Based on these features, it is one of the most versatile engineering plastics.

Over the last 20 years, the use of PET packaging has recorded very strong growth. The first market that PET penetrated was that for carbonated soft drinks (CSD) due to the outstanding properties of PET bottles such as the excellent barrier properties, its low weight and its strength. In addition to its 'unbreakable' features when compared to glass bottles, PET bottle weight is one-tenth of the glass bottle weight. Furthermore PET bottles have taken a big market share for water bottles, fruit juices, oils, sauces, sports drinks and others.

Due to these features and more, the demands for PET resins in Europe (one of the areas most affected by the financial crisis between 2007 and 2009) remains steady, while the demand for other commodity plastic resins fell. For example the demand for Polypropylene (PP) decreased by 15% from 2007 to 2009 and for the same period, the demand for Polyvinyl Chloride (PVC) decreased by 23% and by around 11% for Low Density Polyethylene (LDPE) and Linear Low Density Polyethylene (LLDPE) as figure 1.1 shows.

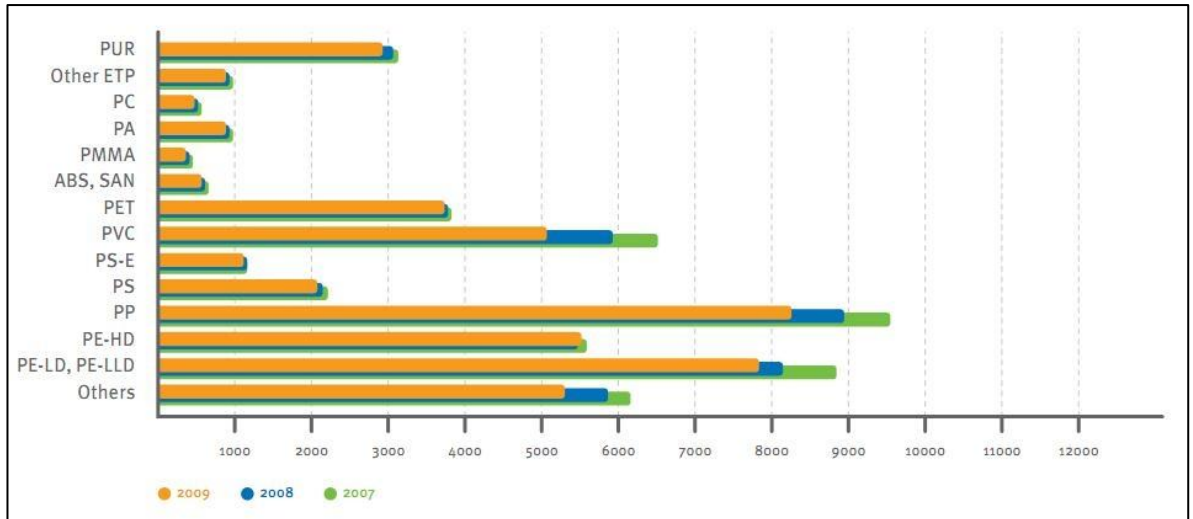


Figure 1.1 European plastics demand by resin type 2009 [Source: Plastics Europe Market Research Group (PEMRG)]

Moreover, according to the US-based consultant CMAI, the average annual growth rate (AAGR) of PET world wide in the period between 2005 and 2010 was 5.3%. CMAI forecasts the AAGR of global PET demand will be 5.7% in the 2010 – 2015 period as figure 1.2 shows.

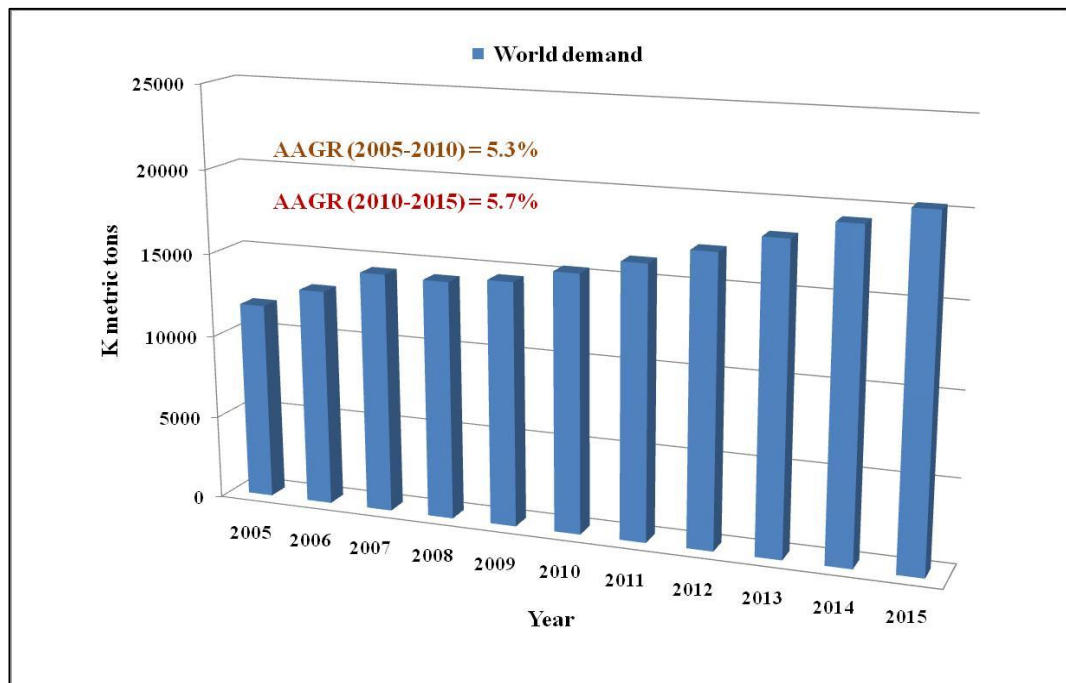


Figure 1.2 World demand of Polyethylene Terephthalate (PET) (actual demand 2005 – 2009 and forecast demand 2010 – 2015) [source: CMAIS]

Demand is increasing for PET packaging as it combines strength and transparency with good barrier properties. Obviously, metalized coatings, cartons and aluminium packaging can not compete with this combination of properties. Furthermore one of the more specialised applications that PET is dominant is the plastic barrier packaging due to the low permeability properties of PET packaging compared with other plastic packaging such as PP and High Density Polyethylene (HDPE) as Table 1.1 illustrate [Lange and Wyser (2003)].

Container composition and size	Oxygen transmission rate at 23 °C, 50% RH [cm ³ /(pack day atm)]
PP, 900 ml	6
HDPE, 500 ml	4
PET, 500 ml	0.2 – 0.4

Table 1.1 Barrier properties of rigid containers

On top of that, recycling the plastic attracts the public interest and this interest continue to grow. According to British Plastic Federation (BPF) in 2006, recycling the plastic in UK saved the emissions of 684,000 tonnes of CO₂ which equivalent to take 216,000 cars off the road. In 2009, 0.55 million tonnes of plastic packaging recycled then export 0.39 million tonnes [source: Liz Smith, WRAP].

PET is one of the most recyclable plastic as post-consumer scrap and the recycled PET can be used in food contact applications. In 1979, 4 million kg of PET beverages bottles were recycled and this number increased to 20 million kg in 1982 and 8 years after the number increased to 125 million kg.

1.2 PET preparation and chemistry

Poly (ethylene terephthalate), commonly abbreviated to PET or PETE, is an aromatic polyester which is a condensation product of Pure Terephthalic Acid (TPA) or Dimethyl Terephthalate (DMT) and Ethylene Glycol (EG). It was first prepared in 1941 by Whinfield and Dickson of the British company ICI [Rubin (1990)]. Their work followed guidelines previously established by W.H. Carothers and J. W. Hill of E. I. du Pont de Nemours and Company whose work in 1932 had yielded a low melt temperature oriented fibre of an aliphatic polyester.

Since its invention, PET has become one of the most important plastics industrially and economically, and it has become one of the most important commercial polymers used for bottles, films, fibres and food packaging. The physical and mechanical properties of PET such as high percentage crystallinity, high strain-induced orientation, high optical clarity and low gas permeability have been well researched by many with regard to these properties [McIntyre (2003) and others].

Jabarin (1996) and McIntyre (2003) reported that PET can be prepared by transesterification of Dimethyl Terephthalate (DMT) with ethylene glycol (EG) or direct esterification of Pure Terephthalic Acid (TPA) and Ethylene Glycol (EG).

In melt polymerization, DMT or TPA is reacted with EG in the presence of one or more combinations of catalysts at a temperature between 190 and 200°C to form bis(hydroxyethyl) terephthalate (BHET) with the elimination of methanol and water. The formed product BHET is polymerized under high vacuum and at a temperature between 275 and 285°C. During this polymerisation process, the excess of Ethylene Glycol is distilled off.

The preparations of the main raw materials are as follows:

- 1- Ethylene glycol (EG) is an essential material for producing PET and it can be obtained by converting ethylene to ethylene oxide then to ethylene glycol, as figure 1.3 shows.

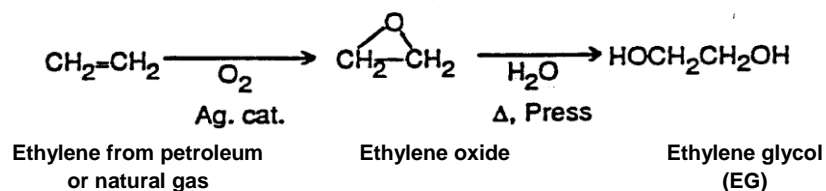


Figure 1.3 Preparing the reaction for ethylene glycol [Jabarin (1996)].

- 2- Para-xylene is oxidized to produce Pure Terephthalic Acid (TPA), then TPA is purified by reaction with methanol to form dimethyl terephthalate (DMT), as Figure 1.4 shows.

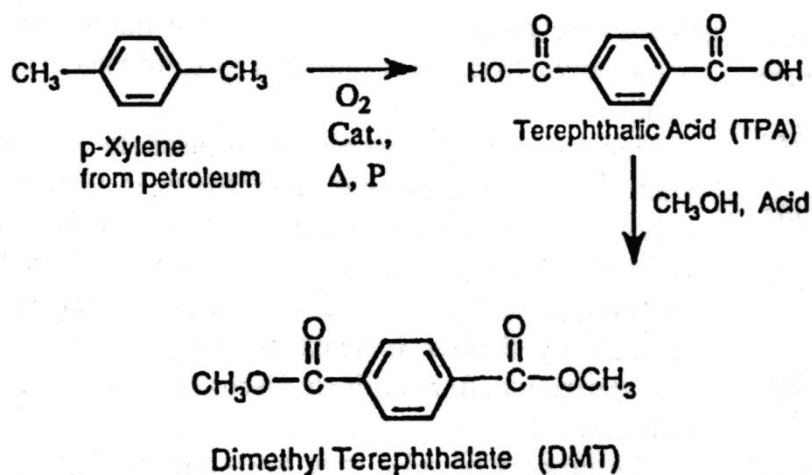


Figure 1.4 Preparation of DMT from Para-xylene [Jabarin (1996)].

3- During the synthesis of PET using TPA or DMT, bis(hydroxyethyl) terephthalate (BHET) is prepared (Figure 1.5)

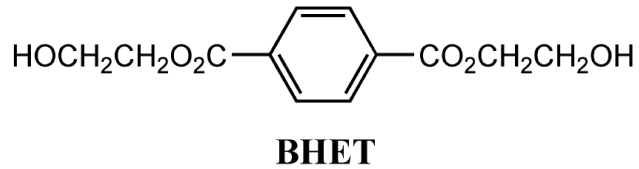


Figure 1.5 Chemical structure of bis (B-hydroxyethyl) terephthalate (BHET) [Jabarin (1996)].

The BHET acts as the monomer for polymerization to yield PET (Figure 1.6).

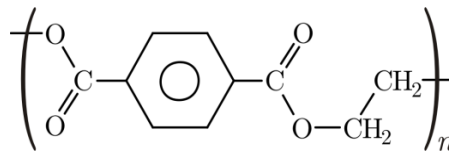
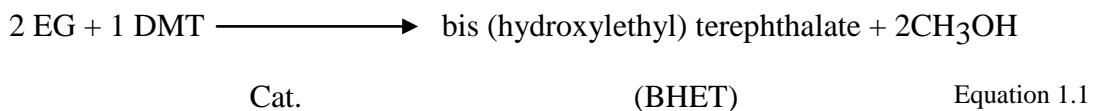


Figure 1.6 Chemical structure of PET [Jabarin (1996)].

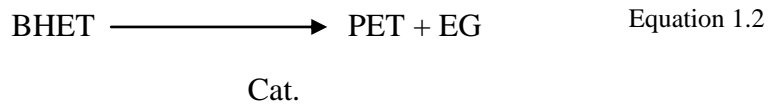
As mentioned above, PET can be prepared by transesterification of DMT or TPA with EG (see section 1.2) as follows [Jabarin (1996)]:

A- Synthesis from DMT follows this scheme:



Conditions: 190-220°C, N₂, and 1 Atmosphere.

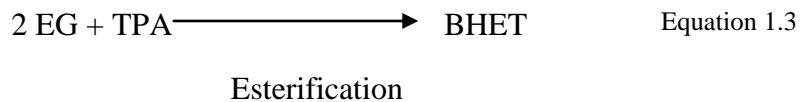
Catalysts: Acetates of Li, Ca, Mg.



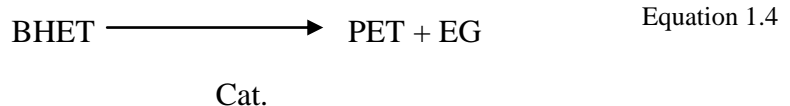
Conditions: 275-285°C, High vacuum.

Catalysts: Acetates of Sb, Zn or Pb. Oxides of Sb, Ge or Pb.

B- Synthesis from TPA follows this scheme:



Conditions: 190-220°C, N₂, 2 Atmosphere, no catalyst.



Conditions: 275-285°C, High vacuum.

Catalysts: Acetates of Sb. Oxides of Sb, Ge.

Melt polymerisation can produce PET with 100 degrees of polymerisation (DP) which can yield an intrinsic viscosity (I.V.) of up to 0.64 dl/g [I.V. is discussed in detail in section 4.3.5].

This PET grade is suitable for some applications such as fibres and carpet. For some products a higher I.V. is required necessitating up to 150 of polymerisation degrees, such as for sheets, films, bottles and other containers. To achieve this, a further process is required to increase the molecular weight of the amorphous pellets. This process is called Solid State Polymerisation (SSP) and is carried out at about 210°C under a nitrogen atmosphere fluidized bed or vacuum pressure [Rieckmann and Volker (2003)].

This process is covered in detail in section 1.3.

1.3 Solid State Polymerisation (SSP)

Producing high molecular weight PET during the melt processing stage provides challenges in handling of the high viscosity PET melt. Increasing the molecular weight of PET using Solid State Polymerisation (SSP) can overcome this problem. This technique is widely applied in the industrial manufacture of bottle grade PET [Papaspnyrides and Vouyiouka (2009)].

Processing of polymeric materials is a broad field consisting of many operations such as extrusion, injection moulding and thermoforming. The processing method is chosen according to the specifications of the final product and the characteristics of the polymer [Culbert and Christel (2003) and Kim et al. (2003)].

Solid State Polymerisation (SSP) aims to increase the molecular weight of the polymer by promoting many reactions between the polymeric end groups. Culbert and Christel (2003) reported that SSP is a relatively simple treatment which results in few side reactions and provides more effective removal of volatile degradation products than other methods of increasing molecular weight.

Three reactions are carried out during the SSP of PET. All these reactions produce high molecular weight PET and some side products. The polycondensation reaction is the main reaction and occurs when two hydroxyl end groups interact and produce a high molecular weight PET with ethylene glycol as a side product (figure 1.7). A second reaction can occur when chains having vinyl ester end groups interact with hydroxyl end groups to produce acetaldehyde (AA) as a side product in addition to the high molecular weight PET (figure 1.8) [Culbert and Christel (2003)].

The third reaction is the esterification reaction which occurs when the carboxyl end groups react with hydroxyl end groups (figure 1.9) to produce PET with high molecular weight and water as a side product [Jabarin (1996) and Wadekar et al. (2009)].

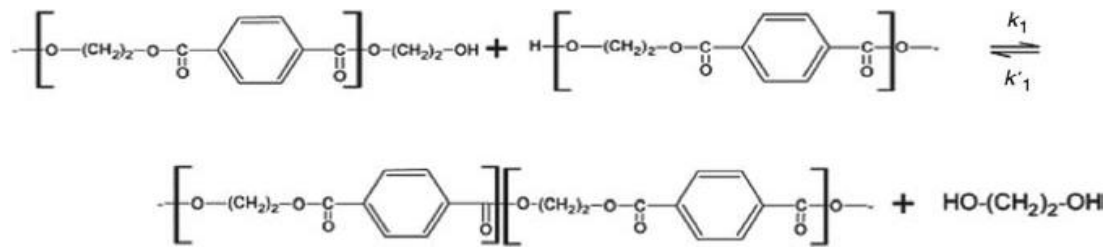


Figure 1.7 Polycondensation reaction

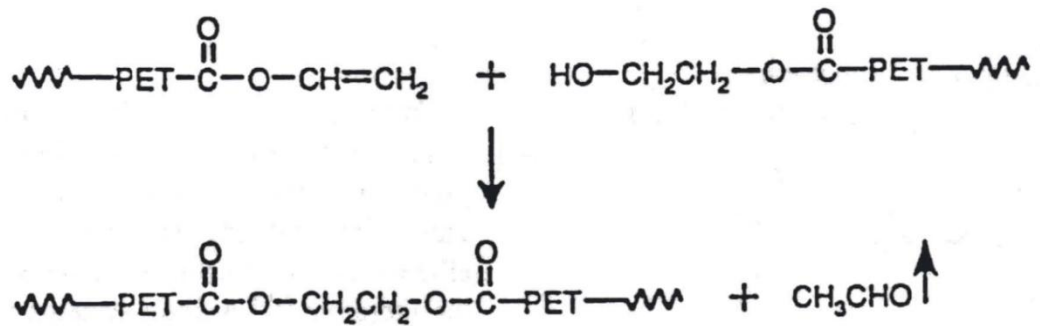


Figure 1.8 Vinyl ester group interacting with hydroxyl end group.

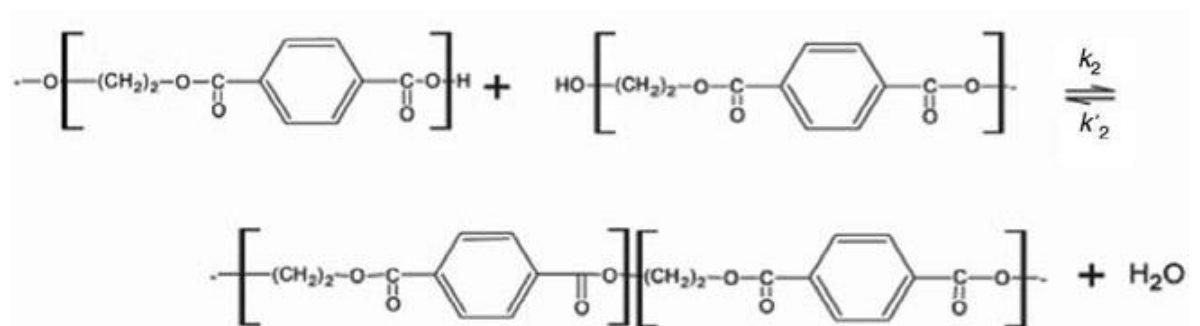


Figure 1.9 Esterification reaction

The SSP process is carried out either in the presence of an inert gas or in a high vacuum environment and at temperatures below the melting point of PET (200 - 240°C), so the risk of PET degradation is low. This processing temperature can lead to sticking of the amorphous pellets inside the SSP reactors thus forming lumps which may hinder the pellets' flow.

Consequently the amorphous pellets should be crystallised prior to entering the SSP reactor. This crystallisation process is carried out in a rotational and vibratory reactor at temperatures between 150 and 180°C. The concentrations of some reactive end groups increase during this crystallisation process. Furthermore, the movement or mobility of the PET molecules decreases.

One of the advantages of the crystallisation process is the prevention of moisture penetrating the crystalline region, which decreases the possibility of hydrolytic degradation. Deactivation of some end groups also occurs during the crystallisation process. SSP can also be used in the recycling of PET bottles. The advantage of using the SSP process in recycling is that the low I.V. flakes can be recycled to high I.V. bottles [Jabarin (1996) and Wadekar et al. (2009)]. The basic flow charts for melt polymerisation and solid state polymerisation processes are shown in Figure 1.10.

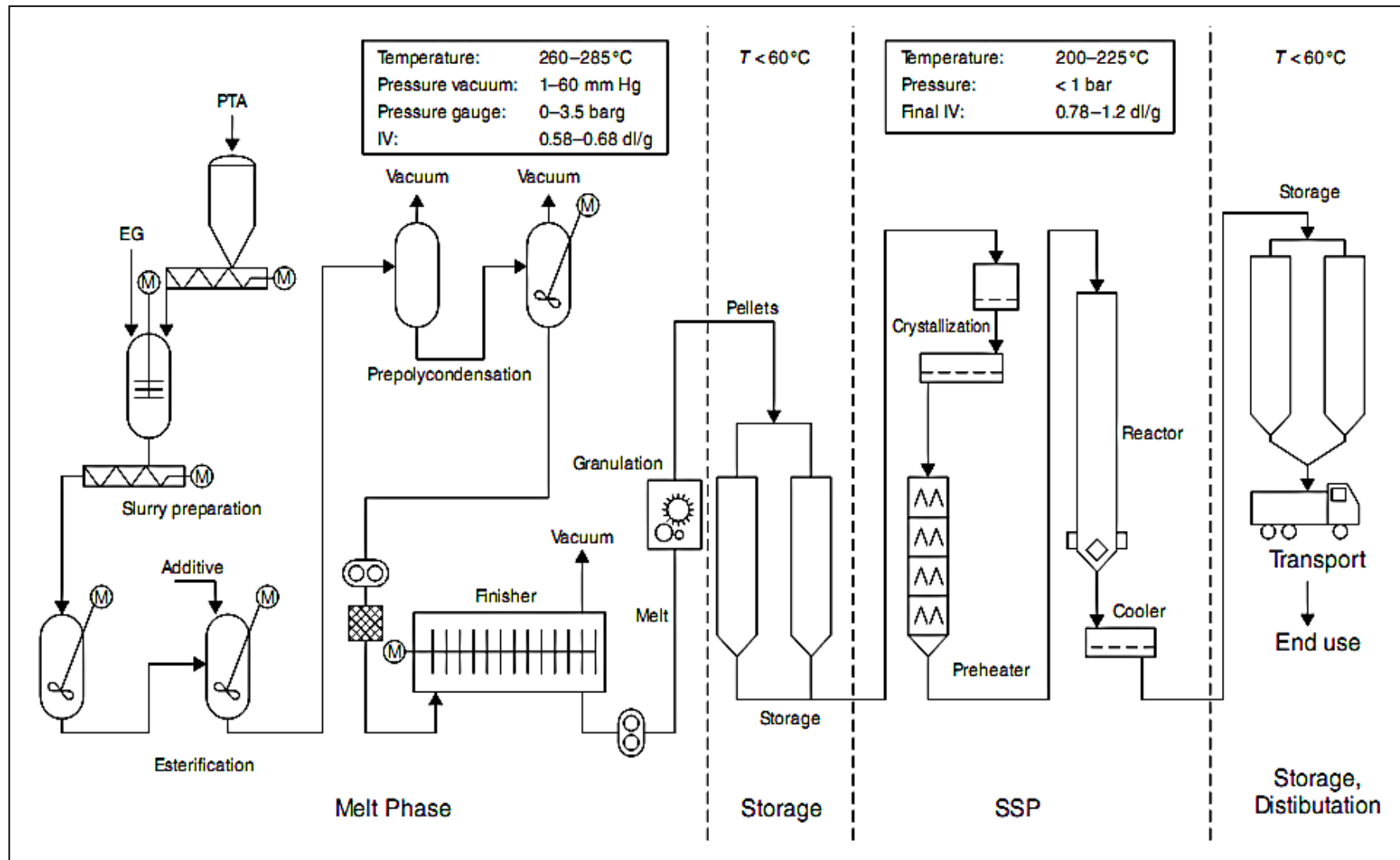


Figure 1.10 Schematic of PET manufacture. [Culbert and Christel (2003)]

1.4 Safety and application of Polyethylene Terephthalate (PET)

The U.S. Food and Drug Administration (FDA) is responsible for the stringent regulations that assure the safety of food in the US. The FDA regulates materials intended to come into contact with a food or beverage, including plastic packaging as an “indirect” food additive. According to the FDA, indirect food additives are substances that may come into contact with food as part of packaging or processing equipment, but are not intended to be added directly to food [FDA’s Center for Food Safety and Applied Nutrition (2004)].

Polyethylene terephthalate (PET) has become the plastic packaging of choice for many food products. This is due to its inherent properties that are well suited for lightweight, large capacity and shatter resistant containers. Castle (1989) determined the levels of compounds that have the potential to transfer from the plastic into food under conditions that simulate the actual use of the material. The author found that the migration of any components of PET plastics under laboratory conditions is well below applicable safety levels.

In a report of PET for food packaging applications issued in July 2000, the International Life Sciences Institute (ILSI) summarized the large body of test data that demonstrates the safety of PET resin and compounds for food and beverage containers:

“PET itself is biologically inert if ingested, is dermal safe during handling and is not a hazard if inhaled. No evidence of toxicity has been detected in feeding studies using animals. Negative results from Ames tests and studies into unscheduled DNA synthesis indicate that PET is not genotoxic. Similar studies conducted with monomers and typical PET intermediates also indicate that these materials are essentially nontoxic and pose no threats to human health. It is important to stress that the chemistry of

compounds that are used to manufacture PET shows no evidence that demonstrates that the use of PET is not a concern and is perfectly safe in this respect” [Packaging Materials (2000)].

Polyethylene terephthalate (PET) has distinguishing properties such as [Brooks and Glies (2002)]:

- Low cost.
- Thermal resistance.
- Chemical resistance. PET can be used for containers for many food and non-food applications such as fruit juice, milk, shampoo and cosmetic containers.
- High barrier, mechanical and physical properties. Preferred for Carbonated Soft Drink (CSD) bottles, other pressurised containers and water drink bottles.
- Excellent transparency and light weight.
- Excellent electrical insulation.
- Crystallisable plastic. Heat setting technology can be used to produce PET bottles which resist deformation during hot filling.
- One of the virtues and attractions of PET products are that it is a fully recyclable plastic and recycling is more practical compared with other commodity polymers.

For all these versatile properties and more, PET has been widely used in a variety of applications (Table 1.2). Its major uses are as food and beverage containers, fibres and films [Brooks and Glies (2002)].

Fibre Form	Film Form	Containers
Textiles, industrial yarn, tyre cord, carpeting, staple fibre.	Film, tapes, bags, photographic film.	Food, beverages, household products, pharmaceuticals, trays.

Table 1.2 Some PET applications

The molecular weight or intrinsic viscosity (I.V.) of PET varies, and the following ranges are suitable for commercial products (Table 1.3):

Application	I.V. (dL/g)
Textiles	0.55–0.65
Films and Tapes	0.65–0.75
Bottles	0.7–1.0
Tyre Cords	1.0

Table 1.3 PET applications by intrinsic viscosity

From time to time researchers and PET producers present new PET applications to the market. Even with these new products, the demands of new PET performance are continuous. There are many methods for meeting these demands such as changing the molecular weight, using new additives, changing the processing conditions, or changing the fundamental properties of PET by copolymerisation of new monomers into the PET backbone.

Poly (ethylene terephthalate)-glycol (PETG) is one of the commercial PET copolymers [Schiraldi (2003)]. It is a non-crystallizing amorphous copolymer of PET. PETG is a random copolymer consisting of (typically) 31 mol% CHDM (Cyclohexanedimethanol) and 69 mol% PET. PETG does not occupy the same industrial niche as PET, precisely

because it lacks the ability to undergo strain-induced crystallisation [Brooks and Glies (2002)]. Dupaix and Boyce (2005) reported that PET and PETG exhibit quite similar deformation behaviour but have a different glass transition temperature. Crystallisation is nearly impossible to achieve in PETG.

Stretched polyester film (PETF) is very different from PETG and indeed PET. It is a semi-crystalline film produced by a roll quenching process; followed by biaxial orientation (stretching the film in machine and transverse directions). Stretched polyester film is used in many applications such as video tape, high quality packaging, professional photographic printing, x-ray film and floppy disks. The primary advantages of the film are high thermal stability, mechanical strength and chemical inertness [Brooks and Glies (2002)].

1.5 Objectives and writing tactic

I. Objectives

This project was initiated and designed to investigate the rheological behaviour, thermal properties, tensile modulus, permeability properties and degradation phenomena of Polyethylene Terephthalate (PET) nanocomposites. Three different types of nanoclays were compounded with PET pellets via a twin screw extrusion. Further melt processing and characterisation followed this compounding stage. The main objective of this project was based on achieving different requirements as follows:

- Choosing the most compatible nanoclay by studying the structure of different nanoplatelets and conducting some characterisation.
- Compounding via twin screw extrusion, feeding the raw materials simultaneous to the extruder by using two motor feeders and processing under optimum temperatures, residence time and screw speed in order to achieve a good mixing process. Drying of the raw material is necessary prior to the compounding process.
- Analysing the rheological behaviour of PET nanocomposites over a wide range of shear rates and investigate the effect of increasing the nanoclay loading on the rheological behaviour.
- Exploring the effect of adding the nanoclay on the thermal properties of PET including its crystallisation properties. Moreover studying the effect of the biaxial stretch process on the thermal properties of PET nanocomposites films.
- Producing PETNCs films via single screw cast film extrusion and PETNCs micro-size samples via micromoulding injection machine to study the effect of nanoclay on the tensile modulus of PET final products.

- Investigating the tensile modulus of PET nanocomposites and correlating these results with TEM micrographs.
- Studying the effect of adding nanoclays on the barrier properties of PET films.
- The degradation phenomenon of PET pellets in the presence of nanoclay was studied over long time scales and through reprocessing the PETNC pellets.

II. Writing tactic

- The thesis was written in the same sequence in terms of PET preparation and processing (i. e. thermal processing and flow behaviour before mechanical and barrier testing on the final PET nanocomposites). The thesis is divided into nine chapters.
- Chapter one covers an introduction and background of Polyethylene Terephthalate (PET) in terms of global market, history, chemistry, preparation and application.
- The fundamentals and concepts of nanocomposite materials, their classification and types are included in chapter two. In addition, an extensive review of previous studies of PET nanocomposites is presented in this chapter while more intensive literature reviews are presented in each of the results and discussion chapters as appropriate.
- The methodology of the project including the details of the raw materials, compounding process, cast film extrusion, micromoulding injection process as well as characterisation techniques are explained in chapter three.
- Chapter four presents the literature review for polymer nanocomposites studies in terms of rheological science and discusses the rheological behaviour of

PETNC over a wide range of shear rates. The results were analysed from different views for more understanding.

- Chapter five covers an introduction to the thermal properties of PET and discusses the effect of nanoclay on these focusing on the crystallisation properties.
- The tensile modulus results for the PETNC films and micromoulded samples are presented in chapter six along with some discussion and a short literature review.
- Chapter seven includes the results and discussion of the effect of the nanoclay platelets on the barrier properties of PET films.
- Analysis of the degradation of PETNCs over long time scales and after additional melt re-processing is covered in chapter eight.
- Chapter nine includes some general conclusions and discussions in addition to the suggested future work in this area.

Chapter Two

2. Polymer nanocomposites

The objectives of this chapter are: 1) to understand the fundamentals of polymer nanocomposite materials by identifying the nanotechnology, nanoparticles and organoclays, 2) review some of the extensive research carried out in this field, and 3) to examine a variety of nanoclays in order to choose three, as well as the proper compounding methodology.

2.1. Introduction

The science of nanocomposites is a branch of nanotechnology, so it is appropriate to define nanotechnology as a prelude to understanding nanocomposites. The prefix “nano”, Greek for “dwarf”, means one billionth or 10^{-9} . To get a sense of the nanoscale, the smallest things that can be seen with the naked human eye are approximately 10,000 nanometers (nm) [Booker and Boysen (2005)]. The thickness of a human hair is about 50,000nm by way of comparison in dimension. Ratner and Ratner (2003) state that nanotechnology is difficult to define as it is difficult to determine. Different scientists define nanotechnology based on the view of their particular field of science. To clarify the definition a new committee was formed in the USA, the National Nanotechnology Initiative. Booker and Boysen (2005) summarized the committee’s definition as follows:

- “1- Nanotechnology involves research and technology development at the 1nm to 100nm range.
- 2- Nanotechnology creates and uses structures that have novel properties because of their small size.
- 3- Nanotechnology builds on the ability to control or manipulate at the atomic scale.”

To fabricate at the nanoscale there are two approaches: bottom-up and top-down. The bottom-up approach seeks to arrange smaller components (e.g. molecules) into more complex assemblies while the top-down approach mimics a large scale assemblies and then reducing size until the nanoscale product is formed.

Buzea et al. (2007) state that nanotechnology has the potential to create many new and novel materials which will affect our lives by increasing standards of living. By producing new medicines and new devices, medical diagnostics will be faster and cheaper and nanotechnology will aid in the delivery of the optimum quantify of medicine to exact spots in the body that need it most. Also security will increase by the production of more powerful and smaller computers and of superior lightweight materials which are ten times stronger than steel but only a tenth of the weight.

2.2 Nanocomposites

Ajayan et al. (2003) defined nanocomposites as multiphase solid materials where one of the phases has a dimension of less than 100nm. The field of nanocomposites is a fast growing area of research and efforts are focused on the ability to obtain control of the nanoscale structures via innovative synthetic approaches. Theng (1979) reported that nanoscale organoclays have been used to control the flow of polymer solutions in cosmetics since the mid 1950s.

Polymer nanocomposites are mixtures of polymers and particles with one of the component dimensions of nanometre length scale. Reducing filler quantities and enhancing some properties are examples of the advantages of nanocomposites. Usuki et al. (1993) stated that the surface area of the fillers is an important factor in achieving

high performance nanocomposites, since nanoparticles have extremely high surface area to volume ratios when good dispersions are achieved.

Clays are one of the nanoscale materials used to form nanocomposites. Koo (2006), Ke et al. (2002), Ray and Okamoto (2003), Carrado (2003) and other researchers have reported that there are three types of polymer-clay nanocomposite structures. The affinity of the clay with the polymer is the main factor in classifying nanocomposites into the three types as follows:

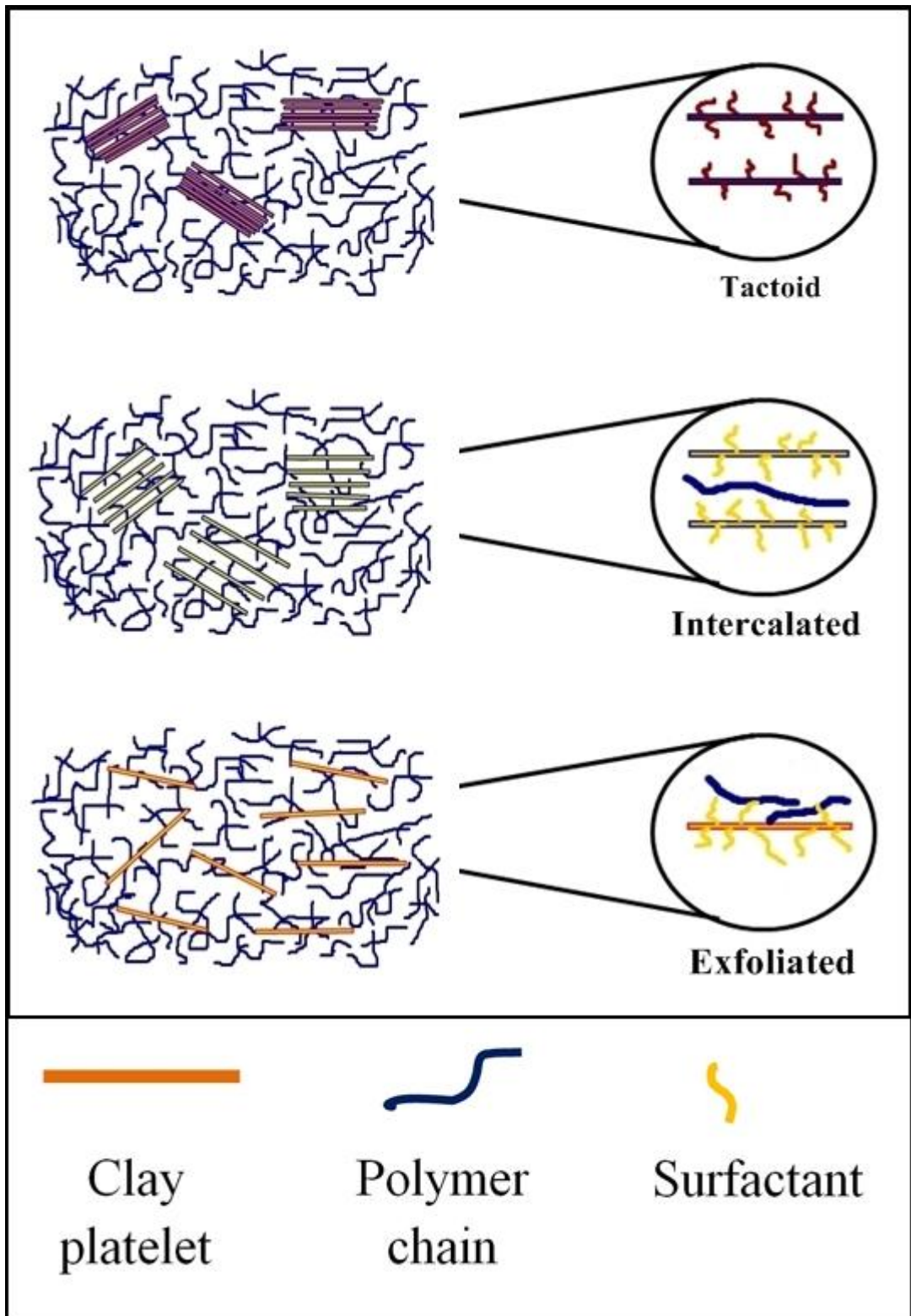


Figure 2.1 Schematic showing polymer-clay nanocomposite classifications

1- Tactoid structures (unmixed)

These structures are obtained when the interlayer space of the clay does not expand, due to its poor affinity with the polymer. These structures are like conventional fillers since improving one property requires a loss of another property.

2- Intercalated structures

Intercalated structures show better dispersion than the first type above. These structures are obtained in the case of a small interlayer expansion of clay. Also, due to some affinity between the polymer and the clay, there is a well-ordered multilayer structure.

3- Exfoliated structures

Due to an excellent affinity between the polymer and the clay, the clay layers are well separated into single layers within a continuous polymer matrix. The exfoliated structure is required to make the best nanocomposite in terms of tensile, thermal and barrier properties, due to the excellent dispersity of clay and the interfacial interaction of clay platelets with the polymer.

Tailoring the morphology (i.e. exfoliated or intercalated structures) of the polymer matrix is the main challenge in enhancing the properties of polymer nanocomposites [Barber et al. (2005)]. Figure 2.1 illustrates these classifications schematically.

Generally, exfoliated structures achieve the most enhancements in the properties of polymer nanocomposites, but in some cases a combination of tactoids and exfoliated structures can exhibit better enhancements. Svoboda et al. (2002) investigated the properties of polypropylene / organoclay nanocomposites and reported that when most of the nanoclay was present in the polypropylene (PP) matrix as tactoid structures and some in the exfoliated form, the mechanical and crystallisation properties were improved when compared with clay present in fully exfoliated structures.

2.3. Nanoparticles

A number of changes in physical properties can occur when materials are reduced in size from microparticles to nanoparticles. As the size is reduced, the ratio of surface area to volume is increased dramatically. For example, the ratio of surface area to volume in sphere shape can be calculated from this equation:

$$\frac{s}{v} = \frac{3}{r}$$

where r is the radius, s is the surface area and v is the volume.

This increase leads to an increasing dominance of the behaviour of the atoms on the surface of the particle over that of those in the interior of the particle. Some of these surface interactions can reflect positively on some properties, for example by increasing the chemical/heat resistance and increasing the strength of the composite material.

Nanoparticles are currently manufactured from a wide variety of materials. Ceramics are the most common of the new generation of nanoparticles. Silicate-nanoparticles currently in use are flakes about 1nm thick and 100-1000nm across. The most common type of clay used is Montmorillonite, a layered alumina-silicate.

Nanoparticles can be divided into three categories based on their dimensions as follows [Utracki (2004)]:

1- Layered nanoparticles

The most interesting of all nanoparticle categories is the layered nanoparticle which can exhibit good dispersion into a polymer matrix. Layered nanoparticles used in polymer nanocomposite processes can exist in different types such as smectite clays (e.g. Montmorillonite (MMT)), synthetic clays (e.g. Sodium fluoromica), and others (e.g. nanotalc). The thickness of the platelet is in the range 0.7 to 2.5nm. The first and second types have been used in this project so they will be discussed in further details later (see section 2.4).

2- Fibrillar nanoparticles

With fibrillar nanoparticles the diameter of the fibres is in the range 1 to 20nm with length 30 to 200nm. The best known fibrillar materials are carbon nanotubes and carbon nanofibres. Carbon nanotubes are molecular-scale tubes of graphitic carbon. They have novel properties that make them potentially useful in many applications in nanotechnology. Nanotubes are categorized as single-walled nanotubes (SWNTs) or multi-walled nanotubes (MWNTs). Carbon nanofibres are a form of vapour-grown carbon fibre. They are available in diameters ranging from 50 to 200nm and are much smaller than conventional milled nanofibres (5 to 10 μ m) but larger than carbon nanotubes (1 to 10nm). They can be used for improving the strength and modulus of the polymer material. One of the carbon polymorphs is graphite which is formed by stacking graphene sheets with an gap spacing of 0.335 nm. Graphite is the stable form of

the element carbon. Exfoliated graphite can replace the CNTs when the high electrical conductivity is required [Utracki (2004)]. Andre Geim and Konstantin Novosrlov were awarded the Nobel Prize in Physics for 2010 for their research “for groundbreaking experiments regarding the two-dimensional material graphene”.

3- Other nanoparticles

Other nanoparticles include spherical particles, sol-gel hybrids and polyhedral oligomeric silsesquioxanes (POSS).

2.4 Structure and properties of Montmorillonite organoclay (MMT) and synthetic mica clay

The preferred layered nanoparticles for preparing polymer nanocomposites (PNCs) are phyllosilicates. The phyllosilicates or smectite clays are used most frequently for non-ceramic applications. The smectites have a triple layer sandwich structure (2:1). This consists of an octahedral sheet in the middle connected to two silica tetrahedral sheets by oxygen ions, as shown in figure 2.2. The two outer layers of silica (tetrahedral) are fused onto an inner layer of alumina (octahedral). A Van der Waals gap occurs when the layers stack on each other and this gap is called a gallery or interlayer [Giannelis et al. (1998), Ray and Okamoto (2003)]. Montmorillonite (MMT) is one of the most common smectites used in different polymers for a variety of applications. MMT is inexpensive and available in nature in large quantities but impossible to obtain in a purified state. Because it is a naturally occurring mineral its composition is subject to variation which can causes variability in the properties of the manufactured polymer nanocomposites. Consequently, synthetic layered nanoparticles with a smectite structure have drawn some attention and interest in the field of polymer nanocomposites. The main

distinguishing features of synthetic clay (e.g. synthetic mica) are its well controlled chemical and physical properties, its high aspect ratio compared with natural clay, and the good reproducibility of its polymer nanocomposite performance [Utracki (2004)]. The major drawbacks of synthetic clay are the material cost and limited availability.

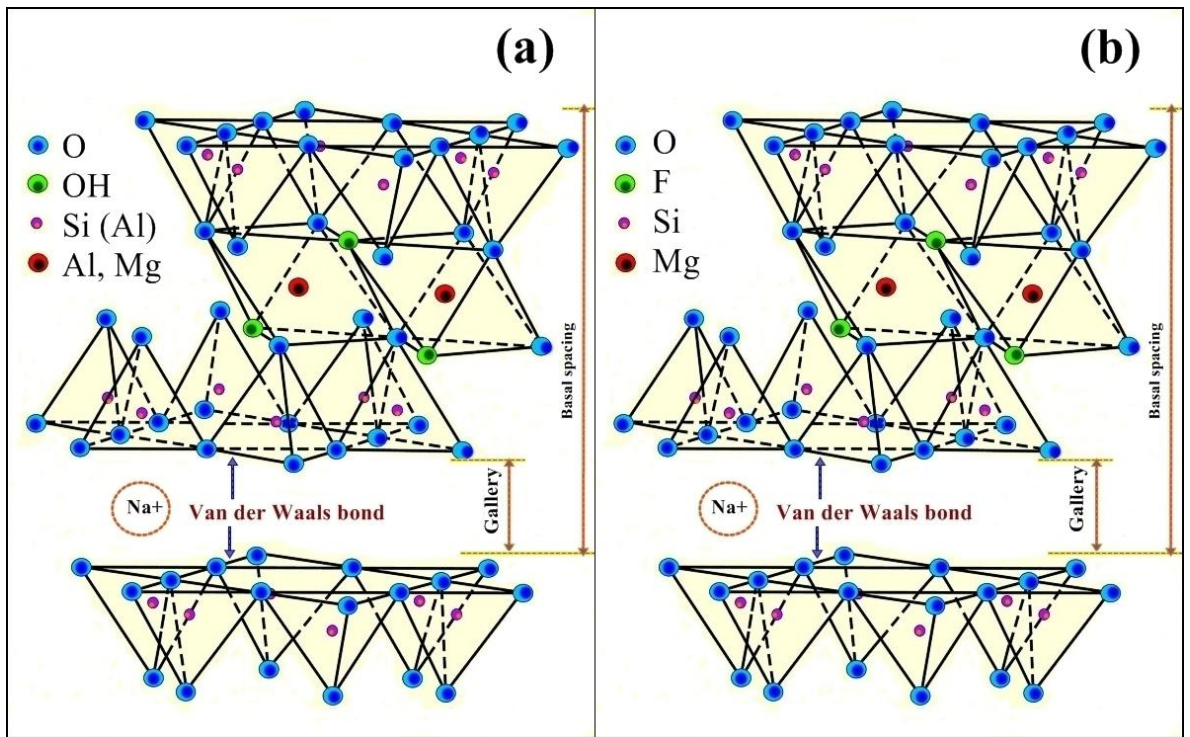


Figure 2.2 The chemical structure of dry phyllosilicates: a) Montmorillonite clay, b) synthetic mica clay.

2.5 Nanoclay modification

MMT clays are highly hydrophilic which means they are immiscible with hydrophobic polymers (e.g. PET). Crystalline swelling occurs when MMT is contacted by water. However, to make these nanoclays compatible with most polymers, they must be made hydrophobic. The laboratory route usually introduces alkylammonium ions in the gallery by an ion exchange reaction which can make the clay surface organophilic. The cations of MMT are commonly hydrated K^+ or Na^+ . However, the ion exchange reaction of an organic cation with a gallery cation can enhance the organophilic nanoclay surface. The amount of the charge which is generated within the layers by replacing Fe^{+2} or Mg^{+2} with Al^{+3} can be measured by the cationic exchange capacity (CEC), which is usually between 0.9 and 1.2 milli-equivalent/g.

The alkylammonium cation contains different types of functional groups which could introduce the polymer to the inorganic clay. Furthermore, the organic cations can allow the organic polymer to expand the gallery by reducing the energy of the nanoclay surface.

The Van der Waals interaction energy causes the platelets to remain stacked together, and the attraction energy depends on the distance between the platelets (h) as shown in figure 2.3.

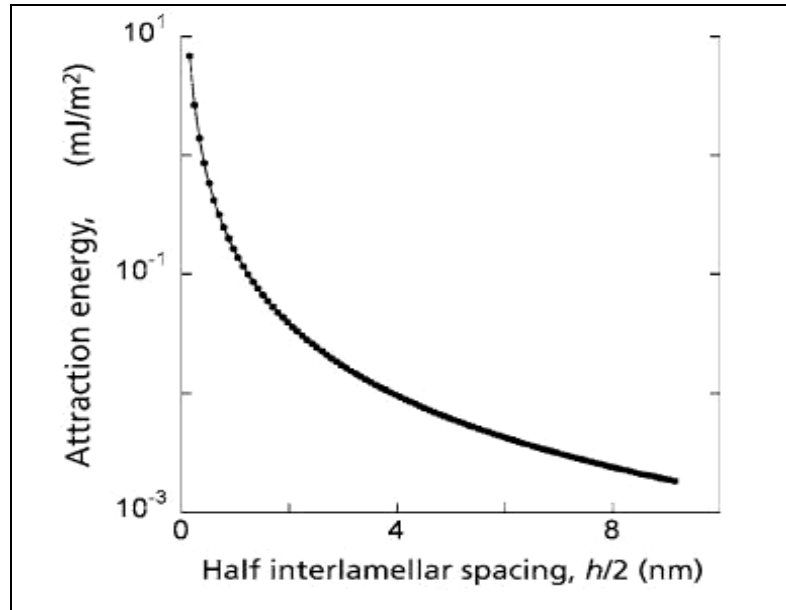


Figure 2.3 Attraction energy vs. the separation distance between two plates between two phyllosilicate layers [Utracki (2004)].

The attraction energy ($U_{\text{attraction}}$) between two plates which have the same thickness is given in Equation 2.1 [Bhattacharya et al. (2008)]:

$$U_{\text{attraction}} = -\frac{A_{11}}{12\pi} \left[\frac{1}{h^2} + \frac{1}{(h+2t)^2} - \frac{2}{(h+t)^2} \right] \quad \text{Equation 2.1}$$

where A_{11} is the Hamaker constant, t is the platelet thickness and h is the separation distance between two plates. The Hamaker constant is a force constant which can be used to define the Van der Waals force.

2.6 Previous studies of polymer nanocomposites

In the following paragraphs some studies of polymer nanocomposites are reviewed to give a general idea about the efforts, work volume, results and observations in this area. Later, each individual chapter will include an extensive literature review covering each specific subject (e.g. rheology and thermal analysis barriers properties).

Ray and Okamoto (2003), Ray (2006), Utracki et al. (2007) and Pavlidou et al. (2008) published review papers covering a wide range of the polymers used to produce polymer nanocomposites. The authors discussed subjects such as the properties and structure of layered nanoparticles, types of polymer used to produce nanocomposites with layered nanoparticles, polymer nanocomposite preparation, and the rheological and mechanical properties of polymer nanocomposites. They reviewed and discussed the results of hundreds of papers.

Furthermore, polyethylene terephthalate (PET) nanocomposites drew the researchers' attention to investigate the effect of nanoclays on the various properties of PET. The researchers compounded the PET with nanoclay via different methods. Some researchers used in situ methods to prepare the PET nanocomposites prior to analysis and characterization, including Chang et al. (2004), Han et al. (2006), Lee and Im (2007), Lu et al. (2007), Chang and Mun (2007), Guan et al. (2008), Antoniadis et al. (2009) and Vassiliou et al. (2010). Other researchers used the melt screw extruder process to compound the clay with PET matrix, then quenched the melt output prior to pelletizing it, including Pegoretti et al. (2004), Sanchez-Solis et al. (2004), Barber et al. (2005), Costache et al. (2006), McConnell et al. (2006), Calcagno et al. (2007), Kim et al. (2007), Kim and Lee et al. (2008), Tzavalas et al. (2008), Ammala et al. (2008), Kim and Choi et al. (2009), Rajeev et al. (2009), Frounchi and Dourbash (2009), and Soon et

al. (2009). In addition, some researchers aimed to enhance various properties of recycled PET (rPET) by adding nanoclays during the recycling process, such as Bizarria et al. (2007), Kracalik et al. (2007) and Giraldi et al. (2008).

The main challenge in achieving success in PET nanocomposite (PETNC) properties is the high processing temperatures during PETNC preparation. PET and nanoclays degrade under high processing temperatures, as reported by Costache et al. (2006) when they prepared PET nanocomposites via an in-situ method in which the polycondensation process took place at 280°C. However, the decomposition temperature of most surfactants, used to modify the hydrophilic clay organophilic, is well below these processing temperatures, as Gupta and Bhattacharya (2008) reported. Furthermore PET is a hygroscopic material, so a high efficiency dehumidifier or vacuum oven is required prior to any melt processing to partially eliminate the effect of hydrolysis degradation. However, many researchers [e.g. Ou et al. (2004)] have suggested a solution method to prepare PET nanocomposites in order to avoid thermal degradation, because this does not require elevated temperatures, which means the PET matrix and the surfactant are not degraded. The use of significant volumes of solvent in this method is a drawback because it is expensive as well as being harmful to the environment.

One of the potential applications for polymer nanocomposites is in compounding a nanofiller with a recycled polymer to enhance the properties of the recycled product (e.g. its mechanical properties). The recycling of polymers is affected by many factors such as the environmental protection regulations of the country and the price of the neat polymer. Therefore, instead of buying the neat polymer, one can add a small quantity of nanofiller to the recycled polymer to attempt to regain the same properties as the virgin material. Pegoretti et al. (2004) aimed to prepare and characterize recycled PET/clay

nanocomposites. Recycled PET (rPET) pellets and two montmorillonite clays (Cloisite Na⁺ and Cloisite 25A) were used to produce PET nanocomposites with 1, 3 and 5 wt.% via melt compounding with co-rotating twin screw extruders. Scanning transmission electron microscopy (STEM) was used to evaluate the dispersity of the nanocomposites and it was found that the Cloisite 25A gave much better dispersion in the nanocomposite compared to Cloisite Na⁺. Also Wide Angle X-ray Scattering (WAXS) measurements indicated increased lamellar periodicity of Cloisite 25A in the composition which infers intercalation. The authors observed that Cloisite 25A increases the rPET nanocomposite tensile modulus. Furthermore, good interfacial adhesion was observed as the yield strength was not reduced with increasing nanoclay fraction. A similar study was carried out by Bizarria et al. (2007) who observed a large reduction in intrinsic viscosity (I.V.) after extrusion and injection moulding processes. The authors tried to avoid hydrolytic degradation by using an antioxidant (Irganox B561) with all nanocomposites during extrusion. They observed some improvement in the modulus and yield strength through addition of the organoclay. They did not explain why the nanoclay they used (Montmorillonite clay (DELLITE1 67G)) did not act as an effective nucleating agent for the nanocomposites which could be because they extruded the nanocomposites under high temperatures (up to 285°C) which may cause degradation in the composite, or they did not select a suitable clay, or both reasons.

The many variables of the melt extrusion method have given researchers concern, such as whether a twin or a single screw extruder was used, the screw design itself as well as the feeding of the two components. McConnell et al. (2006) studied the effect of various organoclays (MAE, MTE, etc.) on the mechanical properties of the PET matrix. Processing methods included compounding via single screw extrusion and injection moulding to produce test specimens. They found that the organoclays enhanced the

mechanical performance and suggested that the organoclays were acting as nucleating agents to form the crystalline phases in the PET during fibre spinning. Through capillary rheometer their results showed that the nanofiller negatively affected the intrinsic viscosity (I.V.) of the PET due to thermal degradation. The researchers also used single screw extrusion which may decrease the mixing efficiency compared to twin screw extrusion and may lead to increased residence time, which could cause thermal degradation. Anoop et al. (2006) used single walled carbon nanotubes (SWNTs) to study the influence of PET crystallization. They found that SWNTs at low concentration (0.03%) enhance the crystallization temperature during melt cooling, increasing it from 200 to 210°C. It was shown that the oriented SWNTs in PET melt enhanced the oriented crystallization of PET.

Researchers studied several ways to enhance the properties of polymer nanocomposites and in particular PET nanocomposites by investigating the effects of different factors on the behaviour of polymer nanocomposites. Many researchers have studied the effect of nanoclay surfactant type or quantity on PET nanocomposite properties. Other researchers have used a compatibilizer with the PET nanocomposites to increase affinity.

Gurmendi et al. (2007) studied the effects of three types of organoclays in producing PET nanocomposites. Cloisite 15A and 20A were used because they have the same surfactant but in different amounts, and this allowed the researchers to study the effect of the amount of surfactant. Also Cloisite 30B was used because it has the same level of surfactant content as 20A but has a more polar chemical nature. This allowed Gurmendi and his team to find out the effects of the polarity of the surfactant on PET nanocomposites. The researchers concluded that a higher surfactant content (Cloisite

15A) does not have a positive effect on the ability of the polymer to intercalate into the clay galleries, and they attributed this to the larger initial interlayer distance of Cloisite 15A, which leads to a decrease in the energy necessary to overcome the attractive interlayer force when the polymer is intercalated into the clay galleries. Also they reported that the surfactant content affected the interaction between the surfactant and the polymer matrix and did not influence the intercalation level. In addition it was found, after comparing Cloisite 30B and 20A, that the polarity was favoured for intercalation. On the other hand it was observed that the modulus increased and was found to be independent of the level and nature of the organic modification of the clay, which means that the parameters that lead to a large increase in the modulus of elasticity differ from those that lead to a large degree of intercalation. The increasing modulus of elasticity was correlated with wide clay dispersion.

Ke et al. (1999) studied the effect of the clay on the crystal morphology and crystallisation processes. Approximately 80% of clay ores are formed as MMT. The clay was treated before mixing it with PET and then refined into small particles with a cation ion exchange range from 0.7 to 1.1 meq/g. The nanocomposites were prepared via an in-situ method. The results show that the clay content affects the crystallisation because the clay acts as a nucleating agent. Also Ke et al. (2002) discussed the relationship between the distribution of intercalated or exfoliated clay and the crystallization of PET. They reported that the increased intercalation with the large number of clay platelets leads to a decrease in crystallization. In the same study it was observed that the dispersion of the clay platelets was controlled by the polymerization method as well as by the surface modification.

Many researchers have tried to improve the dispersion of the clay in the PET matrix by a variety of methods. One of these methods is to use compatibilizer additives to increase the adhesion of the polymer matrix to the clay. Imai et al. (2002) reported making PET/Expandable Fluorine Mica nanocomposites utilizing compatibilizers via a two step polymerization procedure and gained a good dispersion of the mica and enhancement of the mechanical properties of the nanocomposites. Sanchez-Solis et al. (2003) used a compatibilizer (Pentaerythritol and Maleic Anhydride) with PET nanocomposites (Cloisite 15A). The results did not show an exfoliated morphology, while with high clay and compatibilizer content the crystallinity was increased due to the clay acting as a nucleating agent.

Barber et al. (2005) prepared PET ionomer (PETI)/modified MMT clay nanocomposites via melt extrusion. The authors investigated sulfonated PET which contains various incorporated ionic comonomer and modified clays. The interactions between the matrix PET and MMT clay were enhanced by the random merging of ions introduced along the PET backbone. It was found that mixing nanofiller into different ionomers decreased the crystallisation rate and increased mechanical properties.

Tarverdi and Sontikaew (2008) aimed to study the effect of using different concentrations of modifier on the rheology, morphology and product tensile properties, and also studied the effects of different process melt temperatures on these properties. Cloisite 10A and Nanofil-2 (N2) organoclays were used because both are coated with same surfactant, but the percentage of surfactant in 10A (125 meq/100g) is greater than in N2 (75 meq/100g). As discussed before, Gurmendi et al. (2007) worked on a similar study using 15A and 20A to study the effect of using different concentrations, but the 15A and 20A have two long alkyl (dehydrogenated tallow) tails while 10A and N2 have

one alkyl tail (hydrogenated tallow) in the surfactant. Thus it might be expected that the polymer molecules will more easily enter the clay gallery. Also the higher modifier content of 10A means it is probably more easily degraded than N2, which may cause a reduction in the dispersion of clay in the PET matrix. It was observed from TGA results that it is difficult to produce high quality PET nanocomposites because the onset decomposition temperature of both clays is 200°C while the PET melt processing temperature is over 260°C. The TGA results also showed that N2 has better thermal stability than 10A. It was also found that organoclays with more surfactant content gave nanocomposites with higher tensile moduli and better clay dispersion.

Calcagno et al. (2007) studied the effects of the organic modifier of the clays Cloisite 10A, 15A and 30B on the crystallization and morphology properties of PET nanocomposites. The crystallization temperature (T_c) of the pure PET was lower than that of the PET nanocomposites which possibly means that the nanoclay has a nucleation effect on the PET. It was also found that the PET 30B and PET 10A nanocomposites showed exfoliated and intercalated morphologies due to many contributing factors, including the polarity of the surfactant and its chemical structure. In addition they reported that the nanocomposites showed smaller mean spherulite size and more nuclei than in pure PET.

Generally, the thermal stability of polymer nanocomposites can be measured by weight loss (volatile products) upon heating. Blumstein (1965) studied the improvement in the thermal stability of polymer nanocomposites by blending clay with polymethylmethacrylate (PMMA), and reported that adding PMMA to a nanocomposite containing 10% clay causes degradation at a temperature 40-50°C higher than with unfilled PMMA.

On the other hand, unwanted side reactions between the decomposition products and the polymer matrix may also result from surfactant decomposition. These reactions degrade the polymer itself in the nanocomposites. Some active sites can degrade the polymer during the melting process due to clay catalysis effects.

2.7 Nanoclay selection

There are many types of organoclay Montmorillonites (MMT). Commonly used clays produced by Southern Clay Products Inc. include Cloisite 10A, 15A, 20A, 25A and 30B; each one of these clays has a different structure and surfactant. All Cloisite clay types and other clays have been reviewed to find the clay most compatible with a PET matrix. Figure 2.4 shows the chemical structure of the major Cloisite clays. Cloisite 10A has a benzene ring which indicates the possibility of its compatibility with the PET benzene ring. Table 2.1 shows the basal spacing between the layers. It is obvious that Cloisite 15A has the biggest basal space which may mean that the PET chains can penetrate more easily in the interlayer spacing. Cloisite 30B has two hydroxyl groups in the modifier which may lead to compatibility with the hydroxyl group of PET and they may also interact with the carboxyl group of PET.

Cloisite 10A	$\begin{array}{c} \text{CH}_3 \\ \\ \text{CH}_3 - \text{N}^+ - \text{CH}_2 - \text{C}_6\text{H}_5 \\ \\ \text{HT} \end{array}$	Cloisite 15A	$\begin{array}{c} \text{CH}_3 \\ \\ \text{CH}_3 - \text{N}^+ - \text{HT} \\ \\ \text{HT} \end{array}$
Cloisite 20A	$\begin{array}{c} \text{CH}_3 \\ \\ \text{CH}_3 - \text{N}^+ - \text{HT} \\ \\ \text{HT} \end{array}$	Cloisite 25A	$\begin{array}{c} \text{CH}_3 \\ \\ \text{CH}_3 - \text{N}^+ - \text{CH}_2\text{CH}(\text{CH}_2\text{CH}_2\text{CH}_2\text{CH}_3) \\ \qquad \qquad \\ \text{HT} \qquad \qquad \text{CH}_2 \\ \qquad \qquad \qquad \text{CH}_3 \end{array}$
Cloisite 30B	$\begin{array}{c} \text{CH}_2\text{CH}_2\text{OH} \\ \\ \text{CH}_3 - \text{N}^+ - \text{T} \\ \\ \text{CH}_2\text{CH}_2\text{OH} \end{array}$	Figure 2.4 The chemical structure of all Cloisite additives. [Ref. supplier data sheet]	

Table 2.1 shows the concentration of the modifiers. It is clear that Cloisite 20A has a low surfactant content (95 meq/100g clay) which indicates that the lower the content the greater the PET/clay interface and the lower the degradation.

LeBaron et al. (1999) reported that the polarities of the polymer matrix surface and organoclay must be matched. Since PET is a polar polymer, Cloisite 15A and 10A have been removed from our selection list due to their non-polarities (Table 2.1).

Cloisite 20A has an advantage because it has a low surfactant content but contains two alkyl groups (dimethyl, dehydrogenated tallow) similar to those of Cloisite 15A, which indicates the possibility of reducing the interaction between the clay and the polymer chains. This reason was enough to drop Cloisite 20A from our list of potential

candidates. Cloisite 25A and 30B are both polar, which means the surface polarities of the PET matrix match the organoclay.

Khan et al. (1987) reported that these polar interactions are important for the formation of well dispersed systems. As mentioned earlier, Cloisite 30B has two hydroxyl groups and it is expected that this may lead to compatibility with the hydroxyl group of PET, while Kracalik and Puffr et al. (2007) showed the thermal degradation of alkylammonium tethers as well as by chain scission due to water and the hydroxalkyl groups of Cloisite 30B during the melt compounding lead to form low Mw compounds which decreased the melt viscosity of the nanocomposites at higher shear rate.

Kracalik and Puffr et al. (2007) assumed that the degraded and shorter polymer chains could easily penetrate into the gallery of the silicate layers and this may lead to a reduction in the melt viscosity of nanocomposites at higher shear rate compared with recycled PET, due to the inert low molecular weight compounds formed by thermal degradation. The same process has been applied to a Cloisite 25A nanocomposite and this shows improved results. Based on the points made above, Cloisite 25A has been chosen (see Chapter 3 for more details about Cloisite 25A) for the studies reported in this thesis.

Organoclay	Modifier concentration (meq/100 g/clay)	Basal spacing (Å)	Polarity
Cloisite 10A	125	19.2	Non polar
Cloisite 15A	125	31.5	Non polar
Cloisite 20A	95	24.2	Polar
Cloisite 25A	95	18.6	Polar
Cloisite 30B	90	18.5	Polar

Table 2.1 Surfactant content and basal spacing between layers for all Cloisite clays studied [Kracalik and Puffr et al. (2007)].

In order to study the effect of synthetic clays and compare to this natural clay, Somasif clays (MAE and MTE) have been used. These organically modified sodium fluoromica clays were supplied by UniCoop Japan (now CBC Co. Ltd.), Japan (see Chapter 3 for more details about Somasif MAE and Somasif MTE).

Three types of nanoclays have been used in this project. Two are organo-modified, synthetically based on sodium fluoromica (Somasif MAE and Somasif MTE), and the third clay is organically modified (Cloisite 25A). The nanoclays' details have been presented in section 3.2.2.

2.8 Nanocomposite processing methods

After the selection of the appropriate nanoclay, the next challenge is to determine the proper synthetic methods to prepare the polymer nanocomposites. Matayabas and Turner (2001), Li et al. (2001) and Chang (2004), reported that the preparation methods of polymer nanocomposites are divided into many categories. For compounding the thermoplastic polymers with solid nanoclays, there are many common processing methods used:

- I- **Melt intercalation**
- II- **Solution intercalation**
- III- Roll milling
- IV- **In situ polymerization**
- V- Emulsion polymerization
- VI- High-shear mixing

The methods written in bold font will be discussed in brief because it the main three methods which have been used in a wide range of polymer nanocomposite processing methods.

2.8.1 Solution method

Krikorian and Pochan (2003), Ou et al. (2004), Liu and Chen (2008), and others have reported that the solution method has been widely used with water-soluble polymers to produce intercalated nanocomposites. Here the clay layers are swellable in the solvent and the polymer is soluble. The main advantage of this method is that the compounding process is carried out well below degradation temperatures. The major impediment is the high quantity of solvent used in this method.

2.8.2 In-situ polymerisation method

Polymerisation can occur between the intercalated sheets because the layered nanoclay is swollen within the liquid monomer. When the monomer is inserted into the gallery space, polymerisation can occur. This method gained considerable attention after the Toyota research group prepared Nylon-6/MMT nanocomposites via an in-situ method and observed significant enhancements in mechanical and thermal properties [Okada et al. (1995)].

2.8.3 Melt intercalation

The melt intercalation method is the most widely used method to prepare polymer/nanofiller nanocomposites [Bhattacharya et al. (2008)]. Direct compounding is the most common intercalation method. In this method, the polymer and nanofiller are mixed in an extruder (usually via a twin screw due to its superior mixing quality) by

introducing shear to the polymer matrix and nanoclay above the melting temperature of the polymer. This method does not require a solvent. The residence time and temperature of the compounding process in the melt intercalation method are lower than with the in-situ polymerisation method. The method is also well-suited to commercial scale production. This is the method which has been chosen for the present project.

Chapter Three

3. Experimental work

3.1 Introduction

The methodology of this project is covered in this chapter. Section 3.2 gives brief information about the raw materials which were used. The drying of the materials - particular the PET - is a critical step required prior to compounding and carrying out many analytical tests, and so this drying procedure is covered in a separate section 3.3. As mentioned before, the melt intercalation method was used to prepare the PET nanocomposites (see chapter 2) so the compounding procedure and further sample preparation are described in section 3.4. Section 3.5 includes a description of all the equipment used to analyse the raw materials or PET nanocomposites (pellets and films).

Furthermore, a preliminary study was conducted on some PET nanocomposite sheets obtained from Queen's University. These sheets were prepared under the EPSRC funded QBOX project (EPSRC grant EP/C006909/1) by blending PET pellets (Tergal F9) with nanoclays (Somasif MAE and MTE) [Soon et al. (2009)]. This study was initiated to study the effect of different cooling rates when analyzing the thermal properties of the samples. The results and discussion of is preliminary study are covered in appendix 5 (see x5.4).

3.2 Raw materials

3.2.1 Polyethylene terephthalate (PET) pellets

Polyethylene terephthalate (PET) grade T74F9IV080 was supplied by Tergal Fibre, France. It has an intrinsic viscosity (I.V.) of 0.8dl/g in a 50/50 mixture of phenol/o-dichlorobenzene with a PET concentration of 5g^l⁻¹. An AccuPycTM 1330 Pycnometer

(see section 3.5.1) was used to measure the density of the PET pellets, giving a value of 1.4g/cm^3 . [appendix x3.1 shows the data sheet for PET Tergal F9 and appendix x3.2 shows the density results in detail for all raw materials].

3.2.2 Nanoclay additives

As mentioned in section 2.7, Somasif MAE, Somasif MTE and Cloisite 25A were chosen for blending with PET to prepare the PET nanocomposites and can be described as follows:

I. Somasif MAE and Somasif MTE

Somasif nanoclay is a synthetic clay based on sodium fluoromica, modified by dimethyl di-(hydrogenated tallow) ammonium chloride [Utracki, (2007)]. Generally, Somasif is prepared by heating Na_2SiF_6 and talc for several hours in an oven.

Somasif is a swellable synthetic fluoromica having dimethyl di(hydrogenated tallow) ammonium chloride ions between layers (MAE) or methyl trioctyl ammonium chloride ions (MTE). It is supplied by CO-OP Chemical Co., Japan (now CBC Co. Ltd). (See Table 3.1 for more details)

II. Cloisite 25A

Cloisite 25A is a commercial organoclay produced by Southern Clay Products (SCP), Gonzales, Texas, USA. It is a natural Montmorillonite (MMT) and in order to enhance its affinity, dispersibility and miscibility, the clay is modified with a quaternary ammonium salt by the producer (see Table 3.1 for more details).

General comments on the nanoclays

- Pees et al. (2008) reported that swellable Montmorillonite and fluorine mica are preferable for producing polyamide nanocomposites, and fluorine mica is more preferable due to its excellent brightness and its positive effects on final mechanical properties.
- The two platelet-shaped silicates (MAE and MTE) are both based on fluoro-mica. The size of mica particle (6 μ m) is much bigger than Montmorillonites (200nm). The higher negative charge of mica (2.5 times higher than Montmorillonites) can lead to big expansions in the gallery of mica. This advantage can lead to the PET chain penetrating easily into the space of the gallery.
- Somasif clays have a slightly higher tendency to water absorption when compared to Cloisite clay nanocomposites.
- The longer tallow group of the surfactant in MAE is expected to be more reactive than the carbon chain (C8) or methyl group in MTE.
- One of the advantages of Somasif clay is its colour (white). The end products of PET nanocomposites are usually transparent and the colour of the clay affects the final product colour. Therefore, a better product appearance might be expected compared to when using Cloisite 25A which can cause a yellow/brown product. This optical clarity is a much sought after requirement for the use of PET packaging (film or bottle).

	Somasif MAE³	Somasif MTE³	Cloisite 25A³
Density (g/cm ³) ¹	1.55	1.72	1.76
Basal spacing, d ₀₀₁ (nm) ²	3	2.5	1.86
Aspect ratio	1230	1230	218
Surfactant	2M2TA	M3O	2MHTL8
Surfactant formula	Dimethyl di(hydrogenated tallow) ammonium chloride	Methyl trioctyl ammonium chloride	Dimethyl hydrogenated tallow 2-ethylhexyl quaternary ammonium
Cation exchange capacity (CEC) (meq/100g)	200	120	95

Table 3.1 Some properties of the chosen nanoclays

¹ An AccuPyc™ 1330 Pycnometer (see section 3.5.1) was used to measure the density of the nanoclay powder [Appendix x3.2 shows the density results in detail for all raw materials].

² Measured by powder XRD (see section 3.5.9); the results are shown in appendix x3.3.

³ Appendix 3.3 shows the data sheet for Somasif MAE, Somasif MTE and Cloisite 25A.

3.3 Drying process

As mentioned before, polyethylene terephthalate (PET) is highly hydroscopic and absorbs moisture quickly which can cause hydrolytic degradation during melt processing (for more details see section 8.1.2). To avoid this degradation, it is essential to dry the crystallized PET pellets. Drying the PET pellets in the temperature range 140–180°C is effective but above 180°C this may cause a yellowish colour degradation of the pellets. The preferred drying parameters are 160°C for 6 hrs in a dehumidifier

dryer (dew point -40°C) or vacuum dryer [Jones (2002)]. However, prior to any further melt processing or rheological analysis for the amorphous PET nanocomposite pellets produced from the compounding process, a further re-crystallisation process should be applied. This re-crystallisation process is a very important step to simulate the crystallized PET pellets. It was observed and reported (see sections 4.3.1 and 4.3.2) that the rheological behaviour of amorphous PET pellets is significantly different from that of crystallised or re-crystallised PET pellets.

The re-crystallisation process is also applied to eliminate the sticking and lumping of pellets during melt processing which usually occurs with amorphous PET pellets and blocks the process flow (bridging in hopper etc.).

In addition, prior to the compounding process, the organoclays were vacuumed dried at 80°C for 20 hours. Meanwhile, the PET was dried by dehumidifier dryer at 140°C for 20 hours. Also the nanocomposite (NC) master batch (PET/nanoclay 20 wt.%) was dried at 80°C for 20 hours (above the glass transition [$T_g \approx 75^{\circ}\text{C}$] to avoid the pellets sticking) before re-compounding it with dried virgin PET pellets to produce 1, 3 and 5 wt.% NC samples.

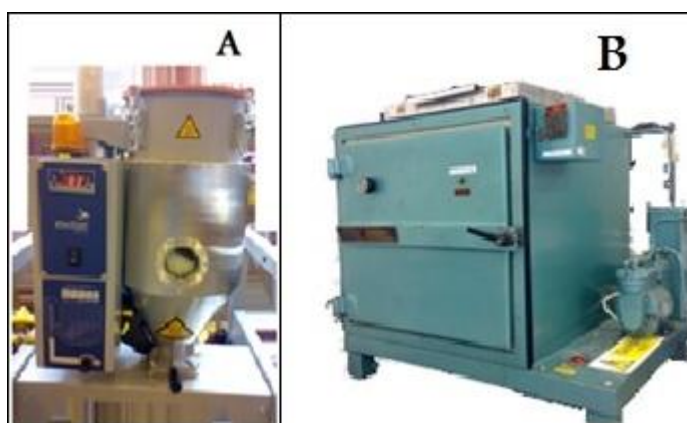


Figure 3.1 Pictures of the driers, A) Motan Drier (Luxor) and B) Vacuum dryer. [IRC, Bradford].

Figure 3.1-A shows the dehumidifier dryer (Luxor CA) which uses hot and very low dew point air to dry the materials. The material in the vacuum oven (figure 3.1-B) is surrounded by a vacuum (- 5bar), to remove sources of contamination and gases such as oxygen.

3.4 Extrusion and injection processes

In preparing polymer nanocomposites by melt processing a compounding technique such as extrusion or batch mixing can be applied. Kim et al. (2007) reported that the twin screw extrusion technique is preferable to batch mixing because the twin screw extrusion breaks up the agglomerates and exhibits better mixing of the nanocomposites than for the batch mixing technique. Furthermore, the method of feeding the polymer and the nanofiller to the twin screw extruder is one of the most important factors in good compounding. Anderson (2002) observed that feeding the materials together leads to better mixing. Cho and Paul (2001) studied the properties of nylon 6 nanocomposites produced by melt compounding using single and twin screw extruders. They found that the single screw extruder failed to show similar levels of exfoliation or dispersion compared with the twin screw extruder. Only a few articles have discussed the relationship between the processing parameters and the degree of mixing with the objective of optimisation. Increasing the melt processing temperatures leads to increase the mobility of the polymer molecules. Decreasing the viscosity resulting in less force applied to the nanofillers, which makes it difficult to break up the nanofiller agglomerates. Furthermore, the degree of mixing may be improved by increasing the residence time of the processing, but at the same time this may enhance the degradation of the nanofiller.

Dennis et al. (2001) studied the effect of screw configuration and screw type on the quality of mixing as measured by TEM. The authors found that improving the clay dispersion can be achieved by increasing the residence time. They observed that by using a co-rotating or counter-rotating extruder with excellent optimization of the screw configuration, good dispersion and exfoliation can be achieved. Fasulo et al. (2004) measured the quality of mixing with changing the temperature, screw speed and feed rate. The authors observed that increasing the processing temperature can cause degradation for the clay surfactant which can lead to agglomeration of the clay into the polymer matrix. They found that introducing the material at high feed rates can lead to the formation of a great mass of clay which can increase the pressure in the extruder thereby causing agglomerated clay.

Kim and Lee et al. (2008) studied the degree of mixing in Alumina/PET nanocomposites through changing melt processing conditions such as temperature, screw speed and feed rate. The authors found that the screw speed had the strongest effect on the degree of mixing with higher screw speeds leading to better mixing. The melt temperatures and feed rate also had significant effects with lower temperatures or lower feed rates giving better degrees of mixing.

3.4.1 Compounding of polyethylene terephthalate (PET) nanocomposite

Twin screw extrusion is widely used for compounding and mixing and can allow relatively simple changes of screw configuration in order to satisfy process requirements. For example, the two screws can be co-rotating or counter-rotating, intermeshing or non-intermeshing. Also the design of the screws themselves can be varied depending on the end product required.

In order to obtain high levels of clay dispersion in the PET matrix, two screw feeders (secondary and main feeder) were used to load the raw material simultaneously at constant feed rates directly to the compounding screws, as shown in Figure 3.2. The main screw feeder was attached onto the machine and used to feed the dried virgin PET pellets. The nanoclays and the master batches were introduced separately through the secondary screw feeder designed within the IRC at Bradford.

Other researchers have premixed PET with clay in a high speed mixer prior to extrusion. The premixing method may lead to agglomeration of the clay due to a relatively uncontrolled clay distribution. The twin screw co-rotating extruder (APV, MP19TC-25, Figure 3.2) with length to diameter ($L/D = 25$, $D = 19\text{mm}$) screws (Figure 3.3) was used in the compounding processes at the first stage. The screws have two mixing zones to allow greater mixing and thus interaction between the polymer and the clay. The first mixing zone has 12 paddles at 90° and the second mixing zone has 8 paddles at 90° , as shown in figure 3.4. The processing parameters are listed in Table 3.2.

Screw speed (rpm)	Output capacity (kg/hr)	Residence time (sec.)	Zone temperature ($^\circ\text{C}$)				
			1	2	3	4	5
			Feed \longrightarrow Die				
100	2.0	60	240	260	265	265	260

Table 3.2 Processing parameters for the compounding process in the APV twin screw extruder.

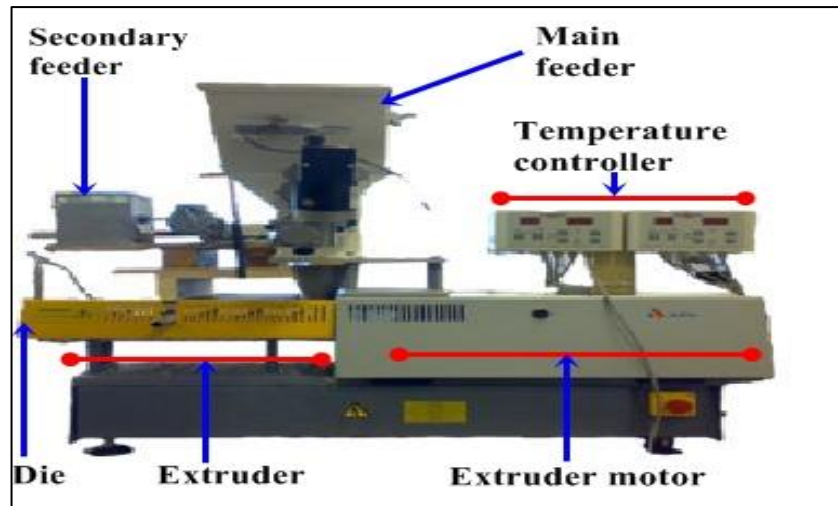


Figure 3.2 The twin screw extruder (APV).

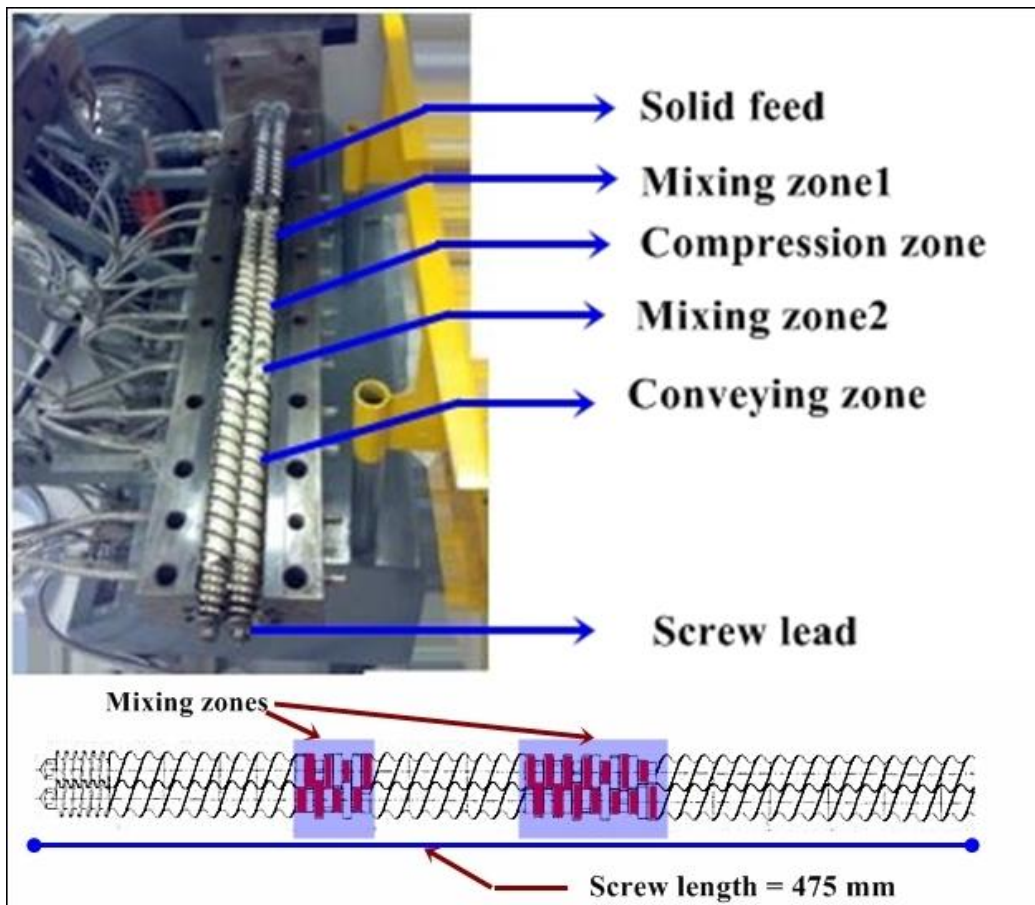


Figure 3.3 Screw design.

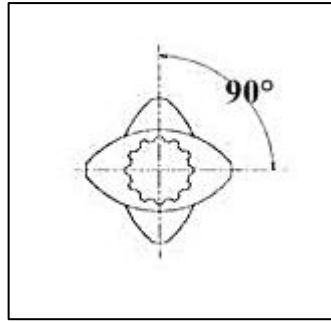


Figure 3.4 The rotating angle of the mixing zones.

To produce the nanocomposites of PET with different clay contents and types, a master batch was prepared (PET/nanoclay 20 wt.%) by mixing the nanoclay particles with dried virgin PET (vPET) pellets via twin screw extrusion. The dried master batch (dried at 80°C for 20 hrs in a vacuum oven) was then diluted by compounding with dried vPET via the same twin screw extrusion and the same extrusion parameters. All the extruded PET nanocomposites were quenched using a cold water bath prior to pelletizing using a Prism pelletizer (figure 3.5 A and B).

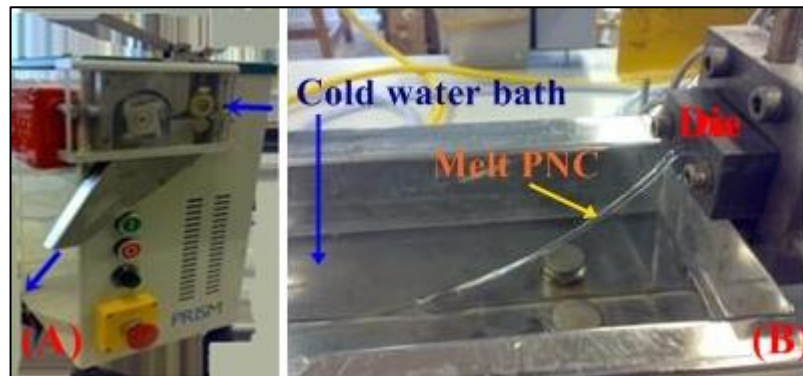


Figure 3.5 (A) the Prism pelletizer and (B) Extruded nanocomposites exit from the die and are then quenched by cold water bath.

The compounding processes produced 13 amorphous pellet samples (2 kg from each sample) in addition to one crystallised pellet sample. Table 3.2 describes the samples.

Sample No.	Sample name	Description of the sample
1	vPET	Virgin PET (as received), crystallised
2	Ext. vPET	Extruded virgin PET (amorphous)
3, 4, 5, 6	PET/MAE (1, 3, 5, 20 wt.%)	4 PET nanocomposites produced from compounding vPET with Somasif MAE clay at various concentrations
7, 8, 9, 10	PET/MTE (1, 3, 5, 20 wt.%)	4 PET nanocomposites produced from compounding vPET with Somasif MTE clay at various concentrations
11, 12, 13, 14	PET/Cloisite 25A (1, 3, 5, 20 wt.%)	4 PET nanocomposites produced from compounding vPET with Cloisite 25A clay at various concentrations

Table 3.3 PET (un-filled) and PET nanocomposite sample descriptions

3.4.2 PET cast film

The process of casting film is important for many applications such as packaging and lamination. To produce films, the PET pellets were plasticated using a Betol 2525 (D=25mm) single screw extruder (see figure 3.6) prior to the melt being extruded through a vertical film die (width = 300mm), as shown in figure 3.7-A. The extruded polymer was then quenched between counter-rotating chill rolls (see figure 3.7-B). One of the advantages of feeding the extruded polymer between two rolls rather than over just one is that the two rolls will give a uniform cooling for the film from both sides, preventing inhomogeneous crystallisation and/or warpage. The rollers are chilled to below the T_g of the polymer (about 16°C). A schematic of the extrusion machine and chill rolls is shown in figure 3.8.

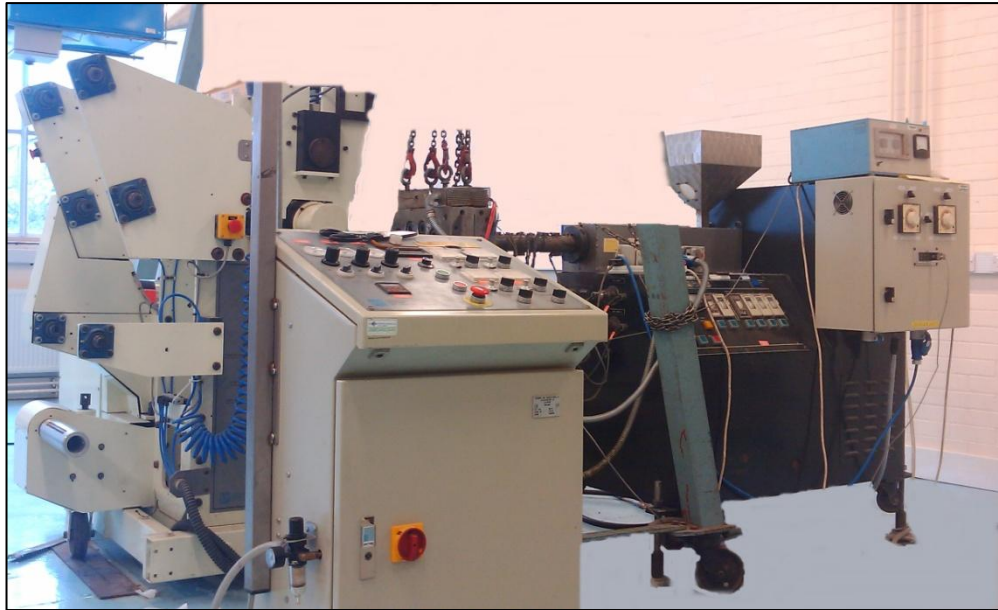


Figure 3.6 Cast film single screw extruder (Betol 2525)

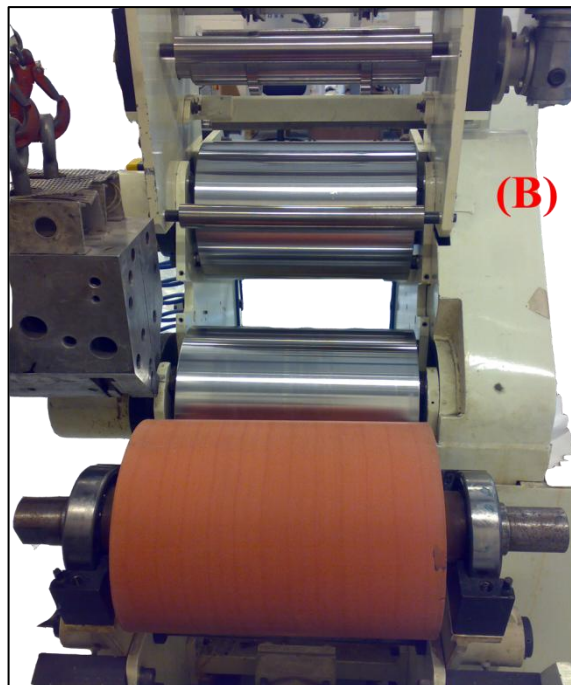
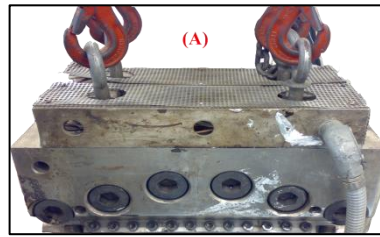


Figure 3.7 Vertical die (A) and chilled rolls (B).

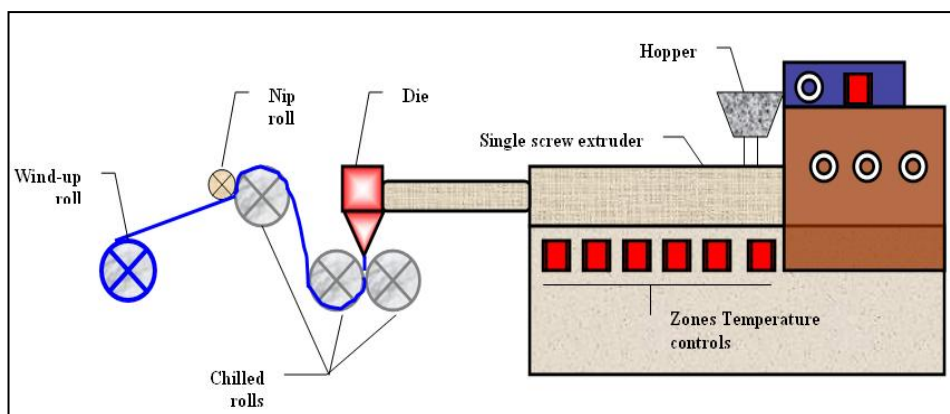


Figure 3.8 Schematic representation of the PET cast film process, showing the single screw extruder and the chill rolls.

In this project, films of 11 PET nanocomposites (thickness = 0.11 mm \pm 0.01) were produced via the single screw extruder. The processing parameters are shown in Table 3.4. The vPET, ext. vPET and PET nanocomposite (1 wt.%) films were transparent but the PET nanocomposite films (3 and 5 wt.%) were translucent. The processing parameters are listed in Table 3.4.

Barrel Temp. (°C)				Die Temp. (°C)		Screw speed (rpm)	Haul off speed m/min	Chiller Temp. (°C)
Feed	→			Die				
Zone1	Zone2	Zone3	Zone4	Zone1	Zone2			
240	255	260	260	255	255	80	5.5	15-17

Table 3.4 PET nanocomposite film processing parameters

3.4.3 Micro-moulding process

The Battenfeld Microsystem 50, shown in figure 3.10 (A) was used in this project to produce micro-specimens at various injection speeds to evaluate the effect of different shear rates on the mechanical properties of PET nanocomposites. The machine consists of three units (plasticating, metering and injection) as shown in figure 3.10 (B). There are many advantages from using this machine over the ordinary injection moulding machines such as the low cycle time for the process to minimise the degradation which is very important to avoid when processing PET nanocomposites. One of the main advantages of using the micromoulding machine is the low sample volume requirements (30g) which allows many samples to be produced with varying set temperatures, piston speeds, mould temperature etc. A typical test specimen is shown in figure 3.9.

The melted polymer is fed to the metering chamber where the exact quantity of the material is accurately controlled using the back pressure control of the metering piston. After the set filling level has been reached, a turn-lock fastener will prevent the molten polymer from back flow. The melted polymer is transferred from metering to injection zone when the injection piston is retracted. The metering piston then transfers the accurately determined material volume via the injection channel to the nozzle from where it is injected into the mould using the injection piston. The screw has been designed with three zones with an L/D ratio of 15 ($D=14\text{mm}$, figure 3.10 (C)) to melt as little polymer as possible to reduce the dwell time in order to minimise sample degradation.

The processing parameters are listed in Table 3.5.

Temperature zone (°C)			Mould temperature (°C)	Injection speed (mm/s)
Nozzle 315	Screw 300	barrel 280	60	100
				400
				700

Table 3.5 Micro-moulding processing parameters

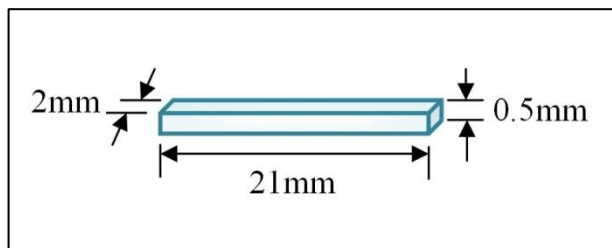


Figure 3.9 Micro-moulding specimen picture and diagram.

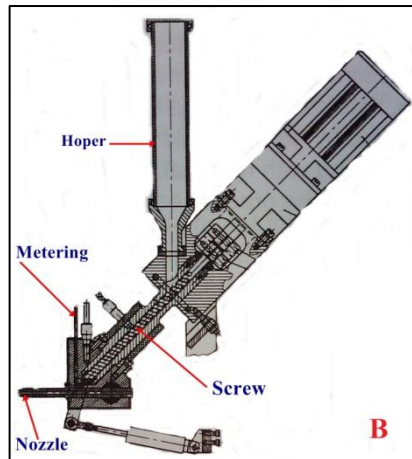


Figure 3.10 Microsystem 50 (A), Plastication unit (B) and the used screw (C).

Crystallised pellets of un-filled PET (vPET and Ext. vPET) and PET/clay (MAE, MTE and Cloisite 25A) at various clay concentration (1, 3, 5, 20 wt.%) were introduced to the Micro-moulding machine and processed at fixed temperature and different injection

speed to produce 42 samples. The tensile tests have been applied on these samples by using Bose machine (see section 3.5.7).

3.5 Characterisation of PET nanocomposites

Various characterisation tests were applied to the output of the extrusion processed samples (e.g. amorphous/crystallised PETNC and PETNC films). In this section all equipment used in this project will be covered. The results from these analyses are presented and discussed in chapter 8.

3.5.1 Density

An AccuPyc™ 1330 Pycnometer (see figure 3.11) was used to measure the density of the raw materials (vPET pellets, nanoclay powder).

I. Test procedure

Calibrating the equipment prior to conducting the test is an essential step. The equipment measures density according to Boyle's law (see equation 3.1) [Gooch (2007)]:

$$\mathbf{P_1 V_1 = P_2 V_2} \qquad \text{Equation 3.1}$$

where **P** is the pressure and **V** is the volume. The equipment has a cup, 75% of which is filled with the weighed material and then inserted into the test chamber. The equipment uses the gas (Helium) displacement technique under 1.5 bar pressure. The equipment shows five readings of the density prior to showing the average density.



Figure 3.11 AccuPyc™ 1330 Pycnometer

II. Density results

The average density results of the raw materials are listed in Table 3.6 and the detailed density results are listed in Table x3-1-x3.4 (appendix x3).

Samples	Density (g/cm³)
vPET (crystallised pellets)	1.4
Somasif MAE	1.55
Somasif MTE	1.73
Cloisite 25A	1.76

Table 3.6 Density of the raw materials

3.5.2 ThermoGravimetric Analysis (TGA) [Hatakeyama (1998), Gabbott (2007) and Menczel and Prime (2009)]

Thermogravimetric analysis (TGA) is an analytical technique used to determine changes in the weight of material as a function of temperature under a controlled atmosphere.

The following diagram (figure 3.12) shows a schematic of the TGA apparatus and figure 3.13 shows the TGA which was used.

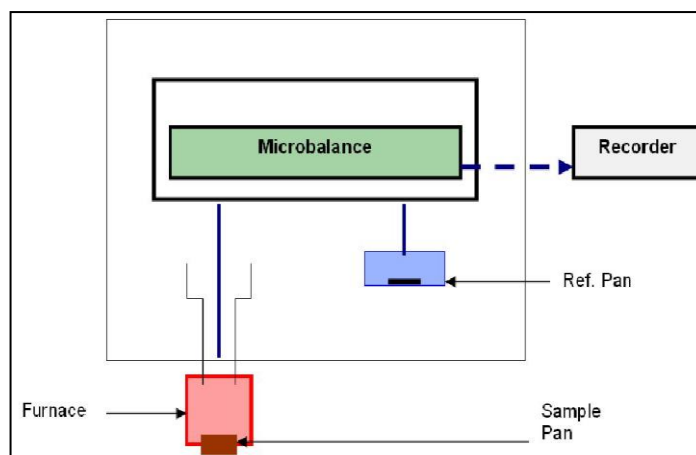


Figure 3.12 Simple diagram for TGA



Figure 3.13 TGA TA instruments Q5000.

A Q5000 TGA from TA instruments was used to analyse the clays. Temperatures up to 500°C under a nitrogen atmosphere with a heating rate of 10°C/min were applied to each sample to study the thermal stability of different types of nanoclays.

3.5.3 Differential Scanning Calorimetry (DSC). [Gooch (2007), Gabbott (2007) and Menczel and Prime (2009)]

Differential Scanning Calorimetry (DSC) was used to study the thermal properties of un-filled PET, extruder un-filled PET (amorphous pellets) and the amorphous PET nanocomposite pellets (PET/MTE, PET/MAE and PET/25A) at various loading

concentrations. The glass transition temperature, crystallisation temperature, melting temperature and crystallinity values were obtained from the DSC thermal scan. A TA instruments Q2000 DSC (see figure 3.14) was used in this study and the analysed results are presented in chapter 5.



Figure 3.14 DSC TA Instruments Q2000.

Differential Scanning Calorimetry (DSC) is a technique in which the difference in the heat flow into a substance and into a reference material is measured as a function of temperature while the substance and reference materials are subjected to a controlled temperature program. DSC is the simplest and most widely used thermal analysis technique for polymers as it enables the study of all major events (transitions) of interest in a polymeric system. The magnitudes of these transitions can be determined as well as the temperatures at which they occur. For instance, the glass transition of a PET material is a region where the material changes from a rigid glassy to softer amorphous form, and this is seen in DSC as a step change in the heat capacity baseline, usually at low temperature.

Heat Flux DSC measures a defined exchange of heat with the environment, which takes place via a thermal resistance. The measurement signal is the temperature difference, which describes the intensity of exchange and is proportional to the heat flow rate. The

principal type of heat flux DSC is the disk-type measuring system with solid sample support.

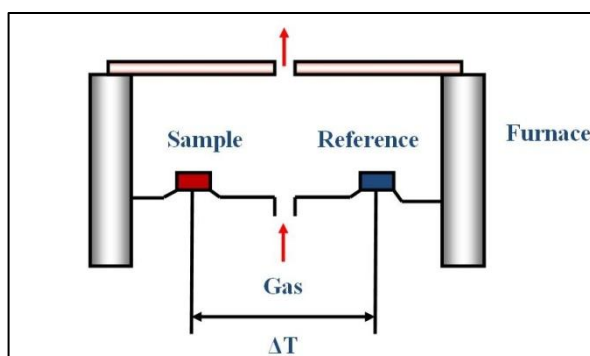


Figure 3.15 Schematic of Heat Flux DSC

This measuring system is based on a design in which the main heat flow from furnace to sample passes symmetrically through a disk of good thermal conductivity. The samples are positioned on this disk symmetrically to the centre. The temperature sensors are integrated into the disk or fixed on the surface (see figure 3.15).

When the furnace is heated, heat flows through the sample disk. Heat flows at proportional rates into the sample and reference container when the arrangement is ideally symmetrical. The difference between the electric potentials (or ΔT) will be recorded as zero. Should an endothermic thermal event (ΔH , which is the amount of heat released or observed when a positive chemical reaction occurs, such as melting) occur in the sample, the temperature of the sample, T_s , would lag behind the temperature of the reference, T_r , which follows the heating programme. However, if an exothermic process (ΔH negative) occurs in the sample, the response will be in the opposite direction of the endothermic events.

The output of a DSC is a plot of heat flux (rate) versus temperature at a specified temperature ramp rate. The heat flux can be converted to C_p by dividing by the constant rate of temperature change.

Once the main features of the heat flux DSC curve have been established, attention can be directed to the correlation of the endothermic or exothermic peaks with thermal events in the sample.

DSC procedure

1. Weigh the pan and the lid for the reference and for the sample
2. Weigh sample of PET sheet in aluminium sample pan
3. Place sample on platform of DSC cell and empty sample pan on rear platform (reference pan). In the DSC Q2000 case, all samples can be loaded at the same time
4. Heat sample in DSC cell from 35 to 300°C with heating rate 10°C/min
5. Cool sample from 300 to 35°C with cooling rate 10°C/min
6. Heat sample again to 300 with heating rate 10°C/min
7. Stop the run

3.5.4 Intrinsic viscosity (I.V.)

The intrinsic viscosity of PET is measured in decilitres per gram (dl/g). The I.V. is determined by dissolving a small sample of PET or PETNC in an appropriate solvent [40-50mg. of PET and 10ml of solvent (60/40 phenol/1,1,2,2-tetrachloroethane)] then measuring the time required for 100ml of the solution to flow through a capillary viscometer (see figure 3.16) which is placed in a constant temperature water bath.

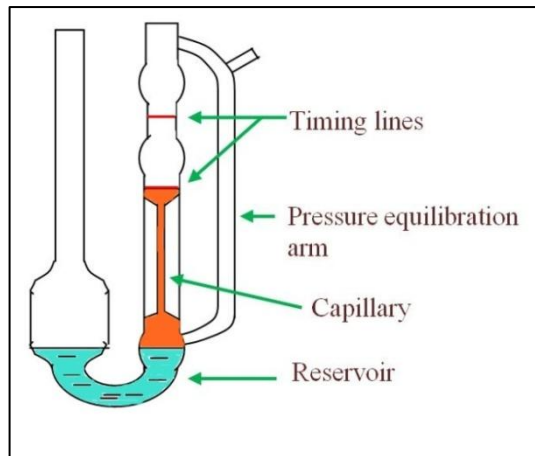


Figure 3.16 Schematic of capillary viscometer

Under the same conditions, the flow time is compared to that for a standard solvent.

Time and concentration are used to calculate the I.V. (ASTM D4603).

3.5.5 Rheometry

Cogswell (1998) defined rheometry as the art of making useful measurements of the deformation and flow properties of materials. A rheometer is a test instrument used to study these rheological properties of polymer melts. It is appropriate to define rheology before talking about the types of the rheometers.

Mezger (2006) explained that the term “rheology” came from the Greek word “rheos” which means “flowing”. Thus, rheology means “flow science”. Dealy and Wissbrun (1990) defined rheology as the science that deals with the way materials deform when forces are applied to them. There are different branches of rheology classified according to the type of material used. Polymer rheology deals with polymeric materials, for biological fluids there is biorheology, and also there is lubricant rheology and suspension rheology to serve different materials. Due to the high demands on polymeric materials, polymer rheology has received the most attention among all these branches.

Dealy and Wissbrun (1990) classified rheometers into two main types as follows:

1. Capillary rheometers
2. Rotational rheometers, which can be divided into:
 - a. Concentric cylinder rotary and rotating cylinder viscometers
 - b. Cone-and-plate (CP) rheometers
 - c. Parallel-plate (PP) rheometers

1. Capillary rheometer

Whelan (1994) defined the capillary rheometer as a test instrument used to study the rheological properties of polymer melts by forcing the polymer melts through a capillary die. It is one of the simplest and widely available types of melt rheometer.



Figure 3.17 Rosand RH10 (A), front view (B) and rods and reservoirs (C)

A capillary rheometer (Rosand RH10) was used in this project (see figure 3.17) and the test procedure is introduced in chapter 4 (see section 4.2.1).

The capillary rheometer provides data in the shear rate range used in (low speed) injection moulding and extrusion. A capillary rheometer consists of a heated reservoir (barrel) and a piston that drives molten material through a calibrated die, as figure 3.18 shows.

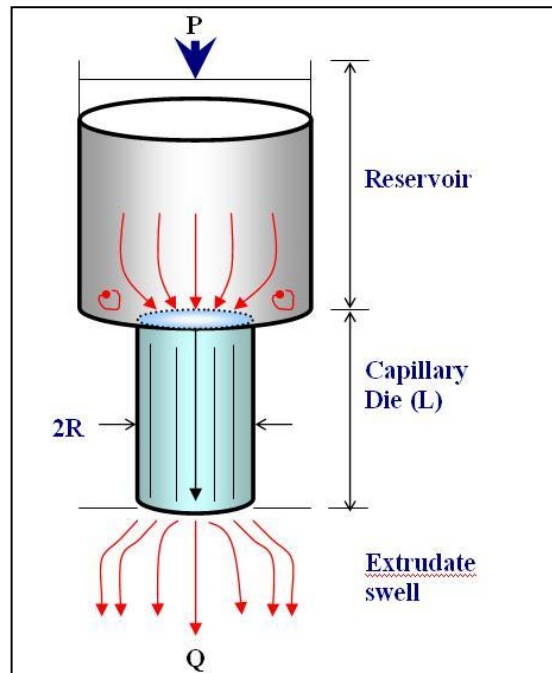


Figure 3.18 The elements of the capillary rheometer.

In addition to the most widely used single-bore configuration, there are also twin bore (dual barrel) instruments which can perform two simultaneous tests under different conditions. Cogswell (1998) recommended the use of one long die and an orifice ($L/R \approx 0$) as a shortcut method for determining reasonably accurate values for wall shear stress (τ_w).

The capillary rheometer is used to calculate viscosity, so it is necessary to know the wall shear stress and wall shear rate. Dealy and Wissbrun (1990) calculated the true viscosity by equation 3.2:

$$\eta = \frac{\tau_w}{\dot{\gamma}} \quad \text{Equation 3.2}$$

where η is the true viscosity, τ_w is the true shear stress at the wall and $\dot{\gamma}$ is the shear rate at the wall.

The shear stress was obtained using the Bagley correction [Tadmor and Gogos (2006)] (equation 3.3):

$$\tau_w = \frac{\Delta P}{2 \left(\frac{L}{R} + e \right)} \quad \text{Equation 3.3}$$

where ΔP is the pressure drop, L is the die length, R is the die radius, and e is the Bagley end correction [Whelan (1994)] which is defined as a negative of the value of L/R at various values of the flow (Q) using a variety of capillaries with different lengths. Bagley plotted ΔP against L/R and drew a straight line through the points as shown in Figure 3.19.

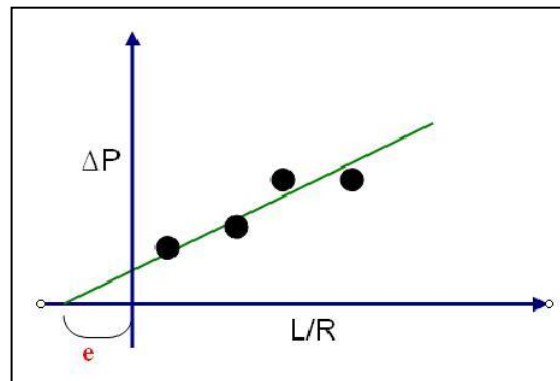


Figure 3.19 Bagley correction curve.

Bagley suggested this scheme as being able to infer viscosity from the simpler procedure of measuring the driving pressure for various flow rates.

The shear rate was obtained and corrected using the Rabinowitch correction (equation 3.4) [Whelan (1994)]:

$$\dot{\gamma}_{\omega} = \dot{\gamma}_{app} \left(\frac{3}{4} + \frac{1}{4} \frac{d \ln Q}{d \ln \tau_{\omega}} \right) \quad \text{Equation 3.4}$$

where Q is the volumetric output rate and $\dot{\gamma}_{app}$ is the apparent shear rate, which can be obtained from equation 3.5:

$$\dot{\gamma}_{app} = \frac{4Q}{\pi R^3} \quad \text{Equation 3.5}$$

II Oscillatory and rotational rheometer

Cogswell (1998) reported that the rotational rheometer is operated at comparatively low shear rates and can have concentric cylinder rotary and rotating cylinder geometries, a Cone-and-plate (CP) rheometer or a Parallel-plate (PP) rheometer. Mezger (2006) and other have showed that the rotational tests typically can have two modes, controlled shear rate (CSR) and controlled shear stress (CSS). When the material to be investigated has no yield point, the CSR method is usually selected. The test method with controlled shear stress is the classic method to determine the yield point of the sample. One widely used rheometer is the MCR rheometer from Anton Paar GmbH, Austria. An MCR 501 (parallel-plate) was used in this project (see figure 3.20) and the test procedure is presented in chapter 4 (see section 4.2.1).



Figure 3.20 The Physica MCR rheometer

There are two modes of operation of the instrument, oscillation and continuous rotation modes. For plastic materials, the oscillation at a narrow angle is most often used, and this can provide information about molecular weight, polymer relaxation, molecular weight distribution and melt viscosity. The output data from this instrument illustrates the relationship between oscillation frequency in radians per second and storage and loss moduli for the sample under test.

The material will gain energy from the rotation motion as long as this motion does not disrupt the structure. This energy is stored in the sample and is called the storage modulus (G'). A structured sample in a rotational shear will create motion between the molecules of the sample. This motion will cause energy to be lost as viscous heating and this is called the loss modulus (G''). The results are usually reported in the form of plots of storage and loss modulus or the complex viscosity (G^*), as a function of frequency. Figure 3.21 shows the typical curve for the storage and loss modulus.

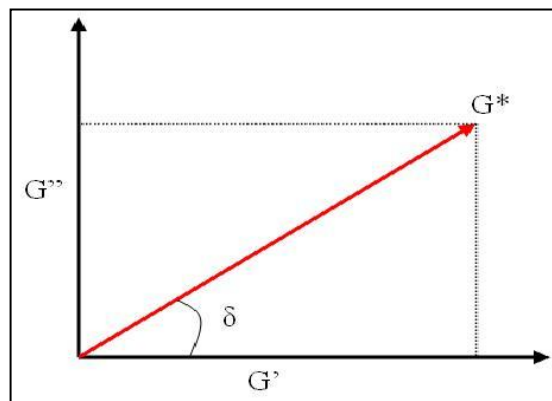


Figure 3.21 The modulus curve.

Loss angle (δ) is associated with the degree of viscoelasticity of the sample. A low value of δ indicates a higher degree of viscoelasticity. Dealy and Saucier (2000) calculated the storage, loss and complex modulus from equations 3.6, 3.9 and 3.10:

$$G' = \frac{2.M.h.\cos(\delta)}{\pi.R^4.\phi_0} \quad \text{Equation 3.6}$$

$$G'' = \frac{2.M.h.\sin(\delta)}{\pi.R^4.\phi_0} \quad \text{Equation 3.7}$$

$$G^* = \frac{2.M.h}{\pi.R^4.Q_0.\omega} \quad \text{Equation 3.8}$$

where M is the torque amplitude, Q_0 is the angular amplitude for oscillatory shear, R is the disk radius, h is the gap between the disks and ω is the angular frequency.

A. Concentric cylinder rotary and rotating cylinder viscometers

Cheremisinoff (1993) reported that cylinder viscometers are most often applied to solution viscosity measurements and are usually limited to shear rates $<100s^{-1}$. Figure 3.22 shows the basic elements of concentric cylinder rotary rheometry.

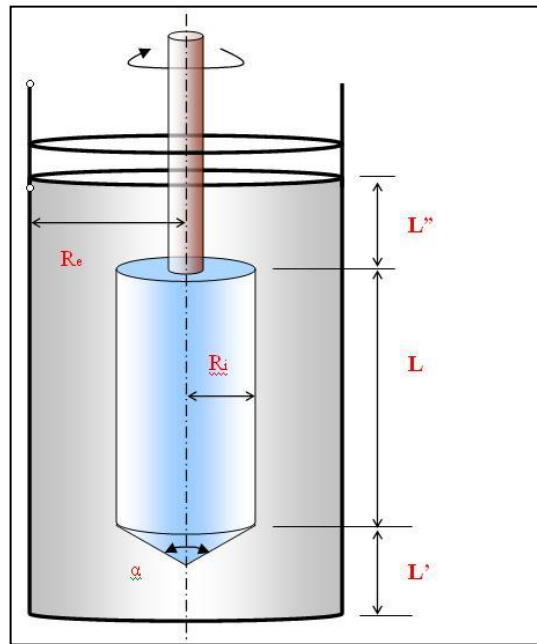


Figure 3.22 The basic elements of the concentric cylinder rotary rheometer

The unit operates by applying shear to a fluid located in the annulus between the concentric cylinders. The viscosity can be obtained via this instrument by equation 3.9:

$$\eta = \frac{(R_e^2 - R_i^2) M}{4.\pi.R_e^2.R_i^2.\omega} \quad \text{Equation 3.9}$$

where R_e is the radius of outer cylinder, R_i is the radius of inner cylinder and L is the length of the inner cylinder.

B. Cone-and-plate (CP) rheometer

Dealy and Wissbrun (1990) reported that the cone-and-plate rheometer is one of the most popular rheometers for studying the viscoelastic properties of molten polymers. The cone-and-plate measuring system consists of a circular disk and a small angle cone as figure 3.23 shows.

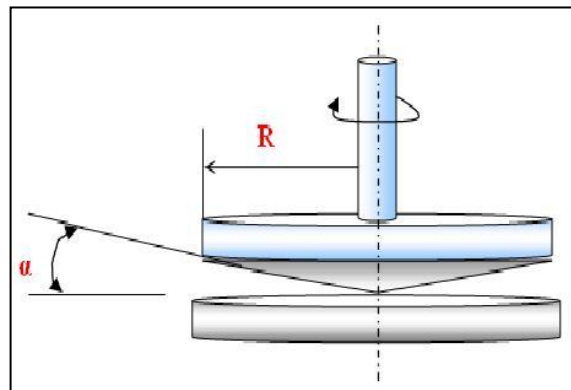


Figure 3.23 The cone-and-plate rheometer.

The sample is inserted between the disk and the cone and the small angle cone is rotated while the disk is held stationary. The cone-and-plate instrument is useful for finding the relationship between angular velocity and torque.

The viscosity can be calculated from equation 3.10:

$$\eta = \frac{3.M.\alpha}{2.\pi.R^3.\omega} \quad \text{Equation 3.10}$$

where α is the cone angle and R is the radius.

C. Parallel-plate (PP) rheometer

The Physica MCR 501 rheometer (see figure 3.24) was used as the parallel plate rheometer. It consists of two plates as figure 3.25 shows. Mezger (2006) explained that when performing oscillatory tests, a large gap dimension H may not be so critical for small angle oscillatory strain.

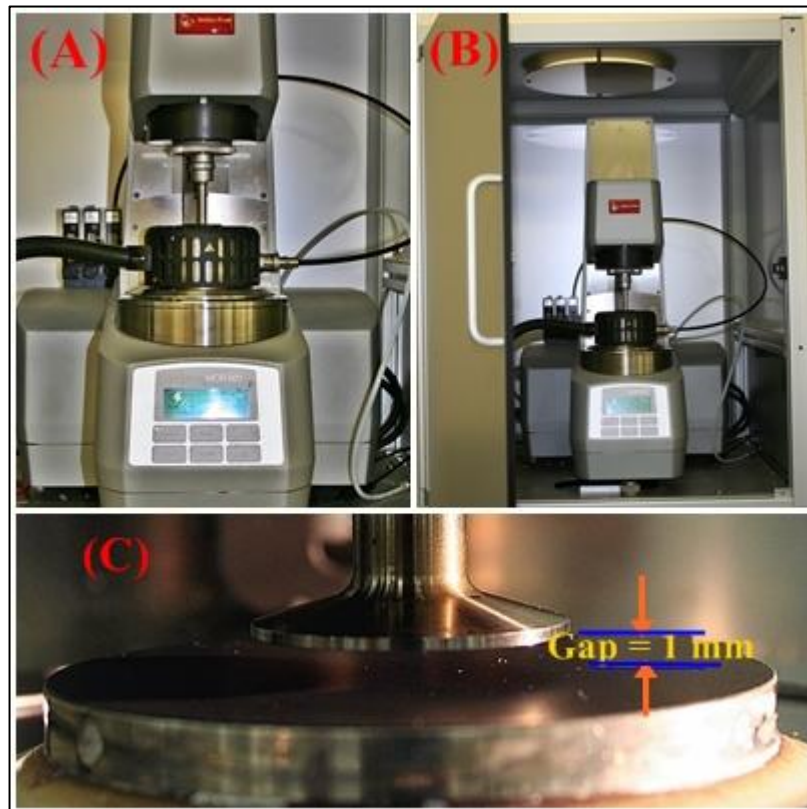


Figure 3.24 The Physica MCR 501 rheometer. Front view for the equipment (A), the equipment located inside the cabinet (B) and the parallel plates (C)

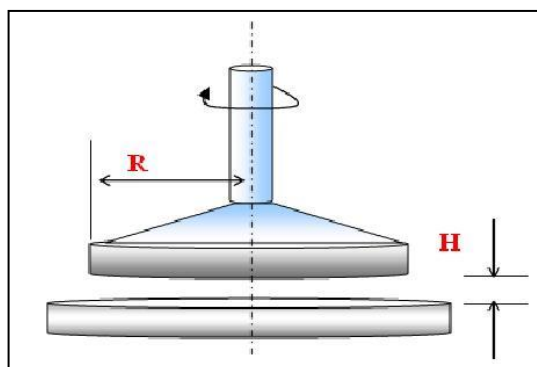


Figure 3.25 The parallel-plate rheometer.

The viscosity also can be calculated from equation 3.11:

$$\eta = \frac{2.M.H}{\pi.R^4.\omega} \quad \text{Equation 3.11}$$

There are many reasons for the popularity of parallel-plates and cone-plate geometrics:

- The small sample quantity needed
- Easy loading and cleaning of the sample

3.5.6 Permeability test

A Mocon Ox-Tran (2/21 MH) permeability tester was used to test the permeability of the produced films at 23°C and relative humidity (RH) 50%. The test is similar to that used for ASTM F-1927-films. OTR (Oxygen Transmission Rate) is a measurement of the quantity of oxygen gas that permeates through a film over a given period under specific conditions of RH and temperature [Brody and Marsh (1997)].

The film sample was clamped into the diffusion cell and acted as the separating membrane. Moist nitrogen was used in the inside chamber (see figure 3.26) to purge residual oxygen. Pure moist oxygen was introduced into the outside chamber. The oxygen diffused through the film to the inside chamber and was carried through the nitrogen to the detector. The difference in pressure created a driving force for the oxygen to pass through the film [Mocon (2010)]. This test has been conduct at SABIC India laboratories.

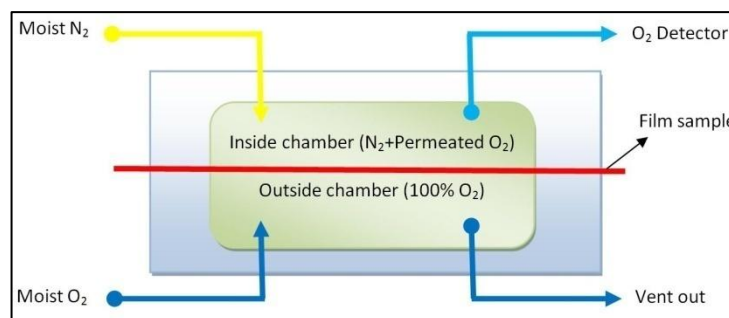


Figure 3.26 Cross section of OTR test cell.

3.5.7 Tensile tests

The tensile tests were carried out using Instron 5564 and Bose ElectroForce 3220 test machines at room temperature. The tensile test for the samples produced from the Micro-moulding machine were carried out using the Bose ElectroForce 3220 (see figure 3.27) with constant cross-head speed of 3mm/min while the samples obtained from the cast films were tested using an Instron 5564 (see figure 3.28) with constant cross-head speeds of 5mm/min and 50mm/min.

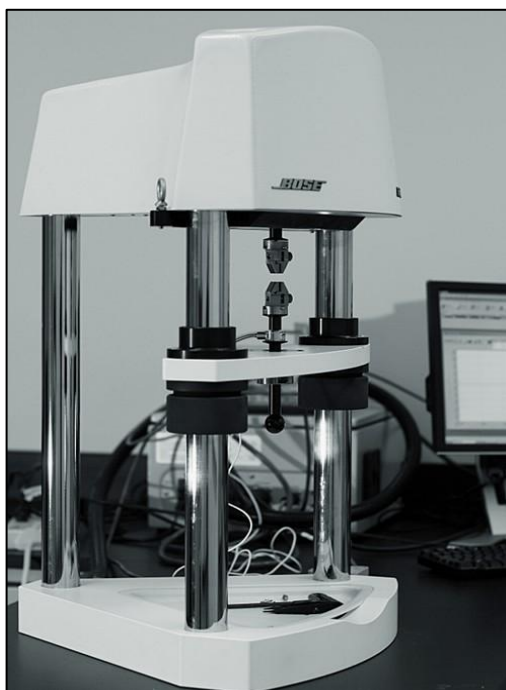


Figure 3.27 Bose ElectroForce 3220

In the Instron 5564, 11 amorphous film samples (un-filled PET and PET nanocomposites) were tested and each test was repeated at least six times at each speed. For the micromoulded samples, 42 amorphous tensile bar specimens were tested.

The amorphous film samples obtained from the cast film process (see section 3.4.2) were cut manually by a hydraulic press machine to produce dumb-bell shapes (ASTM D638 type IV 1998). Their dimensions are illustrated in figure 3.28.

The output data from the machine's software included the load (Newtons, **F**) versus the displacement (Δl mm) of the specimens. The cross sectional area (**A**) of the specimen was considered to be a constant value during the test and was calculated by measuring the width (**w**) and thickness (**t**) of each specimen.

From these data, stress-strain curves can be plotted where nominal stress (MPa) is calculated from the equation $\sigma = F/A$ and strain is calculated from the equation $\varepsilon = \Delta l/l$. The tensile modulus (Young's modulus, MPa) was extracted from all stress-strain curves and analysed in order to investigate the effect of nanoclays on the PET films during the cold drawing. The output results are presented and discussed in chapter 6.

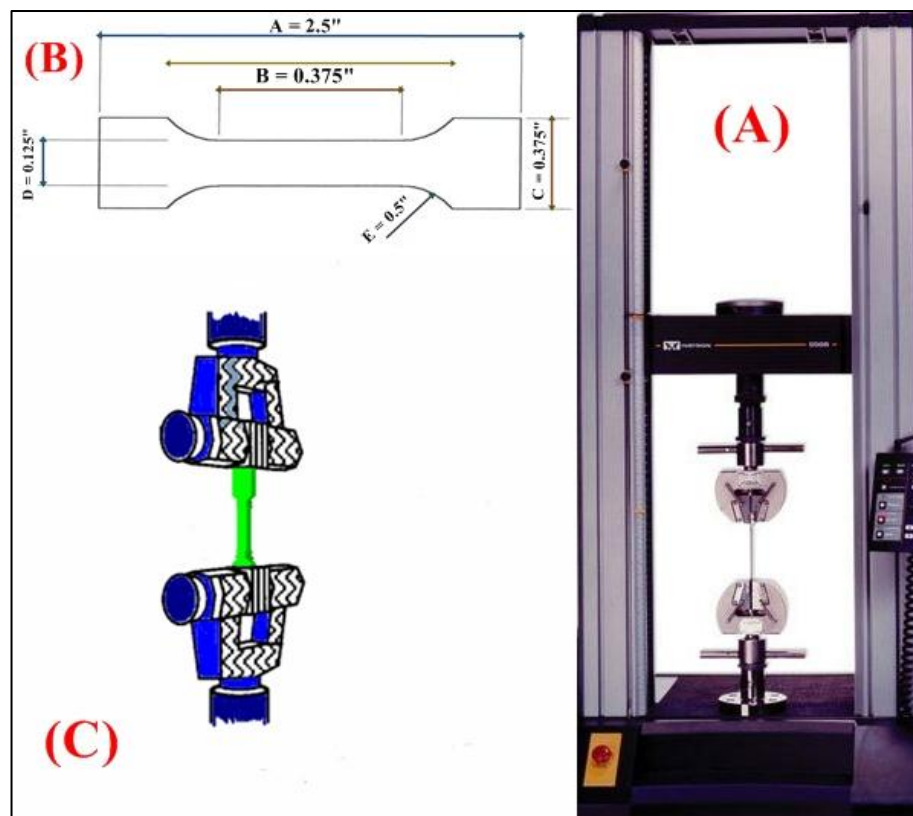


Figure 3.28 Instron 5564 (A), sample dimensions and schematic of the clamp (C)

II Simultaneous equal biaxial stretch test

Simultaneous equal biaxial stretching tests were carried out by using a biaxial testing machine housed at the University of Bradford (figure 3.29). Square specimens (61 x 61 mm) were cut from the cast film samples. Each specimen was clamped into the machine by six grips from each side then heated at 90°C for 60 seconds. An air blower was used to blow hot air below and above the specimen to give the required heat temperature. After 60 second, the heating is stopped and the specimen stretched to a stretch ratio of 2:1.

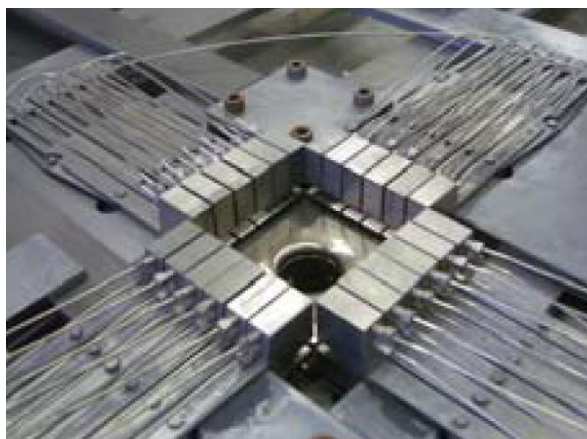


Figure 3.29 Biaxial grips of stretching machine

DSC was used to investigate the effect of biaxial stretch on the thermal properties of unfilled PET and PETNC films.

3.5.8 Transmission Electron Microscopy (TEM)

One of the methods used to characterise the PET nanocomposite films was Transmission Electron Microscopy (TEM). While the wavelength of visible light is limited, electrons are used in this microscopy technique instead of light to get a resolution superior to that for visible light microscopy can present. The TEM

microscope's (see figure 3.30) emission source (electron gun) emits electrons which pass through a vacuum column and are focused into a very thin beam by electromagnetic lenses. This beam travels through the specimen (a PET nanocomposite film in our case). Some of the electrons are scattered then disappear from the beam, while some are not scattered, depending on the density of the material. A fluorescent screen is located at the bottom of the microscope and the non-scattered electrons hit this to produce an image with varying darkness, based on the disparity density of the sample matrix.

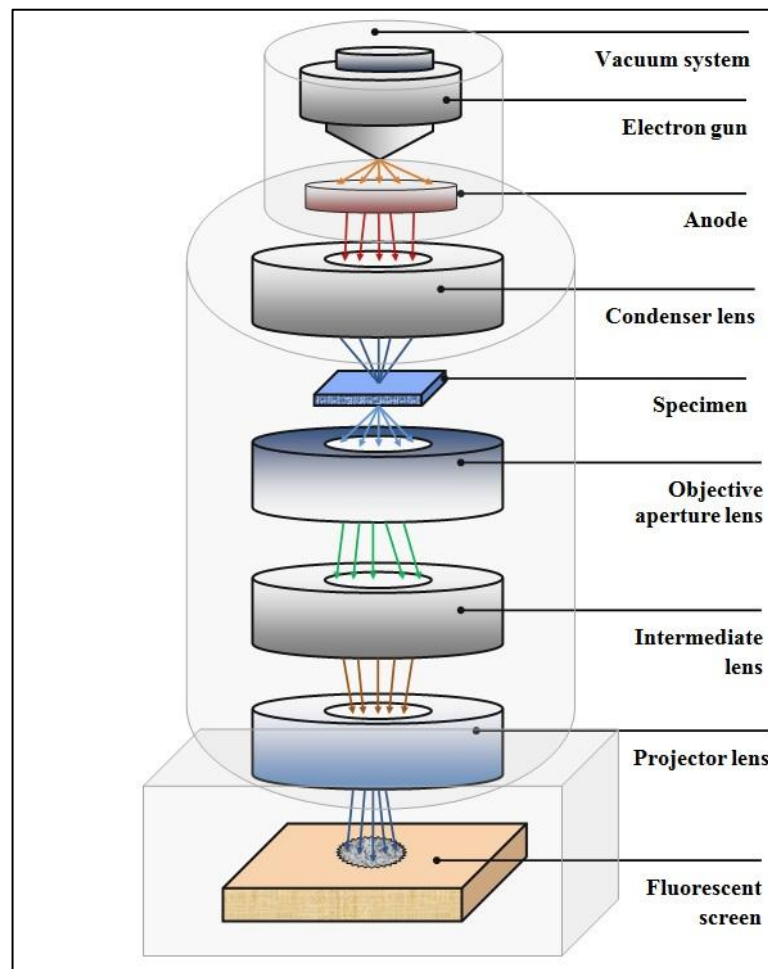


Figure 3.30 Schematic structure of Transmission Electron Microscopy (TEM)

The TEM instrument used in this project is the Tecnai G2 model as shown in figure 3.31.



Figure 3.31 Transmission Electron Microscopy (TEM) apparatus

The TEM specimen should be very thin so a microtoming method is necessary for sample preparation. A diamond blade is used to cut a small piece from the middle core of the sample as shown in figure 3.33. A Leica microtome (see figure 3.32) was used to prepare the specimens. The output results (images) of this test are presented and discussed in chapter 6.



Figure 3.32 Leica microtome

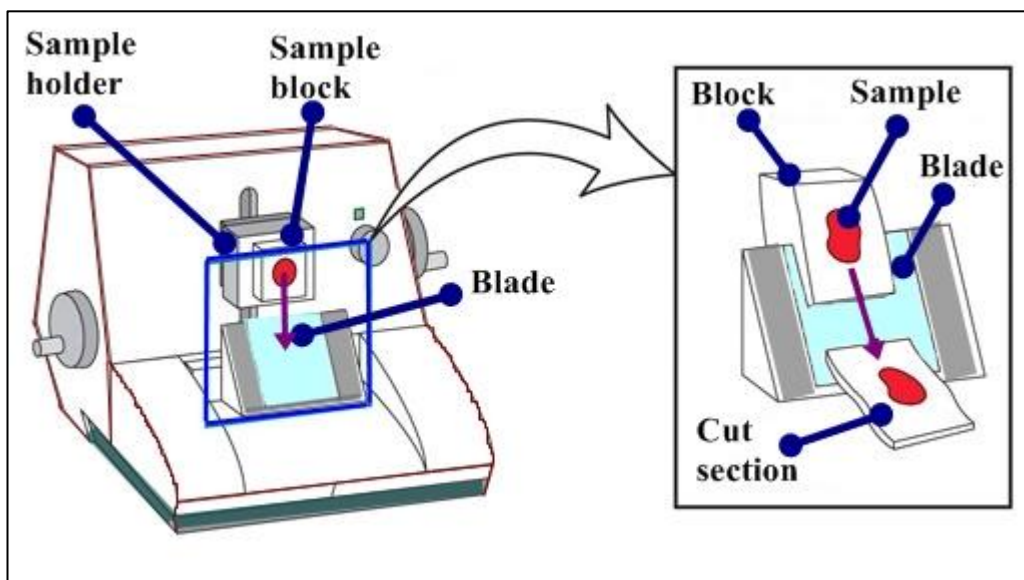


Figure 3.33 Schematic of the Leica microtome

3.5.9 X-ray diffraction

Since the early 20th century x-rays have been used by researchers to explore the structure of matter. Bruker D8 advance model (figure 3.34) was used in this project to measure the basal spacing for the nanoclay powder. The equipment parameters were as follows: wavelength of X-rays 0.154nm Cu source, voltage 40 kV, 175 and filament emission 40 mA. Samples were scanned from 2 to 10° (2 θ) using a 0.01° step width and

a 1s time count. The receiving slit was 1° and the scatter slit was 0.2° . The output curve from measuring the nanoclay powders using the Bruker D8 is shown in appendix x3 (figure x3.3.1).



Figure 3.34 Bruker D8 advance model

Chapter Four

4. Rheological behaviour of polyethylene terephthalate nanocomposites (PETNC)

The main objective of this chapter is to study the rheological properties of unfilled PET and PETNC over a wide range of shear rates, as well as their behaviour on adding different clays with various concentrations. The chapter is divided into three sections: the first covers a literature view on the rheological behaviour of polymer nanocomposites, the second describes the rheological measurements and intrinsic viscosity (I.V.) test procedures, and the third, covers the current rheological and I.V. results and analysis.

4.1 Literature review

There are two main reasons to study the rheological properties of polymer nanocomposites (PNCs). First, since nanofillers have different particle sizes, structures and shapes, different rheological properties may be expected, which may provide a means to assess the nanofiller dispersion state. Second, the rheological properties of PNCs are indicative of the behaviour of the polymer melts during downstream processing (e.g. extrusion injection moulding) [Pavlidou (2008)].

Han (1976) reported that a good and deep understanding of rheological phenomena and of the behaviour of polymers leads to excellent polymer processing. Bhattacharya et al. (2010) attributed the complications of polymer processing to the fact that polymers exhibit viscoelasticity during melt processing.

The main reason for studying the rheology of polymers is that rheological science provides a clear understanding of the effects of molecular weight of polymers under different flow conditions, and this allows optimised control of melt processing and the creation of a good final product.

Wang and Xie et al. (2006) studied the rheology of Polycarbonate (PC)/CaCO₃ nanocomposites by using a capillary rheometer. The author observed that the viscosity of nanocomposites reduces with an increase in CaCO₃ content and this viscosity reduction can be attributed to CaCO₃ enhancing the chain mobility of the PC in the melt. Giannelis et al. (1998) also reported that the nanoparticles do not chemically change the structure of the polymer matrix, but they reduce polymer viscosity in the melt by enhancing chain mobility.

Cho and Paul (2001) studied the rheological properties of nylon-6/organoclay nanocomposites at high shear rates. The authors showed that nylon 6 NC viscosity decreases with increasing nanoclay content over a similar range of shear rates. The authors assumed two mechanisms caused this reduction: first, the slip between the clay platelets and the polymer matrix, and second, degradation of the polymer which can lead to this viscosity reduction.

Yao et al. (2009) identified three types of interaction between PET chains and silica. Firstly a branched structure occurs between silica and PET forming a primary entanglement. Secondly a lightly crosslinking structure between silica and PET chains. Thirdly a secondary entanglement occurs in the free PET chains. The authors proposed a collapse in the primary and secondary entanglements at high shear rates which may lead to weak connections between the polymer chains themselves or between polymer

chains and the silica. These weak connections were counted as one of the main reasons for viscosity reduction.

Potschke et al. (2002) investigated the rheological behaviour of PC/Multiwall nanotube (MWNT) nanocomposites. The experiments were carried out in an oscillatory rheometer (ARES, parallel plate, 260°C). Masterbatches of PC/CNT (15%) were prepared and then diluted in neat PC to produce PC/CNT nanocomposites of 0.5 to 5 wt.% content. The authors observed that increasing the aspect ratio of the filler led to increases in the melt viscosity of polymer nanocomposites. The authors reported that using carbon nanotubes as an additive increased the melt viscosity of the polymer nanocomposites more than for carbon nanofibres or other nanofillers, due to the high aspect ratio of the nanotube. Their results show that the complex viscosity of neat PC does not exhibit any shear rate dependency, while on increasing the shear rate the master batch (PC/CNT (15 wt.%)) exhibits strong shear thinning behaviour. This study also shows that on adding more CNT (2, 5 wt.%) the composite tends to exhibit shear thinning behaviour and an increase in shear rate dependency. PC/CNT at 0.5 and 1wt.% loading did not show any significant change in complex viscosity with increasing shear rate. The authors also investigated storage (G') and loss (G'') modulus behaviour with changing shear rate for PC/CNT nanocomposites. They found that G' and G'' increased with increases in filler content as well as with increases in shear rate. The G' and G'' behaviour for the master batch exhibited an independence of shear rate and this phenomenon was attributed to the increase in filler-filler interaction on increasing the filler content (e.g. 15wt.% CNT). The Cole-Cole plot (G' vs. G'') for PC/CNT nanocomposites shows that the melt elasticity increased after adding 5 wt.% and higher of CNT. This plot is a useful way to show the differences initiated in the polymer nanocomposite structure due to adding more filler content to the matrix.

In 1987, Nakayama and Harrell used Cole-Cole plots to investigate the effect of branching and broadening of the distribution of polyethylene molecular weight on the microstructure [Potschke (2002)]. They found that G' (for a given value of G'') increased with increases in the degree of long chain branching. Also, the viscoelastic behaviour of poly(ϵ -caprolacton) (PCL)/attapuligite (AT) nanocomposites was studied by Liu and Chen (2008). The authors used Cole-Cole plots to investigate the structural differences between the PCL matrix and AT systems at fixed temperatures. They found that the slope of the storage modulus (G') versus the loss modulus (G'') decreased on increasing the filler (AT) content. Furthermore, at a given G'' , increasing the AT content led to increases in G' . The interaction between the polymer matrix and the filler can be observed from the changes in the slopes of the curves of G' vs. G'' , and this change was magnified on adding further AT.

Wu et al. (2007) investigated the relationship between the crystallisation temperature and the clay dispersion of Polybutylene terephthalate (PBT)/Montmorillonite (MMT) nanocomposites. They found that a sample isothermally crystallised at a high temperature exhibited high dispersion. They also observed that the storage modulus increased on increasing the crystallisation temperature (T_c). The authors reported that the value of G' for the sample crystallised isothermally at 210°C was higher than the value of G'' at a lower shear rate, indicating a solid-like rheological phenomenon. This phenomenon was attributed to the fact that network percolation had occurred. The TEM images showed that the clay had delaminated and became distributed within the matrix for the sample crystallised isothermally at 210°C, compared with a sample crystallised under normal processing.

Shen et al. (2005) explored the rheological behaviour of polyamide-attapulgite fibre (modified) nanocomposites. The authors observed that the composites' rheology became shear rate dependent at low shear rates as well as when the clay content increased. They found that at high frequencies the samples take on a liquid-like behaviour, and they attributed this phenomenon to the fact that the clay particles could be oriented in the flow direction.

Ammala et al. (2008) investigated the effect of two different types of clay (Cloisite 10A and Somasif MEE) on a PET matrix. The clays were modified to improve their affinity prior to mixing with PET. The samples were characterised by many techniques in order to explore dispersion level, thermal stability and rheological behaviour. In the rheological terms, the neat PET exhibited Newtonian behaviour in the relationship between the steady shear viscosity and shear rate. The PET nanocomposites exhibited higher shear viscosities and tended to take on shear thinning behaviour. The authors attributed this to the fact that the clay plates hinder the free rotation of PET chains (a percolated network structure). The authors took the higher shear viscosity for modified clay as evidence that excellent clay dispersion and exfoliation occurred, and this suggestion was supported by TEM images. The results and observations found by Ammala et al. (2008) are in agreement with Anoop et al. (2007), who studied the rheological behaviour of PET/single-walled carbon nanotube (SWNT) nanocomposites. The nanofillers were compounded with PET via a melt extrusion method at different concentrations. The authors found that the storage and loss moduli and complex viscosity increased on increasing the SWNT loading. They observed strong shear thinning behaviour for PET/SWNT (3%) at low shear rate and attributed this to the fact that the carbon nanotubes act as effective entanglements during the melt state.

Durmus et al. (2007) studied the effects of compatibilizer polarity and structure on the physical properties and rheological behaviour of linear low density polyethylene (LLDPE)/clay nanocomposites. The authors state that the storage modulus (G') is a rheological factor sensitive to any change in polymer nanocomposite structure, more than the loss modulus (G''). They found that the storage modulus becomes independent of frequency in the low shear rate region. This is indicative of pseudo-solid-like behaviour, or 'yielding solid-like behaviour'. This behaviour has been referred to as a strong interaction between the LLDPE matrix and clay layers. The authors observed that increasing the compatibilizer polarity led to a high storage modulus, indicative of good dispersion.

Drozdov et al. (2008) studied the pseudo-solid-like behaviour of low density polyethylene (LDPE)/MMT nanocomposites, which they observed in low shear rate oscillatory tests. The storage and loss moduli started to lose their frequency dependency on increasing the nanoclay loading. The increases in G' and G'' led to increases in the complex viscosity at low frequencies. The authors proposed three reasons for this phenomenon: first, the frictional interactions between the silicate layers, second, the stock of polymer chains within the layers, and third, the clay platelets stacking onto one another, which may lead to the formation of a percolated network.

Kracalik and Kovarova et al. (2007) studied the effect of additional organoclays (Cloisite 25A, 10A and 30B) on the rheological properties of recycled PET (rPET). The complex viscosities of all rPET nanocomposites exhibited shear thinning behaviour. This phenomenon can be attributed to the clay particles which tend to orient in the flow at high shear rates, while the network structures are disrupted at low shear rates. The authors observed that Cloisite 25A showed the best dispersed organoclays in rPET

compared with Cloisite 10A and 30B. The rheological results were complemented by TEM, WAXD, DSC and TGA techniques. G' and G'' results inferred internal changes in the structure of rPET nanocomposites. Both moduli increased on increasing the organoclay concentration till the moduli exhibited weak frequency dependency. The authors attributed this to exfoliation occurring in the organoclays in the polymer matrix.

4.2 Experimental process

4.2.1 Rheological behaviour

A. *Materials*

The rheological properties of crystallised and dried pellets of unfilled polyethylene terephthalate (PET) and PET nanocomposites (PETNCs) were studied. Fourteen samples were used in this study. Each test was repeated 3 times and showed good repeatability. The rheological properties of vPET pellets (as received) and extruded vPET (ext. vPET) and PETNCs pellets, produced during the compounding processes (see Chapter 3), were studied using capillary and oscillatory rheometers over a wide range of shear rates. The details of the samples are listed in Table 4.1.

Sample (pellets)	Description
vPET	PET as received (crystallised)
Ext. vPET	Extruded PET, unfilled (amorphous)
PET/MAE (4 samples)	PET/MAE (1, 3, 5 and 20wt.%), (amorphous)
PET/MTE (4 samples)	PET/MTE (1, 3, 5 and 20wt.%), (amorphous)
PET/Cloisite 25A (4 samples)	PET/Cloisite 25A (1, 3, 5 and 20wt.%), (amorphous)

Table 4.1 Description of the samples used in the rheological study

All amorphous pellets were recrystallised in the vacuum oven for 20 hrs at 150°C (dried in the case of vPET) prior to rheological testing.

B. *Procedure and parameters*

The rheological behaviour of all samples was studied using a capillary rheometer and oscillatory rheometer; both items are discussed in chapter 3 (see section 3.5.6). The capillary rheometer (Rosand-RH10) was used to study the rheological properties of the

samples over a ‘high’ shear rate range ($50\text{--}5000\text{s}^{-1}$) at 260°C . Furthermore, the oscillatory rheometer (Anton Paar MCR 501) with parallel-plate geometry (25mm diameter) was used to measure the complex viscosity, storage modulus and loss modulus as a function of shear rate ($0.1\text{--}100\text{s}^{-1}$). All measurements in the oscillatory rheometer were performed at 260°C under an air atmosphere. The gap between the plates was 1mm and the strain rate was 0.5%, this having been determined to lie within the linear viscoelastic range for all samples through amplitude sweep testing. Prior to measurement all samples were placed in the oscillatory and capillary rheometers at the measurement temperature for 3 and 8 minutes (respectively) to allow the samples to relax and become isothermal throughout. The measurements were carried out in the IRC Laboratories at the University of Bradford.

4.2.2 Intrinsic viscosity

A. *Materials*

The intrinsic viscosity (I.V.) of all samples used in the rheological study was measured (Table 4.1). In addition to these samples, the I.V. of the films produced during the cast film process (see section 3.4) was measured. Table 4.2 lists the amorphous film samples.

Sample (films)	Description
vPET	PET film, unfilled (amorphous)
Ext. vPET	Extruded PET film, unfilled (amorphous)
PET/MAE (3 samples)	PET/MAE films (1, 3, and 5wt.%), (amorphous)
PET/MTE (3 samples)	PET/MTE films (1, 3, and 5wt.%), (amorphous)
PET/Cloisite 25A (3 samples)	PET/Cloisite 25A films (1, 3, and 5wt.%), (amorphous)

Table 4.2 Description of the film samples used in intrinsic viscosity (I.V.) analysis

B. Procedure

The intrinsic viscosity tests were performed in SABIC Laboratories at Riyadh, Saudi Arabia. The procedure was covered in section 3.5.4.

4.3 Results and discussion:

In this section, the results of the rheological properties virgin PET (vPET), extruded virgin PET (ext. vPET) and PET nanocomposites (PETNCs) for all clays (Somasif MAE, Somasif MTE and Cloisite 25A) at various concentration (1, 3, 5 and 20 wt.%) are presented and discussed. As mentioned in previously in section 4.2, all samples were dried (in vPET case) or re-crystallised (in amorphous ext. vPET and PETNC cases) prior to the tests. The importance of this step will be explained in this section. Furthermore the question why the oscillatory test procedure started from high frequency to low and not vice versa was answered. This section is divided into five subsections as follows:

- I. The rheological behaviour of the samples at high shear rate (50s^{-1} to 5000s^{-1}).
- II. The rheological behaviour at low shear rate (0.1s^{-1} to 100s^{-1}).
- III. Investigation into the Cox-Merz rule for PETNCs over wide shear rate range.
- IV. The shear viscosity behaviour at fixed shear rate and varying clay concentration.
- V. The intrinsic viscosity (I.V.) of PETNCs.

4.3.1 Capillary rheometer (High shear rates):

The importance of drying or re-crystallising samples is presented in section *A*. Section *B* shows the effect of adding clay to the PET matrix on the rheological phenomena. Section *C* shows the rheological behaviour of the samples at the same concentration levels for the various clays.

A. *Shear rate (1/s) vs. shear viscosity (Pa.s) for virgin PET, extruded vPET (re-crystallised and amorphous).*

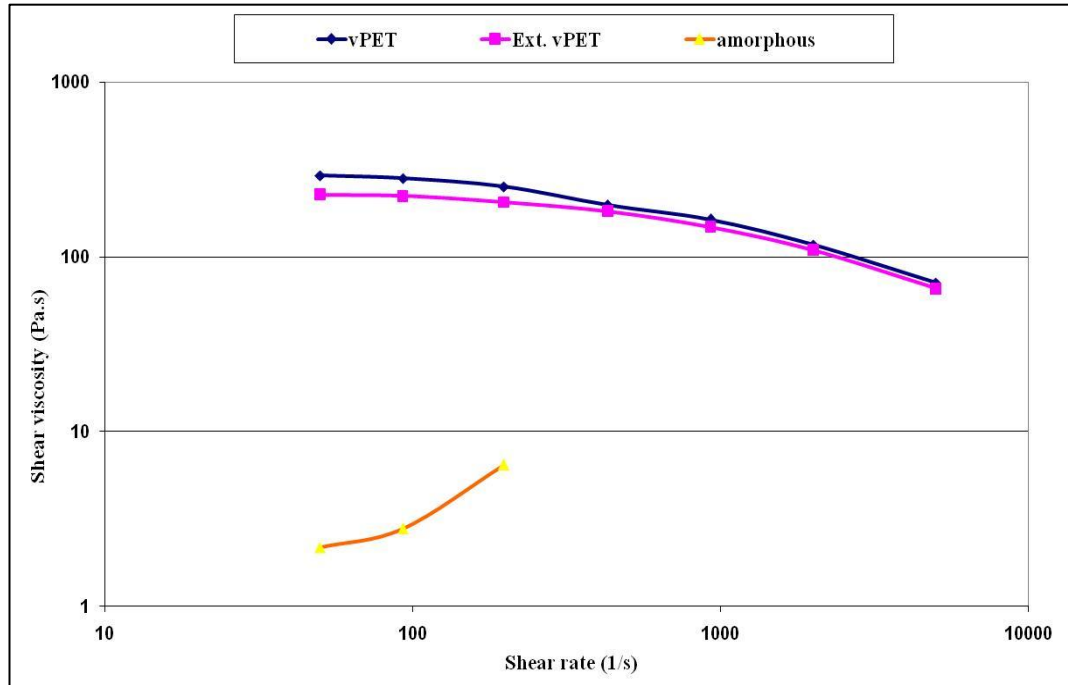


Figure 4. 1 Shear rate vs. shear viscosity for neat PET (vPET) and extruded PET (re-crystallised and amorphous)

Figure 4.1 shows the viscosity of amorphous PET over high shear rates and compares it with that for crystallised PET. The purpose of the experiment was to prove the importance of re-crystallising amorphous pellets prior to investigation of the rheological properties of PET. This result also shows the essential requirement of re-crystallising the amorphous PETNC pellets prior to any downstream melt processing (e.g. extrusion or injection). Applying high shear rate (over 200s^{-1}) cause a huge reduction in the viscosity of amorphous pellets material.

B. Shear rate (1/s) vs. shear viscosity (Pa.s) for all PET nanocomposites at different clay loadings:

At high shear rates, figures 4.3 - 4.5 show the rheological behaviour of PETNC for each nanoclay (MTE, MAE and Cloisite 25A) with different weight loading of clays (1, 3, 5 and 20 wt. %). It is clear that the absolute value of the melt viscosity of PETNC is significantly lower than for un-filled PET, and the extent of this reduction increases with adding more nano-filler at a given shear rate. These figures confirm of shear thinning behaviour (i. e. pseudoplastic) and illustrate the dependence of the shear viscosity for the un-filled PET and PETNC on the shear rate. Generally speaking, shear thinning behaviour can be explained by two mechanisms which can occur simultaneously. The first mechanism proposed is that some polymer has entangled and few oriented molecular chain at rest. When applying high shear rates, the level of entanglements is reduced and the molecular chains tend to orient with the flow direction. The other mechanism which may cause pseudoplastic behaviour is caused by the presence of the nanoparticles. The nanoparticles align with the flow direction at high shear rate. The combined two mechanisms or either one of them in isolation reduce the viscosity of the polymer matrix [Muksing et al. (2008)].

The status of the PET chains, the nanoclay plate to plate variation and the interactions between the PET chains and the nanoclay prior to and during melt processing are illustrated in figure 4.2.

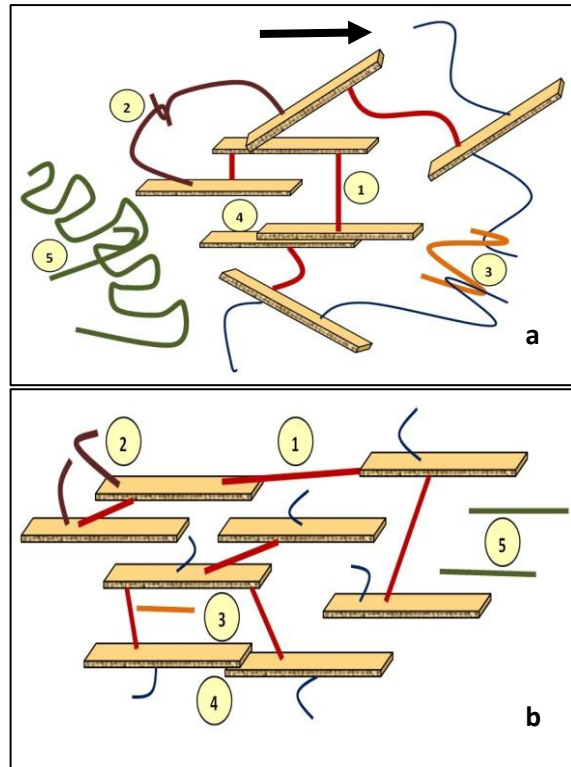


Figure 4.2 Sketch map exhibiting the different types of PET-nanoclay interactions. (a) Interactions at rest state. (b) Interaction during flow.

Figure 4.2 includes the two PETNC matrix statuses, at rest (a) and during melt flow (b). Five cases have been assumed to occur during both states. Case (1) defines the direct bridge between the PET chains and the nanoclay plates (crosslink structure). Cases (2 and 3) show the primary and secondary entanglements respectively. Case (2) occurs between PET chains which have already interacted with the nanoclay plates from both ends. Case (3) illustrates the interaction between the free PET chains. Case (4) assumes some stacking or connection between the nanoclay plates though this phenomenon is not always exhibited in the nanocomposites unless poor dispersion remains. Case (5) defines the PET chains when unoriented. Figure 4.2 shows how these cases behave during melt flow. Cases 2 and 3 interactions collapse and become weak under high shear rates while case 1 shows the interaction between the PET chains and nanoclay

plates. For case 4, interactions the plates tend to align in the flow direction and the stacked plates tend to diverge. In case 5, interaction the un-oriented chains become oriented and less resistant to flow.

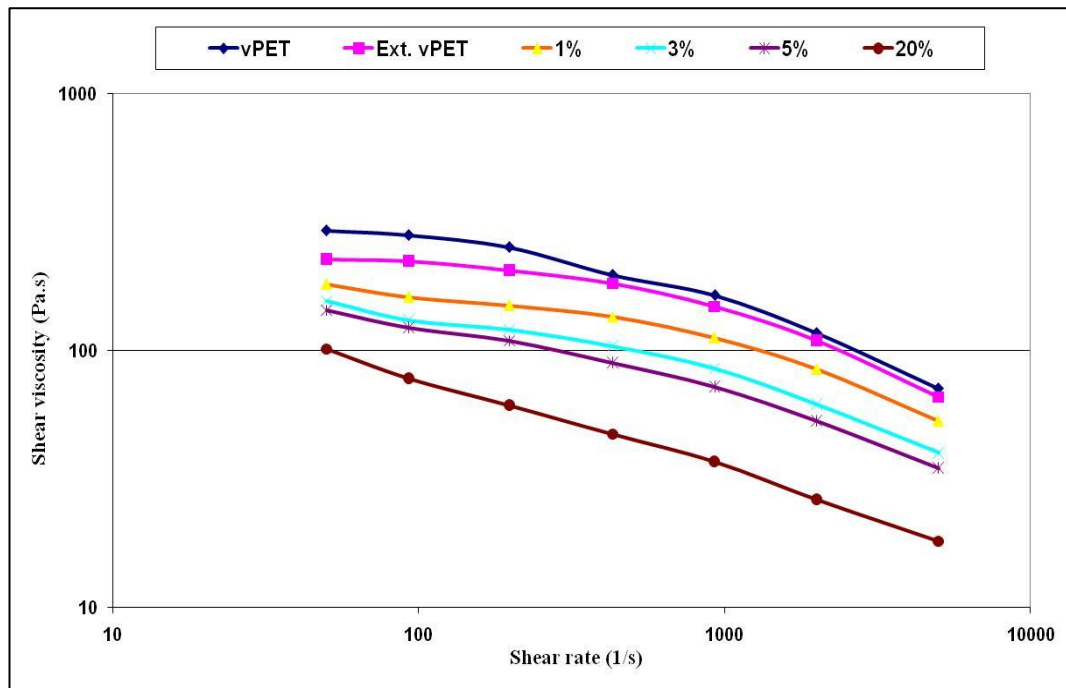


Figure 4. 3 Shear viscosity variation of PET/MAE nanocomposites at different MAE concentration with shear rate.

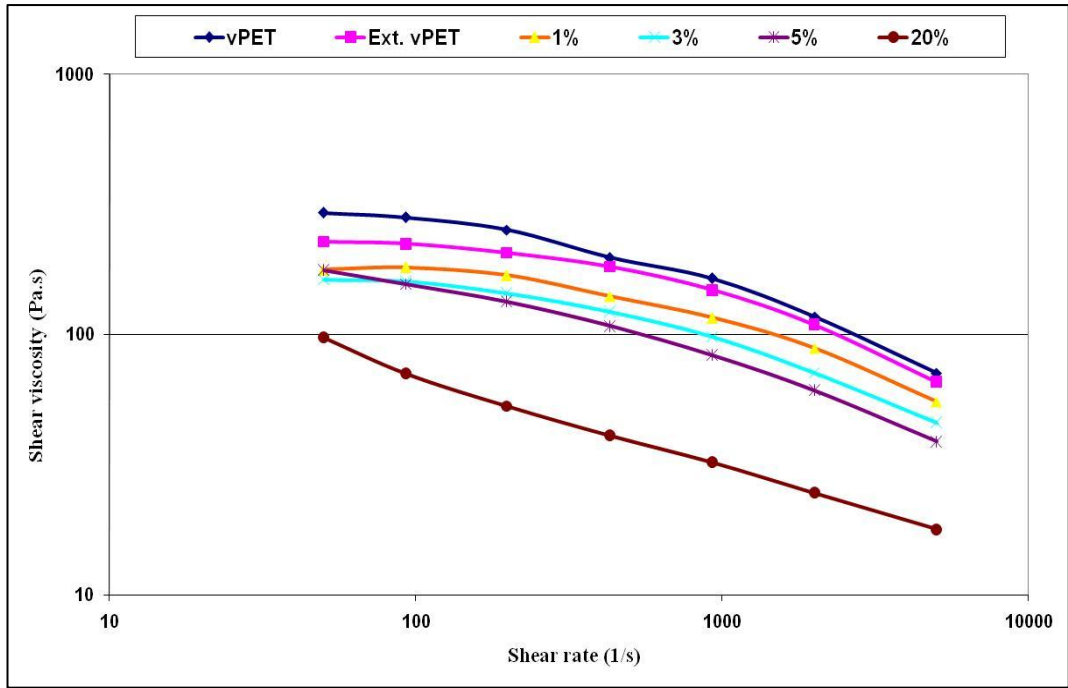


Figure 4. 4 Shear viscosity variations of PET/MTE nanocomposites at different MTE concentration with shear rate.

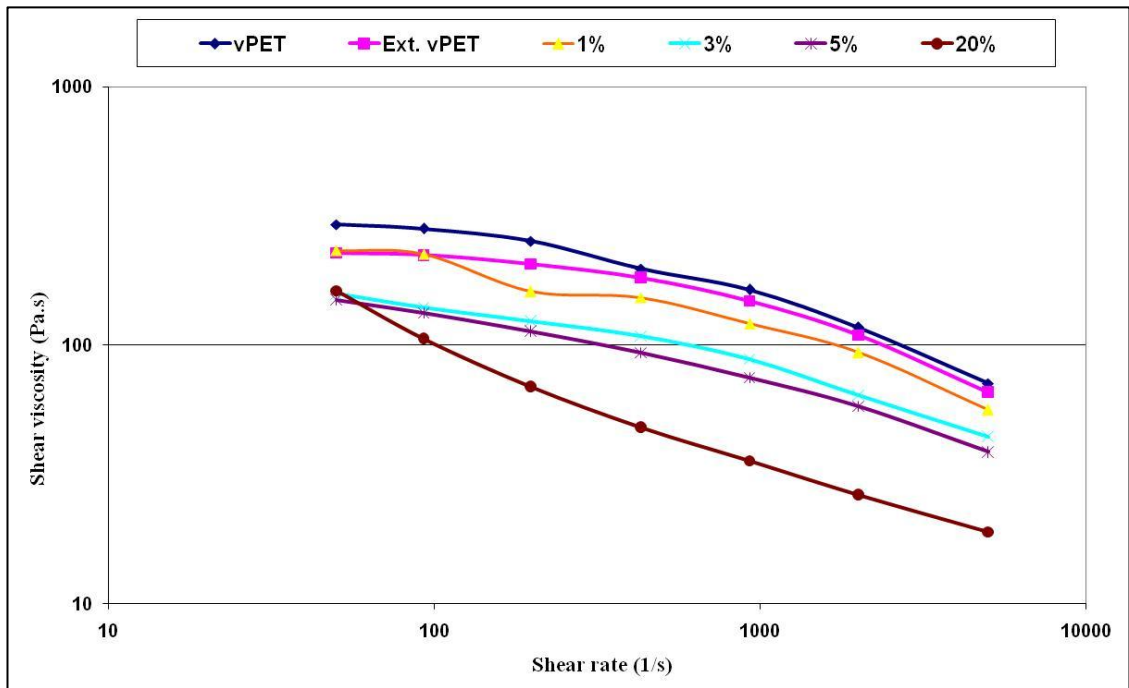


Figure 4. 5 Shear viscosity variations of PET/Cloisite 25A nanocomposites at different Cloisite 25A concentration with shear rate.

Figures 4.3 - 4.5 illustrate that the viscosity of unfilled PET and PETNC decrease monotonically with increasing clay loading and decrease substantially with increasing shear rate. While this reduction in the viscosity of most PETNCs is exhibited from the onset of the shear rate, figure 4.5, shows that the rheological behaviour of PET/Cloisite25A (1 wt.%) shows similar behaviour between unfilled PET (ext. vPET) which may be attributed to delays in the particle alignment process. It is also clear in the same figure at 20 wt. % loading a delay in the viscosity reduction at the onset of the shear rate can also be observed.

PET/Cloisite 25A (3 wt.%) shows a big reduction in the melt viscosity, to almost the 5 wt.% values. The size of the reduction may infer that some relatively poor dispersion occurred in the Cloisite 25A (3 wt.%) compounding.

It seems that apparent unusual behaviour of the PET/Cloisite 25A (3 wt.%) samples can be attributed to relatively poor dispersion of the nanofiller. The consistent results of PET/Cloisite 25A (3 wt.%) seem to suggest good distribution, but not good dispersion. Having said that, others analytical results also exhibit similar anomalies. Fornes et al. (2001) observed a similar rheological behaviour trend with Nylon 6 NC. Wang and Xie et al. (2006) also presented some rheological results in agreement with our own when investigating the rheological behaviour of PC/CaCO₃.

C. Shear rate (s^{-1}) vs. shear viscosity (Pa.s) for different types of PET nanocomposites with the same nanofiller content

This section presents the differences in the effects of each nanoclay at the same level of content. It is clear from figures 4.6 – 4.9 that Somasif MAE clay exhibits the maximum reduction in the shear viscosity of PET compared with the other clays used (Somasif MTE and Cloisite 25A). This observation may be attributed to either the fast alignment

of MAE plates with the flow direction due to the big gap (d-spacing) between the platelets compare with other nanoclays used, or to the higher degradation level of PETNC in the presence of MAE due to the high surfactant content, or to both causes.

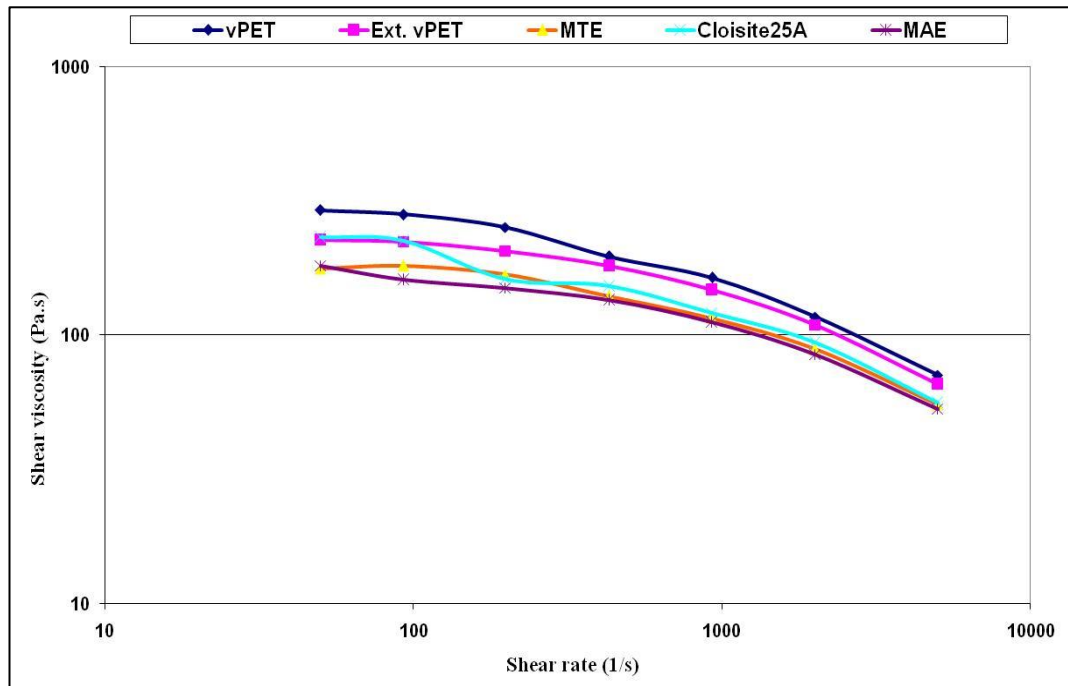


Figure 4.6 Shear viscosity variation of PET NC with different nanofillers (MTE, MAE and Cloisite 25A) with 1wt.% clay concentration.

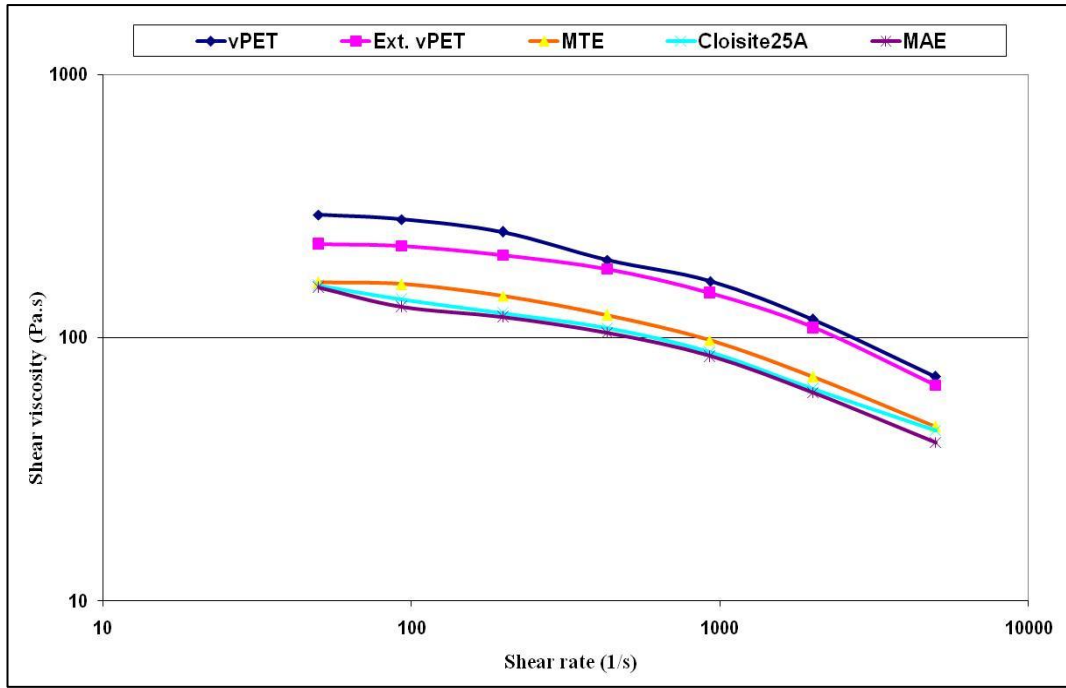


Figure 4.7 Shear viscosity variation of PET NC with different nanofillers (MTE, MAE and Cloisite 25A) with 3 wt.% clay concentration.

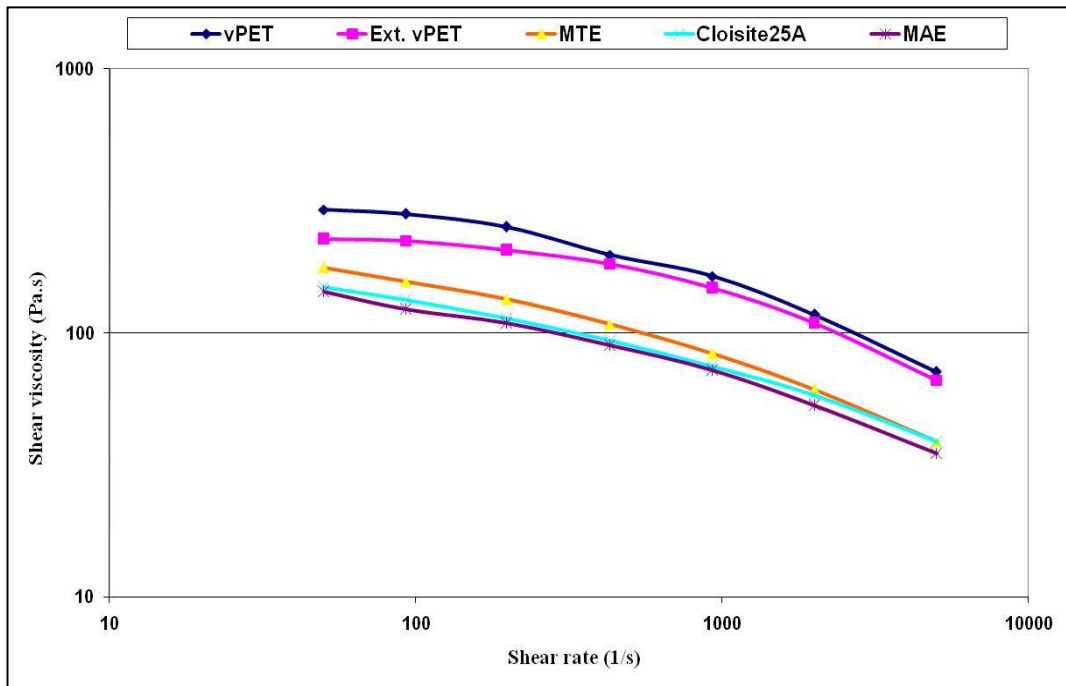


Figure 4.8 Shear viscosity variation of PET NC with different nanofillers (MTE, MAE and Cloisite 25A) with 5 wt.% clay concentration.

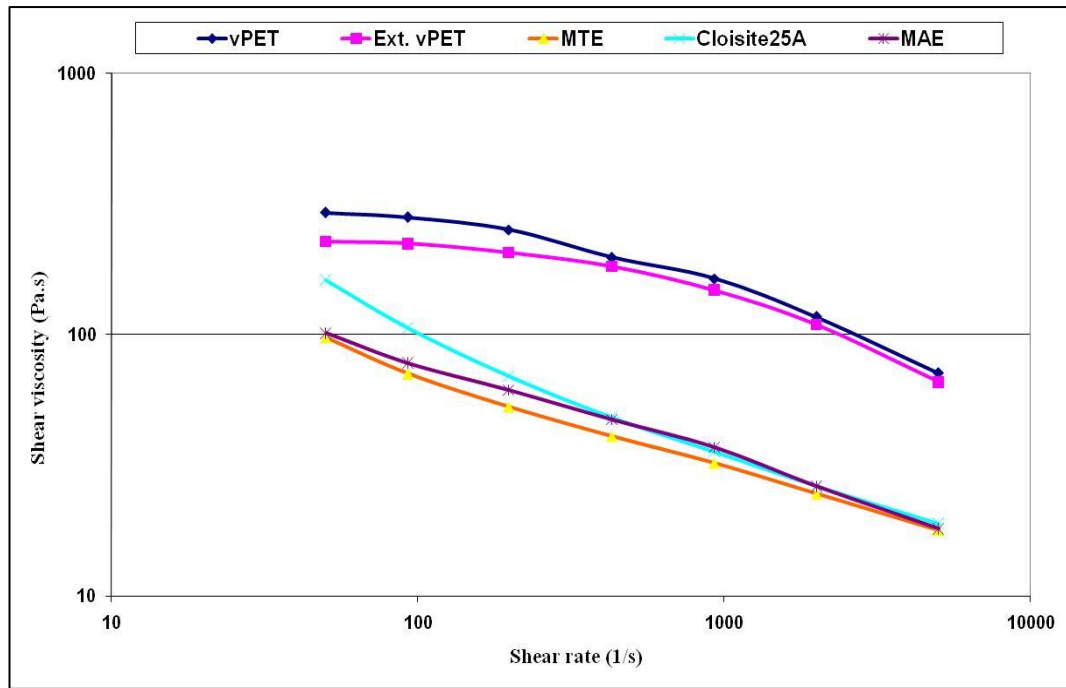


Figure 4.9 Shear viscosity variation of PET NC with different nanofillers (MTE, MAE and Cloisite 25A) with 20 wt.% clay concentration.

4.3.2 Oscillatory rheometer (low shear rate)

This section investigates the rheological behaviour of PETNCs at low shear rates. Prior to conducting the tests with the oscillatory rheometer, the linear viscoelastic (LVE) range should be defined. Amplitude sweep tests were performed at constant frequency and variable amplitudes (strains). As shown in figure 4.10, a strain rate of (0.5 wt.%) was chosen as the ideal strain rate. In choosing the right strain it is not enough to define LVE for unfilled PET, and that is proved by analysing the LVE range of PET/MTE (5 wt.%) as figure 4.10 shows. Determination of the rheological properties of PETNC requires a lower value of strain.

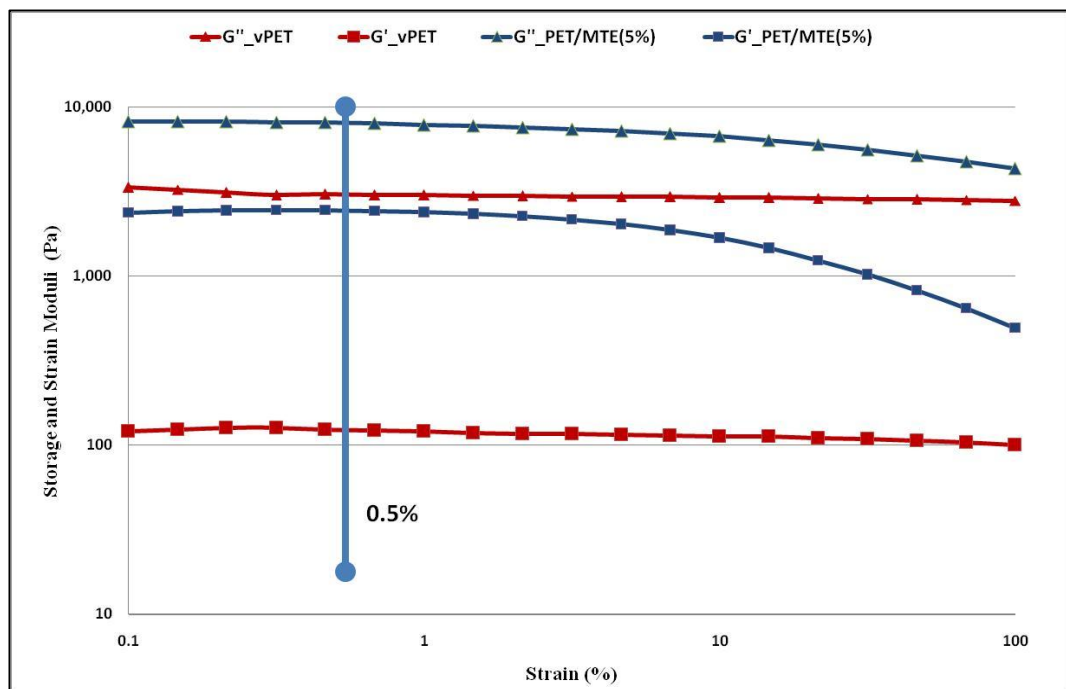


Figure 4.10 Strain amplitude sweep of vPET and PET/MTE (5 wt.%) nanocomposites at 260°C, $\omega=10\text{rad/sec}$.

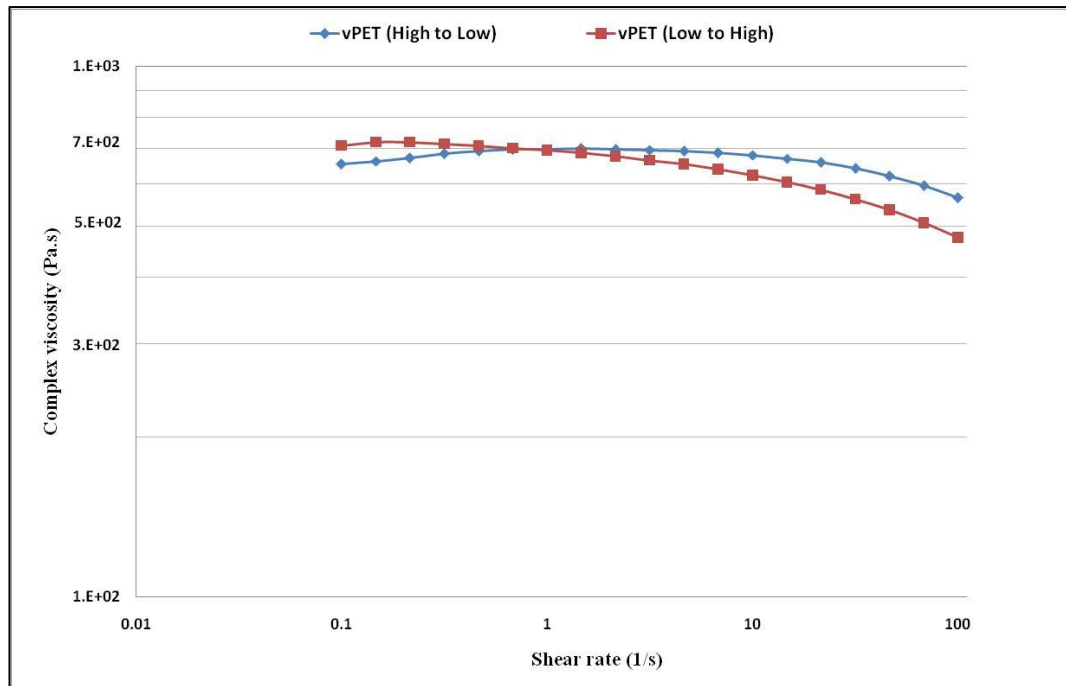


Figure 4.11 Complex viscosity of vPET tested under shear rates from 0.1 to 100 s^{-1} and 100 to 0.1 s^{-1} .

As mentioned before (see section 4.2), the shear rates for the oscillatory rheometer ranged from 0.1 – 100 s^{-1} though in reality the test was run from 100 to 0.1 s^{-1} . This action was taken after studying the residence time of the melt sample over the shear rate range. It was found that the melt PET spent longer in the range 0.1 – 1 s^{-1} compared to 1 – 100 s^{-1} . Spending time in the range from 0.1 upward can lead to more degradation of the material. Figure 4.11 shows the viscosity trend of vPET as a function of shear rate going from 0.1 to 100 s^{-1} . It is obvious that the viscosity tends to lose Newtonian behaviour and decreases with increases in the shear rate. On other hand, the viscosity of vPET under the same shear rate but going from 100 to 0.1 s^{-1} exhibits Newtonian behaviour all the time.

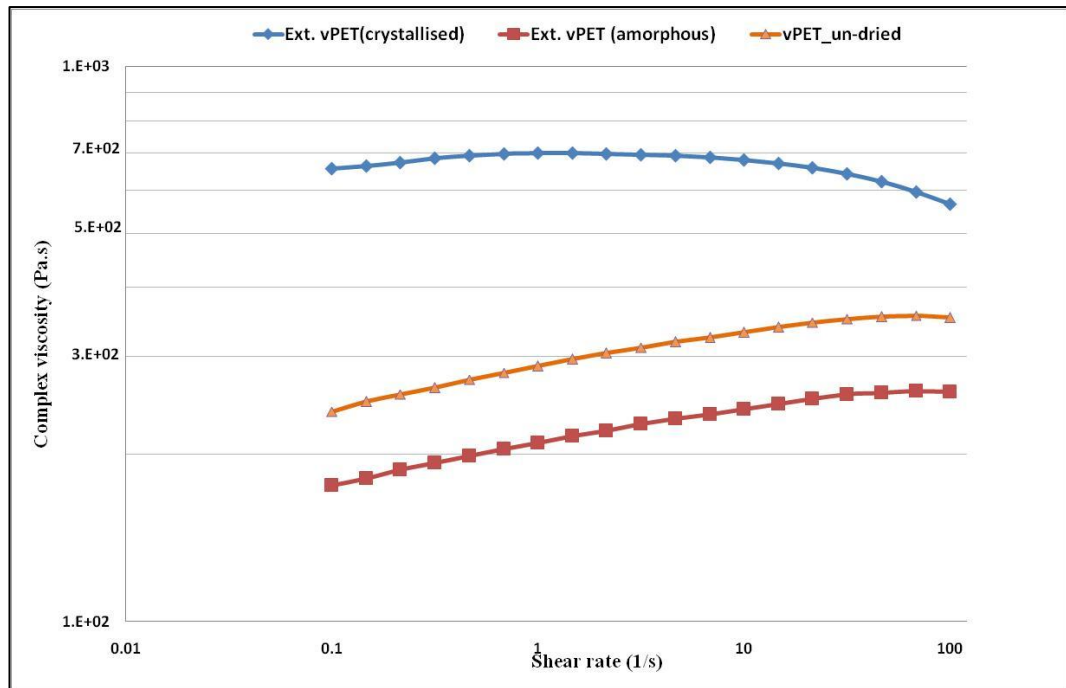


Figure 4.12 complex viscosity vs. shear rate for Ext. vPET (amorphous and re-crystallised).

Sufficient drying as described before (section 3.3) is an important step prior to any PET melt processing to avoid hydrolysis degradation. To assess the importance of the drying stage, the rheological properties of dried and un-dried vPET were studied. Figure 4.12 shows how the absence of a drying step affects the PET viscosity. A big reduction in viscosity was observed and this reduction being magnified at lower shear rates (longer times). This reduction can be attributed to hydrolysis degradation of the PET matrix due to moisture content in the pellets.

One mistake often made during investigations of the rheological properties of PET is to analyse the amorphous PET (e.g. amorphous film or amorphous pellets) in its state. This procedure may be valid for other polymers (e.g. PP) but not for PET. Figure 4.12 also shows the rheological behavior of amorphous PET compared with behavior of crystallised PET. It is clear that the drying of crystallised PET or re-crystallised amorphous PET is an essential step that must be taken prior to studying the rheological properties of PET.

A. *Shear rate (s^{-1}) vs. complex viscosity (Pa.s) for PET nanocomposites with different clay contents*

This section shows the behavior of the complex viscosity of un-filled PET and PETNCs in various composites over low shear rates ($0.1 - 100s^{-1}$).

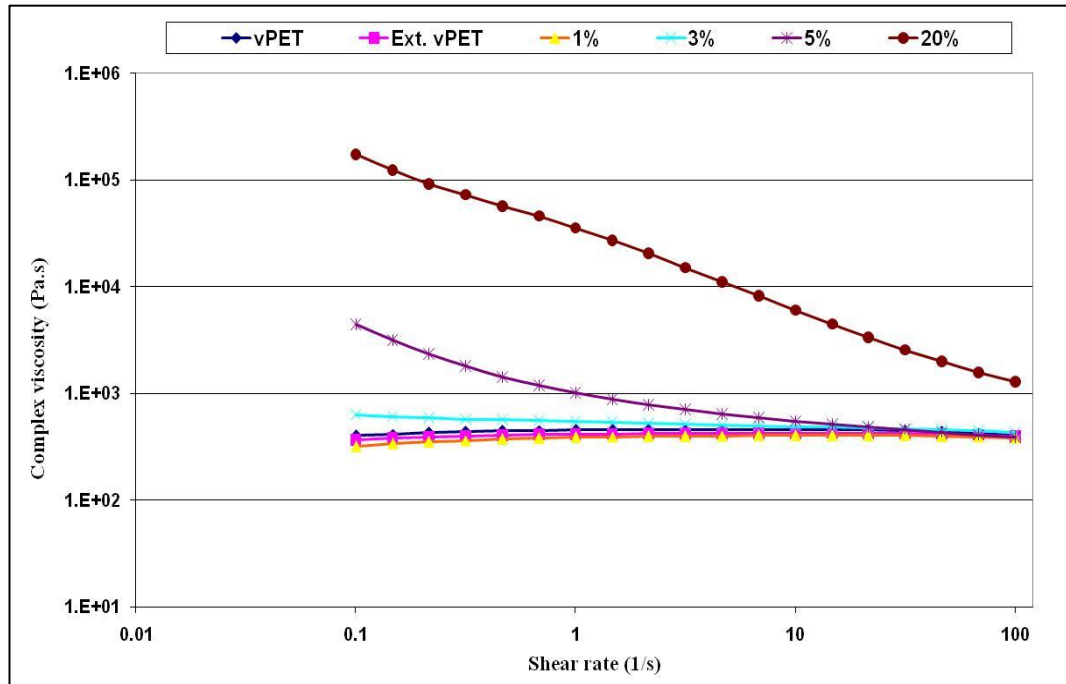


Figure 4.13 Complex viscosity variation of PET/MAE nanocomposites at different MAE concentrations with low shear rate.

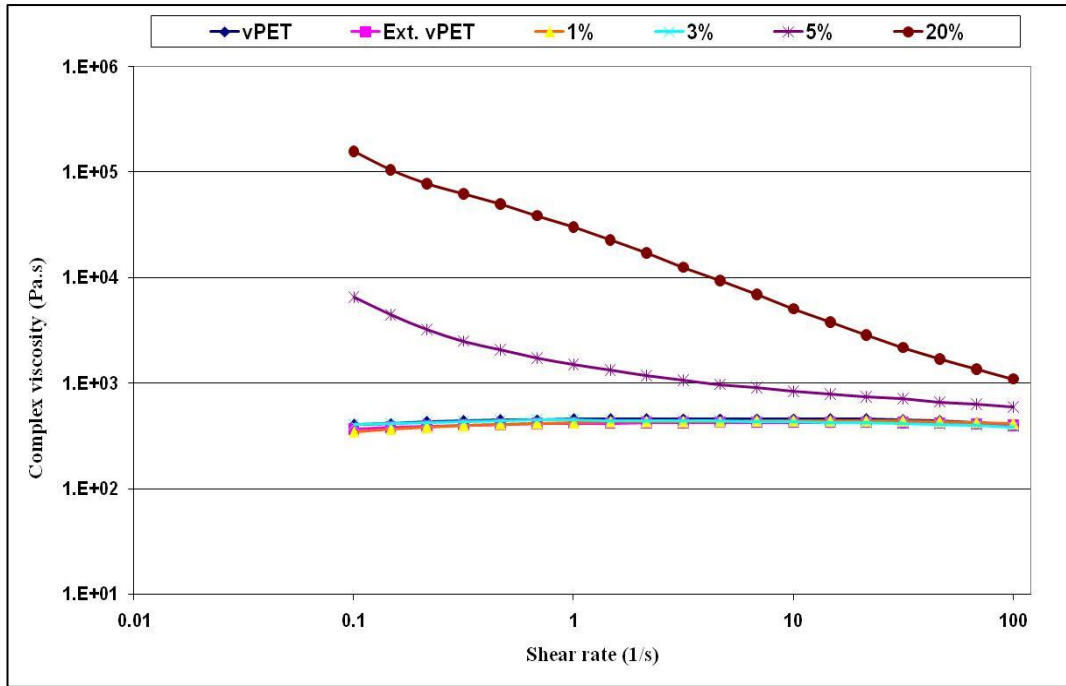


Figure 4.14 Complex viscosity variation of PET/MTE nanocomposites at different MTE concentrations with low shear rate.

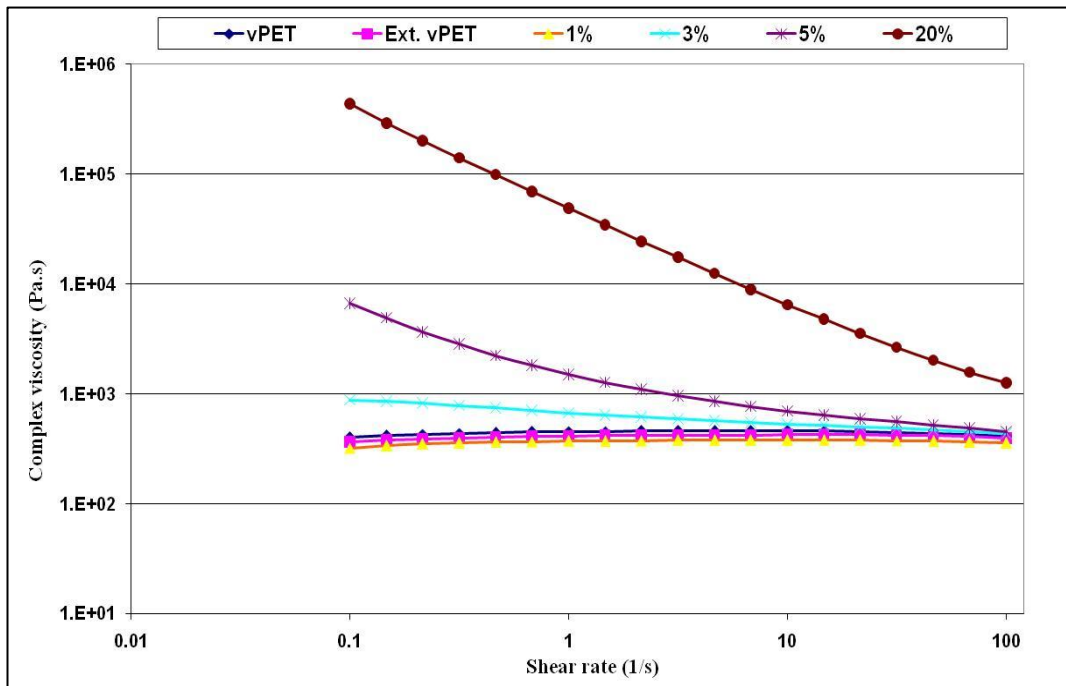


Figure 4.15 Complex viscosity variation of PET/Cloisite 25A nanocomposites at different Cloisite 25A concentrations with low shear rate.

Figures 4.13 – 4.15 show the shear rate dependency of the complex viscosity of different nanocomposites at different clay concentrations. The magnitudes of the complex viscosity are clearly dependent on the nanoclay concentrations and processing shear rate. In terms of PET nanocomposites, the nanoclay leads to increases in complex viscosity with increases in nanoclay concentration over 1 wt.%. The vPET, ext. vPET, and PET nanocomposites (1 wt.%) and PET/MTE (3 wt.%) exhibit Newtonian behavior for low shear rate ranges. The complex viscosity for PET/MTE deviated from Newtonian behavior and behaved in a shear thinning manner at 5 and 20 wt.% loading of nanoclay, while Cloisite 25A and MAE started to deviate at a 3 wt.% concentration. For example, at a shear rate of 0.1 s^{-1} , PET/Cloisite 25A (20 wt.% loading) showed 575 times the complex viscosity of vPET.

B. Shear rate (s^{-1}) vs. complex viscosity (Pa.s) for different types of PET nanocomposites with the same nano-filler content

This section includes plots showing the viscosity behavior of PETNC at the same content level for various clays over low shear rates. As seen in the previous section, PETNC at 1 wt.% does not exhibit any significant change in its polymer viscosity matrix compared to un-filled PET (see figure 4.10 in appendix 4). However the nanoclay at this low loading (1 wt.%) act nucleation agent to increase the crystallization rate and temperature (see chapter 5).

Figures 4.16 – 4.18 reveal that the PET nanocomposites exhibit Newtonian behavior at low nanoclay content and tend to show shear thinning behavior with increasing clay content. A PET/Cloisite 25A nanocomposite was the first to respond to increasing the content followed by PET/MAE and lastly PET/MTE nanocomposites. Usually the formation of aggregates is responsible for an increase in complex viscosity.

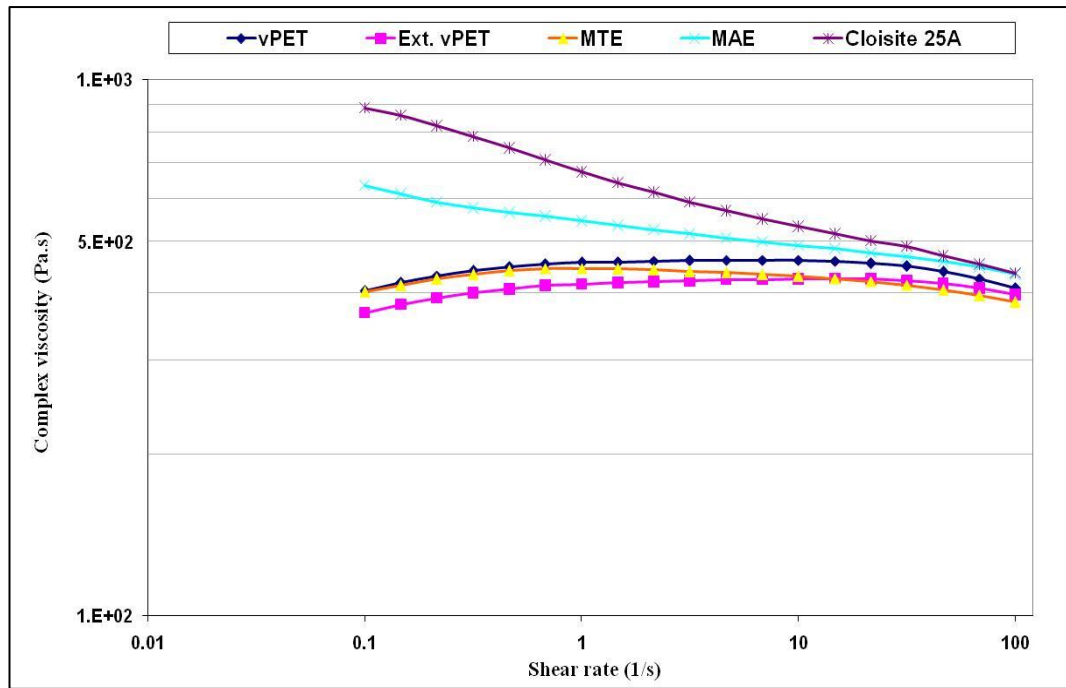


Figure 4.16 Complex viscosity variation of PET nanocomposites at the same concentration (3 wt.%) with low shear rate.

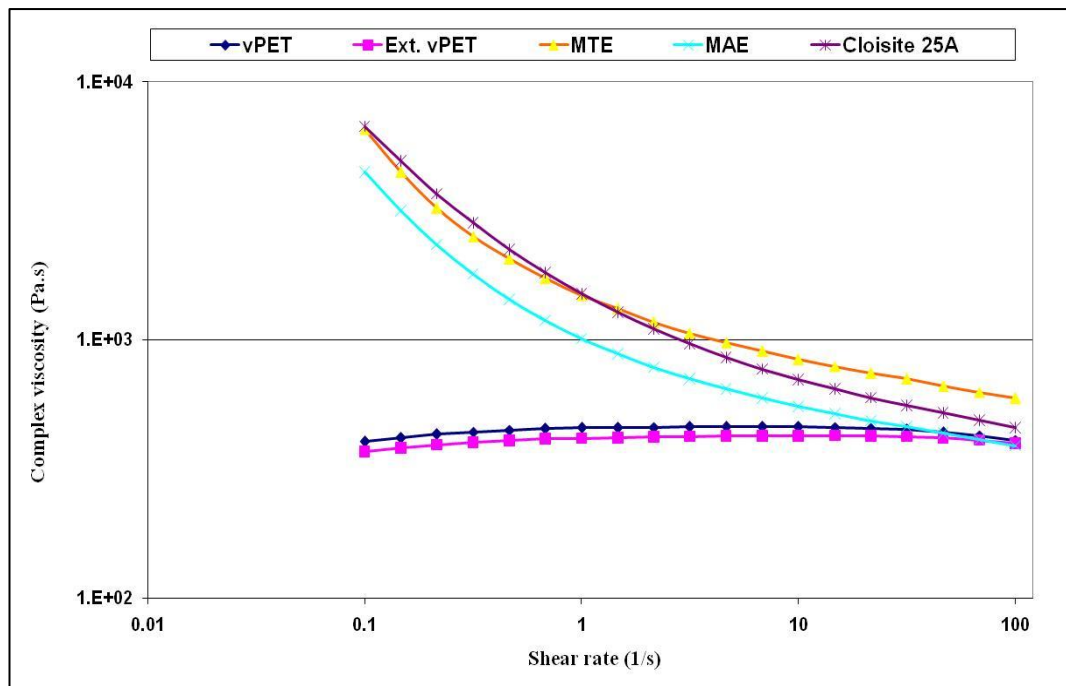


Figure 4.17 Complex viscosity variation of PET nanocomposites at the same concentration (5 wt.%) with low shear rate.

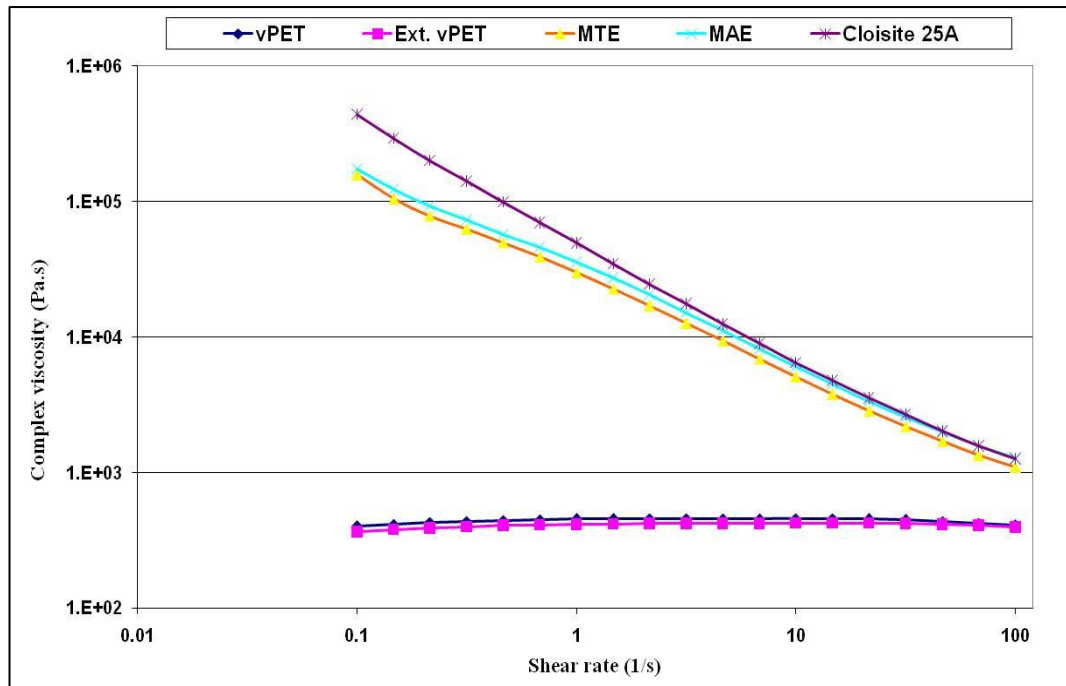


Figure 4.18 Complex viscosity variation of PET nanocomposites at the same concentration (20 wt.%) with low shear rate.

These results match the results obtained by Jin et al. (2007). The rheological properties of PET/MWCNT (multi-walled carbon nanotube) were studied using oscillatory rheometry. It was found that the complex viscosity increased on increasing the nanofiller content. Also, at higher content, the shear rate curve showed non-Newtonian behavior. Reinking and Rufener (2005) reported that the complex viscosity of an HDPE/clay nanocomposite increased in a low shear rate range. Also Kim et al. (2008) reported that a PET/AM-POSS-1 (aminoisobutyl-polyhedral oligomeric silsesquioxane) nanocomposite leads to an increase in the complex viscosity with increases in the POSS concentration

C. Storage modulus (Pa) vs. shear rate (s^{-1}) for PET nanocomposites with different clay contents

This section shows the behavior of the storage modulus over low shear rates (0.1-100 s^{-1}). It has been reported that the storage modulus is very sensitive to any change in

polymer structure [Durmus et al. (2007)]. Therefore this factor can be plotted against shear rate to investigate the internal change in the structure of a PET matrix with adding a nanoclay. It is believed that the effect of the nanoclay on the viscous properties of the polymer nanocomposites can be defined in terms of the degree of dependence of the storage modulus (G') on the low shear rates at very low shear rates [Wu et al. (2005)]. It is clear in figures 4.19 – 4.21 that the dependency of the storage modulus (G') on the shear rates at low nanoclay loading (1 wt.%) is similar to that of the vPET, while the dependency of G' on the shear rate decreased with loadings of 3 wt.% and above.

Figures 4.19–4.21 show increases in the storage modulus of PETNC especially at the lowest shear rates studied. The increase in G' means the PETNC matrix has a strong tendency to store energy which suggests increases in the composite relaxation time. The slopes of $\log(G')$ vs. $\log(\text{shear rate})$ are less than 2 which means that a network structure has been formed during the melt processing due to the presence of the clay. Usually the non-crosslinked polymer exhibits a value of 2 during the melt process [Yoon et al. (2003) and Kim (2009)]. The figures showing the loss modulus (G'') vs. shear rate are presented in appendix x4 (see figures x4.4 – x4.6). The slopes of $\log(G'')$ vs. (\log) shear rate curves are less than unity which is also an indication of the formation of a network structure during melt processing. G' and G'' for PETNC show a significantly diminished shear rate dependence and this becomes obvious on increasing the clay content. When the polymer behavior transfers from fluid-like to solid-like behavior at a certain filler concentration, the phenomenon is known as the percolation threshold [Krishnamoorti (2001) and Cassagnau (2008)]. It seems clear that the percolation threshold in figures 4.19 – 4.21 is reached at 3 wt.% loading.

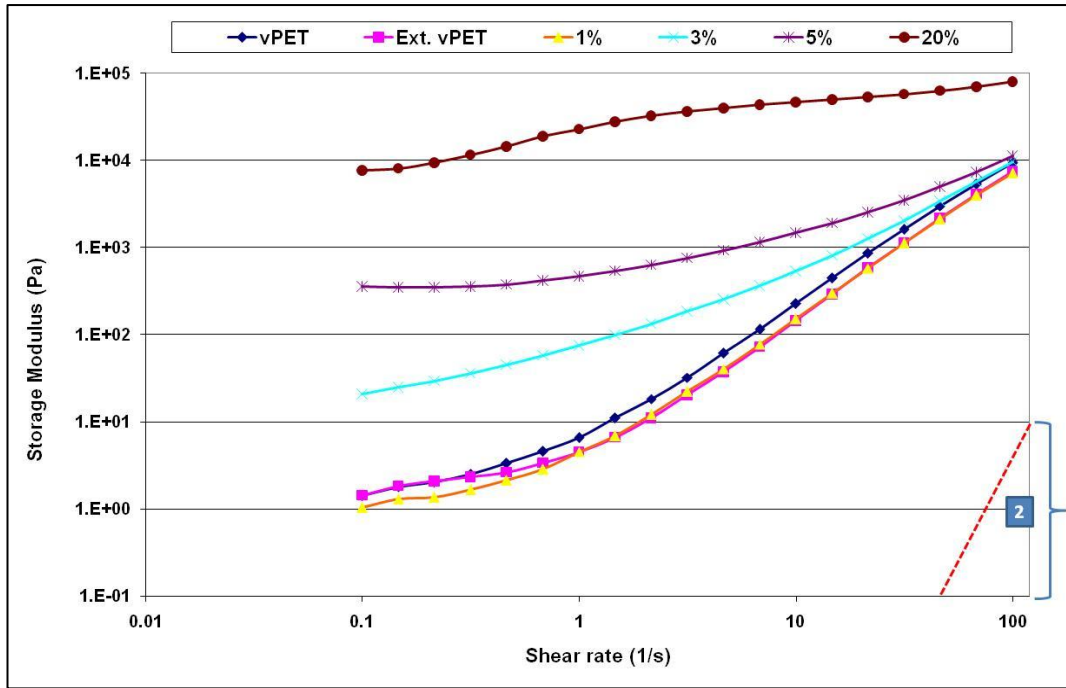


Figure 4.19 Storage modulus behaviour for PET/MAE NC at different clay concentrations with low shear rate.

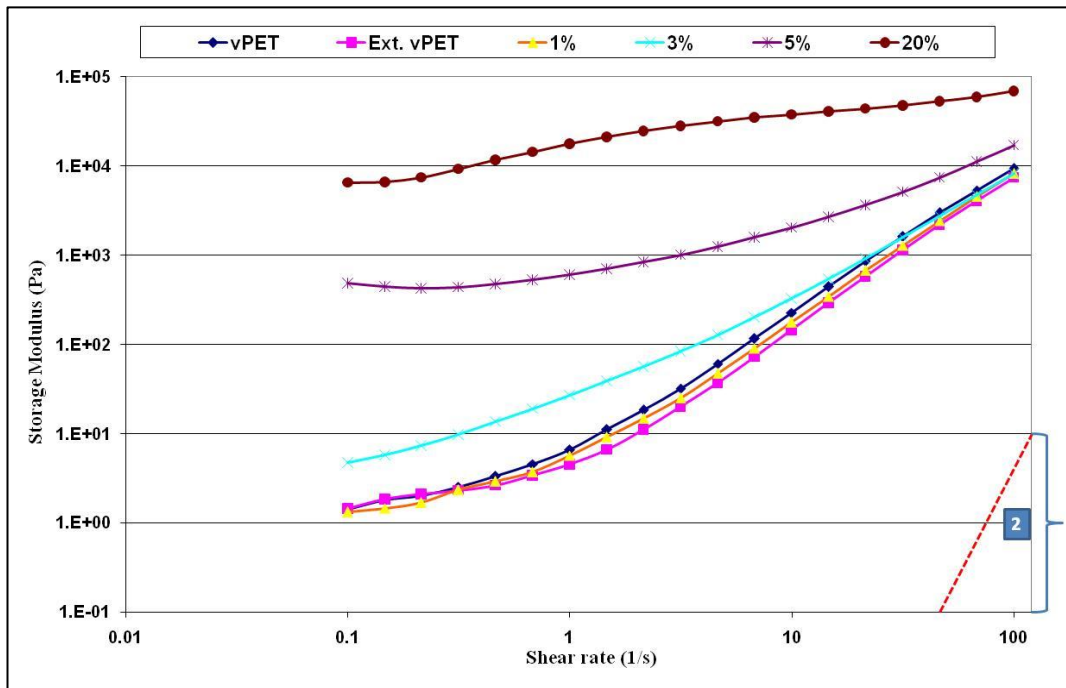


Figure 4.20 Storage modulus behaviour for PET/MTE NC at different clay concentrations with low shear rate.

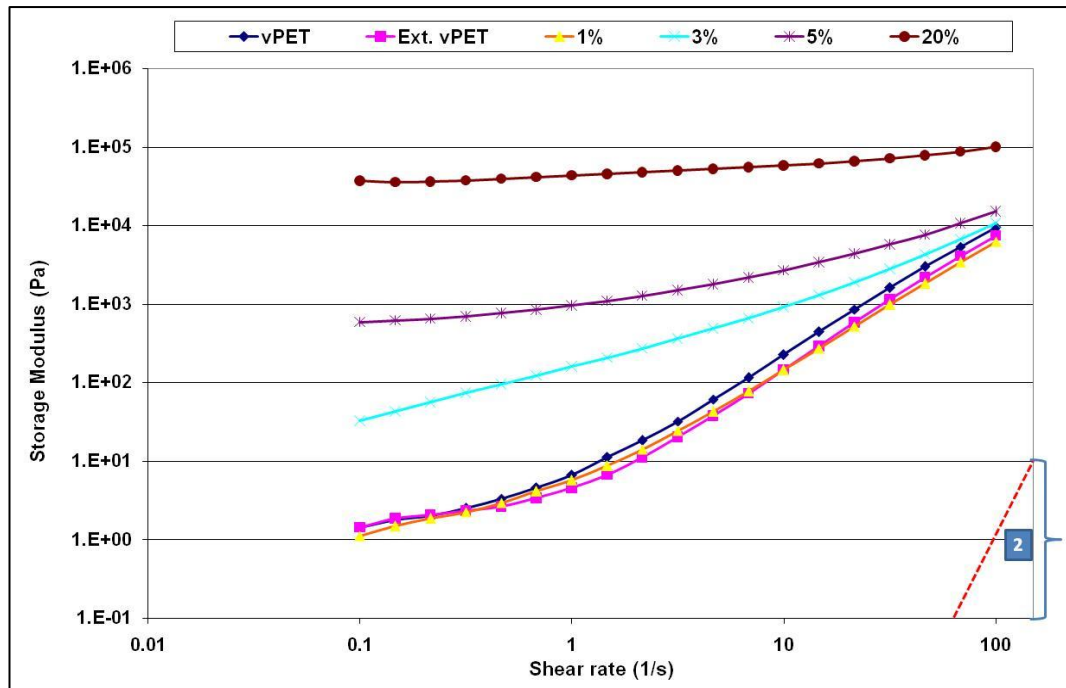


Figure 4.21 Storage modulus behaviour for PET/Cloisite 25A NC at different clay concentrations with low shear rate.

D. Storage modulus as a function of shear rate for different nano-fillers at certain loading concentrations

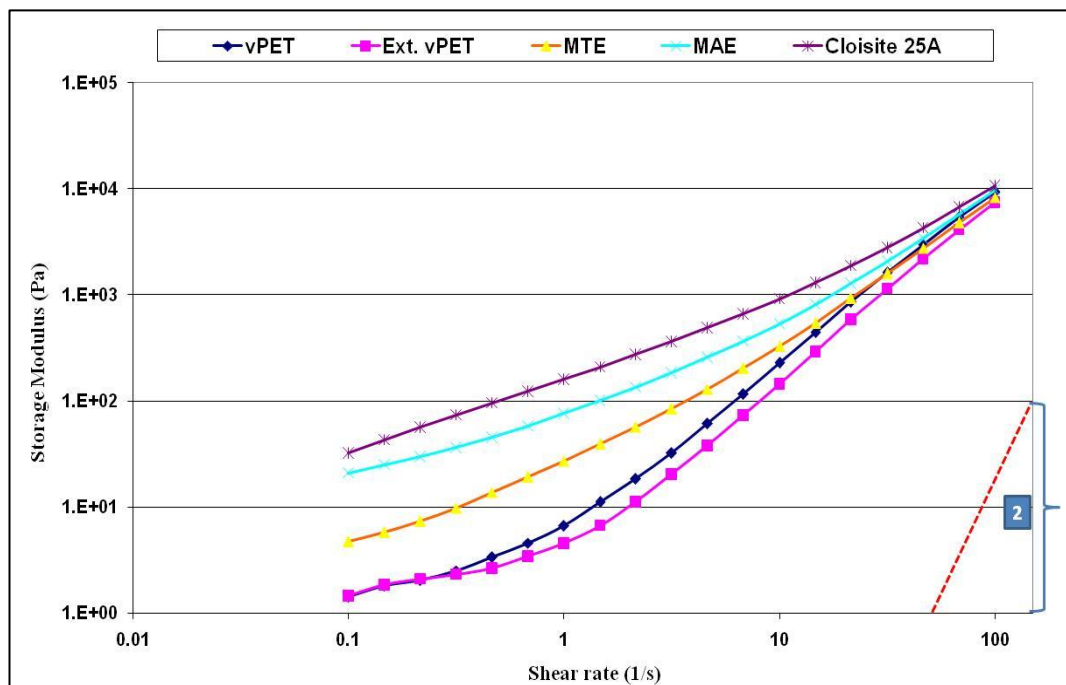


Figure 4.22 Storage modulus behaviour for PETNCs at 3 wt.% loading with low shear rate.

As discussed in section C and as figures 4.19 – 4.21 show, the percolation threshold started at a clay loading of around 3 wt.%. The percolation threshold decreases with increasing exfoliation [Cassagnau (2008)]. Figure 4.22 shows which clays form the network structure faster and have an absolute storage modulus value higher than other clays at the same concentration loading (3 wt.%). It is clear that PET/MTE shows the lowest G' value among the PETNCs at the same concentration (3 wt.%) which can be attributed to excellent exfoliation in the MTE case. This observation is further assisted by the good dispersion for MTE into the PET matrix shown by TEM images (see 6.4.1). Similar plots but at 1, 5 and 20 wt.% are presented in figures x4.7-x4.9 in appendix x4.

E. The Cole-Cole plot (G' vs. G'') for PET/CNT nanocomposites

This section shows the Cole-Cole plots (G' vs. G'') for PET/nanoclay nanocomposites at various concentrations. This plot is an effective method to explore the influence of adding a nano-filler on the structure of a PET matrix at a fixed temperature.

Figures 4.23–4.25 show a decrease in the slope of G' vs. G'' on increasing the nanoclay content and significantly increasing the storage modulus G' at a certain loss modulus G'' . The change in the slope of the curves is an indication of increasing the interaction between the PET matrix and the nanoclay platelets. For example the slope of the curve at content 3wt.% is near unity which implies that the PETNC at this point is rheologically heterogeneous and further energy can be dissipated. Furthermore, some slopes of the curves at high shear rates are nearer 2 which indicates that the rheological back to homogenous system, and this can be attributed to the effect of a high shear rate on the network structure, or in other words, the high shear rate induces a collapse in some interactions.

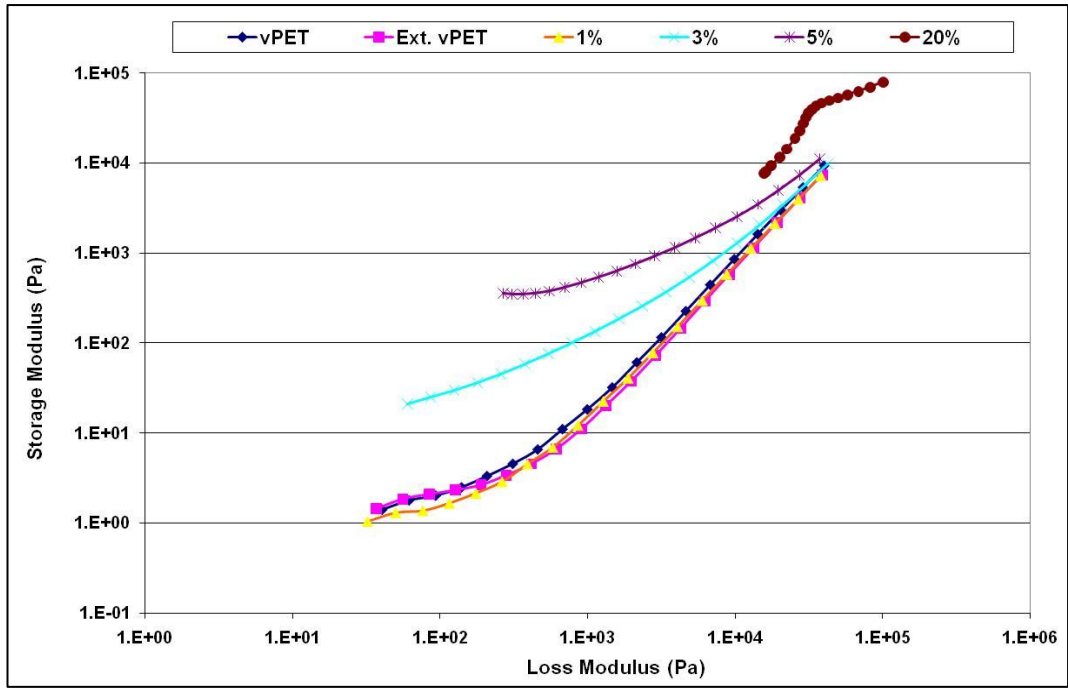


Figure 4.23 Cole-Cole plot for vPET, ext. vPET and PET/MAE nanocomposites at different clay concentrations.

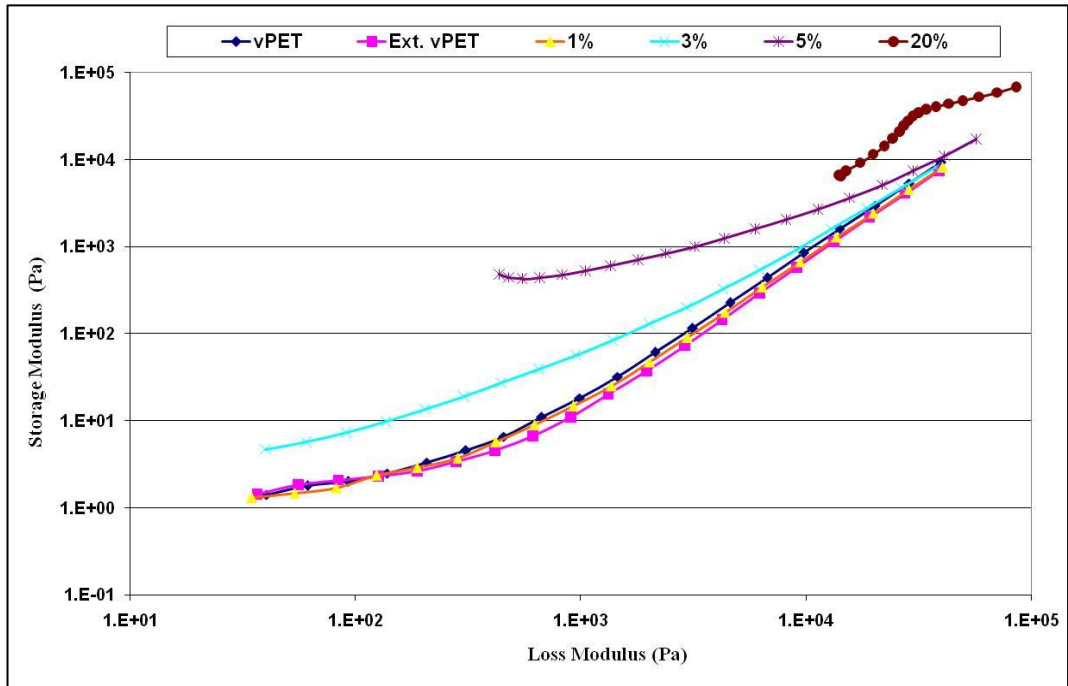


Figure 4.24 Cole-Cole plot for vPET, ext. vPET and PET/MTE nanocomposites at different clay concentrations.

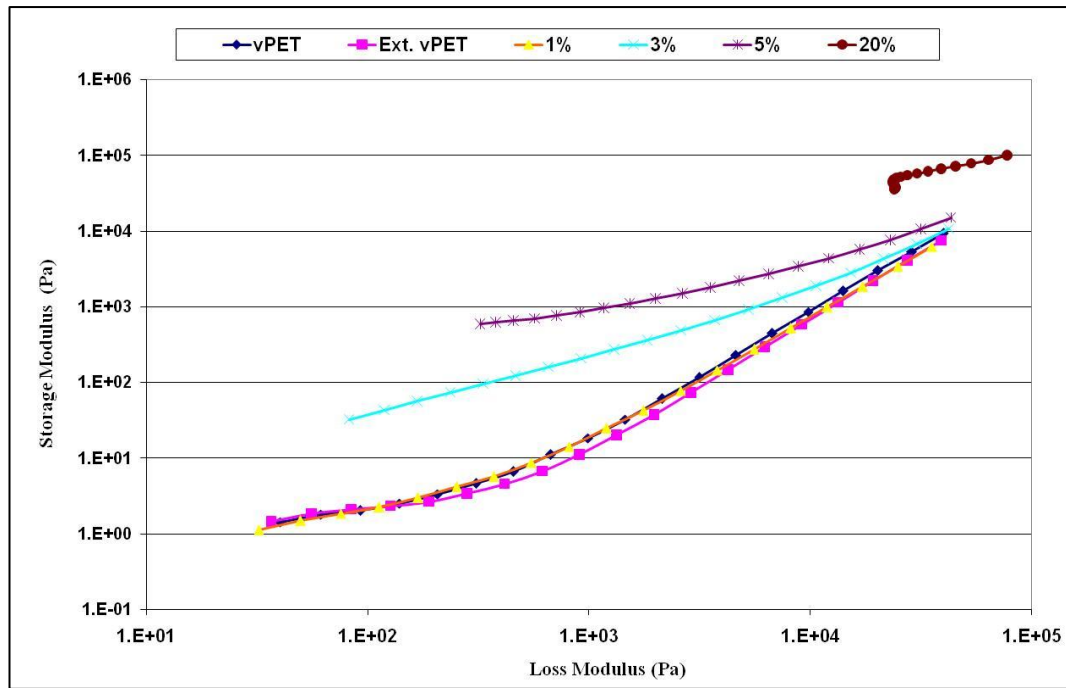


Figure 4.25 Cole-Cole plot for vPET, ext. vPET and PET/Cloisite 25A nanocomposites at different clay concentrations.

F. Storage and loss modulus behavior over low shear rates

This section shows the plots of the complex shear modulus (G' and G'') versus the shear rate. Figures 4.26 – 4.28 illustrate this relationship for all PET nanocomposites at various concentrations (3, 5 and 20 wt.%). Since the percolation threshold started at 3 wt.%, the un-filled PET and PETNC at 1 wt.% are not included in these figures. In general, figures 4.26 and 4.27 show that the absolute values of the storage modulus G' are always lower than those of the loss modulus G'' , indicating that the PET matrix is still dominant in determining the viscoelastic properties of PET nanocomposites (fluid-like behavior). However, figure 4.28 shows that PET/Cloisite 25A (20 wt.%) has an absolute value of G' that is always higher than that of G'' , which indicates strong solid-like behavior. In the same figure, this PETNC at 5 wt.% also tends to exhibit solid-like behavior at very low shear rates, but this changes on increasing the shear rate. This phenomenon may be due to the formation of a percolation network.

Some crossover occurs on increasing the shear rate, which can be observed at the higher clay loadings when loss modulus G'' becomes higher than storage modulus G' , resulting in a change from solid-like behavior to liquid-like behavior. This phenomenon can be attributed to the orientation of the nanoclay plates in the flow direction.

These results are in agreement with results presented by other researchers, such as Wu et al. (2005) and Tang et al. (2011).

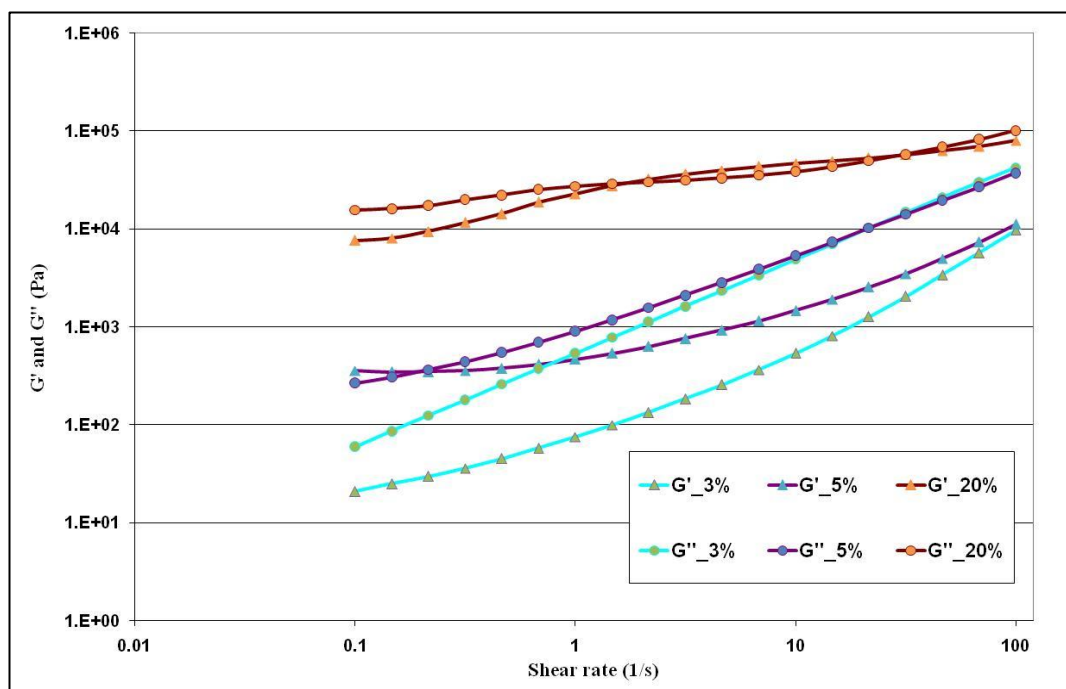


Figure 4.26 Storage and loss modulus behavior on increasing the shear rate for PET/MAE nanocomposites.

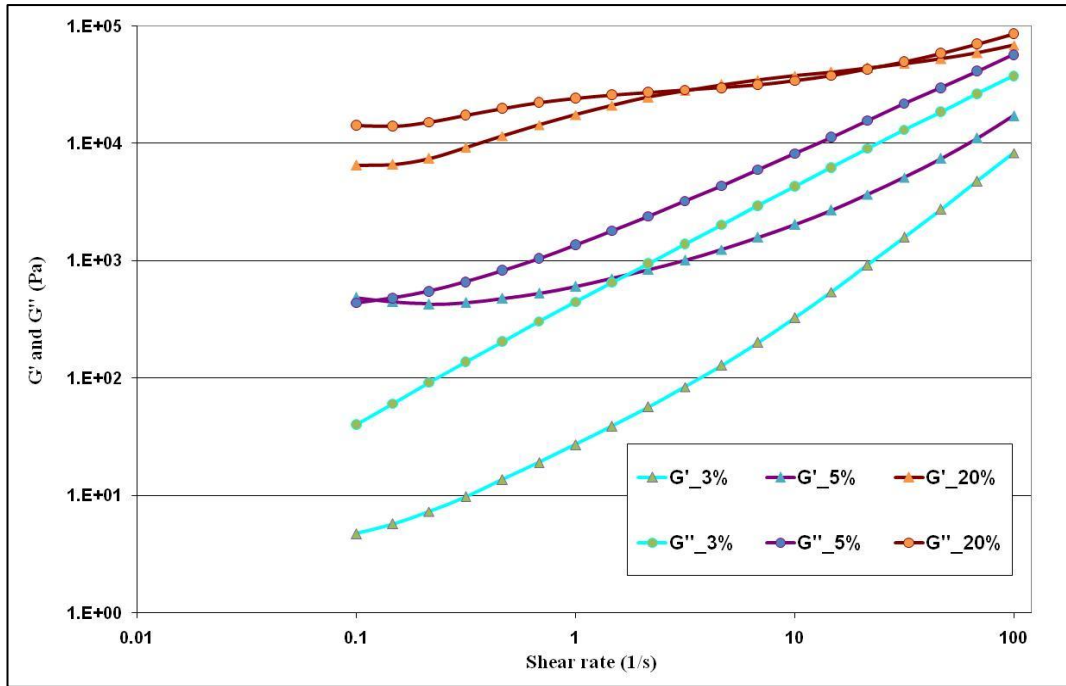


Figure 4.27 Storage and loss modulus behavior on increasing the shear rate for **PET/MTE** nanocomposites.

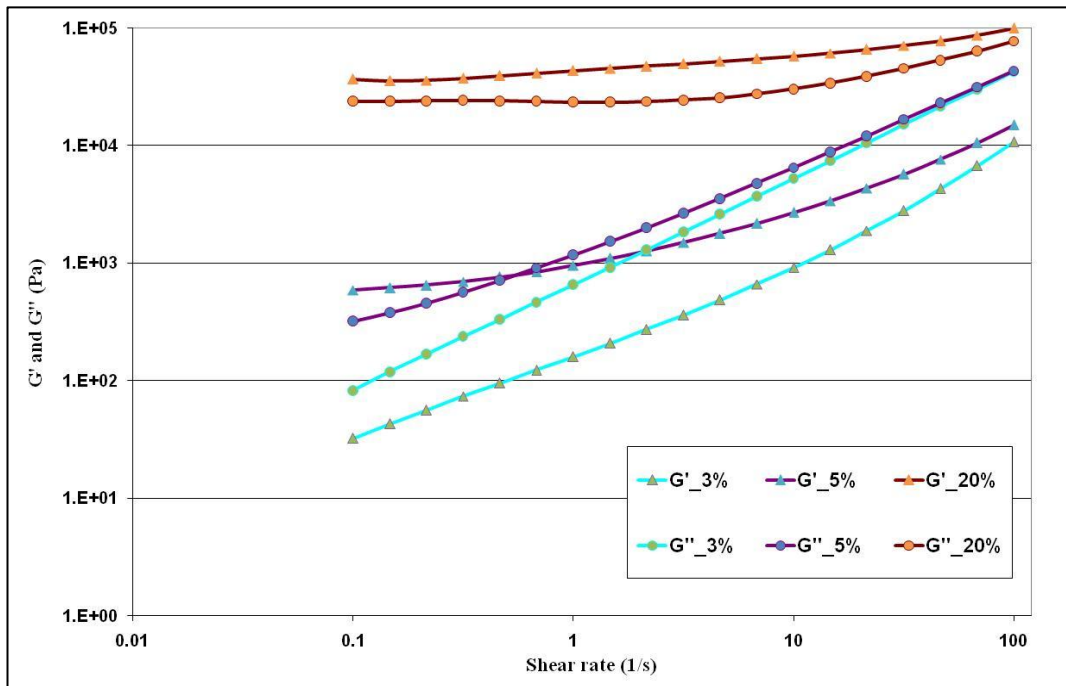


Figure 4.28 Storage and loss modulus behavior on increasing the shear rate for **PET/Cloisite 25A** nanocomposites.

G. The relaxation time (λ) of PET nanocomposites at various nanoclay concentrations

Another important rheological property is the relaxation time of the polymeric material. The relaxation time (λ) of the polymer can be calculated from the following equation (Equation 4.1) [Chae and Kim (2007)]:

$$\lambda = \frac{G'}{(\eta \cdot \dot{\gamma}^2)} \quad \text{Equation 4.1}$$

where η is the complex viscosity, G' is the storage modulus and $\dot{\gamma}$ is the shear rate.

Chae and Kim (2007) studied the rheological and thermal properties of PET/ferrite nanocomposites. The authors reported that the relaxation time of PET nanocomposites increased on increasing the ferrite content at very low shear rates, even with high ferrite content. They attributed this to the reduction in the polymer chain mobility at very low shear rates.

When the storage modulus G' of the polymer nanocomposites is higher than that for pure polymer this indicates the polymer NC matrix has big tendency to store energy rather than lose it as compared to the pure polymer. This behaviour tips about a possibility increase in relaxation time [Bhattacharya et al. (2010)].

Ray et al. (2005) studied the rheological behaviour of Poly [(butylenes succinate)-co-adipate] (PBSA)/Cloisite 30B. They found that the PBSANC (6 and 9 wt.%) tended to have a long relaxation time which suggests pseudo-solid-like behaviour. Krishnamoorti and Yurekli (2001) observed solid-like behaviour when the relaxation time was over 1000s and the filler content was greater than 6.7 wt.%. The authors attributed this phenomenon to the anisotropic nature of the silica layer which tends to form a percolation network at very low shear rates.

As figures 4.29 – 4.31 show, the relaxation time increased with decreasing shear rate, and this can be attributed to the reduction in PET chain mobility at low shear rates. The physical interaction between the PET chains and nanoclay platelets can be broken with increases in the shear rate, which can lead to shorter relaxation times.

While the relaxation time of PET/(MTE or MAE) at 20 wt.% is lower than that for PETNC at 5 wt.% at the lowest shear rate (0.1s^{-1}), as figures 4.29 and 4.30 show, the relaxation time of PET/Cloisite 25A at the same concentration and shear rate remain constant (see figure 4.31). This phenomenon can define the phase of the PETNC during the rheology test and can be correlated with the behavior of G' and G'' over low shear rates, as discussed in the previous section. Focusing on figures 4.29 and 4.26 (from the previous section), at a certain shear rate (0.1 s^{-1}) it is clear from figure 4.29 that the relaxation time of PET/MAE (5 wt.%) is higher than the relaxation time of PET/MAE (20 wt.%), and it is obvious for the same points in figure 4.26 that G' is higher than G'' for PET/MAE (5 wt.%) and lower than G'' for PET/MAE (20 wt.%). This indicates solid-like behavior of the material at a loading of 5 wt.%, while the PET/MAE (at shear rate 0.1s^{-1}) tends to exhibit fluid-like behavior at a loading of 20 wt.%. The same results have implications for PET/MTE relaxation time behavior as shown in figure 4.30.

On the other hand, at the same shear rate (0.1s^{-1}) and the same concentrations (5 and 20 wt.%) for PET/Cloisite 25A, the relaxation time did not decrease after a loading of 5 wt.%, and at the same time G' is greater than G'' for both loading concentrations at very low shear rates (figure 4.28). Increasing the shear rate leads to a change in the behavior of PET/Cloisite 25A (5 wt.%) from solid-like behavior to fluid-like behavior, and also a decrease in relaxation time, while for the same NC but at (20

wt.%) the NC kept its solid-like behavior even on increasing the shear rate as shown in figure 4.30.

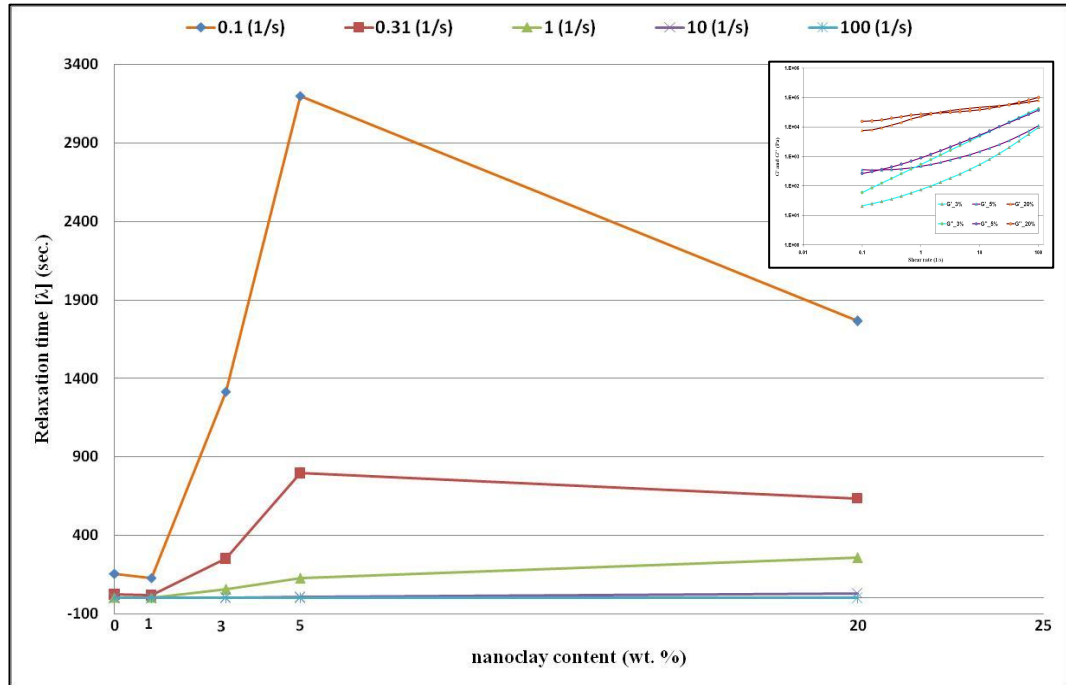


Figure 4.29 Relaxation time of PET/MAE nanocomposites at different composite loadings over several shear rates. (window, Figure 4.26)

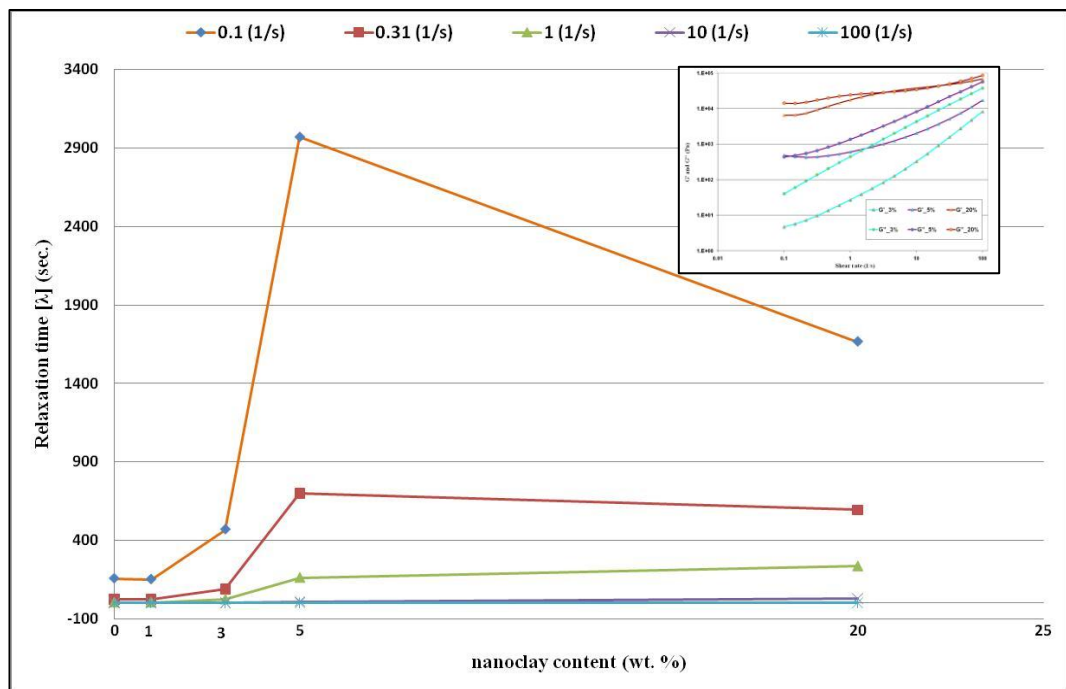


Figure 4.30 Relaxation time of PET/MTE nanocomposites with different composite loadings over several shear rates. (window, Figure 4.27)

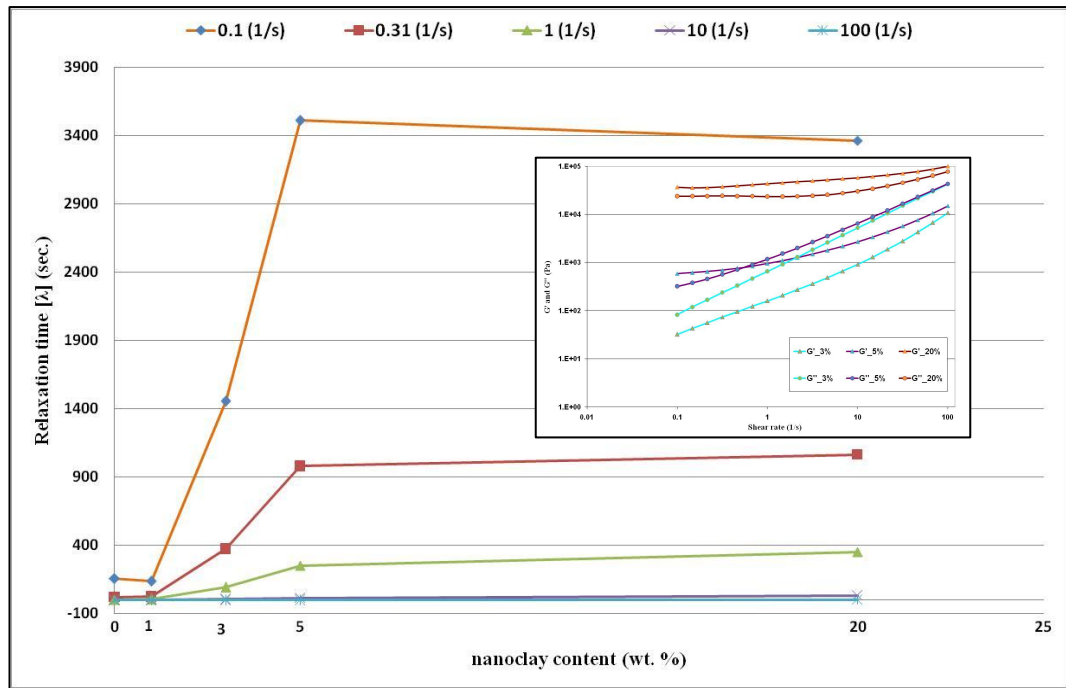


Figure 4.31 Relaxation time of PET/Cloisite 25A nanocomposites with different composite loadings over several shear rates. (window, Figure 4.28)

4.3.3 The Cox-Merz Rule

Generally for many polymer melts there is a close relationship between the shear viscosity $\eta(\dot{\gamma})$ and complex viscosity $\eta^*(\omega)$. In 1958 Cox-Merz introduced the following rule (Equation 4.2) [Mezger (2006)]:

$$\eta(\dot{\gamma}) = |\dot{\eta}^*(\omega)| \quad \text{Equation 4.2}$$

The Cox-Merz rule is of great value in polymer rheology. It can be used in many applications for many reasons such as:

- If an expensive oscillatory rheometer is not available, the complex viscosity can be predicted from the shear viscosity measurement.
- It is difficult to measure the shear viscosity for many polymers at high shear rates due to secondary flows, sample fracture etc., so the shear viscosity can be predicted from oscillatory measurements by the Cox-Merz rule.

- How close to or far from the rule the materials behaviour is can be used as an analytical tool to give a sense of the material structure.

Kelly et al. (2009) observed that polypropylene (PP) exhibits a correspondence between complex viscosity and shear viscosity as shown in figure 4.32.

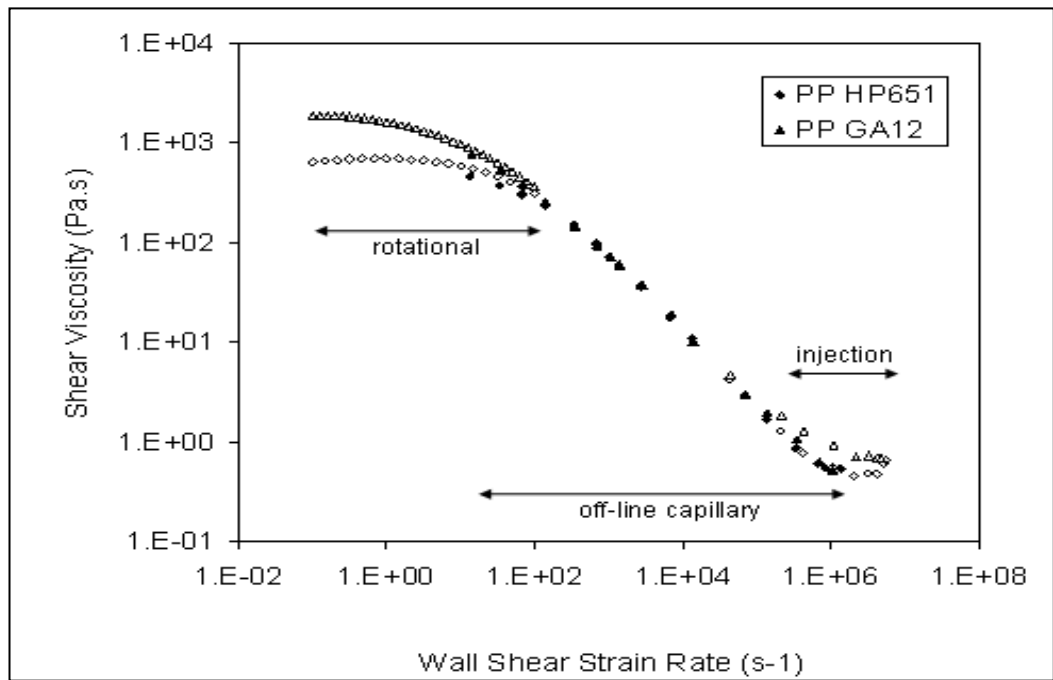


Figure 4.32 Shear viscosity of high density PP at 200 °C [from Kelly et al. (2009)].

Also Han et al. (1995) observed a good agreement with the Cox-Merz rule in homopolymer Polystyrene (PS), as shown in Figure 4.33.

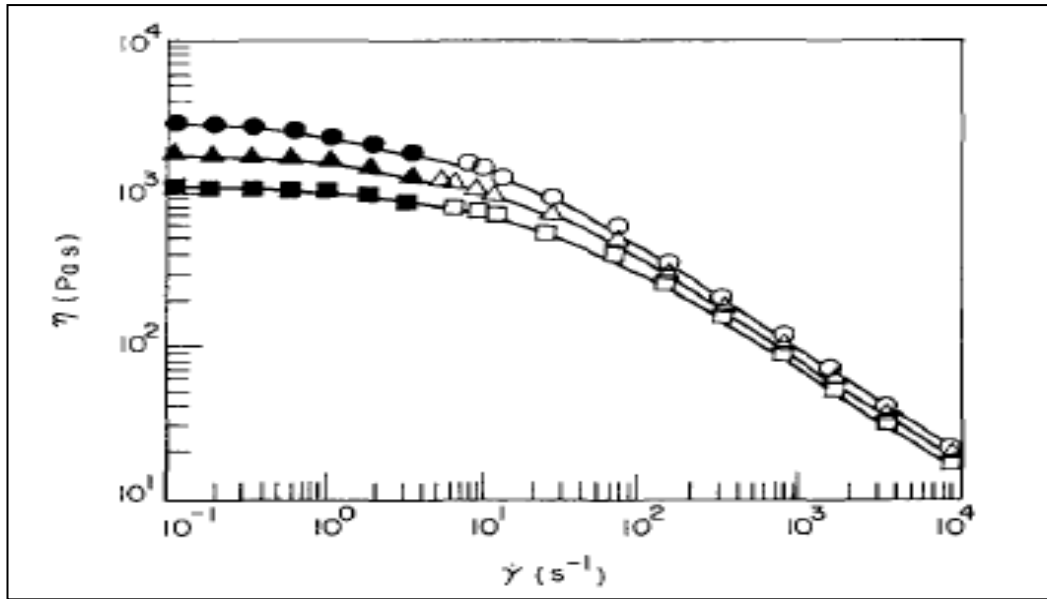


Figure 4.33 Plot of $\log \eta$ vs. $\log \dot{\gamma}$ for homopolymer PS [from Han et al. (1995)].

The Cox-Merz rule is not useful for complex structured fluids, such as liquid crystalline polymers, crosslinked polymer or gels [Larson (1999)].

Many researchers have proved the failure of the Cox-Merz rule in polymer nanocomposites and blends [Fornes et al. (2001)]. Han et al. (1995) studied the effect of flow geometry on the rheological properties of PS/PMMA (poly (methacrylate)) blends. They found that the logarithmic plots of shear rate vs. shear viscosity obtained by a capillary rheometer do not overlap those obtained by a cone-plate rheometer, and this is due to the difference in morphological states of PS/PMMA blends in the non-uniform shear flow in a capillary rheometer (due to the effects of die exit and entrance) versus the uniform shear flow in a cone-plate rheometer. No big changes were observed when the Bagley correction was used. Also, it was reported that the blends do not obey the Cox-Merz rule because the flow geometry affected the rheological behaviour of the blends, which exhibited different morphological states in the two rheometers. Krishnamoorti et al. (2001) observed a failure in this rule in polystyrene-polyisoprene block copolymer nanocomposites. Nakajima et al. (1977) reported deviations from the

Cox-Merz rule in carbon black/rubber composites. They observed that the complex viscosity obtained by dynamic shear measurements was higher than the shear viscosity measured by capillary rheometer, and attributed this to strain hardening with extension in the oscillatory rheometer.

Ray and Okamoto (2003) proposed two reasons to explain the deviations of polymer nanocomposites from the Cox-Merz rule. First, the nanocomposites tend to change the structure formation of the matrix when applying a dynamic oscillatory test. Second, while the Cox-Merz relation applies for many homogenous systems, polymer nanocomposites are a heterogeneous system. The Cox-Merz rule works for many polymers but the relation is not supported by a theoretical background that shows it must be obeyed by all polymers.

Figure 4.34 illustrates the shear viscosity vs. shear rate over a wide range of shear rates for vPET, ext. vPET and PET nanocomposites.

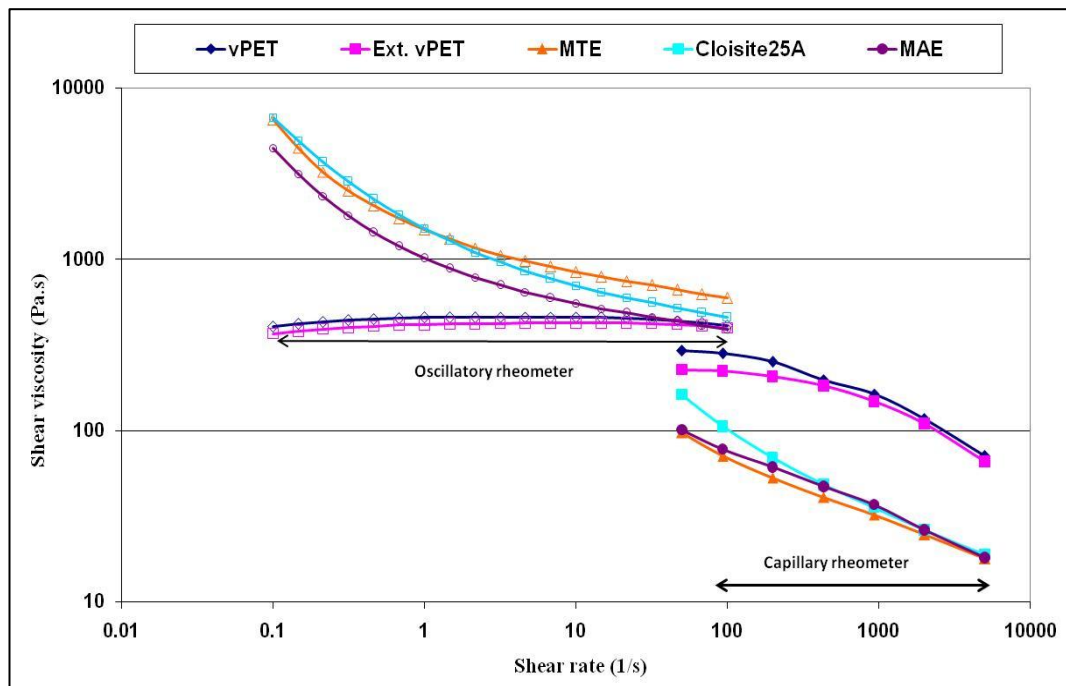


Figure 4.34 Plots of shear rate vs. shear viscosity for PET nanocomposites at 5 wt.% nano-filler concentrations.

The result revealed in figure 4.34 (also see figures x4.1-x4.3 in appendix x4) matches the results obtained by others [Nakajima et al. (1977) and Krishnamoorti and Yurekli (2001)] proving that the Cox-Merz rule does not hold for PET nanocomposites. However, un-filled PET also does not obey the Cox-Merz rule, as observed in previous figures, and this result is in agreement with the results of Xanthos et al. (2000).

4.3.4 Shear viscosity behaviour at fixed shear rates and varying clay concentrations.

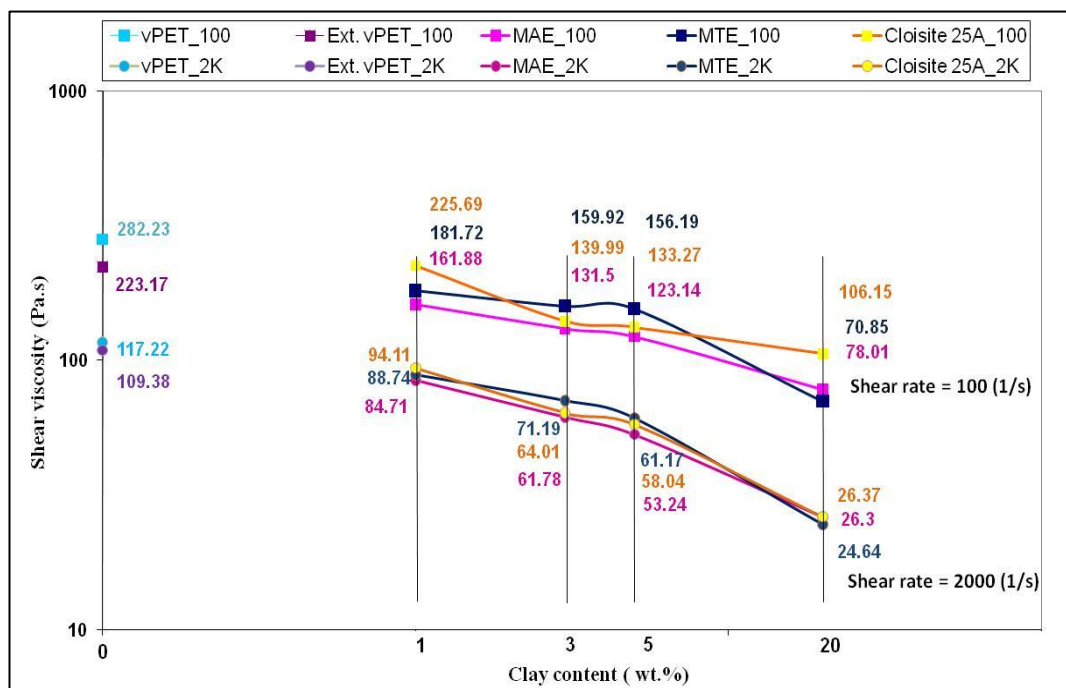


Figure 4.35 Shear viscosity as a function of nano-filler concentration at two constant shear rates (100 and 2000s⁻¹).

The aim of this section is to study the effect of adding different nanofillers at a variety of fill levels on the shear viscosity of PET at a constant shear rate. The shear rates were chosen (100 and 2000s⁻¹) to cover the range of shear rates in normal melt processing such as sheet extrusion and preform injection. The relationship between shear viscosity and clay content for different PET nanocomposites at shear rates 100 and 2000s⁻¹ is shown in figure 4.35. It is obvious that the shear viscosity decreases on adding more

nanofillers. For example, a 5 wt.% MAE loading gives a one-fold decrease in shear viscosity compared to ext. vPET at shear rate 100s^{-1} . Furthermore, increasing the shear rate leads to a decrease in shear viscosity for the same PETNC and loading level. For example, the shear viscosity for PET/MTE (3 wt.%) reduced by 55% when the shear rate increased from 100 to 2000s^{-1} . So prior to processing PETNC, knowing the shear rate is essential in predicting the viscosity of the melt in order to achieve a good final product.

Increasing the nanofiller content means increasing the small platelet size quantity, which means the platelets can easily align in the matrix on applying the shear rate. Therefore the viscosity slightly drops when compared to vPET or ext. vPET. Also due to working under high temperatures (260°C) there exists a possibility of degradation which may lead to a reduction in the molecular weight, and therefore a reduction in viscosity.

4.3.5 The intrinsic viscosity (I.V.) of polyethylene terephthalate (PET) nanocomposites

Intrinsic viscosity (I.V.) is one of the simplest, cheapest and most precise measurements in polymer science and it is one of the most important characteristics descriptors of PET. Intrinsic viscosity is related to the composition and molecular weight of the PET resin and it is a common description of PET flowability. When the PET has high I.V. the material becomes stiffer which means the chains are longer. During the polymerization process, the average chain length can be controlled and that affects the final I.V. value.

Mark-Houwink's equation (Equation 4.3) is used to calculate the molecular weight from the intrinsic viscosity value [Culbert and Christel (2003)].

$$[\eta] = K M^a \quad \text{Equation 4.3}$$

where $[\eta]$ is the intrinsic viscosity (I.V.), M is the molecular weight, and K and a are known as Mark-Houwink constants. There is a specific constant value for each solvent-polymer combination so it is not possible to use this equation to calculate the molecular weight of a newly invented polymer. On top of that, the constant (a) is affined to the stiffness of the polymer chains. So the polymer nanocomposites need another (a) value different from that of the un-filled polymer due to the presence of nanoclay platelets.

Sanches et al. (2005) evaluated the molecular weight of PET using different techniques such as solution intrinsic viscosity, intrinsic viscosity from melt flow (MFI) and size exclusion chromatography (SEC). The aim of their study was to obtain a correlation between the viscosity of diluted solutions and molecular weight. One of the main restrictions on obtaining this correlation is the presence of branched chains in the polymer structure. The authors found that the molecular weights measured by SEC and the M-H equation were different. This difference in the values was attributed to the different test parameters such as the temperature and solvents used in the tests. Based on their observations, the molecular weight of PETNC (pellets or film) cannot be calculated from the I.V. data obtained in this project.

Figure 4.36 shows the intrinsic viscosity (I.V.) of crystallized vPET and amorphous pellets of ext. vPET and PETNC at various clay concentrations. The test procedure is covered in section 3.5.4. It is worth mentioning that the I.V. measurement method for vPET at the Tergal Fibre Ltd. Company (PET supplier) is different from the method that SABIC used to measure the I.V. It is therefore not surprising that different values for

same material were observed. For example, the I.V. of vPET was found to be 0.8 dL/g at the producer's laboratory (Tergal) and 0.77 dL/g at the external laboratory (SABIC). This difference may come from the differences in solvent mixture ratios. While Tergal used 50/50 %, SABIC used 60/40 %.

The I.V. of the pellets was measured while in the amorphous phase (except vPET which was in the crystallized phase) in order to see the effect of the compounding process and avoid any inconsistency in the re-crystallisation process. The absolute value of I.V. of ext. vPET is expected to drop (see figure 4.36) compared with vPET for two reasons: first, the state of the pellets is amorphous, and second, the pellets were exposed to thermal processing which means a possibility of thermal-oxidative degradation during the compounding process, leading to a reduction in molecular weight. Furthermore, the absolute value of I.V. of PETNC reduced on increasing the clay concentration, and this reduction can be attributed to two reasons: first, the presence of clay platelets which align with the flow and increase the flowability of the dissolved solution during the I.V. test, and second, the possibility of thermal-oxidative degradation of nanoclay during the compounding, which can increase the magnitude of this reduction.

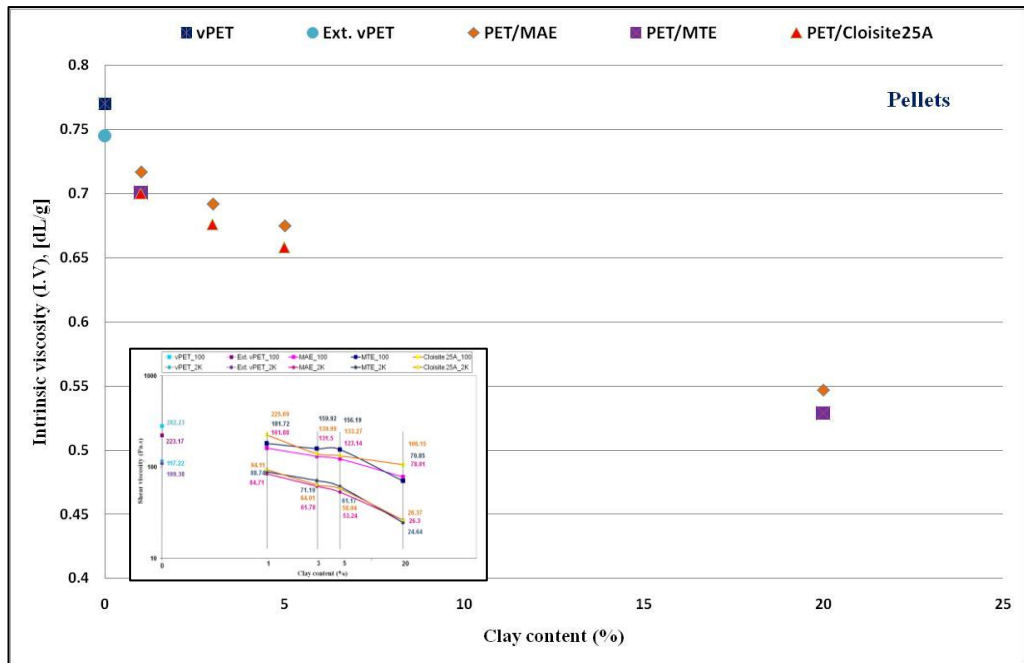


Figure 4.36 Absolute values of intrinsic viscosities (I.V.) of PET nanocomposites (pellets) at different clay concentrations. [Figure 4.35 in the window].

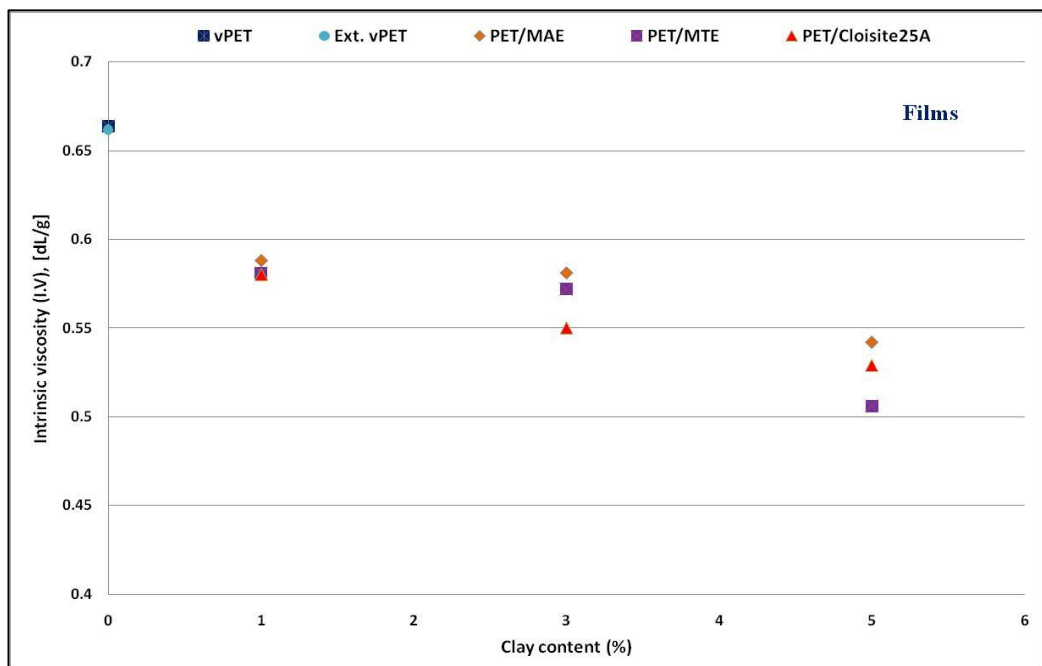


Figure 4.37 Absolute values of intrinsic viscosities (I.V.) of PET nanocomposites (amorphous films) at different clay concentrations.

The trend of the I.V. reduction is quite similar to the trend in the melt viscosity behaviour of PETNC which was obtained from the rheological behaviour of PETNC (figure 4.36 has both plots). Based on this observation, the capillary rheometer curves

can be used to predict the behaviour of the I.V. trend, but not the absolute values. Furthermore, figure 4.37 shows the intrinsic viscosity of amorphous films of un-filled PET and PETNC. It is clear that adding more clay leads to a reduction in the I.V. values. It is worth mentioning that the reduction in the I.V. values of the films compared to those of the pellets is due to the fact that the films were exposed to two melt processing stages (compounding and film casting), while the pellets were exposed only to the compounding process, which means more clay platelet alignment and an increased possibility of thermal-oxidative degradation. The absolute values of vPET film and ext. vPET film are quite similar, indicating the importance and the good efficiency of the re-crystallisation process carried out prior to the cast film processing for ext. vPET and PETNC amorphous pellets (see figure 4.37).

4.4 Conclusions

- Studying the rheological properties of unfilled PET and PET nanocomposites over a wide range of shear rates, as well as their behaviour on adding different clays with various concentrations were the main objective of this chapter.
- The importance of re-crystallising the amorphous pellets prior to investigation the rheological properties of PET was proved.
- At high shear rates, it is clear that the absolute value of the melt viscosity of PETNC is significantly lower than for un-filled PET, and the extent of this reduction increases with adding more nano-filler at a given shear rate. This reduction follows the shear thinning behaviour which shows the dependence of the shear viscosity for the un-filled PET and PETNC on the shear rate.
- Shear thinning behaviour occurred at high shear rate can be explained by two mechanisms which can occur simultaneously. The first mechanism proposed is that some polymer has entangled or oriented molecular chain at rest. When applying high shear rates, the level of entanglements is reduced and the molecular chains tend to orient with the flow direction. The other mechanism is the presence of the nanoparticles. The nanoparticles align with the flow direction at high shear rate.
- At high shear rate, Somasif MAE clay exhibits the maximum reduction in the shear viscosity of PET compared with the other clays used. This observation may be attributed to either the fast alignment of MAE platelets with the flow direction due to the large gap (d-spacing) between the platelets when compared to the other nanoclays used, or to the higher degradation level of PETNC in the presence of MAE due to high surfactant content, or to both causes.

- The rheological test shown a big reduction in the viscosity of amorphous pellets or un-dried crystallised pellets which prove the importance of re-crystallised/dried the pellets prior the melt processing.
- At low shear rates, the magnitudes of the complex viscosity are dependent on the nanoclay concentrations and processing shear rate. The nanoclay leads to increases in complex viscosity with increases in the clay loading above 1 wt.%. The vPET, ext. vPET, and PET nanocomposites (1 wt.%) and PET/MTE (3 wt.%) exhibit Newtonian behaviour for low shear rate ranges. The complex viscosity started to deviate from Newtonian behaviour and behaved in a shear thinning manner at a 3 wt.% concentration. Usually the formation of aggregates is responsible for an increase in complex viscosity.
- Storage and loss moduli for the PETNCs show a significantly diminished shear rate dependence and this becomes more obvious on increasing the clay content. The polymer transfers from fluid-like to solid-like behaviour at certain filler concentrations, this phenomenon being known as the percolation threshold. From the results presented it seems that the percolation threshold is reached approximately at 3 wt.% loading.
- PET/MTE shows the lowest storage modulus value among other PETNCs at the same concentration (3 wt.%) or in other word lowest percolation threshold, which can be attributed to an excellent exfoliation occurs in MTE case.
- Cole-Cole plots has been used to explore the influence of adding a nano-filler on the structure of a PET matrix at a fixed temperature. The change in the slope of the curves is an indication of increasing interaction between the PET matrix and the nanoclay platelets. The slope of the curve at 3 wt.% content is near unity which implies that the PETNC at this point is rheologically heterogeneous and

further energy can be dissipated. Furthermore, some slopes of the curves at high shear rates are nearer 2 which indicates that the rheology is that of a homogenous system, and this can be attributed to the effect of a high shear rate on the network structure, or in other words, the high shear rate induces a collapse in some interactions.

- The behaviour of storage and loss modulus over low shear rate used to explore the behaviour of the PETNC. When the storage modulus higher than the loss modulus indicates strong solid-like behaviour and the opposite case indicates that the PET matrix is still dominant in determining the viscoelastic properties of PET nanocomposites (fluid-like behaviour).
- The relaxation time of the PETNCs increased with decreasing shear rate, this being attributed to the reduction in PET chain mobility at low shear rates. The physical interaction between the PET chains and nanoclay platelets can be broken with increases in the shear rate, which can lead to shorter relaxation times.
- The rheological results over a wide range of shear rates show that the Cox-Merz rule does not hold for PET nanocomposites or induced for unfilled PET.
- The absolute value of intrinsic viscosity (I.V.) of PETNC reduced on increasing the clay concentration, and this reduction can be attributed to two reasons: first, the presence of clay platelets which align with the flow and increase the ‘flowability’ of the dissolved solution during the I.V. test, and second, the possibility of thermal-oxidative degradation of nanoclay during the compounding, which can increase the magnitude of this reduction.

Chapter Five

5. Thermal properties of polyethylene terephthalate (PET)

The thermal properties of PET nanocomposites (PETNCs) in the amorphous, semi-crystalline and melting phases on adding nanoclay content were studied and the results presented and discussed in this chapter. In order to understand these results, it is appropriate to present some introduction and definitions regarding the fundamental features of these polymer phases.

5.1 Introduction

Polyethylene terephthalate (PET) exhibits three phases on increasing the temperature from ambient temperature to 280°C as follows: firstly an amorphous phase, secondly a semi-crystalline phase and third the melt phase. Prior to presenting the results on thermal properties, the fundamental qualities of these phases are discussed. Since the semi-crystalline structure can affect the properties of the final product significantly and the nanoclay can have a significant effect on the crystallisation temperature and overall crystallinity, most attention has been given to this state.

5.1.1 Amorphous phase

There are two types of polymer morphology in the solid state: that for a semi-crystalline polymer and that for an amorphous polymer. Sperling (2006) reported that the older literature often referred to the amorphous state as a liquid state. In an amorphous polymer, the molecules are twisted together and oriented randomly. A polymer with an amorphous morphology tends to have a transparent appearance. If the amorphous polymer is linear, it will flow above the glass transition temperature (T_g). It is usually a hard, clear, rigid material with low shrinkage and low impact strength; examples are

polystyrene (PS) and polycarbonate (PC). Semi-crystalline polymers are made up of discrete crystal structures in coexistence with regions of amorphous chains. In this amorphous region, the polymer does not contain any crystalline structure and does not exhibit any crystalline pattern upon application of x-ray diffraction techniques.

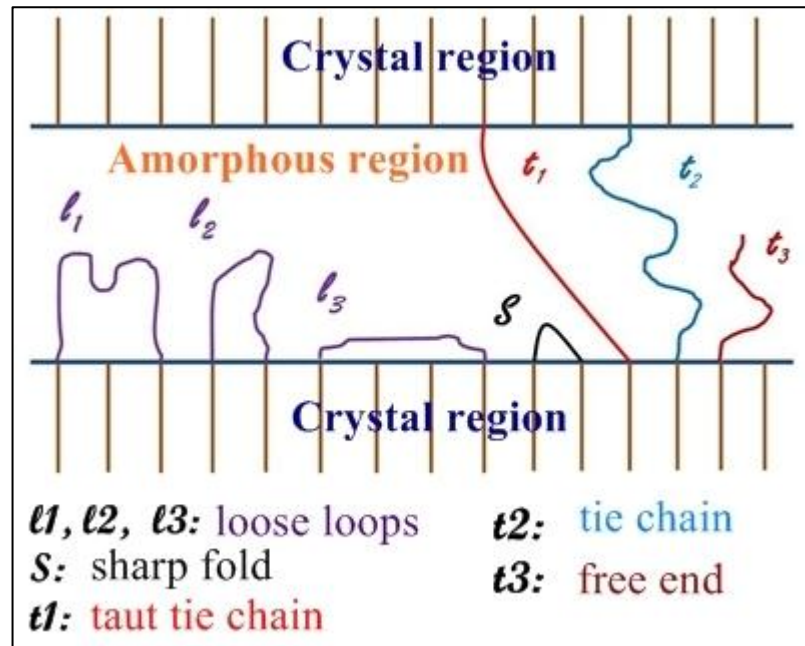


Figure 5.1 Schematic representation of the different types of amorphous chain.

For a semi-crystalline polymer the amorphous region different chain types, as shown in figure 5.1. Some kinds of chain connect between two different crystal regions while others have a loose loop state.

Usually, amorphous PET (e.g. amorphous pellets, bottles etc.) have left the brittle glassy state and take on a tough and brittle state as the temperature is raised above the glass transition temperature (T_g). When there is sufficient thermal energy in the polymer matrix to create enough free volume to allow sequences of a few chains of the polymer to move as a unit, the glass transition occurs. Actually, it is more important to know and understand the glass transition temperature (T_g) than the melting point, because

knowing T_g tells us how the polymer behaves at ambient temperature and about the limitations of the PET application temperature. The T_g for PET is about 75°C.

5.1.2 Melting phase

The melt phase of polyethylene terephthalate (PET) is an amorphous state and an isotropic liquid. PET transfers from solid phase (semi-crystalline) to a molten phase as the temperature is raised above the melting temperature (T_m) which is around 250°C. The melting temperature and melt state of PET have received relatively good attention in the polymer science literature, probably because PET is very sensitive to high temperatures which may lead to thermal degradation. Furthermore, the melting step in polymer processing is usually the rate-controlling step. In other words, the melting process consumes 70-80% of the energy used in the processing.

5.1.3 Semi-crystalline polymers

Usually, polymers have some irregularity in their structure so they cannot be 100% crystallised. The amount of the crystalline material is expressed as a percentage. Semi-crystalline polymers have both regions (amorphous and crystalline) and combine the flexibility of the amorphous state with the strength of the crystalline forms.

PET is a semi-crystalline polymer whose morphology can vary widely depending upon the fabrication process. Amorphous thermoplastic materials such as polycarbonate tend to be transparent, while crystalline thermoplastic materials such as polyethylene tend to be opaque. PET is a unique thermoplastic material. Since depending on the processing conditions, PET can be an amorphous or semi-crystalline material. Furthermore, the crystalline structure of PET material can exist in a clear or opaque state.

The crystal structures of PET materials are either rod-like in shape (small size) or spherulitic (large size). The spherulitic shape is induced by heating the amorphous region while the rod-like shape is induced by biaxial orientation or molecular strain. The rod-like crystal has a wavelength smaller than light and the spherulitic form has a wavelength larger than light. Consequently, light passes through the rod-like crystal shape without any reflection which gives it transparency while the spherulitic crystal shape reflects most of the light trying to pass through the wall [Brody and Marsh (1997)].

The polymer can be obtained as a “glassy” or “amorphous” transparent solid by rapidly quenching the melt below the glass transition temperature. However when the polymer is heated above its T_g , it crystallises rapidly forming an opaque material exhibiting spherulitic crystalline morphology. This morphology can also be obtained by slow cooling of the polymer melt. The crystallinity is usually induced by heating from the glassy state and is often accompanied by orientation. The conversion of PET into most commercial products requires that the polymer be highly crystalline. Fast crystallization melt becomes a crucial factor when these systems are processed from the melt. A fast crystallization response is favourable from an economic perspective as it leads to lower cycle times.

Ke et al. (2007) reported that PET has molecular chains connected with aromatic ethyl and ester groups. The twist or torque motion between PET rigid aromatic segments and the ethyl connector greatly slows down its crystallization rate and prolongs its processing cycle. Xanthos et al. (1997) reported that the maximum growth rate of the spherulites for PE is $5000\mu\text{m}/\text{min}$ while it is only $10\mu\text{m}/\text{min}$ for PET.

In the injection moulding process, a polymer melt is injected into a cold mould and crystallisation occurs during cooling in the mould. When a polymer has a fast crystallisation, it is an ideal candidate for injection moulding applications. Many factors affect the final crystalline morphologies such as the cooling and shearing conditions of the injection step. Thus it is essential to understand the crystallization process and to be able to predict it under different moulding conditions.

Crystallization consists of nucleation followed by crystallite growth. Nucleation is very important in determining the final crystalline morphology. In many cases where there is a deliberate attempt to control the properties of a given polymer by manipulating its morphology, it has been achieved via the use of nucleating agents.

In general, nucleation represents the initial step of a phase transformation and can be defined as “The formation of short range ordered polymer aggregates in a melt or solution, which act as growth centers for crystallization.” [Gooch (2007)].

The first step crystallization is the formation of the primary nuclei. This is followed by the continuation of the crystallisation process on the growth surface by induction of more polymer molecules. Nucleation at an edge is called tertiary nucleation.

When all nuclei start forming at approximately the same time, this is called athermal nucleation, and it leads to spherulites of roughly the same size. When the nuclei start forming at different times, this is called thermal nucleation, and leads to different spherulitic sizes.

I. Nucleation classification

Sharples (1966) classified nucleation into two types: homogenous and heterogeneous.

A. Homogeneous nucleation

The homogenous nucleation process occurs with much more difficulty in the interior of a uniform substance. Homogenous nucleation phenomena occur when there is no second surface or existing nuclei present, and the nuclei formation takes place spontaneously due only to supercooling.

B. Heterogeneous nucleation

Chatterjee et al. (1975) reported that heterogeneous nucleation arises from adventitious impurities, either randomly distributed throughout the bulk, or possibly localized on a surface. Crystallization of polymers usually takes place via heterogeneous nucleation, because of the large amount of impurities (catalyst residues, etc.) present that act as substrates for nucleation.

In the case of PET some chemical interaction has been observed between the polymer melt and certain nucleating agents. Whelan (1994) defined a nucleating agent as an additive used to increase the crystallization rate in the polymers by increasing the number of nuclei at which crystal growth is initiated (nucleation density). In this project, the nanoclay additives were used as nucleating agents; therefore the nucleation of PET can be categorized as heterogeneous.

For thermodynamics, it is useful to consider the Gibbs free energy of any system related to the enthalpy and entropy (Equation 5.1):

$$G = H - T.S$$

Equation. 5.1

where G is Gibbs free energy, a thermodynamic quantity which can be used to determine if a reaction is spontaneous or not, H is the enthalpy, S is the entropy and T is the temperature.

In the nucleation step, a few molecules pack together to form a crystalline embryo. This process will change the Gibbs free energy; the incorporation of molecules in the crystal will cause a decrease in G , while the creation of a crystal surface will cause an increase in G , as Figure 5.2 shows.

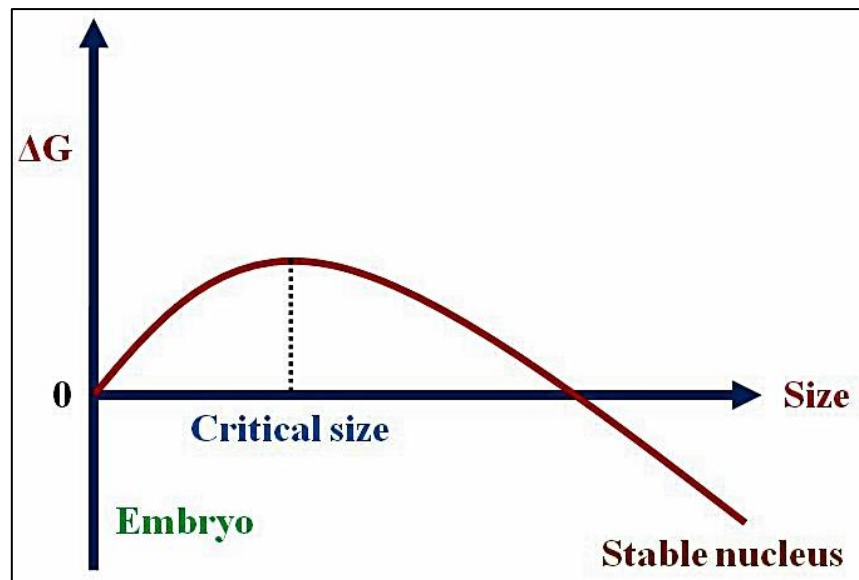


Figure 5.2 The change in free energy for the nucleation process during polymer crystallisation.

The peak in the curve may be regarded as an energy barrier. The stable nucleus in primary or secondary nucleation needs to overcome the free energy crystallisation barrier in order for formation to take place.

Once the nucleus is greater than the critical size it will grow spontaneously as this will cause G to decrease.

II. Structure of semi-crystalline polymers

Historically, the study of polymer crystallinity was important in proving the macromolecular hypothesis developed in 1922 by Staudinger [Mulhaupt (2004)].

Daubeny et al. (1954) found that the pure polyethylene terephthalate (PET) crystal belongs to the triclinic system (Figure 5.3). The cell dimensions are [Daubeny et al. (1954)]:

$a = 4.56 \text{ nm}$, $b = 5.94 \text{ nm}$, $c = 10.75 \text{ nm}$ with the angles being $\alpha = 98.2^\circ$, $\beta = 118^\circ$, $\gamma = 112^\circ$.

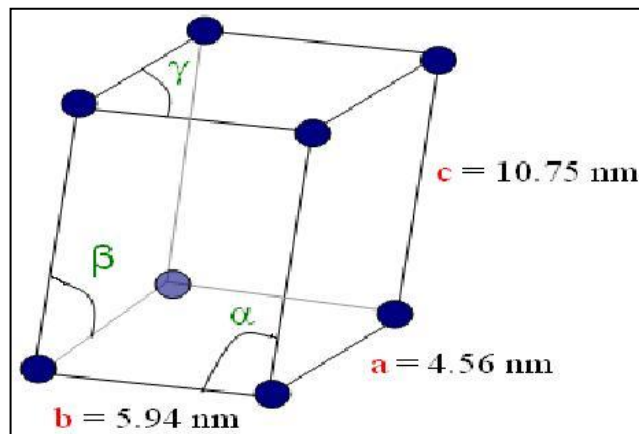


Figure 5.3 The triclinic crystal structure of PET.

Goltner (2003) reported that the triclinic crystal structure for the PET gave a crystalline density of 1.455 g/cm^3 , while the amorphous density is 1.335 g/cm^3 .

III. Crystallization from the melt

The lamellar shaped single crystals are formed when polymers are crystallized from the melt. In most polymers processing, the most obvious of the observed structures are the spherulites. Odian (2004) described spherulites as having a complex, polycrystalline structure, as shown in figure 5.4. As the name implies, spherulites are sphere-shaped crystalline structures that form in the bulk [Sperling (2006)].

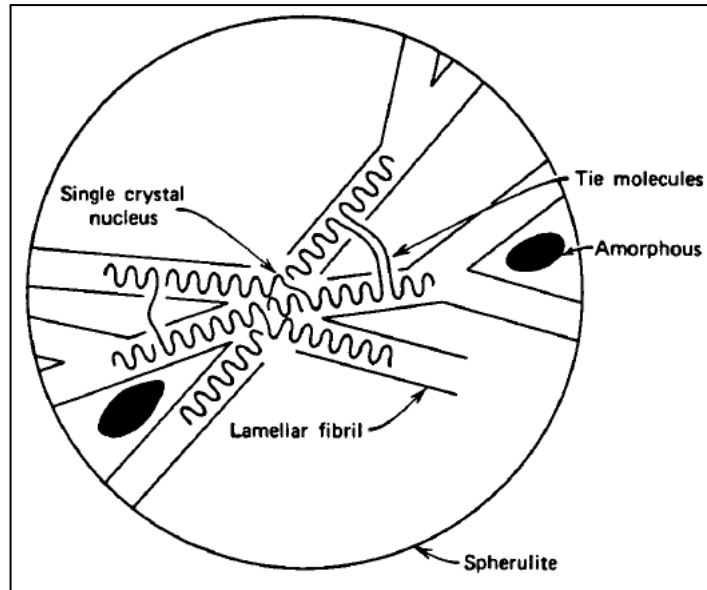


Figure 5.4 Structural organization within spherulites in melt-crystallized polymers [O'dian 2004].

The spherulites are really spherical in shape only during the initial stages of crystallization, while during the later stages the spherulites impinge on their neighbours. When the spherulites are nucleated simultaneously the boundaries between them are straight, but if the nucleation happens at different times the boundaries form hyperbolas, due to their different sizes when impinging on one another.

On cooling from the melt, the single crystal structure is the first structure formed. During the early stages of the growth of polymer spherulites, the single crystal structures divert into sheaf-like structures, and this represents an intermediate stage in the formation of spherulites. Figure 5.5 shows the development of a spherulite. Row (a) represents the edge-on view of the growth of a spherulite while row (b) represents the flat-on view. Row (a) column (III) and row (b) column (III) illustrate the intermediate stage (sheaf-like structure).

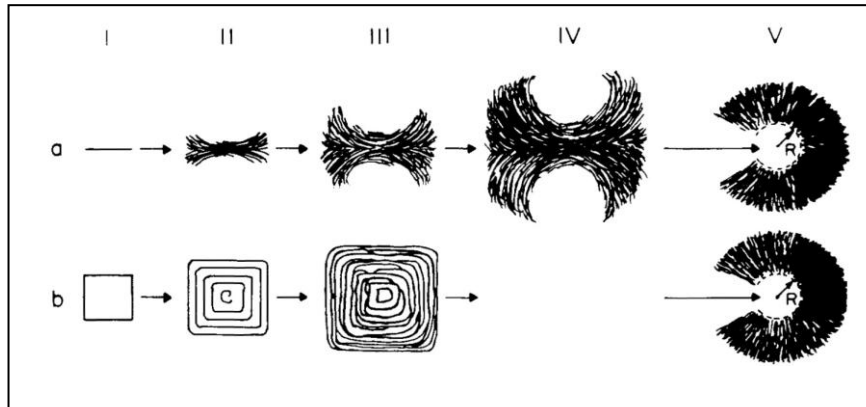


Figure 5.5. Schematic development of a spherulite from a chain-folded precursor crystal. Rows (a) and (b) represent, respectively, edge-on and flat-on views of the evolution of the spherulite [Sperling (2006)].

IV. The mechanism of PET crystallization

In the PET crystallisation mechanism, Brink (2003) proposed that the effective nucleation was either due to hydrolysis of PET or to the localized supercooling of PET by released water in the vicinity of the particles.

Two regions can describe the crystallization rate of polyethylene terephthalate. Figure 5.6 illustrates the spherulitic growth curve as a function of temperature.

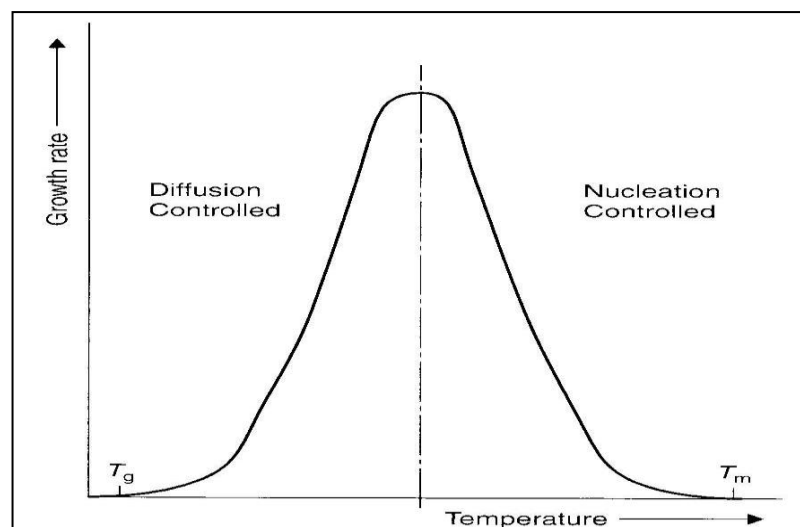


Figure 5.6 Spherulitic growth as a function of temperature [Brink (2003)].

As the PET cools from the melt during the moulding process, it is obvious that it first transitions into the nucleation-controlled region and the crystallization process begins. Often in a spherulitic microstructure, the crystal lamellae structure grows from each nucleation site. In this region, the lamellar growth rate is the slow step in the overall crystallization process.

For better mechanical properties and more rapid crystallization a high level of nuclei is needed [Brink (2003)]. Some PET chains incorporate into more than the lamellae due to the growth and impingement of spherulites on one another. These chains are called “tie chains” which can concentrate and distribute stresses throughout the material, effectively increasing the toughness of the resin.

The crystallization of PET first involves the formation of nuclei and their subsequent growth, whether heating amorphous PET from the glassy state or cooling from the melt state. The lamellae form by radiating outward from the nucleus by chain folding normal to the direction of growth, as figure 5.7 shows.

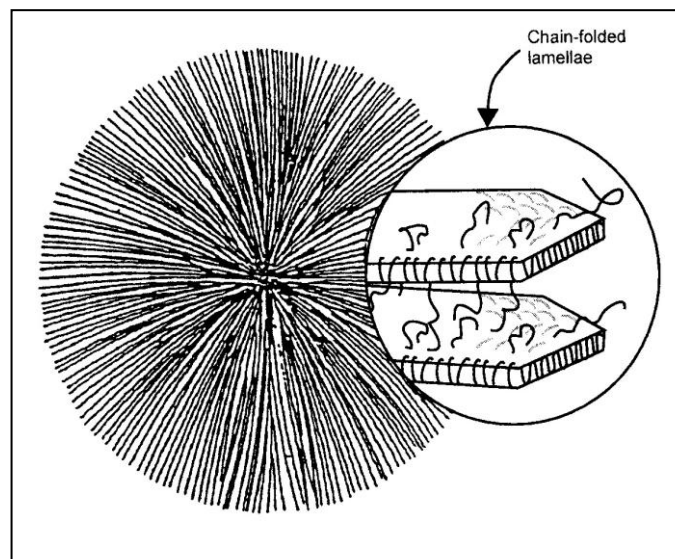


Figure 5.7 Illustration of a spherulite growing into a melt [Culbert and Christel (2003)].

The spherulites spread at the expense of amorphous material until surface impingement with other spherulites occurs, thereby limiting further growth.

Crystallizing the PET from a glassy state by the thermal method leads to an isotropic structure while the anisotropic structure can be achieved by drawing, as Kattan et al. (2001) reported.

5.2. Thermal properties of the polymer nanocomposites (literature review)

The thermal properties of polymer nanocomposites have received wide attention in the literature because changing any thermal properties of the polymer (e.g. glass transition or crystallisation temperature) affects the melt processing parameters and the properties of the final product.

Natarajan and Wu (1994) stated that the slow crystallisation rate of PET hindered crystallisation at low moulding temperatures (below glass transition (T_g)). Injecting PET melt in a mould at low temperatures (e.g. 27°C) leads to completely amorphous PET products, and reheating above T_g reduces the dimension stability of the final part. In order to avoid sticking of the PET inside the hot mould (above the T_g), it is necessary to increase the crystallisation rate. However, some undesired properties of the PET final product can result, due to over-increasing the crystallisation rate. When the crystallisation rate becomes too fast, the final product is hazy, especially at high nanofiller concentrations. Therefore it is very important to control the crystallisation rate of PET nanocomposites by controlling the nanofiller loading level or the nanofiller type, or by modifying the nanofiller.

Recently, many researchers have given attention to the thermal behaviour of polymer nanocomposites. The incorporation of nanofillers (e.g. MMT, CNT) not only enhances the properties of the polymer but it also alters the crystallisation properties.

Chan et al. (2002) studied the thermal and mechanical properties of a polypropylene (PP) nanocomposite (CaCO_3). They observed that the melting temperature of the PP did not change on adding CaCO_3 while the crystallisation temperature significantly increased by 10°C . They attributed this to the filler acting as a nucleating agent. The absolute value of the crystallisation did not change with adding the filler. Cho and Paul (2001) investigated the rheological, mechanical and thermal properties of nylon 6 nanocomposites (MMT, organoclay and glass fibre). Differential Scanning Calorimetry (DSC) results exhibited a slight (negligible) change in the glass transition temperature (T_g) and melt temperature (T_m) in the presence of fillers. The fillers acted as nucleation agents, leading to increases in the crystallisation rate and crystallisation temperature (T_c) compared with neat nylon 6.

PET/silica nanocomposites were prepared and characterized by Liu and Tian et al. (2004). The PETNC was prepared via in-situ polymerisation at two low silica contents (0.5 and 2.5 wt.%) and the thermal properties were analysed using DSC. The authors observed significant changes in the thermal properties with the crystallisation temperature increasing by 15 and 18°C for PET/silica (0.5 and 2.5 wt.%) respectively, compared with neat PET. They found that the melting temperature of PETNC increased by 9 and 11°C with adding 0.5 and 2.5 wt.% respectively. The authors attributed this significant change in T_m to the good dispersion of the fillers which can enhance the PET segment during crystallisation and lead to formation of a good crystal structure. An increase in the melting temperature was also observed by Mucha and his co-workers in a study of the crystallisation of isotactic PP on adding carbon black [Mucha et al.

(2000)]. The authors attributed the increase in T_m to the iPP chains forming perfectible crystals on adding carbon black, which may lead to a hindrance or delay in the beginning of T_m .

Li et al. (2006) however did not observe any significant change in the melting temperature of PET when compounded with carbon nanotubes (CNT). The obvious change was in the crystallisation temperature (T_c) because the nanotubes act as nucleating agents for the crystallisation. Moreover, this change was obvious with lower carbon nanotube contents (0.5 wt.%) in PET, and the increases in crystallisation temperature became slower with adding more CNT. Increasing the concentration of CNTs means that most of the CNTs will form networks.

Kracalik and Kovarova et al. (2007) studied the rheological, mechanical and thermal properties of recycled PET (rPET) and its behaviour on adding nanoclays, and compared this with virgin PET (PET) nanocomposites. The authors did not report any remarkable decrease in the glass transition (T_g) or melting temperature (T_m). On the other hand, they observed an increase in the crystallisation rate and temperature on adding more clay and attributed this to the nanoclay (silica platelets) acting as a nucleating agent in the heterogeneous crystallisation of the PET matrix. The rPET exhibited a faster crystallisation rate than PET and this was attributed to the fact that the melt viscosity of rPET is lower and thus allows an easier arrangement of polymer chains into a lamellar structure. On the other hand, Bizarria and co-workers (2007) studied the morphology of recycled PET (rPET)/ organoclay [MMT (Dellite 67G)] nanocomposites and did not observe any differences in the crystallisation rate or temperature of an rPET nanocomposite matrix. Only slight (negligible) decreases were found in the glass transition temperature and melting temperature, and the authors attributed this to clay agglomeration and degradation. The authors compounded the nanocomposites via twin

screw extruder at a screw speed of 250rpm and high processing temperatures (up to 285°C) which may slightly damage the nanoclay before the DSC measurement. A TGA test is convenient if applied to investigate the thermal stability of the nanoclay. With the same process and materials, Girald et al. (2008) found that a lower screw speed (150rpm) achieved higher mechanical properties and better dispersion as well as observing changes in the crystallisation temperature.

Chung et al. (2002) modified a surface fume silica filler then compounded it with PET via a melt compounding process to investigate the effect of various nano fume silicas on PET polymers at various concentrations. The authors observed that the crystallisation temperature from solid (T_{gc}) decreased on increasing the nano fume silica content, which indicated that the filler acted as a nucleating agent in the PET matrix. On the other hand, there were no significant changes in the melting temperature or glass transition temperature with adding more filler. They also found that the crystallinity of the PET nanocomposites increased on increasing the filler loading. Furthermore, the crystallinity and crystallisation rates of PET nanocomposites are more proportional to filler content than filler type with the range studied.

Guan et al. (2008) investigated the crystallisation behaviour of PET/clay which was prepared through in situ synthesis. The study was conducted in terms of POM, SEM and DSC. The surface of the clay (Na-MMT) was modified by Hexadecyltriphenylphosphonium (HTPP) and 1-hexadecyl-2,3-dimethylimidazolium (HDMI) salts to produce HTPP-MMT and HDMI-MMT. The authors did not find any significant change in the melting temperature but observed that the crystallisation rate of PETNC (MMT) was highly dependent on the surface modification of the clay (MMT). Frounchi and Dourbash (2009) studied the permeability properties of PET/clay (Cloisite 15A and Nanolin) film nanocomposites. They found a significant decrease in the glass

crystallisation temperature (T_{gc}) on adding nanofillers and no change in the glass transition (T_g). Furthermore the nanofillers increased the melting temperature, and this was attributed to the dispersion of the platelets in the polymer matrix hindering the heat from conducting the crystallized matrix. This study is covered in more detail in chapter 8 (Permeability of PET nanocomposites). Calcagno et al. (2007) studied the effect of the organic modifiers of clays (Cloisite 10A, 15A and 30B) on the crystallization and morphology properties of PET nanocomposites. The crystallization temperature (T_c) of the pure PET was lower than that for the PET nanocomposites which possibly means that the nanoclay had a nucleation effect on the PET. It was also found that the PET 30B and PET 10A nanocomposites exhibited exfoliated and intercalated morphologies due to many reasons, including the polarity of the surfactant and its chemical structure. In addition, the authors reported that the nanocomposites showed smaller mean spherulite size and more nuclei than for pure PET. Anoop et al. (2006) used single-walled carbon nanotubes (SWNTs) in a study of their influence on PET crystallization. The authors observed that SWNTs at low concentration (0.03%) enhance the crystallization temperature during melt cooling by increasing the value from 200 to 210°C. They showed that the oriented SWNTs in the PET melt enhanced the oriented crystallization of PET.

Wang and Gao et al. (2006) used XRD, TEM, DSC and TGA to study the thermal stability, crystallization behaviour and mechanical properties of PET/organic Montmorillonite nanocomposites (the trade name of the organic MMT was DK₂; it has a cation exchange capacity of 120meq/100g and is supplied by Zhejiang Fenghong Clay, Chemical Co. Ltd. (China)). The composite was prepared via melt-blending through the clay and the PET was pre-mixed in a high speed mixer prior to twin screw extrusion. This may lead to non-uniformity in clay dispersion and could cause a variation in

results. They observed that adding DK₂ increased the crystallization temperature from the melt (T_{mc}), and decreased the half peak width and sharpness in the crystallization rate curve. The researchers attributed these phenomena to PET molecules stacking on each other to grow into crystals, due to the fact that DK₂ itself helps in this stacking. Also this may occur because DK₂ acts as an effective heterogeneous nucleation agent. In addition to enhancing the crystallization rate, DK₂ can increase the heat distortion temperature (HDT) possibly due to the higher crystallinity for the nanocomposites or the high interaction force between the PET matrix and the DK₂. Most of the results showed that the composite had optimum mechanical properties when the DK₂ content was approximately 1%.

Ke et al. (1999) studied the effect of the clay on the crystal morphology and crystallisation processes. The nanocomposites were prepared via the in-situ method. The results showed that the clay content affects crystallisation as the clay acts as a nucleating agent. Also Ke et al. (2002) discussed the relationship between the distribution of intercalated or exfoliated clay and the crystallization of PET. They reported that the increased intercalation with the large number of clay platelets leads to a decrease in crystallization. In the same study, it was observed that the dispersion of the clay platelets was controlled by the polymerization methods as well as the surface modification.

Chen et al. (2007) prepared PET/antimony doped tin oxide (ATO) through an in situ polymerisation method and studied the effect of ATO loading on electrical properties, dynamic mechanical properties and crystallisation behaviour. The authors observed that the ATO nanoparticles increased the crystallisation temperature from the melt (T_{mc}) and the crystallisation rate. This phenomenon may be attributed to the fact that the ATO has a very large surface area which can lead to the formation of strong heterogeneous

nucleation in the polymer crystallisation. It was also found that ATO decreased the crystal size of PET. Chae and Kim (2007) also noticed an increase in the crystallisation temperature of PET/ferrite nanocomposites. The effect of treatment of MMT on the crystallisation behaviour of PET/MMT nanocomposites was investigated by Yin and his team in 2009. They observed, using DSC, SEM and POM, that the MMT acted as a heterogeneous nucleating agent and impeded the crystal growth of PET no matter how the MMT was treated. The physical impeding of the clay was negligible when the MMT agglomerated in the PET matrix so the PET/MMT nanocomposites had too fast a crystallisation rate.

5.3 Experimental work

A. Materials

Semi-crystallised PET pellets as received from the supplier (Tergal F9) were used to investigate the double endotherm melting temperatures exhibited in the first heating stage of the DSC test and the results presented in section 5.4.7.

Extruded vPET amorphous pellets and PET nanocomposite amorphous pellets produced during the compounding processes (see chapter 3) were used to investigate the effects of the nanoclays (MAE, MTE and Cloisite 25A) on the thermal properties of PET. Between four and six pellets were chosen from each batch (from the beginning, middle and end of the compounding run) to measure their thermal properties and compare them with unfilled PET.

In order to study the effect of nanoclays on the thermal properties of stretched films, unfilled PET and PET/MTE (1, 3 and 5 wt.%) films were analysed by DSC before and after the equal biaxial stretch. These films were produced by the film cast process and

the equal-biaxial stretch films were additionally processed using the biaxial stretcher at 90°C as discussed in section 3.5.7.

B. Procedure

The thermal properties of the un-filled PET and PET nanocomposites (pellets and films) (including crystallisation temperature, glass transition temperature and melting temperature) were investigated by TA Instruments Q2000 DSC. The amorphous pellets and films were investigated during the first heating stage from 30 to 280°C at a heating rate of 10°C/min, and during the first cooling stage from 280 to 30°C at a cooling rate of 10°C/min, while a second heating stage was applied to the semi-crystallised PET pellets (vPET) from 30 to 280°C, in addition to the first heating and cooling stages.

The degree of crystallinity (X_c) of the samples was calculated by using the following equation [Karagiannidis et al. (2008)]:

$$X_c(\%) = \left(\frac{\frac{\Delta H_m - \Delta H_{mc}}{1 - x}}{\Delta H_m^{100}} \right) \cdot 100$$

Where X_c is the degree of crystallinity, ΔH_m is the enthalpy of melting, ΔH_{mc} is the enthalpy of crystallinity in cooling stage, ΔH_m^{100} is the theoretical enthalpy of melting when the PET 100% crystallised (140 J/g) [Mehta (1978) and Bizarria et al. (2007)] and x fraction weight of nanoclay.

5.4 Results and discussion

The objective of this chapter is to analyse the thermal property results obtained from analysing PET nanocomposites using DSC in order to study the effect of adding nanoclays on the thermal behaviour of PET. The first section in this chapter (5.4.1) presents some typical DSC curves for amorphous and semi-crystalline PET, and also defines some abbreviations used during the discussion of the results. Sections 5.4.2, 5.4.3 and 5.4.4 cover the thermal property diagrams for PETNCs (PET with MAE, MTE and Cloisite 25A). Section 5.4.5 covers the comparative study between PET nanocomposites with different nanoclay types and constant loading concentrations. Section 5.4.6 investigates the thermal behaviour of PET/MTE films before and after the equal-biaxial stretch. It was noticed that the vPET (Tergal F9, as received) showed double melting endotherms, so this phenomenon is discussed in section 5.4.7.

Furthermore, a preliminary study was conducted on some PET nanocomposite sheets obtained from Queens University. These sheets were prepared under the EPSRC funded QBOX project by blending PET pellets (Tergal F9) with nanoclays (Somasif MAE and MTE). This mini-study was initiated to study the effects of cooling rates on the crystallisation properties, and also to compare other thermal properties such as glass transition temperature (T_g), melting temperature (T_m), and crystallization temperature from the solid (T_{gc}) and from melting (T_{mc}), of the PET nanocomposite sheets (QBOX project) with PET nanocomposites prepared at Bradford. This preliminary study is covered in appendix 5 (see appendix x5.4).

5.4.1. Introduction

Amorphous PET exhibits different thermal behaviour to semi-crystallised PET. During the heating of the amorphous sample from ambient temperature to melting temperature, it goes through three zones: first the glass transition zone, second the cold crystallisation zone and third the melting zone. Semi-crystalline PET, however, exhibits only one zone in the first heating stage (melting zone) and two zones in the second heating stage (glass transition and melting zones). During the cooling stage, only one zone appears for both PET states (amorphous or semi-crystallised) which is called the melt crystallisation zone.

Each zone has a peak and starting point so it is appropriate to define these zones and points prior to the discussion.

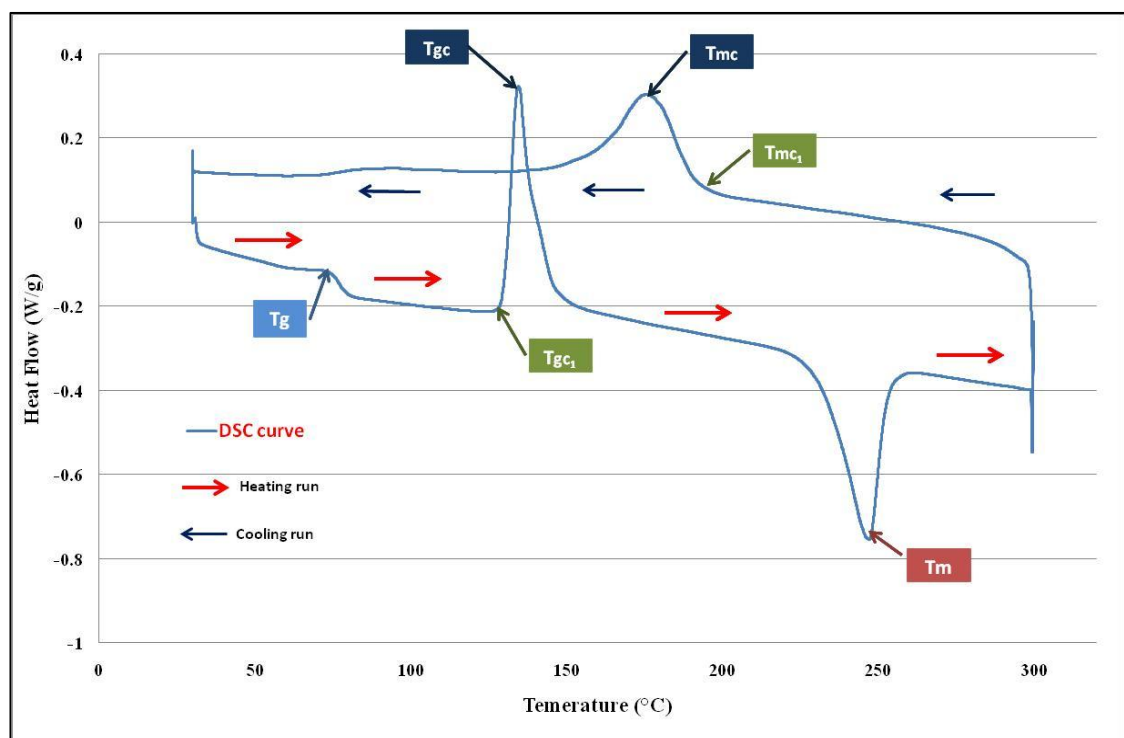


Figure 5.8 Typical DSC curve for PET amorphous.

The DSC curve for amorphous PET is shown in figure 5.8. This shows the thermal behaviour of amorphous PET during the first heating and cooling. Some abbreviations

are used to explain temperature points observed during the thermal measurements and can be defined as:

- **T_g**: Glass transition temperature.
- **T_{gc}**: Crystallisation temperature from solid.
- **T_{gc1}**: Onset crystallisation temperature from solid.
- **T_m**: Melting temperature.
- **T_{mc}**: Crystallisation temperature from melt.
- **T_{mc1}**: Onset crystallisation temperature from melt.

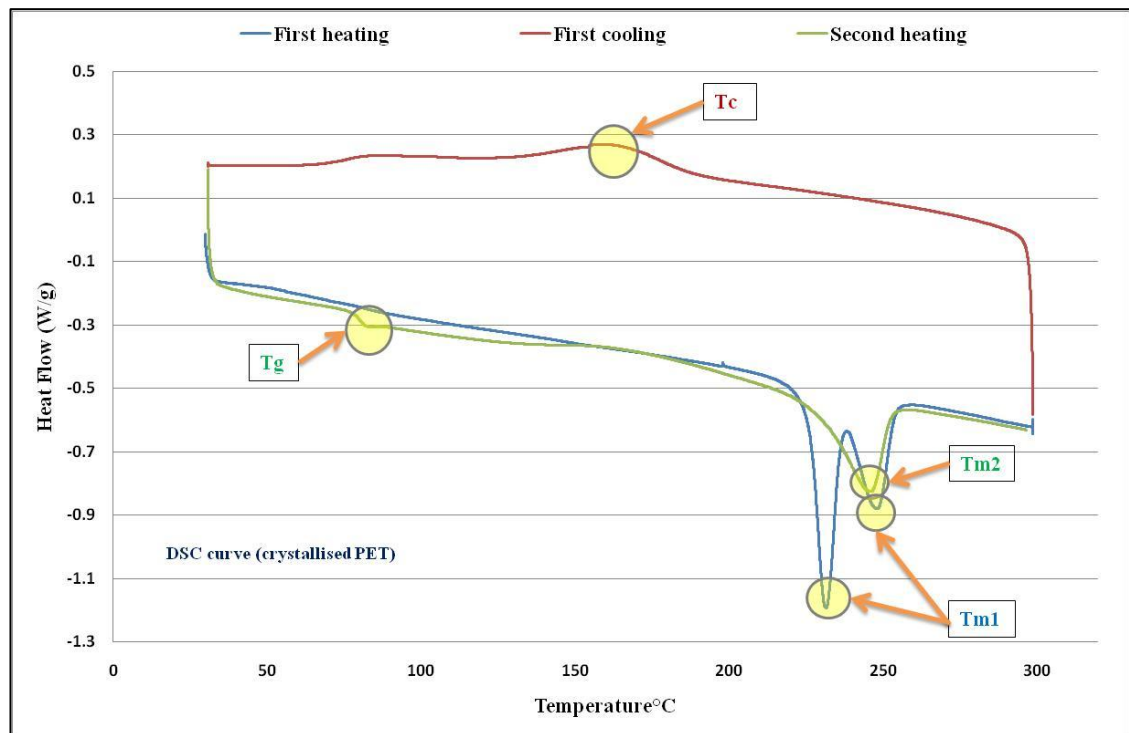


Figure 5.9 DSC curve for crystallised PET pellets (Tergal F9)

The thermal behaviour of semi-crystallised vPET (Tergal F9) is different from the amorphous PET, as mentioned before, and this is obvious from a comparison of figures 5.8 and 5.9. The unusual thing here is the double melting endotherm which PET Tergal F9 exhibits (this phenomenon is covered in detail in section 5.4.7).

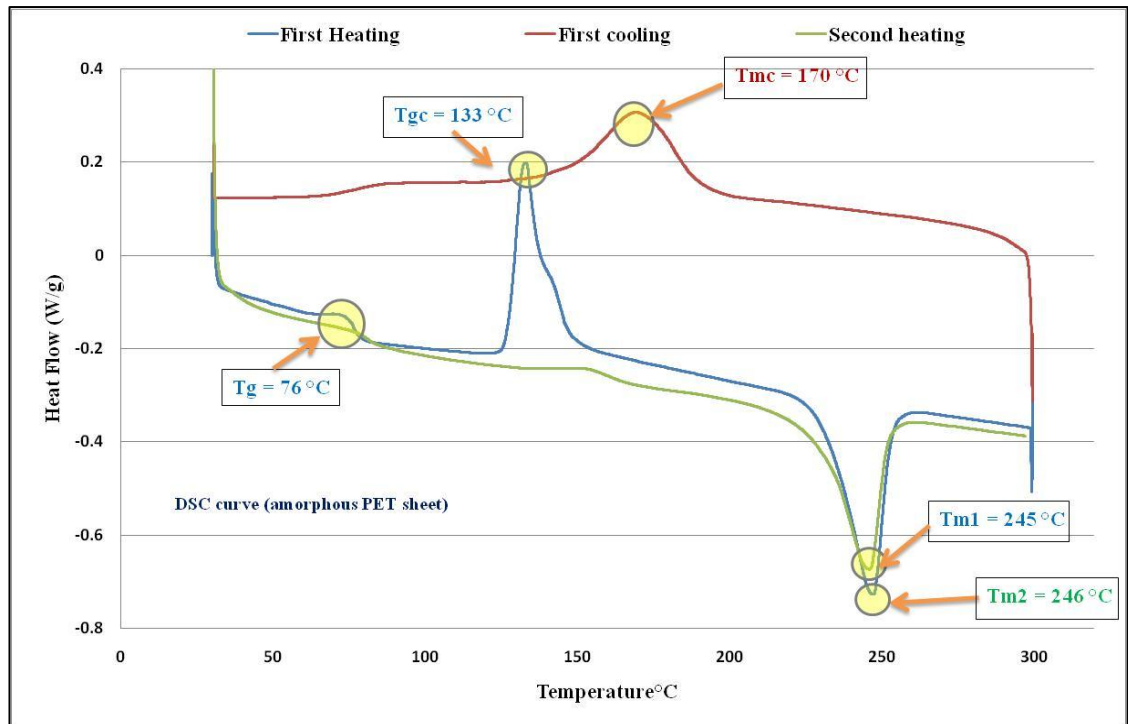


Figure 5.10 DSC curve for amorphous PET film

It is obvious in figure 5.10 that the T_{gc} peak disappeared from the curve in the second heat run, hence the first heating and cooling were used to analyse the thermal properties of amorphous PET.

5.4.2. PET/MAE nanocomposites

The objectives of this section are to study the effects of the nanoclay (Somasif MAE) with different clay contents on the thermal properties of PET and compare it with unfilled PET.

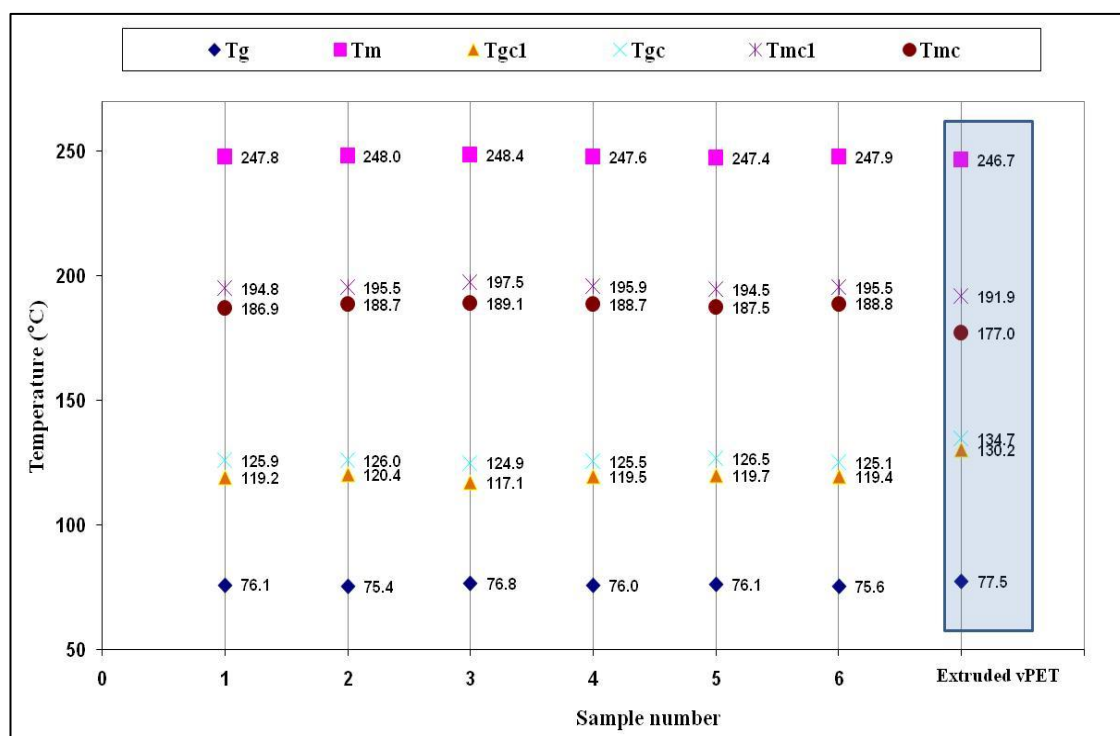


Figure 5.11 DSC results for 6 samples from the same run to produce PET/MAE (1 wt.%).

Six samples from the same run were taken at different times (from the beginning, middle and end of the compounding run of PET/MAE 1 wt.%) then analysed by the DSC. Figure 5.11 (each sample weight was about 3mg \pm 0.5) shows the consistency of the results of the nanocomposites (NC) (1 wt.% MAE), which can be attributed to good nanoclay distribution. The effect of the nanoclay on Tg and Tm was negligible while a significant change occurred in Tgc and Tmc. The small increase in Tm can result from a good dispersion of the nanoclay. During the crystallisation, the good dispersion of nanoparticles into the polymer matrix can make the PET to form crystals in perfectible

structure, as observed by Liu and Tian et al. (2004) in their study of PET/silica nanocomposites. Mucha et al. (2000) attributed the increase in T_m in PP/carbon black to some hindrance at the beginning of the melting process.

The repeatability of the thermal property results of PET/MAE (3, 5 and 20 wt.%) is shown in appendix 5 (see figures x5.1-x5.3). These results show good repeatability and close results for all thermal temperatures which again indicates good nanoclay distribution. Regardless of the small variation between some samples of PET/MAE (5 wt.%) indicated in T_{gc} , all samples started to crystallise (T_{gc1}) at similar temperatures, indicating good sample homogeneity and that the nanoclay changed the crystallisation temperature and crystallisation rate. The acceptable repeatability of most of the sample results may be attributed to a good mixing process. The T_g even at high contents did not show any significant decrease above 1 wt.% MAE content.

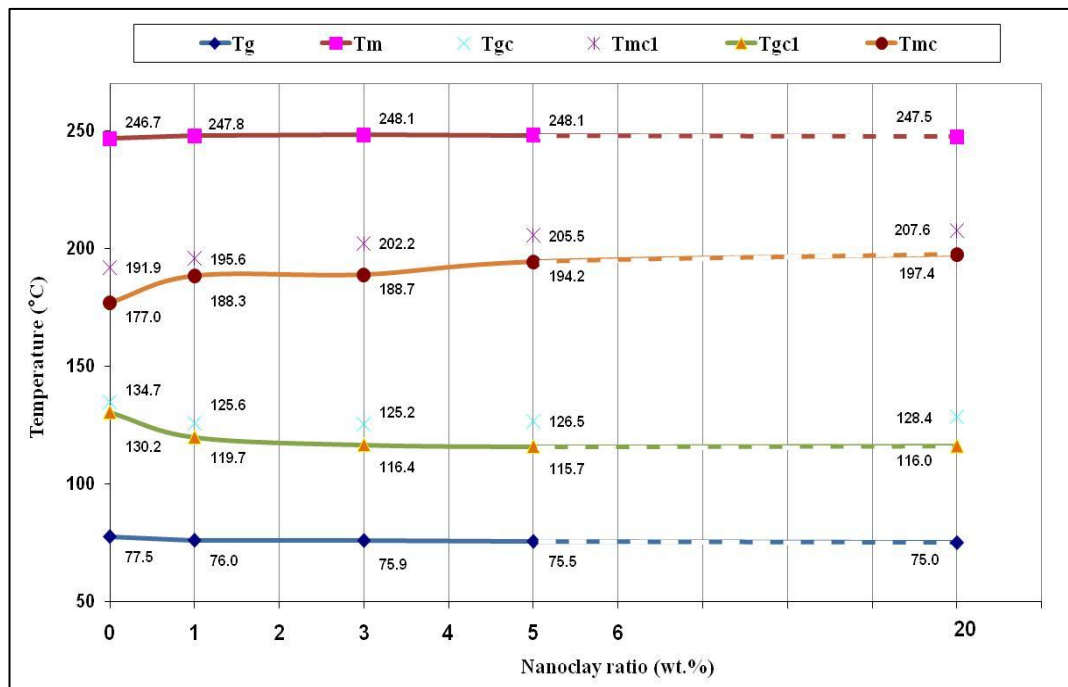


Figure 5.12 Average of thermal analysis results of PET nanocomposites (MAE) for various MAE contents.

Figure 5.12 is a combination of the average values shown in figures (5.11 and x5.1 - x5.3) indicating the relationship between the PET nanocomposites at various nanoclay contents (0, 1, 3, 5 and 20 wt.%) and the thermal analysis temperatures. It is clear that the absolute values of the crystallisation temperatures (T_{gc} and T_{mc}) follow a certain trend in decreasing or increasing with the addition of clay. While T_m did not show any significant change, it is observed from the T_g results that the nanoclay has a limitation in increasing the flexibility between the PET molecules (decrease T_g) which can be achieved by adding 1 wt.% MAE. It was found that adding 5 wt.% MAE to the PET matrix produced more change in the crystallisation temperatures (T_{gc} and T_{mc}) than adding 1 or 3 wt.% of MAE. Furthermore, PET/MAE (3 wt.%) exhibited differences in T_{gc} and T_{mc} larger than those of PET/MAE 1 wt.%, and all crystallisation temperatures (T_{gc} or T_{mc}) showed significant changes compared with the un-filled PET, which can be attributed to the fact that the nanoclays acted as nucleation agents for crystallisation. T_{mc} showed further increases but with small values for PET/MAE nanocomposites at concentrations over 5 wt.%, while T_{gc} did not exhibit further decreases for PETNC with clay contents over 5 wt.%.

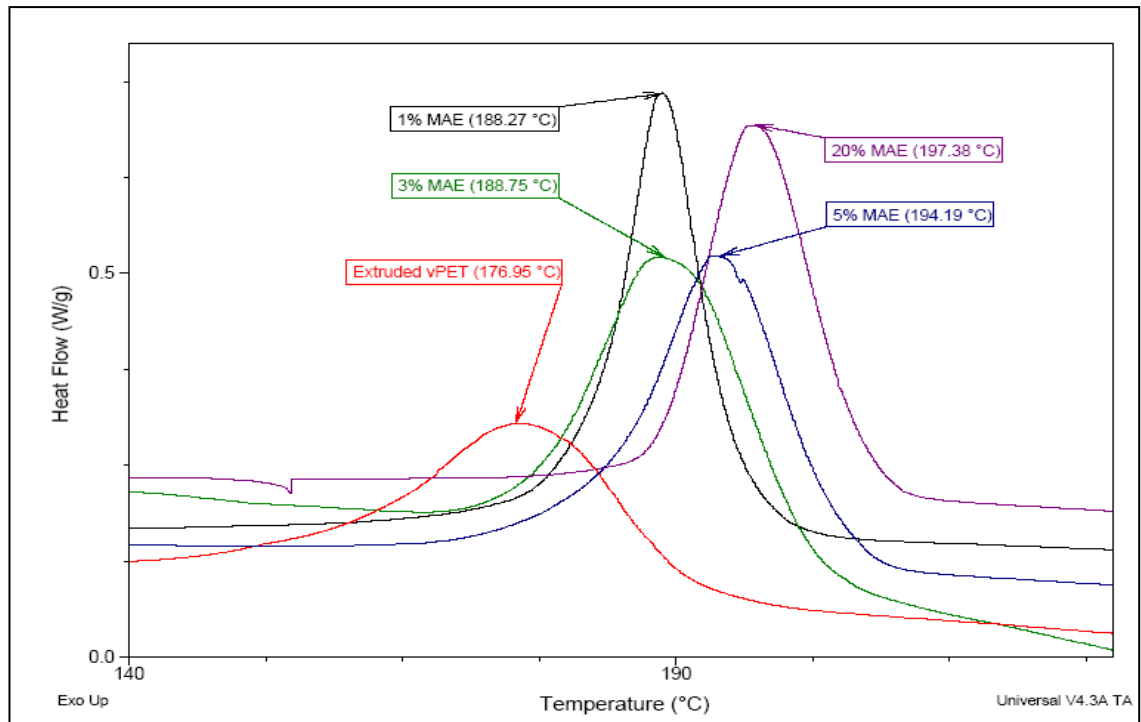


Figure 5.13 Tmc curves obtained from the DSC for all NC (PET/MAE).

In figure 5.13 the location and the shape of the curves for Tmc indicates that the crystallisation rate improved in the case of the PET/MAE nanocomposites curves. The exothermal peaks tend to become sharper with adding clay content, which has been observed by many researchers such as Xue and Hara (2006).

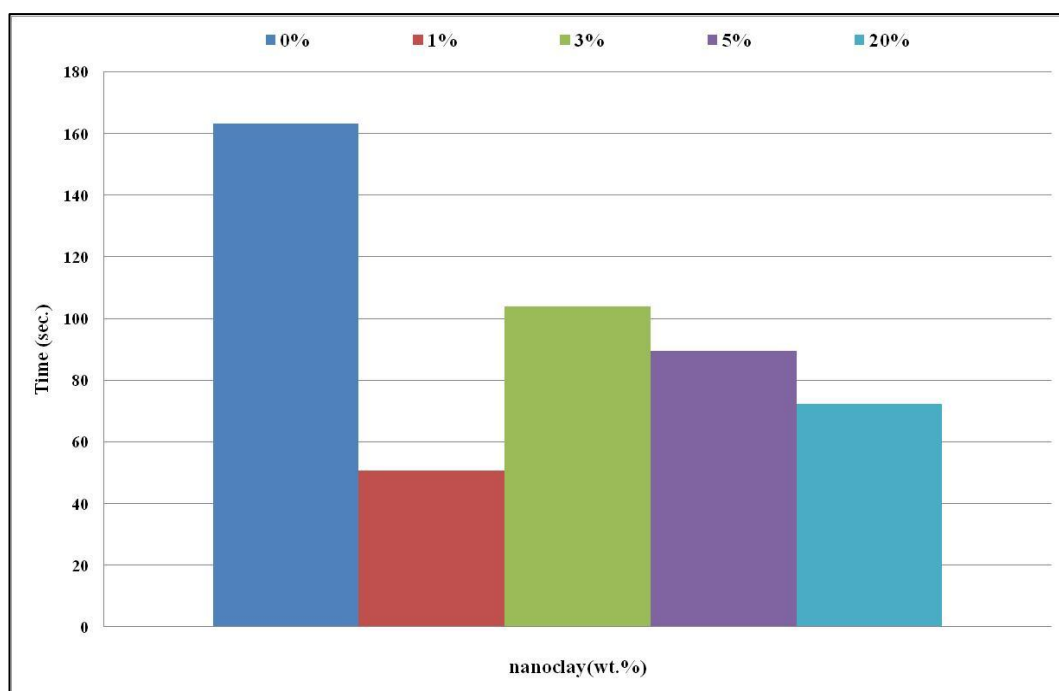


Figure 5.14 Crystallisation half-time for crystallisation from melt states for PET/MAE

It is evident that T_{mc} shifts to higher temperatures and the half peak width reduces (becomes sharper), indicating higher crystallization rate with increasing clay content as figure 5.13 shown. PET/MAE (1 wt.%) shows the shortest half-time for crystallisation (figure 5.14) but the PET/MAE (3, 5 and 20 wt.%) commence the crystallisation process earlier. There are many reasons for the enhancement of the crystallisation rate in nanocomposites. One is that the structure of the nanoclay can help the molecules of PET to stack on each other to grow into crystallites, and that leads to the high crystallisation rate. Another possible reason is that the clay may act as an effective heterogeneous nucleating agent. Similar results have been found by many researchers such as Wang and Gao et al. (2006).

5.4.3. PET/MTE nanocomposites

The objective of this section is similar to the previous section but with a different nanoclay Somasif MTE.

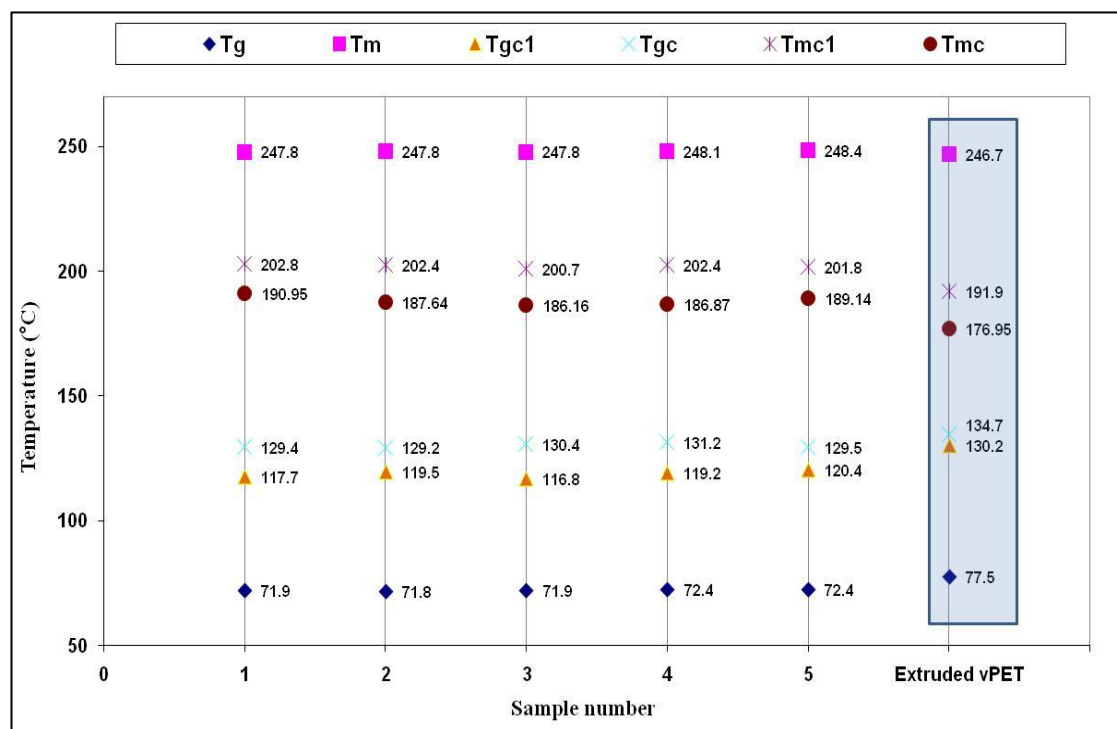


Figure 5.15 DSC results for 5 samples from the same run to produce PET/MTE (20 wt.%)

Similar analyses were applied to the nanocomposites of PET/MTE for the same purpose. Figure 5.15 shows the excellent repeatability for 5 samples of the masterbatch of PET/MTE (20 wt.%) nanocomposites. Tmc (+ 10°C) and Tgc (- 10°C) were affected by adding 20 wt.% of MTE to the PET matrix. The glass transition temperature of the PET/MTE masterbatch was reduced by 5°C and this may be attributed to the high amount of nano-platelets in the MTE increasing the mobility and the flexibility of the PET chain, which can lead to Tg reduction.

Though the results for the five samples indicate good mixing, there were no sizeable benefits from adding more clay to the PET matrix since the crystallisation temperatures did not improve significantly, while the Tg dropped by around 6°C.

The repeatability results for PET/MTE at 1, 3 and 5 wt.% were plotted and are shown in appendix 5 (see figures x5.4 – x5.6). These figures also exhibit good stability in the results.

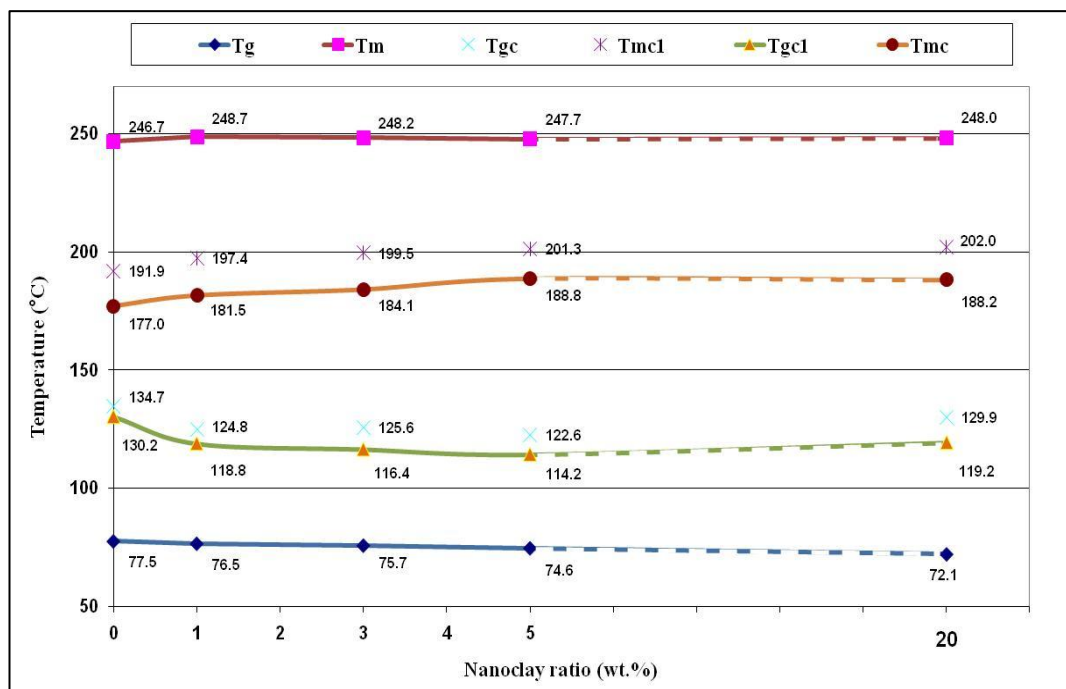


Figure 5.16 Average of thermal analysis results of PET/MTE nanocomposites for various MTE contents

The average results for all PET/MTE nanocomposites are combined in figure 5.16. The slight change in melting temperature is negligible, especially given that the processing temperatures are around 260°C. The Tgc and Tmc of PET/MTE at various contents exhibit a similar trend in both temperatures for PET/MAE nanocomposites. The changes in crystallisation temperatures are evidence that the MTE clay works as a nucleating agent for the crystallisation.

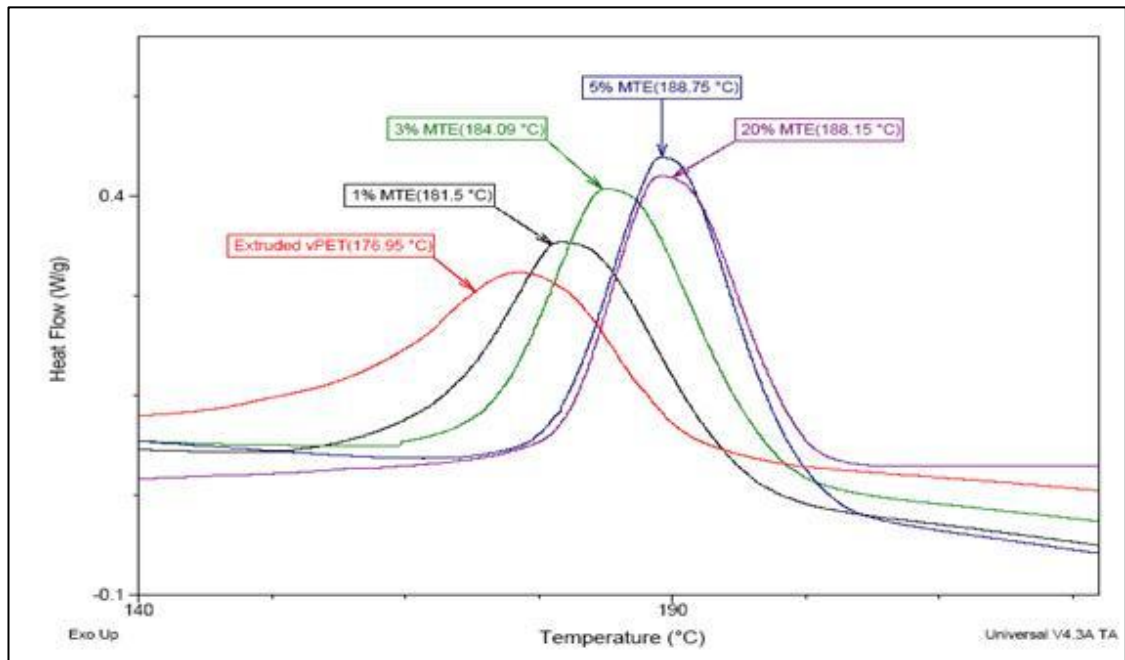


Figure 5.17 Tmc curves obtained from the DSC for all NC (PET/MTE)

Figure 5.17 shows symmetrical crystallisation peaks and distinct exothermic peaks. With increasing clay content, the curve moves to the right (higher T_{mc} temperature) and gets sharper (decrease in the $t^{1/2}$) which indicates the crystallization rate is increased (see figure 5.18). Chen et al. (2007) and others have reported similar results.

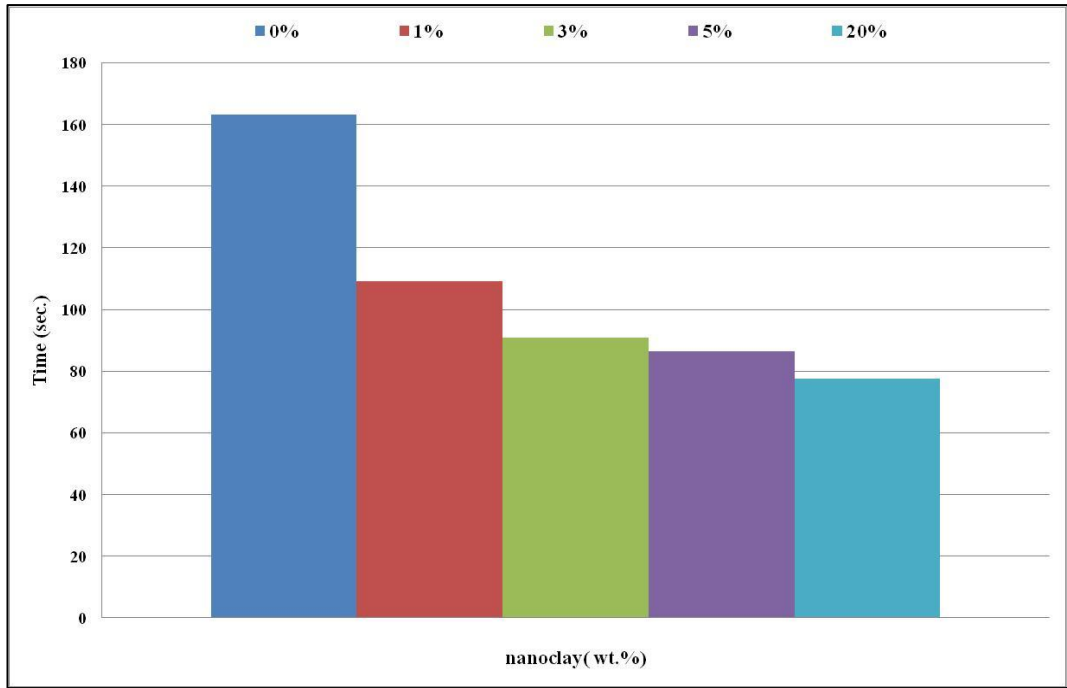


Figure 5.18 Crystallisation half-time for crystallisation from melt states for PET/MTE

5.4.4. PET/Cloisite 25A nanocomposites

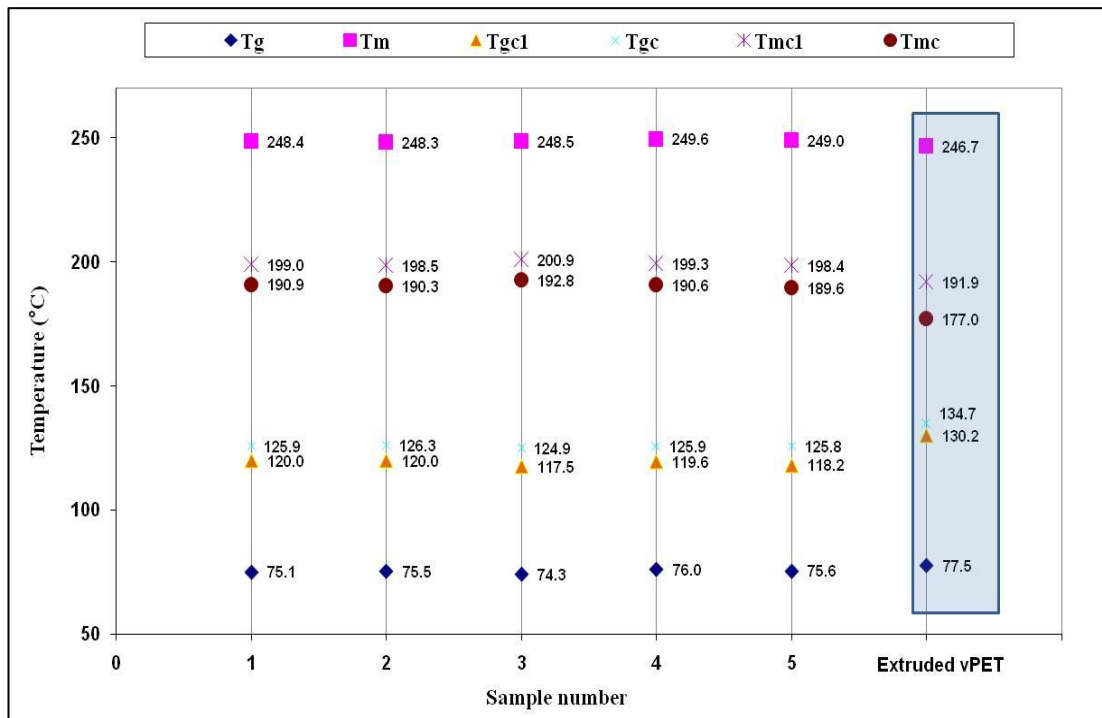


Figure 5.19 DSC results for 5 samples from the same run to produce PET/Cloisite 25A (3 wt.%)

The repeatability of thermal temperatures of PET/Cloisite 25A nanocomposite pellets after the compounding process is represented in figure 5.19 at loading 3 wt.%, and in appendix 5 for the other clay concentrations (see figures x5.7 - x5.9). It is apparent that fair consistency in the DSC results has been achieved.

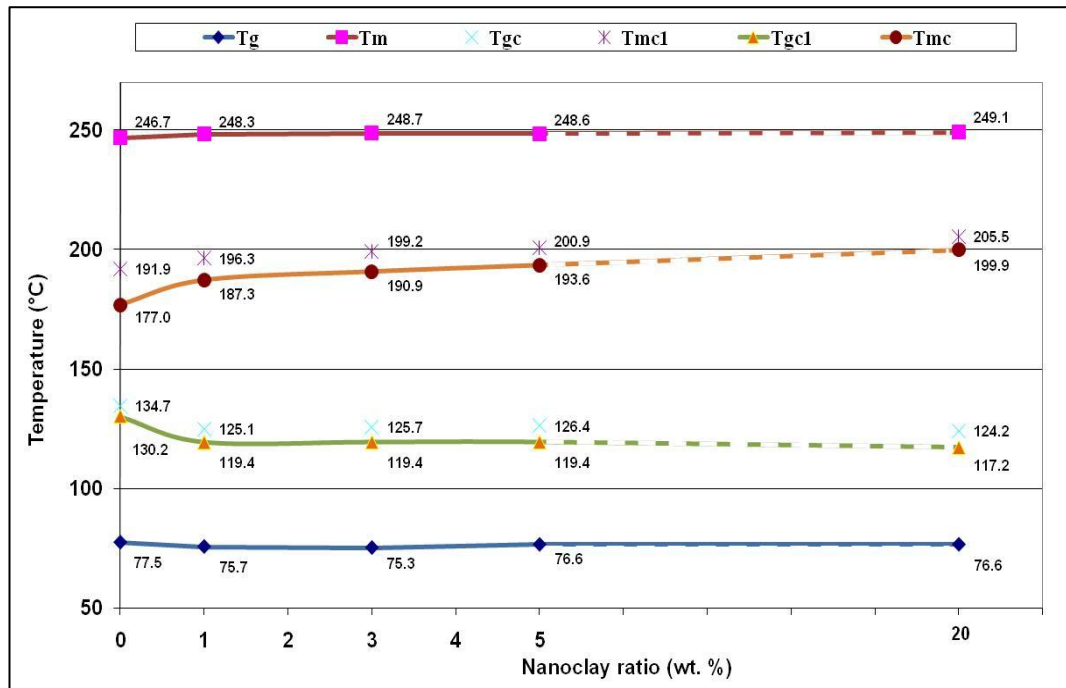


Figure 5.20 The average of thermal analysis results of PET/Cloisite 25A nanocomposites for various Cloisite 25A contents

Figure 5.20 represents the behaviour of the thermal properties of PET/Cloisite 25A nanocomposites at various nanoclay concentrations. It is obvious that the Cloisite 25A acts as a nucleating agent for crystallisation by changing the absolute values of Tgc and Tmc. It is worth mentioning that the Cloisite 25A continues to increase the Tmc even at high clay content (20 wt.%). As observed with MTE and MAE, the melting temperature did not show any significant change. The distinctive effect of Cloisite 25A on the thermal properties of PET is that the reduction in Tg is less than 1°C, even at 20 wt.%.

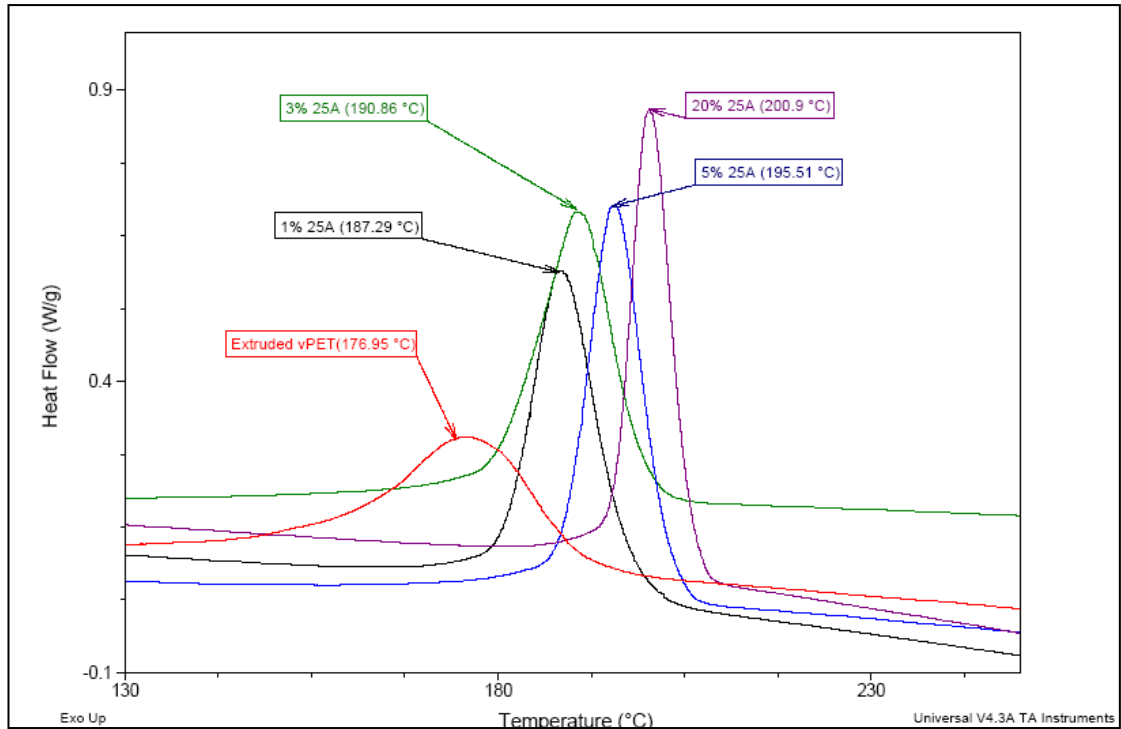


Figure 5.21 Tmc curves obtained from the DSC for all NC (PET/Cloisite 25A)

Figure 5.21 illustrates the curves of Tmc for PET/Cloisite 25A at various clay concentrations. The addition of more clay leads to an increase in the Tmc value and higher crystallisation rates. The exothermic peaks tend to become sharper with adding clay content which mean decreasing in the half-term of crystallisation as figure 5.22 shown.

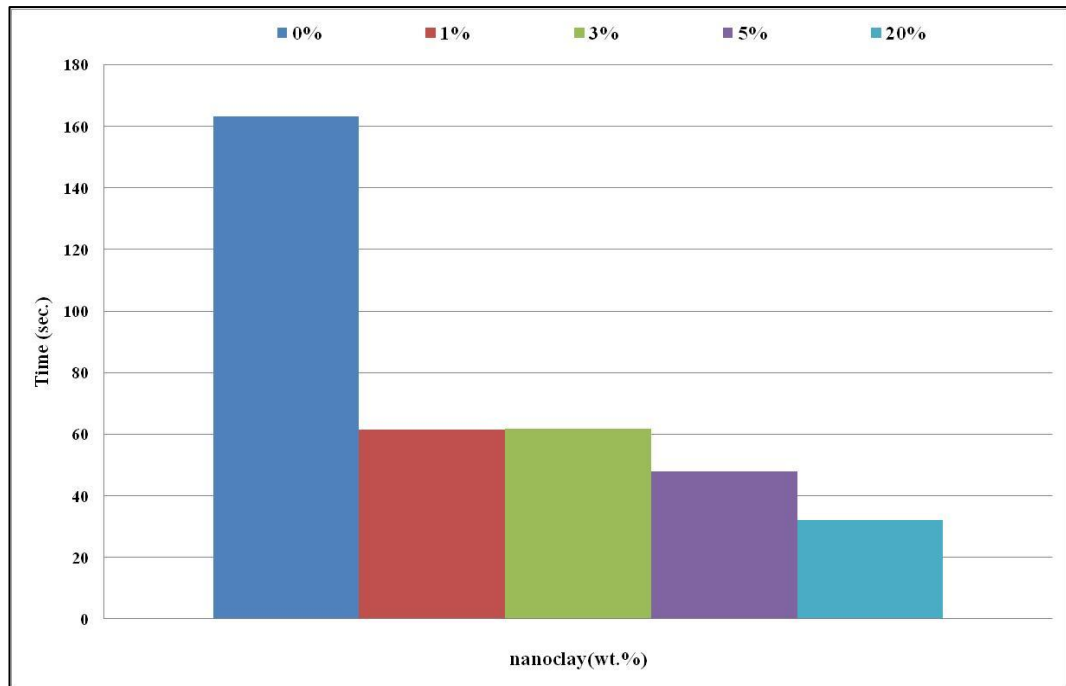


Figure 5.22 Crystallisation half-time for crystallisation from melt states for PET/Cloisite 25A

It seems apparent after reviewing the results of the thermal properties of PET nanocomposites with three different nanoclays at various concentrations that the nanoclay acts as a nucleation agent for the crystallisation process by increasing the T_{mc} and decreasing the T_{gc} , while causing no constant trends in the absolute crystallisation values (Table 5.1). The final application of PETNC depends on whether this change is a disadvantage or an enhancement. Some applications require a high crystallisation rate and others a lack of crystallinity in the matrix. For example, hot filling of PET requires a heat setting treatment for PET bottles, which also requires high crystallisation rates, especially for the bottle neck. However, controlling the crystallisation rate is an essential factor. High crystallisation rates can lead to opaque PET products.

Sample name	X _c (%)
Ext. vPET	10.06
PET/MTE (1%)	11.61
PET/MTE (3%)	11.4
PET/MTE (5%)	11.12
PET/MTE (20%)	8.41
PET/MAE (1%)	8.65
PET/MAE (3%)	10.29
PET/MAE (5%)	10.1
PET/MAE (20%)	8.96
PET/Cloisite25A (1%)	9.42
PET/Cloisite25A (3%)	11.36
PET/Cloisite25A (5%)	9.76
PET/Cloisite25A (20%)	10.73

Table 5.1 Crystallinity degree of PET nanocomposites

Generally, the melt processing temperature of PET is about 10°C above the melting temperature. However it is preferable in some regions to avoid a big reduction in the glass transition temperature (T_g), and this is a crucial issue in hot countries. For example, the distribution of carbonated soft drink (CSD) bottles in some hot countries is carried out via uncovered vehicles, which exposes the bottles to the sun. This can raise the bottle temperature above 60°C, reaching the deformation stage.

5.4.5. Comparative study of PET nanocomposites with different clay types and the same loading concentrations

Figures 5.23 - 5.26 and figures x5.14 - 5.17 (see appendix 5) summarise the effect of all three clays (MTE, MAE and Cloisite 25A) at 1, 3, 5 and 20 wt.% contents. From these figures, it can be observed which clay exhibits faster and greater changes in thermal temperatures or crystallization rates of PET nanocomposites when compared to other clays or un-filled PET. For example, an earlier crystallisation onset temperature (e.g. high T_{m1}) does not mean a higher T_{mC} .

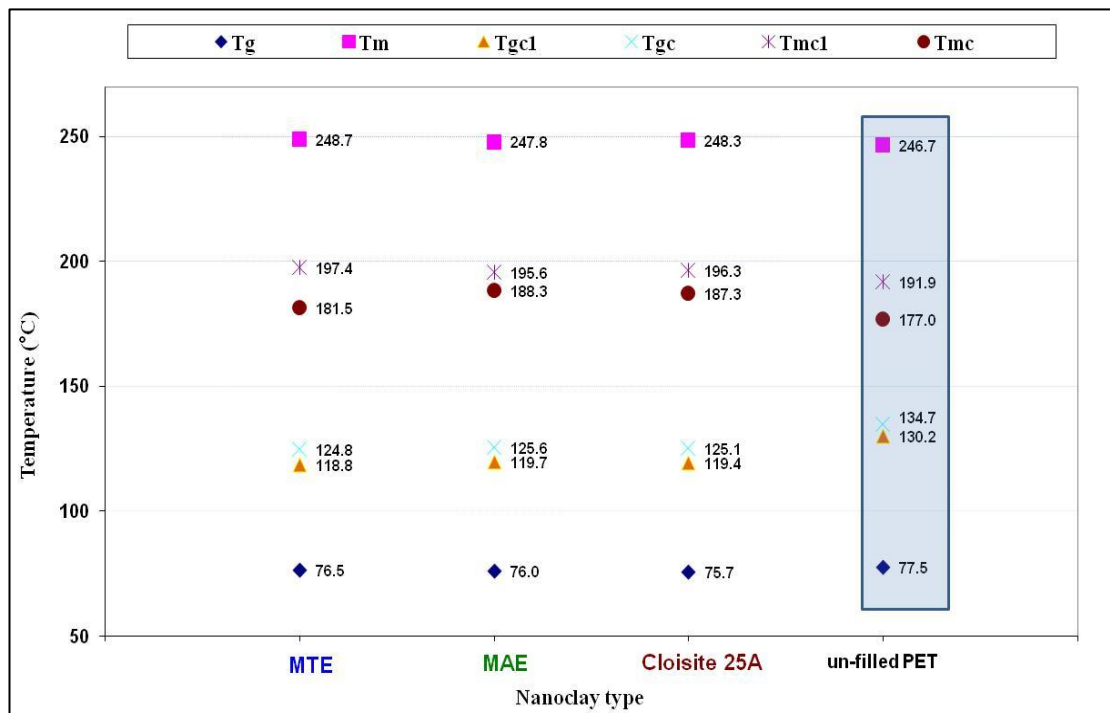


Figure 5.23 DSC results of PET nanocomposites at 1 wt.% for all nanoclay types

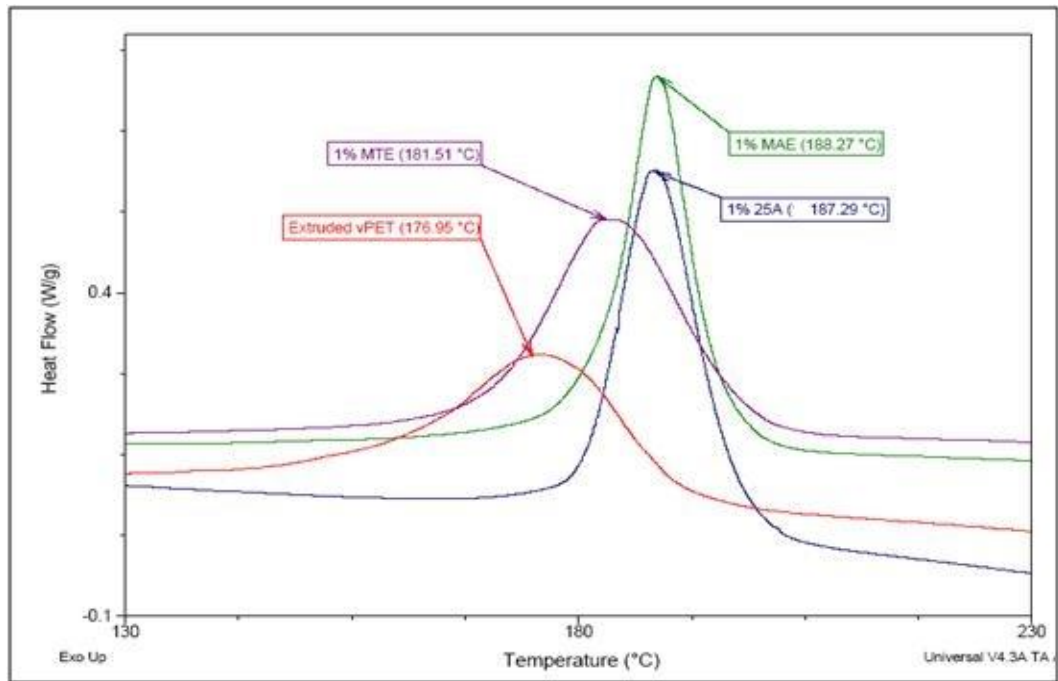


Figure 5.24 Tmc curves obtained from the DSC for all clays at 1 wt.%

Figure 5.23 illustrates the DSC results for PET nanocomposites (MAE, MTE and Cloisite 25A) at loading concentration 1 wt.%. It is apparent that the T_m and T_g did not show any significant variation among the PET nanocomposites themselves or compared with unfilled PET. Furthermore, it was found that the MTE (1 wt.%) started the crystallisation from melt earlier than the other clays (higher T_{mc1}), but spent longer in reaching the peak of the curve (T_{mc}), while the other nanoclays (MAE and Cloisite 25A) at the same concentration started late but recorded a higher T_{mc} (figure 5.24 shows this phenomenon clearly). This means that the crystallisation rate of PET nanocomposites with MAE or Cloisite 25A is faster than PETNC with MTE, although all nanoclays similarly reduced T_g by around 10°C compared with the un-filled PET. However figure 5.14 exhibits similar conclusion for PET nanocomposites at a loading concentration of 3 wt.% and the rheological behaviour for the same materials as presented before in figure 4.16 assist this observation showing Cloisite 25A responds to form a network earlier than the other two nanoclays.

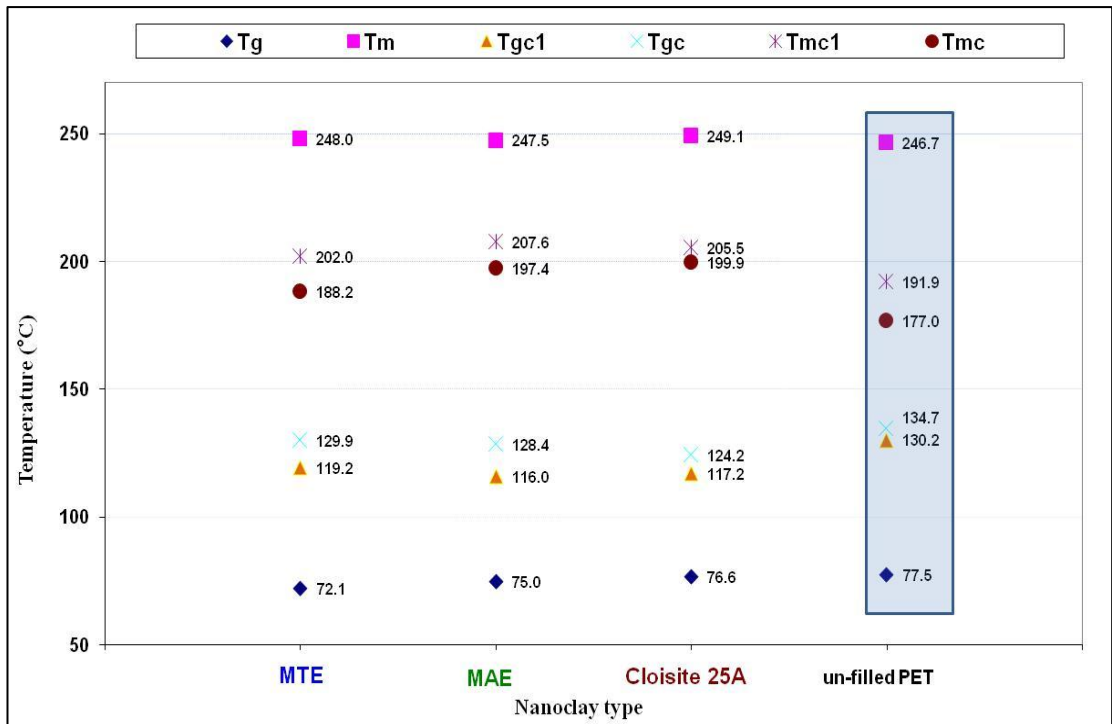


Figure 5.25 DSC results of PET nanocomposites at 20 wt.% for all nanoclay types

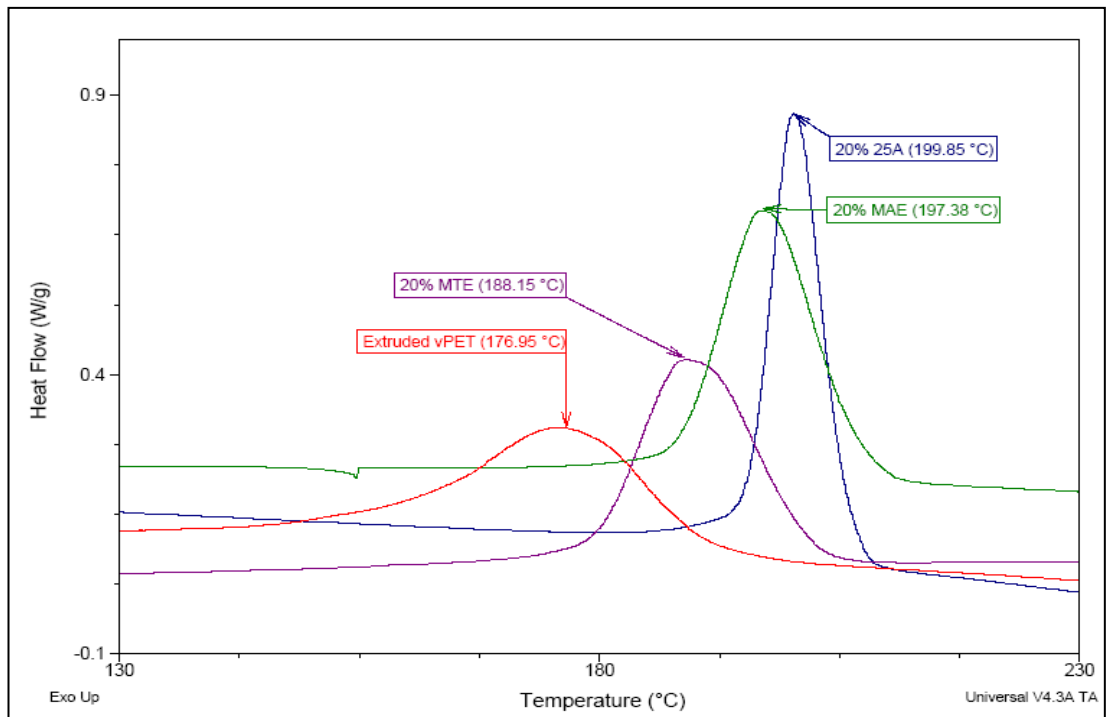


Figure 5.26 Tmc curves obtained from the DSC for all clays at 20 wt.%

A comparison of the thermal properties of PET nanocomposites at the masterbatch concentration of 20 wt.% is illustrated in figures 5.25 and 5.26. Cloisite 25A again

exhibits a faster crystallisation rate with MTE being the slowest to crystalline. MTE shows the lowest T_g, and this may be attributed to the MTE increasing the PET chain flexibility more than the other nanoclays. The same comparison study but for levels 3 and 5 wt.% is shown in figures x5.14-x5-17 with similar conclusion. Most of these results agree with other studies of PET nanocomposites or general polymer nanocomposites, such as Cho and Paul (2001), Chen et al. (2002), Lie et al. (2006), Kracalik and Kovarova et al. (2007), and Calcagon et al. (2007).

5.4.6. Thermal properties of PET/MTE films (un-oriented and equal-biaxial stretch)

In this study, un-filled PET and PET/MTE nanocomposite (1, 3 and 5 wt.%) films before and after biaxial stretch were analysed using DSC to investigate the effect of the equal biaxial stretch film process on the thermal properties of the film. Generally, un-oriented PET films are in an amorphous state while oriented films (stretched) have a partially crystallised state (anisotropic structure) which is formed during the stretching process [Kattan (2001)]. The film was stretched at 90°C, above T_g but below T_{gc}, to avoid spherulitic crystallisation [Joel et al. (2007)].

The area under the glassy crystallisation curve indicates the quantity of crystallisation formed by thermal treatment (during DSC) for PET film. While the oriented film already exhibits anisotropic crystallisation and amorphous structure, a lower area under the glassy crystallisation curve was expected for an oriented PET film, and that is clearly apparent from Table 5.2.

Film type	ΔH_{gc} (oriented)	ΔH_{gc} (un-oriented)
Ext. vPET	28.09	19.07
PET/MTE (1 wt. %)	27.32	19
PET/MTE (3 wt. %)	26.92	16.48
PET/MTE (5 wt. %)	27.63	16.06

Table 5.2 The enthalpy of crystallinity in heating stage for un-oriented and oriented of un-filled PET and PET/MTE films at various concentrations.

It was mentioned earlier that the crystallinity value did not significantly change due to the presence of nanoclay, and here the stretch process shows a similar result.

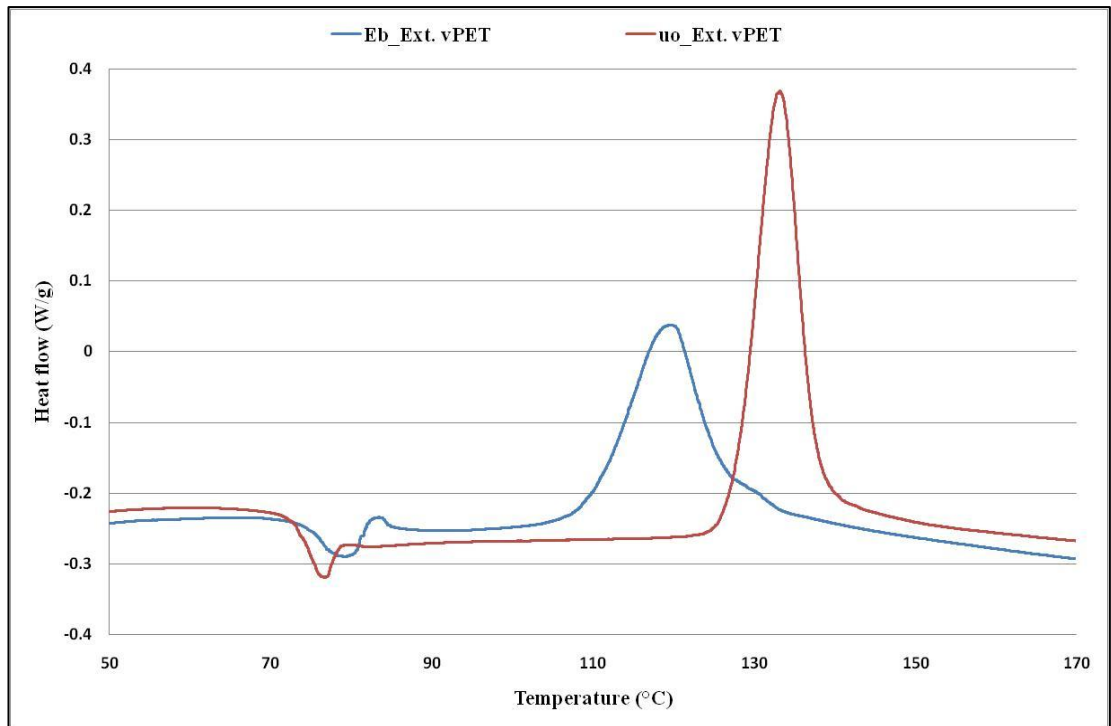


Figure 5.27 Part of the DSC curves for extruded vPET film (un-oriented and equal biaxial stretch) showing the Tg and Tgc curves

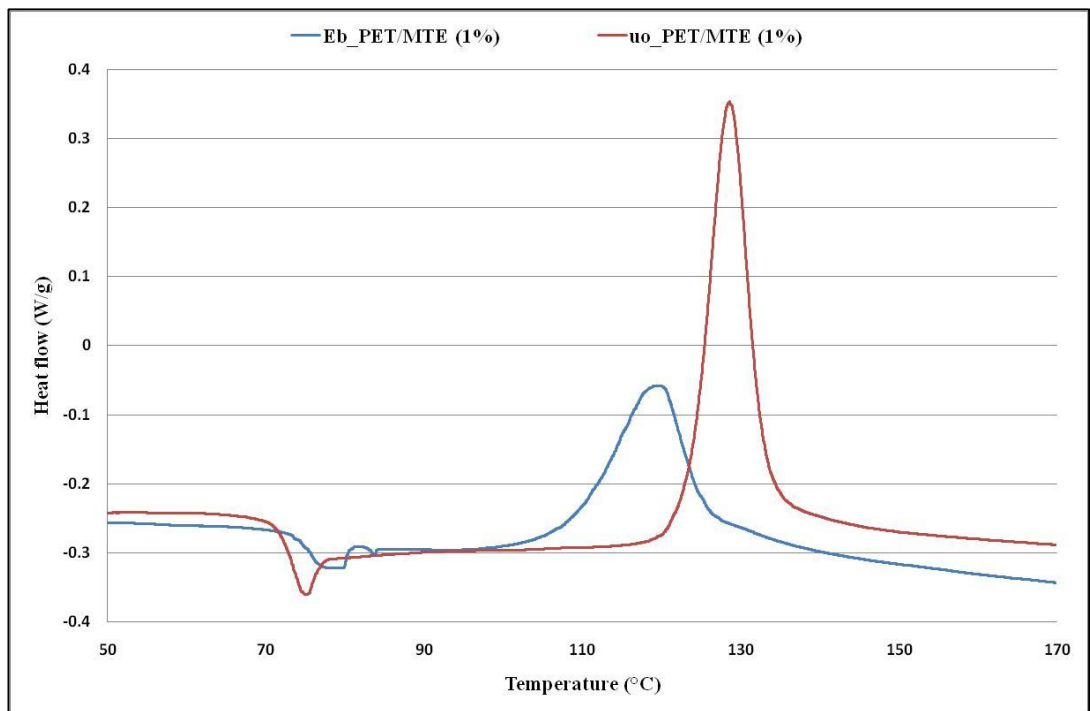


Figure 5.28 Part of the DSC curves for extruded PET/MTE 1 wt.% film (un-oriented and equal biaxial stretch) showing the Tg and Tgc curves

It is apparent from figure 5.27 that stretching the un-filled PET decreased chain flexibility and this is indicated by the increase in glass transition temperature (T_g). Stretching the film also accelerates the crystallisation temperature of the film from the solid phase (T_{gc}). Similar behaviour was found in PET/MTE at low loading content (1 wt.%) as figure 5.28 shows.

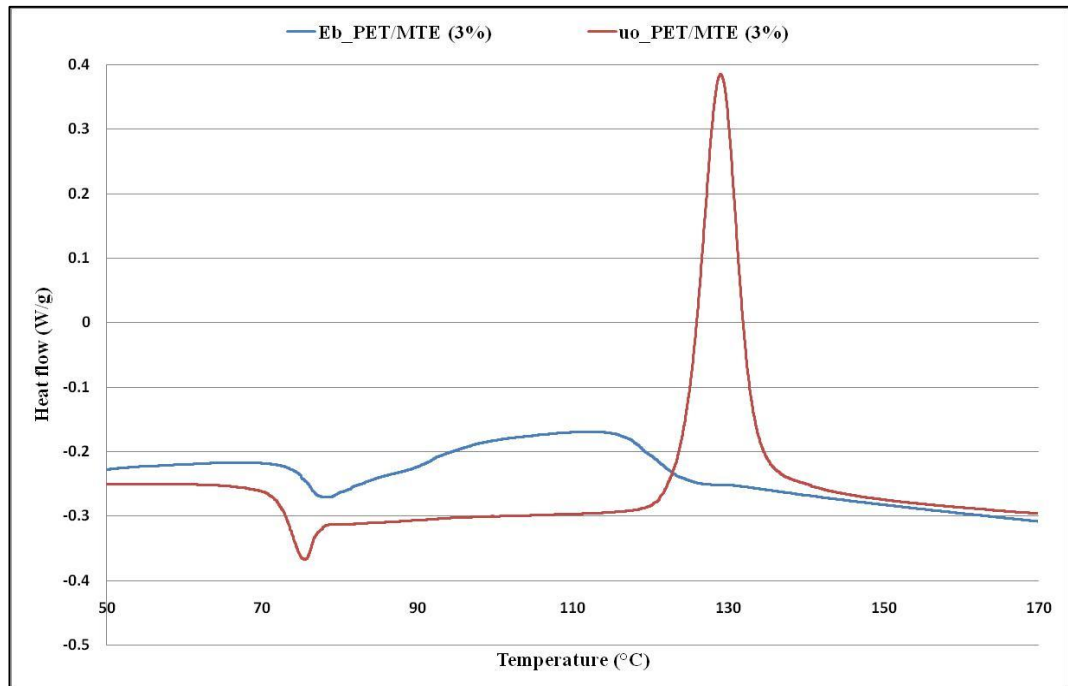


Figure 5.29 Part of the DSC curves for extruded PET/MTE 3 wt.% film (un-oriented and equal biaxial stretch) showing the T_g and T_{gc} curves

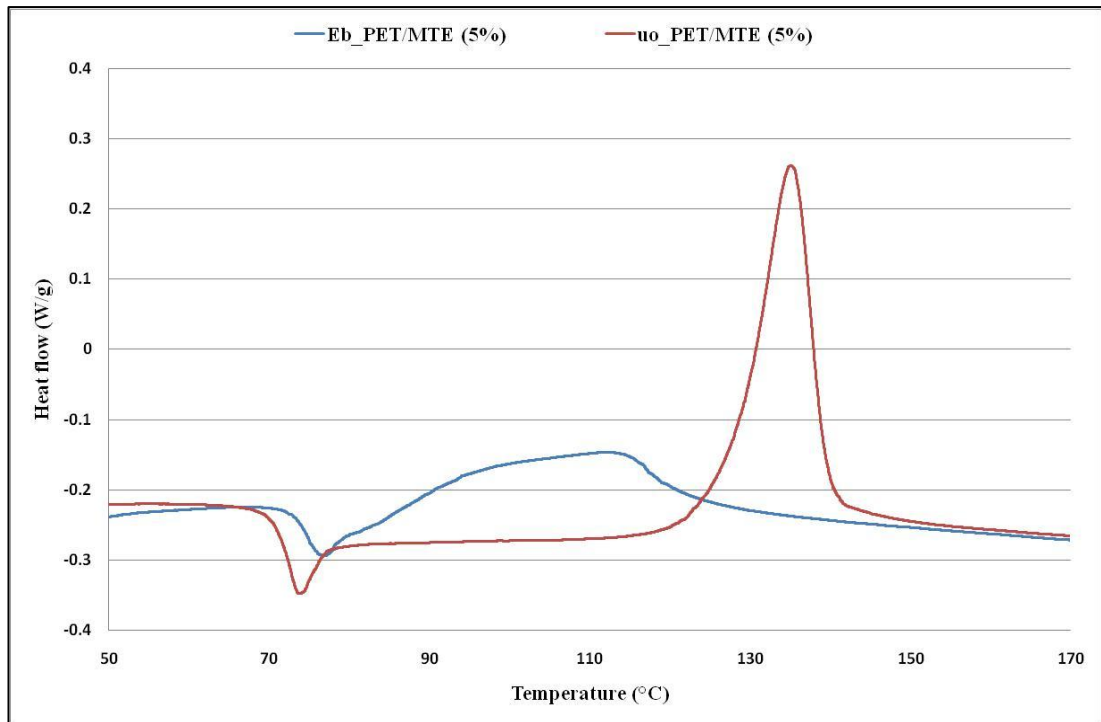


Figure 5.30 Part of DSC curves for extruded PET/MTE (5 wt.%) film (un-oriented and equal biaxial stretch) showing the Tg and Tgc curves

Adding further MTE filler (e.g. 3 or 5 wt.%) leads to the MTE starting to build up crystallinity immediately after the glass transition temperature in the case of the stretched film, as figures 5.29 and 5.30 show.

This confirms that the stretch process forms crystalline structures inside the PET matrix. The above figures show that the stretching accelerated Tgc and this acceleration increases in the presence of a nanoclay. The faster start in building the crystallisation structure in the presence of the nanoclay could be attributed to the fact that the stretch process expands the gallery space (d-basal), which means a high contacting surface between the nanoclay platelets and the PET matrix, which may lead to an earlier nucleation process.

The decrease in crystallisation temperature from solid (Tgc) for un-filled PET films (see figure 5.27) agrees with other researchers' results, such as Zaroulis and Boyce (1997), who investigated the effect of uniaxial stretch on the crystallisation temperature (Tgc) of

PET films at various stretch ratios and different temperatures. The T_{gc} decreased markedly on increasing the stretch ratio, and the authors attributed this to the orienting of the macromolecular network leading to the formation of the crystallisation structure.

The changes in thermal temperatures of the film due to stretching were only seen in the glass transition temperatures (T_g) and crystallisation temperatures from the solid (T_{gc}), while no significant change occurred in melting temperatures (T_m) or crystallisation temperatures from melt (T_{mc}). The full DSC curves for the un-filled and PET/MTE films are shown in appendix 5 (see figures x5.10 - x5.13).

5.4.7. Double melting endotherm behaviour of PET

I. Introduction

Multiple melting endotherms have been observed with many semi-crystalline polymers, copolymers and blends. Many reasons have been invoked to explain this phenomenon and it seems clear that this can be explained by one of the following mechanisms: the presence of more than one polymorphism; changes in morphology; and/or the effect of molecular weight distribution [Kong (2003)].

Bell and Murayama (1969) and Bell and Dumbleton (1969) observed two endotherms and proposed that the lower represented the melting of imperfect or smaller crystals with partially extended chains while the higher was associated with the melting of folded chain crystals. Also they considered in their results that more extended crystals were preferred kinetically and the folded chain crystals converted to extended chain crystals, on annealing during heating.

Furthermore, Roberts (1969) observed two endotherms and proposed that the lower melting endotherm represented the melting of folded chain crystals and the higher represented bundle-like crystals. Both Bell's and Robert's conclusions were based on the assumption that the melting endotherms were directly related to the structures that developed on crystallisation. These authors did not consider the effect of the heating rates.

Holdsworth and Turner-Jones (1971) observed two endotherms and suggested that the lower endotherm was due to the melting of crystals formed at the crystallisation temperature while the higher endotherm was due to annealing on heating. Zhou and Clough (1988) were the first to report three melting endotherms in the melting of PET

and they labeled the endotherms I, II and III. They attributed endotherm I to the melting of crystals formed during secondary crystallisation, endotherm II to the melting of crystals formed during primary crystallization, and endotherm III to those formed as a result of re-crystallisation on heating.

Medellin-Rodriguez et al. (1996; 1997) reported a different view from that of Zhou and Clough. The melting behaviour of PET was studied using DSC, polarised light microscopy and small angle x-ray scattering (SAXS). They found that melting was the morphological reversal of crystallisation with respect to the primary and secondary structures produced. They considered that endotherm I occurred in metastable crystalline material when the small branches melted, endotherm II resulted from the melting of metastable secondary branches, and endotherm III was associated with dominant branches, which underwent some recrystallisation on heating.

Normally, PET pellets (e.g. bottle grade) have one melting temperature around 250°C. The double melting endotherm is generally caused by an insufficient solid state polymerisation (SSP) process treatment for the PET pellets. During the standard SSP process, the material goes through certain stages and each stage exhibits a typical DSC profile, as shown in figure 5.31 [Culbert and Christ (2003)].

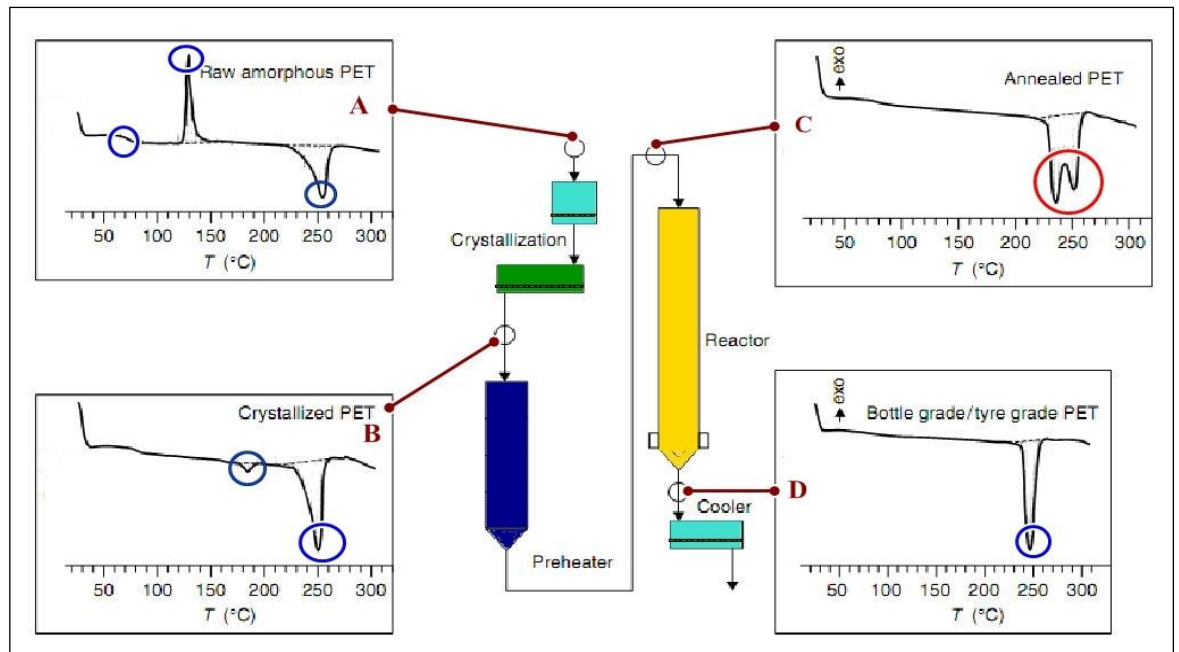


Figure 5.31 Schematic of DSC diagram for PET pellets during SSP process

It can be seen in figure 5.31 that the exothermic peak of the PET pellets caused by primary crystallisation before the crystallisation stage (figure 5.31-A) has disappeared and an endothermic low melting peak has taken its place (figure 5.31-B) due to crystals formed in the crystallisation section. This is necessary to raise the temperature above the intended SSP temperature before processing at a higher SSP temperature. This action can reduce the risk of sintering later on the SSP column. Also the polymer has a tendency to stick at lower temperatures and so this higher range is again preferred. The phenomenon of sticking is a very severe engineering problem in SSP and indeed in any drying process. This low melting peak (figure 5.31-B) tends to move to a higher temperature and its size increases during drying which obviously leads to the formation of a double melting peak (figure 5.31-C). With sufficient SSP processing through the SSP reactor, the double melting behaviour becomes a single melting peak (figure 5.31-D).

Jabarin and Lofgren (1986) studied the effect of SSP processing parameters on melting endotherms and they found that the temperature and residence time have major effects.

Table 5.3 summarises their results.

SSP process	T _m °C (1 st endotherm)	T _m °C (2 nd endotherm)
200°C for 4 hrs	233	254
210°C for 4 hrs	239	254
220°C for 4 hrs	245	248
225-230°C for 8 hrs	---	246

Table 5.3 First and second melting endotherms under various SSP processes.

As Table 5.3 shows, on increasing the temperature and time for the SSP process the first endotherm will disappear. A typical residence time in the SSP process is in the range of 10 – 20 hrs at a temperature of 210°C.

II. Study of the experimental technique for double melting endotherms

Polyethylene terephthalate (PET) resin was supplied by Tergal Industries (France) at grade F9 and intrinsic viscosity 0.8dl/g. A Differential Scanning Calorimeter (DSC) was used with different scenarios as follows:

[A] Heat from 35 to 300°C with heating rate 20°C/min.

[B] Heat from 35 to 300°C with heating rate 10°C/min.

[C] Heat from 35 to 190°C with heating rate 10°C/min, then keep isothermal for 20mins, then heat from 190 to 300°C with heating rate 5°C/min.

[D] Heat from 35 to 300°C with heating rate 0.5°C/min.

[E] Heat from 35 to 300°C with heating rate 0.1°C/min.

Furthermore, a Modulate Differential Scanning Calorimeter (MDSC) was used for further investigation with an experimental protocol of:

[F] Heat from 35 to 300°C with heating rate 4°C/min and modulation of ($\pm 0.4^\circ\text{C}$) every 40seconds.

III. Results and discussion of the double melting endotherms study

Figure 5.32 shows the DSC curves for scenarios A–E. It is clear that each curve shows two melting endotherms. Also it is clear that on decreasing the heating rate the two endotherms tend to separate from each other to form individual peaks, and the first endotherm peak tends to disappear.

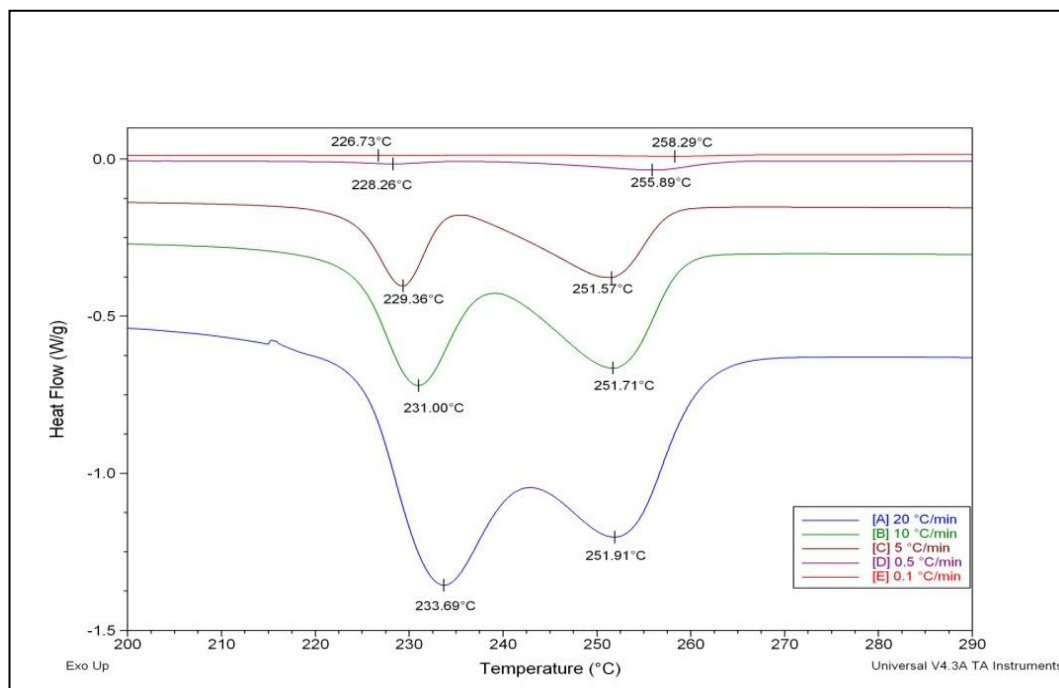


Figure 5.32 Double melting endotherm behaviour with different heating rates

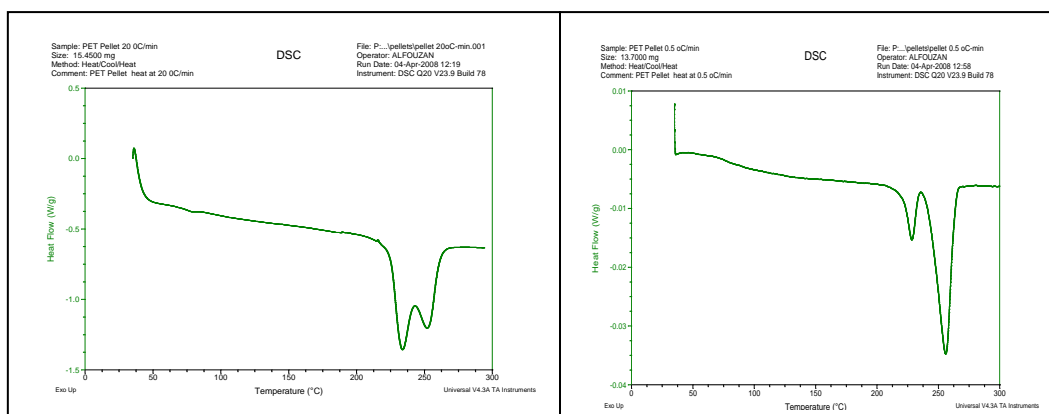


Figure 5.33 Shape of double melting endotherms for heating rates of 20°C/min and 0.5°C/min, in sequence

Figure 5.33 shows that on decreasing the heating rate the two endotherms mentioned earlier become clearer, tending to form separate peaks, while the first peak tends to disappear

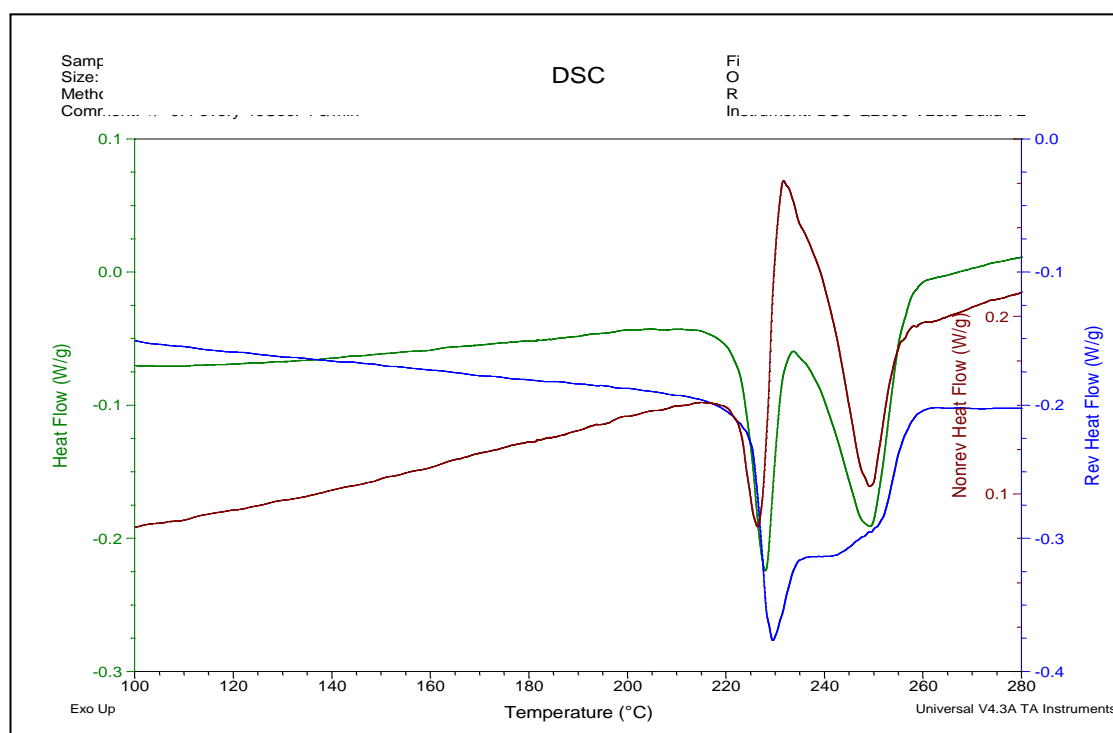


Figure 5.34 MDSC curves for the [F] scenario.

From the MDSC curves (figure 5.34) the total heat flow curve (green line) confirms the availability of double melting endotherms, which means the material has more than one

polymorphism. The non-reversible heat flow (brown line) shows that the non-stable or imperfect crystals start to melt at a low temperature and simultaneously the melt recrystallises until the temperature rises to around 243°C, where the polymer completely melts the stable crystal or the crystal forms as result of recrystallisation during heating. The reversible curve (blue line) averment the simultaneously melting crystallinity by showing that the melt starts at a low temperature and continues till the polymer completes melting, which means while the recrystallisation occurs the melting also occurs.

5.5 Conclusions

- The main objective of this chapter is to analyse the thermal property results obtained from analysing PET nanocomposites using DSC in order to study the effect of adding nanoclays on the thermal behaviour of PET.
- It was observed that all three nanoclays used in this project (MAE, MTE and Cloisite 25A) act as nucleation agents for the crystallisation process by increasing the T_{mc} and decreasing the T_{gc} , while causing no consistent trends in the absolute crystallisation values.
- It also noticed that the change in the T_g and T_m in the presence of nanoclay was small.
- With increasing clay content, the curve moves to the right (higher T_{mc} temperature) and gets sharper (decrease in the $t^{1/2}$) which indicates the crystallization rate is increased.
- Unfilled PET and PET/MTE nanocomposite (1, 3 and 5 wt.%) films before and after biaxial stretch were analysed using DSC to investigate the effect of the equal biaxial stretch film process on the thermal properties of the film.
- Stretching the un-filled PET film decreased chain flexibility and this is indicated by the increase in glass transition temperature (T_g). Stretching the film also accelerates the crystallisation temperature of the film from the solid phase (T_{gc}).
- Adding further MTE filler (e.g. 3 or 5 wt.%) leads to the MTE starting to build up crystallinity immediately after the glass transition temperature in the case of the stretched film. This confirms that the stretch process forms crystalline structures inside the PET matrix. It is also observed that the stretching accelerated T_{gc} and this acceleration increases in the presence of a nanoclay.

The more rapid start in building the crystallisation structure in the presence of the nanoclay could be attributed to the fact that the stretch process expands the gallery space (d-basal), which means a high contact surface between the nanoclay platelets and the PET matrix, which may lead to an earlier nucleation process.

- Semi-crystallised PET pellets as received from the supplier (Tergal F9) were used to investigate the double endotherm melting temperatures exhibited in the first heating stage of the DSC test. With sufficient SSP processing through the SSP reactor, the double melting behaviour becomes a single melting peak.

Chapter six

6. The cold drawing of polyethylene terephthalate (PET) amorphous film:

The objectives of this chapter are to investigate the mechanical properties of the amorphous film of PET nanocomposites which are produced via cast film extrusion (see section 3.3.2) and amorphous micro-size samples of PET nanocomposites which have been prepared by a micromoulding injection machine (see section 3.3.3) using tensile testing or cold drawing. The injection speed in the injection processing of polymer nanocomposites can have major implications for the mechanical properties of the polymer NC product and the dispersion of the nanofiller into the polymer matrix. The micromoulding injection process has been run under various injection speeds to investigate this injections' effect on the final product mechanical properties. The final PET forming process (e.g. for bottles, films etc.) exposes the material to some physical effects such as biaxial tension for film packaging or bottle production so this study may give an indication on nanoclay effects on these properties.

The effect of uniaxial stretch ratio on the tensile modulus of the amorphous films has been studied. The tensile modulus results of PETNC films are correlated to the TEM images results for the same films. This chapter starts with a brief introduction about the mechanical properties and then presents the observations and outputs of some previous studies on the effect of nanofillers on the mechanical properties of the polymer. Prior to the discussion of this study's results, the experimental procedures of the tests are presented.

6.1 Introduction:

Polymer matrices have much lower modulus than the hard particles and this can be derived from the Halpin-Tsai equation [Ke et al. (1999)]. In general, it has been found that mechanical properties of polymer nanocomposites are greatly improved when the nanoclay particles have a high degree of exfoliation and have good affinity with the matrix polymer. [Sanchez-Solis et al. (2003)].

Some polymers (have high modulus at room temperature) such as polystyrene, polymethyl methacrylate and amorphous PET (when quenched from the melt state) but other polymers have low modulus at room temperature such as natural rubber.

Stretching the amorphous PET can produce orientation and this orientation leads to juxtaposition of the molecules to produce small regions in three-dimensional orders known as crystallinity. [Ward and Sweeney (2004)]

Brittleness of polymer nanocomposites is a common problem. The impact strength decreases with increases the tensile modulus [Utracki et al. (2007) and Pavlidou (2008)]. The nanometric scale additive may lead to restriction in the mobility of the PET molecules.

Direct evidence of the dispersion of the nanoclay into the polymer matrix can be provided by TEM technique. TEM images cannot be taken individually as evidence of good dispersion of the platelets but can assist other results especially the tensile test. Because the images represent a very small area the dispersion within the whole matrix can still be unclear. The distinguish and unique of TEM test is that it can be used to demonstrate whether the platelets are exfoliated or intercalated.

6.2 literature review:

Brandao et al. (2006) reported a successful attempt to prepare PET nanocomposites with lamellar zirconium phosphorous via twin-screw extrusion at 280 °C with a screw speed of 90 rpm in order to investigate the mechanical and thermal properties of the composites. It was observed that the moduli increased with addition of filler, this being attributed to the enhancement of crystallinity degree which was induced by the nanofiller nucleation, and the presence of the inorganic phase. It was found that increasing filler level from 2 to 5 wt.% did not show any significant increase in the mechanical modulus. Usuki et al. (1995) ascribed the enhancement of the mechanical properties to the strong interaction between the filler layers and the polymer molecules while Wang and Gao (2004) attributed this phenomenon to decrease in spherulite size as well as physical crosslinking associated with the nanofiller.

Frounchi and Dourbash (2009) studied the permeability properties of PET/ (Cloisite 15A and Nanolin DK₂) nanocomposites prepared by twin screw extrusion (this paper is covered in detail in chapter 7). In addition to the barrier properties presented, the authors reported that the tensile modulus of PET were nanocomposites enhanced compared with un-filled PET. PET/Cloisite 15A shows fluctuation in the tensile results with increasing tensile modulus at 1 wt. %; this decreasing at 2 and 3 wt.% prior to an increase for 4 wt.%. This may be attributed to many reasons such as the incompatibility of Cloisite 15A with the PET matrix due to the differences in the polarity or the high thermal processing temperature used during preparation of the films (melted at 275 °C for a long time). DK₂ addition increased the tensile modulus gradually at 1 and 2 wt. % but to lower than values for the Cloisite 15A nanocomposites. The authors state that

adding the nanoclay at high concentrations may lead to reduction in the tensile modulus due to aggregation of the nanoclay. The organic montmorillonite (DK₂) has been also used by Wang and Gao et al. (2006) in order to prepare PET nanocomposites via twin screw extrusion.

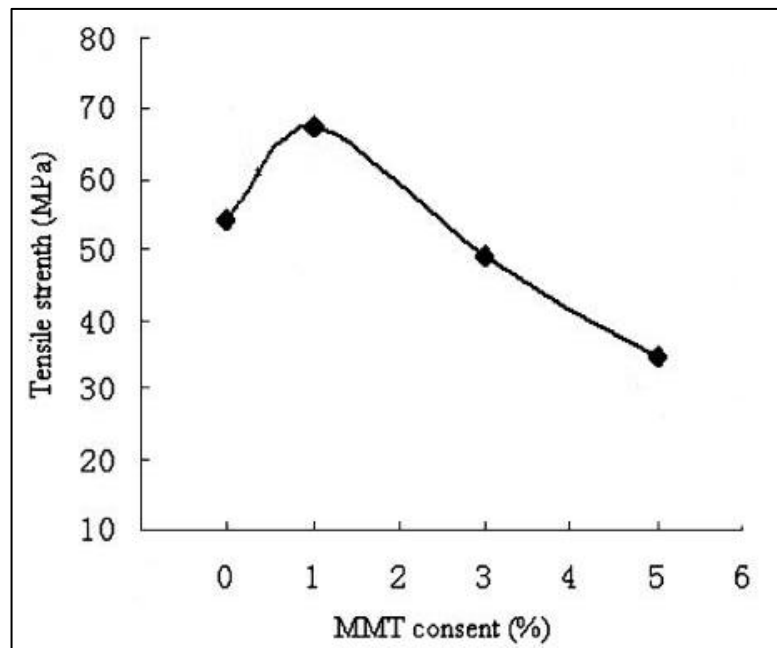


Figure 6.1 Tensile strength vs. DK₂ content. [Wang and Gao et al. (2006)]

The authors observed that adding greater than 1 wt.% of DK₂ decreased the tensile modulus of the PET (figure 6.1). It was reported by the authors that the large specific area of DK₂ leads to a strong interaction between PET matrix and the organoclay and this interaction is not complete at high organoclay concentrations.

Fornes et al. (2001) studied the effect of the molecular weight of nylon 6 on the nanocomposites properties. Three different molecular weights (Mw) of nylon 6 ($M_{n(\text{low})} = 16400$, $M_{n(\text{medium})} = 22000$ and $M_{n(\text{high})} = 29300$ g/mol) were compounded with organoclay via a twin screw extruder then the nanocomposite pellets were injection

moulded into tensile specimens. The authors observed that adding the organoclay enhanced the stiffness of the nylon 6 nanocomposites for all molecular weights. The improvement continued with adding more nanoclay. It was found that at any given nanoclay concentration, the stiffness increased with increasing Mw of nylon 6.

A studying on the effect of ionic groups on PET/nanoclay nanocomposites was conducted by Barber and co-workers (2005). Three different types of nanoclay (Cloisite Na, 10A and 15A) at the same concentration (5 wt.%) were compounded via melt extrusion process (twin screw extruder) with PET-ionmers (ionic content 1.8, 3.9 and 5.8 mol %). The authors reported that the mechanical properties of non-ionic PET increased with adding nanoclay and Cloisite 10A NCs exhibited the highest tensile modulus. Furthermore, adding ionic to the PET nanocomposites further enhanced the tensile modulus.

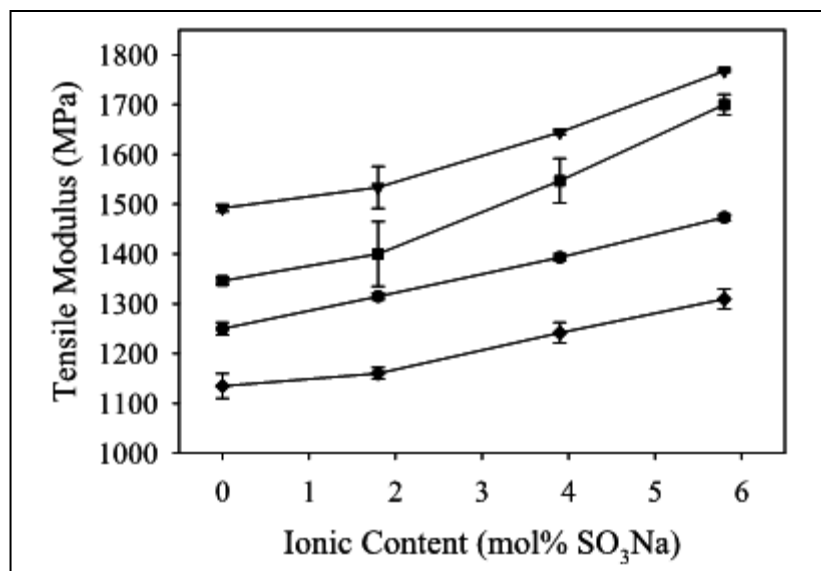


Figure 6.2 Tensile modulus vs. ionic content for nanocomposites made with different types of nanoclays. No Cloisite (♦), 5% Cloisite Na (●), 5% Cloisite 10A (▼) and 5% Cloisite 15A (■). [Barber et al. (2005)].

As figure 6.2 shows, the tensile moduli of PET ionomers/nanoclay nanocomposites exhibit greater improvement compared with PET nanocomposites without ionomers and the authors attribute this to strong interactions between the silicate layers and the sulfonic acid groups in the PET ionomers which leads to a high degree of exfoliation. This conclusion was backed up with TEM and XRD results.

Enhancing the mechanical properties of recycled PET (rPET) by adding nano-fillers has been studied and reported in many papers. Bizarria et al. (2007) prepared rPET/nanoclay nanocomposites by twin screw extruder and generally found that nanoclays enhance the tensile strength and stiffness of rPET compared with un-filled rPET. This enhancement was attributed to a good clay dispersion as observed in TEM and WAXS results. Figure 6.3 shows the Young's modulus of rPET/nanoclay nanocomposites.

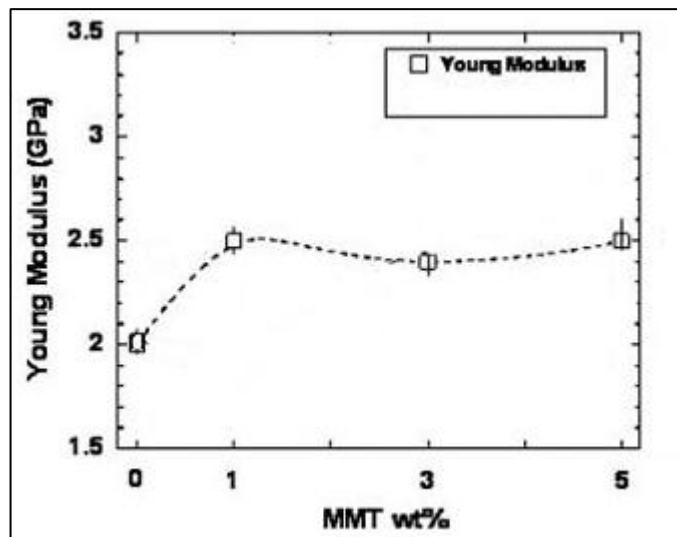


Figure 6.3 Tensile modulus of rPET/clay nanocomposites [Bizarria et al. (2007)].

It seems clear from figure 6.3 that nanoclay levels greater than 1 wt.% did not show any further significant enhancement in the tensile modulus. Preparing the rPET nanocomposites tensile specimens under high processing temperature during the compounding and then the injection processes may have degraded the rPET matrix and

the nanoclay which may hinder further investigation of the rPET nanocomposites tensile modulus.

Kim et al. (2009) introduced carboxylic acid groups on the surface of carbon nanotubes (CNT) prior to compounding with high intrinsic viscosity PET (I.V approximately 1.07 dl/g). The authors aimed to increase the interaction between the PET matrix and the nanotubes through modification since the mechanical, thermal and rheological properties mainly depend on the interfacial interaction between the nanotubes and the PET matrix. It was observed that the modified CNTs achieved higher mechanical properties more than un-modified CNT. Furthermore, adding more modified CNT significantly increased the mechanical properties of PET nanocomposites and this was attributed to the possibility of interaction occurring between the ester groups in the PET and the carboxylic acids groups which can lead to better interfacial adhesion between the CNT and PET matrix. Adding CNT to the PET matrix leads to increase in the stiffness of the matrix which results in the decrease of elongation at break.

Tarverdi and Sontikaew (2008), aimed in their work to study the effect of using different concentrations of modifier on the rheology, morphology and product tensile properties, also studying the effects of different process melt temperatures on these properties. Cloisite 10A and Nanofil-2 (N2) organoclays were used in this study as both of them are coated with the same surfactant but the percentage of surfactant in 10A (125 meq/100g) is greater than for N2 (75 meq/100g). It was observed that the processing temperature (255 and 280 °C) did not produce different effects on the tensile properties of un-filled PET and PET nanocomposites amorphous films. The PET/Cloisite 10A nanocomposite exhibited better tensile modulus enhancements compare with PET/N2 nanocomposite though both were improved upon un-filled PET. Furthermore, SEM

results showed the degree of Cloisite 10A dispersion in the PET matrix to be greater than for N2.

Sanchez-Solis et al. (2003) added compatibilizer to increase the compatibility between the PET matrix and nanoparticles (Cloisite 15A) and studied the thermal behaviour and the mechanical and rheological properties of the PET nanocomposites. The authors reported that even without reaching the complete exfoliation, the tensile and strength modulus increased by 32% and 30 % respectively with increasing the clay concentration in the presence of the compatibilizer.

Pegoretti et al. (2004) prepared and characterized recycled PET/clay nanocomposites. Recycled PET (rPET) pellets and two montmorillonite clays (Cloisite Na⁺ and Cloisite 25A) were used to produce PET nanocomposites with 1, 3 and 5 wt.% via melt compounding with a co-rotating screw extruders. Scanning Transmission Electron Microscopy (STEM) was used to evaluate the dispersity of the nanocomposites and it was found that the Cloisite 25A gave much better dispersion compared to Cloisite Na⁺. Also Wide Angle X-ray Scattering (WAXS) measurements indicated increased lamellar periodicity of Cloisite 25A in the composition which implies intercalation occurred. It was observed that both nanoclays enhanced the modulus of rPET nanocomposites.

The micromoulding process becomes a key process for the manufacture of very small scale polymer nanocomposite products. Nanocomposites are suitable for micromoulding applications since they provide benefits in terms of ease of processing as well as enhanced final properties. Polymer materials are exposed to harsh process conditions in the micromoulding process compared with conventional injection moulding [Zhao et al. (2003)].

By controlling the orientation of the polymer chains during the injection moulding process, the mechanical properties of the polymer product can be enhanced. The shear extension flow of semi-crystalline polymers during injection moulding can induce high molecular orientation [Zhong et al. (2006)]

Wang et al. (2004) studied the effect of the shear rate on clay dispersion in a polypropylene matrix during the injection moulding process. The authors observed that using chemical modification of the clay with shear, the dispersion of the clay into polymer matrix was enhanced exhibiting an exfoliated morphology within the core and an intercalated morphology in an oriented zone. Yalcin et al. (2003) investigate the effect of processing conditions and nanoparticles on local microstructure of nylon 6 by variation of the injection speed and mould temperature. The samples were prepared at two different injection speeds (2.02 and 17 cm/s) and mould temperatures (50 and 130°C). The authors found that the orientation of the polymer matrix can be enhanced by the nanoplatelets throughout the mould thickness due to the effect of shear amplification that occurs in the narrow gap between the tightly packed nanoplatelets at different speeds. The authors also observed high orientation levels in the core of moulded parts.

Hsiung et al. (1993) and Hsiung and Cakmak (1993) observed similar behaviour for liquid crystal polymers. Furthermore Yalcin and his team (2003) presented schematics of the organization and orientation of the nanoplatelets from skin to core for the samples moulded at 50 and 130°C as shown in figures 6.4 and 6.5.

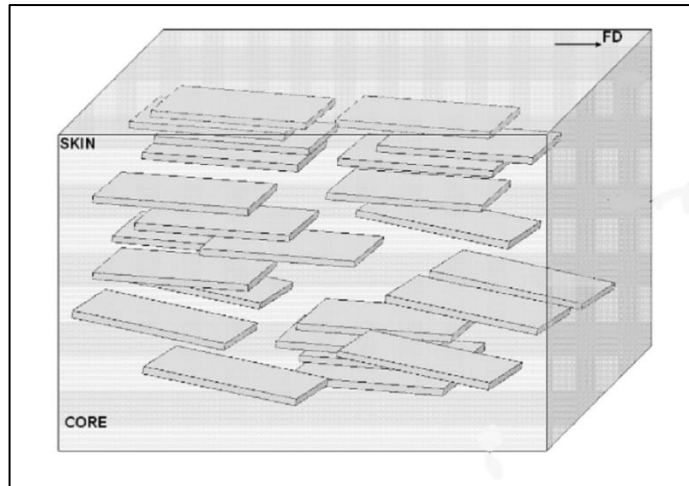


Figure 6.4 Schematic of nanoplatelets orientation from skin to core for specimens moulded at 50°C

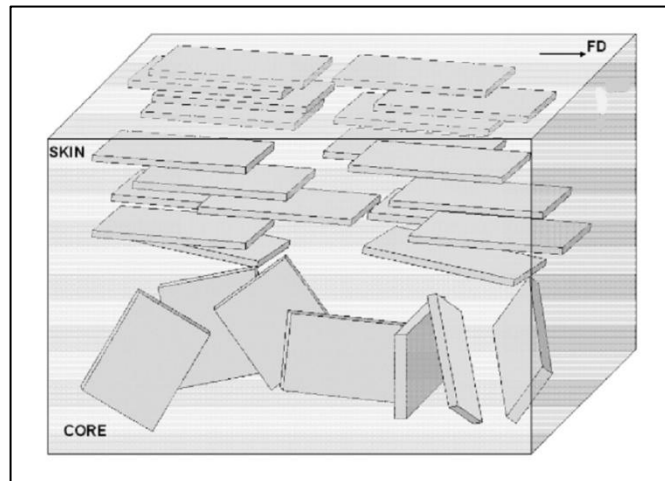


Figure 6.5 Schematic of nanoplatelets orientation from skin to core for specimens moulded at 130°C

6.3 Experimental work:

The tensile tests in this study were applied on samples produced via both extrusion and injection moulding process. The method of producing the un-filled PET and PETNC films using the cast film extrusion was covered in section 3.4.2 while section 3.4.3 covered the micro-moulding injection process used to prepare the micro-size tensile bars.

Tensile tests applied on the film and micro-size samples. An Instron 5564 tensile test machine was used to test the mechanical properties of the films PET and a Bose ElectroForce machine was used to test the mechanical properties of the micro-size tensile bars. Section 3.5.7 described these equipments in detail.

Transmission Electron Microscopy (TEM) was used to characterise the PET nanocomposite films as described in section 3.5.8. These TEM micrographs of PET nanocomposites were used to assist the results from the tensile tests.

6.4. Results and discussion:

In this section, the results of the tensile tests of un-filled PET and PET nanocomposites films (using Instron 5564) are discussed to show the effect of nanoclays on the mechanical properties of the samples. The tensile tests of un-filled and PET nanocomposites micro-moulded samples (using the Bose Electroforce (see 3.5.7)) are also discussed to investigate the effect of injection speed on the mechanical properties of the samples.

6.4.1 Tensile testing for un-filled PET and PET nanocomposites films

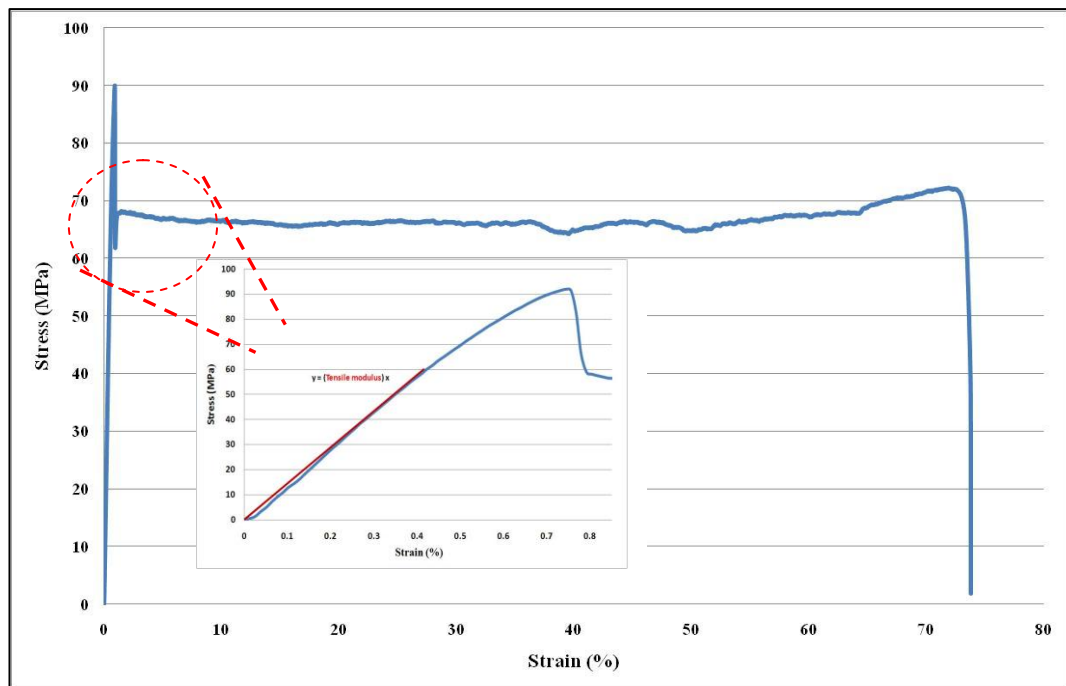


Figure 6.6 Typical stress-strain curve for cold drawing of PET film. (window shows method for calculation of tensile modulus)

Figure 6.6 shows a typical cold draw plot for PET films obtained from our tensile tests. The stress increases linearly with strain as load is applied to reach the maximum point prior to necking occurring which leads to a drop in the stress to a local minimum. The necking is associated with an initial maximum point in the stress-strain curve. This

necking phenomenon can not be attributed to the changes in the sample geometry alone. Whitney and Andrews (1967) and Brown and Ward (1968) showed that the stress used for initiation of the yield is greater than the stress required for yield propagation.

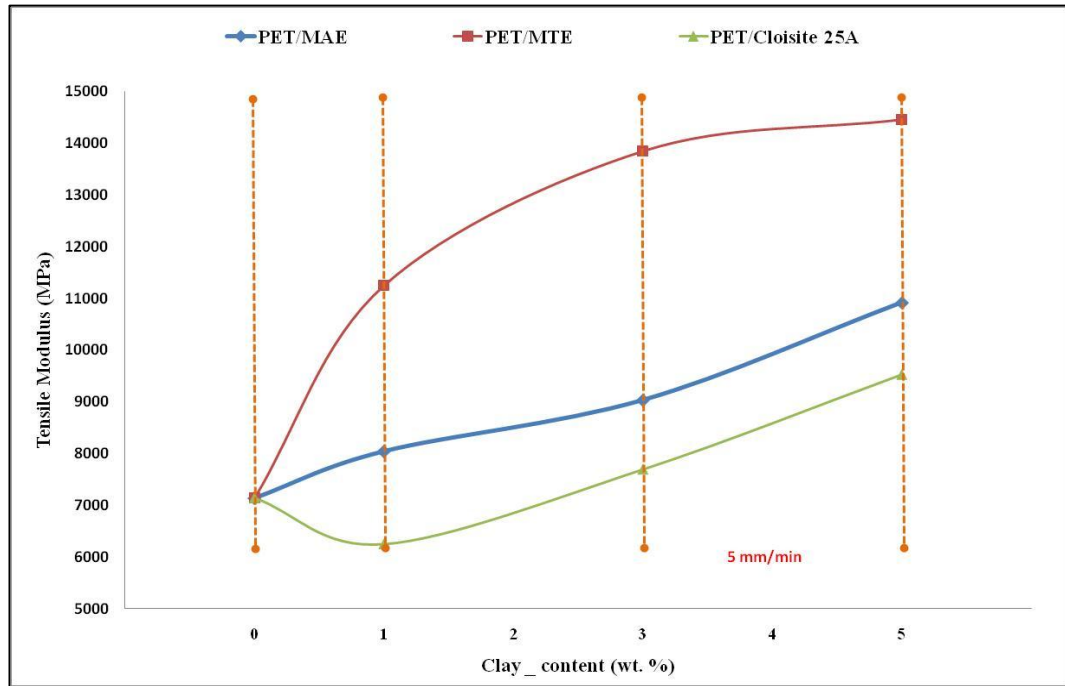


Figure 6.7 Tensile modulus of PETNCs films vs. clay contents at tensile test speed of 5 mm/min

The tensile test for the PET nanocomposite films was conducted at two different crosshead speeds; 5 and 50 mm/min. The influence of adding nanoclay to the PET matrix on the tensile modulus of un-filled PET and PETNC films at different test speeds is illustrated in figures 6.7 and 6.8. At the lower speed test (5 mm/min), Somasif MTE exhibits the greatest increase in the tensile modulus. In contrast Cloisite 25A (1 wt.%) reduced the tensile modulus then enhanced these values at higher loadings.

It is enlightening to consider the reasons leading to these results. The improvement in the tensile modulus when adding MAE or MTE can be attributed to many reasons such as the good dispersion of these clays within the PET matrix as the TEM images in figures 6.9 and 6.10 show. The good compatibility between the PET chain and MTE or

MAE clays contribute to this improvement. The large intergallery spacing and greater aspect ratio of the MTE and MAE platelets compared with the Cloisite 25A platelets may increase the diffusion rate of PET macromolecules into the Somasif (MAE and MTE) intergallery space compared to the Cloisite 25A. This may enable the Somasif clays to enhance the interfacial adhesion between the clay platelets and the PET matrix. The orientation of the PET chain which occurs during the tensile stretch also increases the strength of the material as well as aligning the nanoclays' platelets.

Although the poor dispersion may lead to a reduction or very small increase in the mechanical properties of the polymer. Here we have Cloisite 25A as good example to show what is the effect of relatively poor dispersion (little intercalation around tactoids area) on the polymer behaviour especially the mechanical properties. The drop in the tensile modulus of PET/Cloisite 25A (1 wt.%) may be attributed to the agglomeration of the nanoclay within the PET matrix as TEM images show (see figure 6.11) and the orientation of the PET chain eliminates some of the failure caused by the nanoclay by increasing the strength of the chain and aligning the nanoclay's platelets. The small d-space and the shorter aspect ratio of the Cloisite 25A platelets may also be counted as one of the reasons. Nevertheless the failure to enhance the mechanical properties does not necessarily means corresponding deterioration in other properties. PET/Cloisite 25A films exhibit excellent gas barrier improvements (see chapter 7) and act as nucleation agents as seen in the crystallisation temperature and rate results shown in chapter 5.

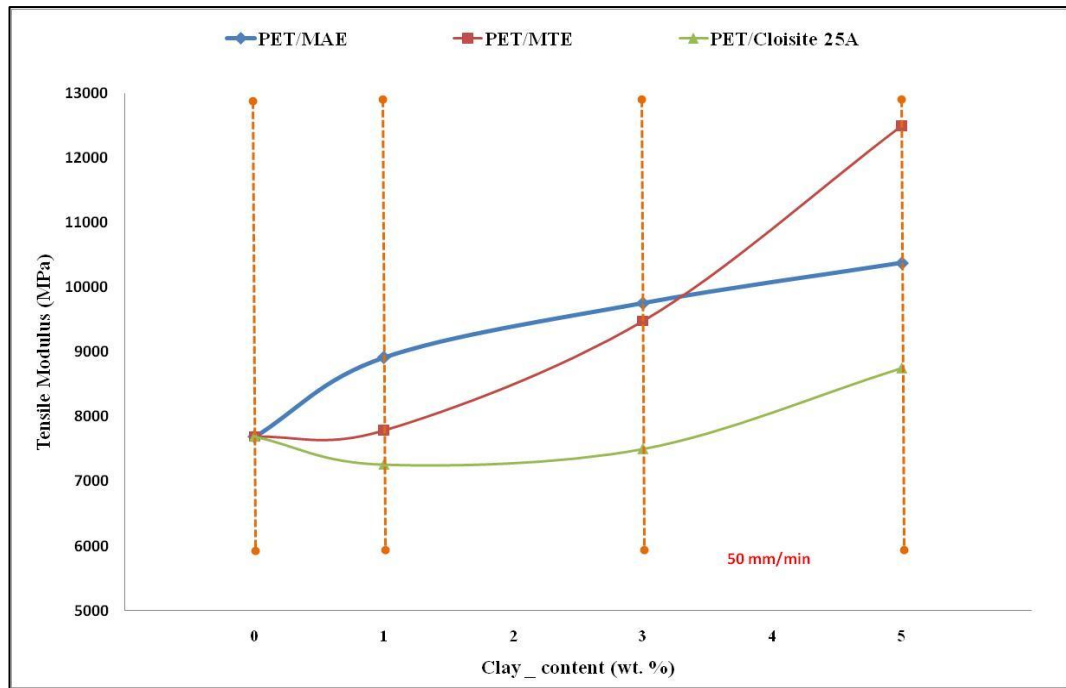


Figure 6.8 Tensile modulus of PETNCs films vs. clay contents at tensile test speed of 50 mm/min

The higher speed tests may be expected to produce high modulus values because it will simulate stiffer molecules while the slower speed will allow the molecules to respond flexibly and exhibit lower tensile modulus. Un-filled PET and PET/MAE nanocomposites films tested at 50 mm/min show increases in the tensile modulus compare to the same samples tested at the lower speed (5 mm/min). However PET/MTE nanocomposites films exhibited higher modulus values at the lower speed, this being attributed to excellent dispersion of the MTE within the PET matrix or, in other words, the dispersion aspect was few exfoliations around intercalation and the slower speed gave more time to the nanoclay platelets to align and reinforce the matrix. This phenomenon was not observed for PET/MAE while it exhibit a good dispersion aspect, may be because the dispersion aspect did not hold any exfoliation aspect so most of the platelets already align.

The above results are further presented in figures x6.1-x6.12 showing the tensile modulus vs. clay content at the two crosshead speeds (5 and 50 mm/min.).

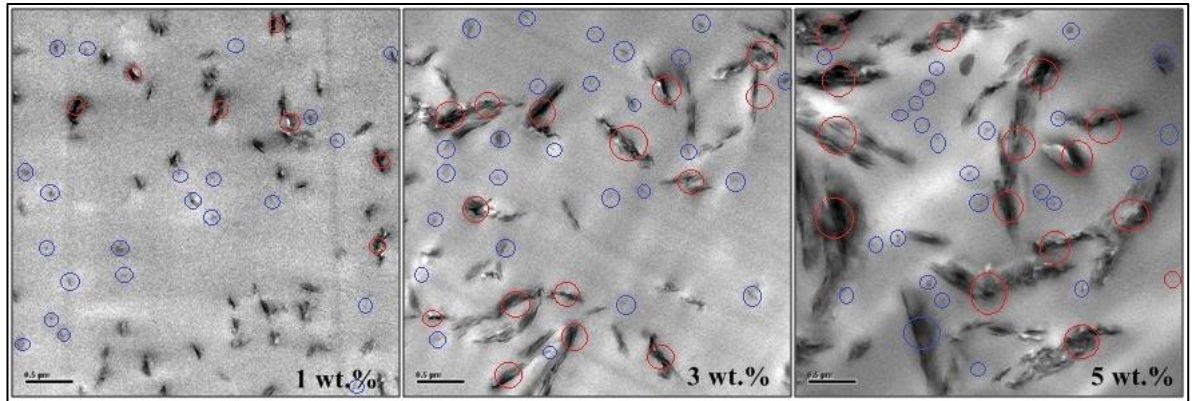


Figure 6.9 TEM micrographs for PET/MAE nanocomposites films at various clay concentrations

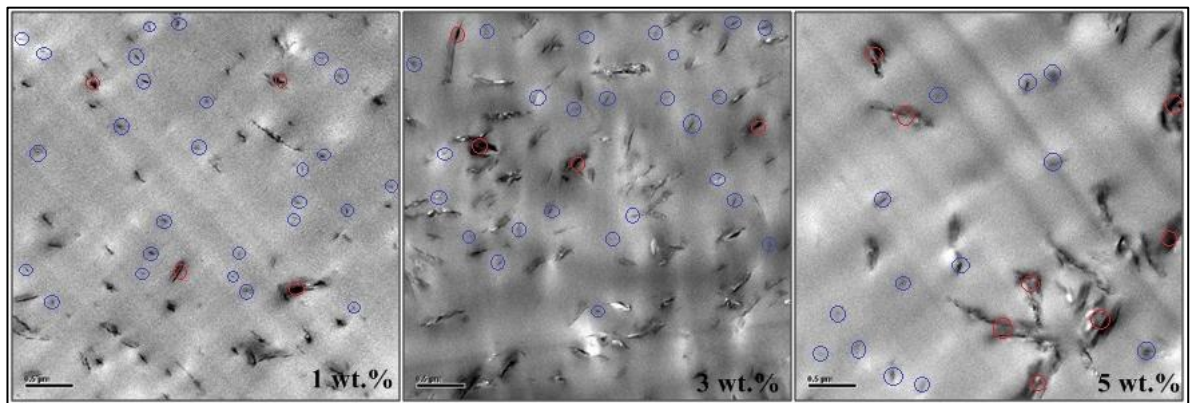


Figure 6.10 TEM micrographs for PET/MTE nanocomposites films at various clay concentrations

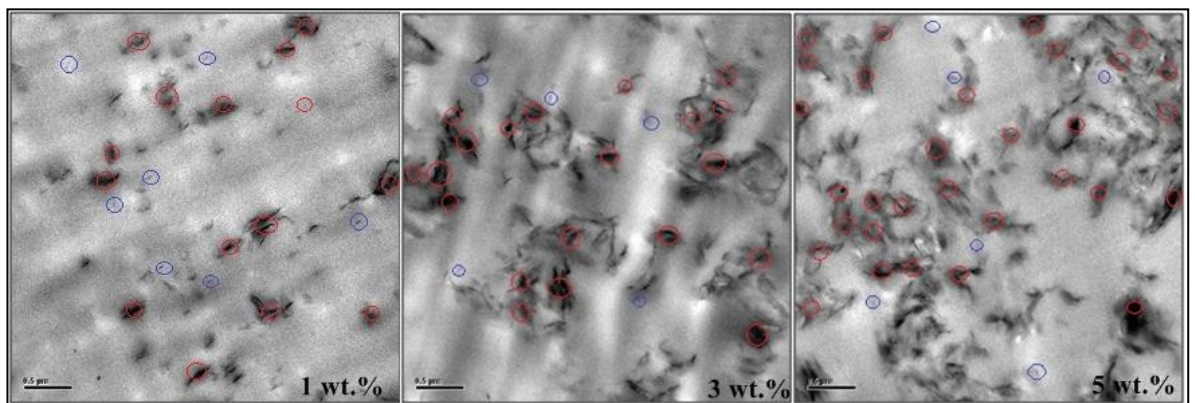


Figure 6.11 TEM micrographs for PET/Cloisite 25A nanocomposites films at various clay concentrations

All TEM micrographs have been taken at one resolution and the scale bars (0.5 μm) are specified for each image. From the TEM images, it seems clear that the use of the synthetic clay (Somasif MAE or Somasif MTE) provides better dispersion when compared to Cloisite 25A. This can be attributed to smaller the gallery space for Cloisite 25A, the larger aspect ratio of the Somasif clays as well as the organic modifier used in the synthetic clays which can help 'bond' the clay to the polymer matrix and thus enhance the affinity more than for the non-synthetic Cloisite 25A. Also as mentioned before (see section 2.4), the synthetic clay has well controlled chemical and physical properties while the nature clay shows variability with properties of polymer nanocomposites.

TEM images shown in figure 6.11 show PET containing various Cloisite 25A loading which show large grouping of Cloisite 25A platelets appearing as dark spots or, in other words the images show a tactoid morphology. Little intercalation occurs around these tactoid regions.

Figure 6.10 contain 3 images of PET/MTE nanocomposites films and demonstrate that the MTE nanoparticles exhibit good dispersion with in the PET matrix without large tactoids being present.

6.4.2 The interplay of injection speed and nanoclay levels on the mechanical properties of PET nanocomposites

In this section the stress-strain curves obtained from the Bose Electroforce are discussed. The effects of nanoclay on the tensile modulus of the PETNC were covered in section 6.4.1 so we will focus this discussion on the area after the yield point until the break point. Due to the limitation of tensile elongation that the equipment can offer (12 mm), the break point for some samples was not reached. Figures 6.12 - 6.15 show the stress-strain curves for extruded vPET and some PETNCs at various injection speeds (100, 400 and 700 mm/s). The rest of the PETNC stress-strain curves are shown in appendix 6 (see figures x6.13-x6.18).

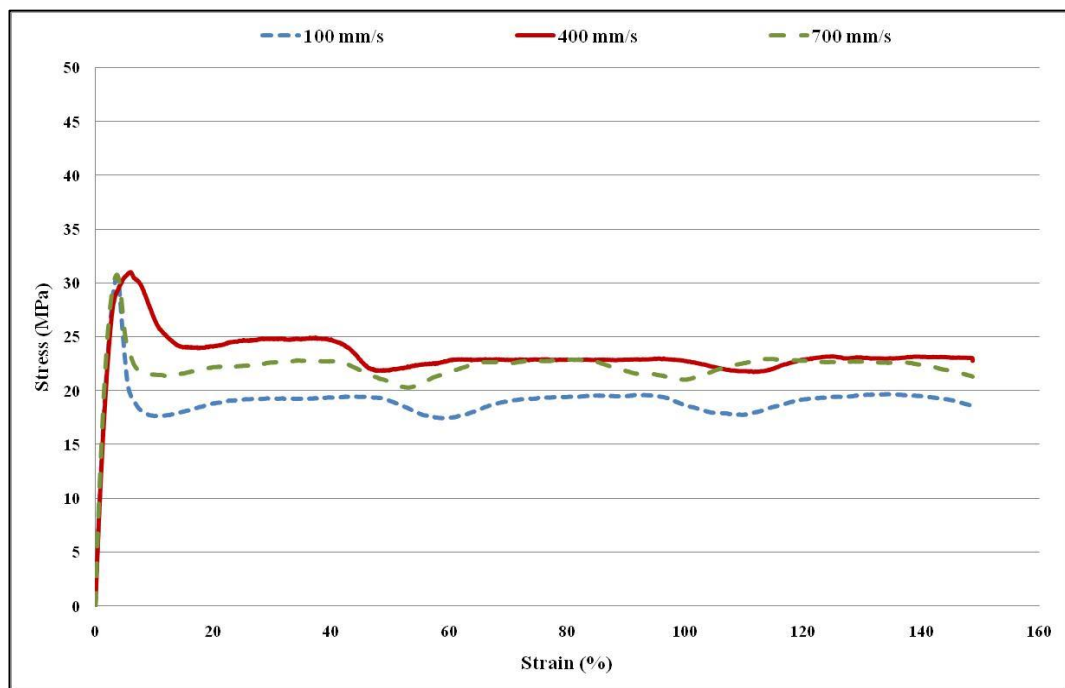


Figure 6.12 Stress-strain curve for extruded vPET micro size sample prepared at different injection speeds

The stress-strain curves for extruded vPET are shown in figure 6.12 and it is clear that the samples at various injection speeds exhibit such long elongation that the equipment did not allow the materials break point to be reached. The extruded vPET samples

produced at injection speed 400 mm/s show the highest stress values and the samples produced at injection speed 100 mm/s record the lowest stresses.

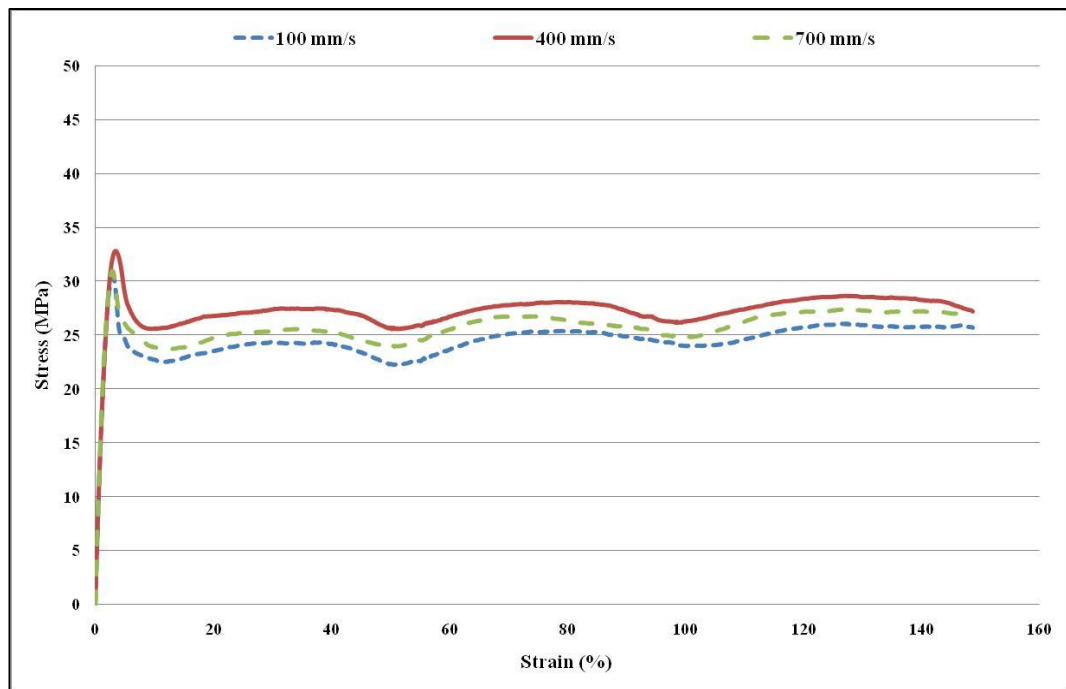


Figure 6.13 Stress-strain curve for PET/MTE (1 wt.%) micro size sample prepared at different injection speeds

Moreover the stress-strain curve for PET/MTE (1 wt.%) exhibits the same trend and phenomenon as the ext. vPET samples (figure 6.13). It is again clear that the samples produced at 400 mm/s exhibit the higher stress of the three samples.

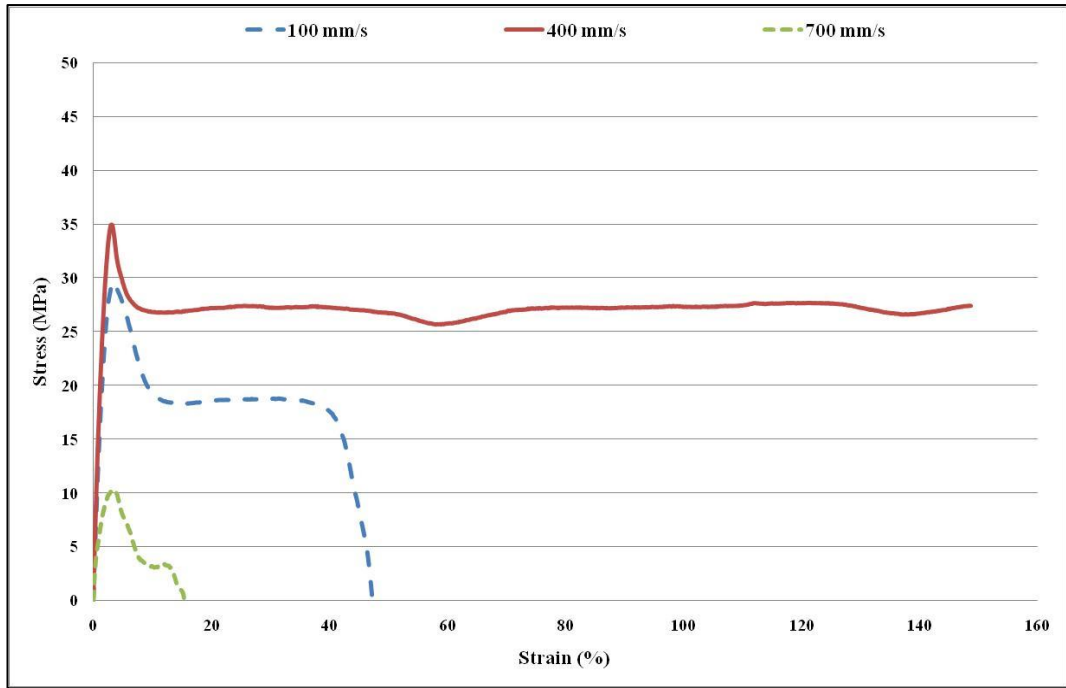


Figure 6.14 Stress-strain curve for PET/Cloisite 25A (3 wt.%) micro size sample prepared at different injection speeds

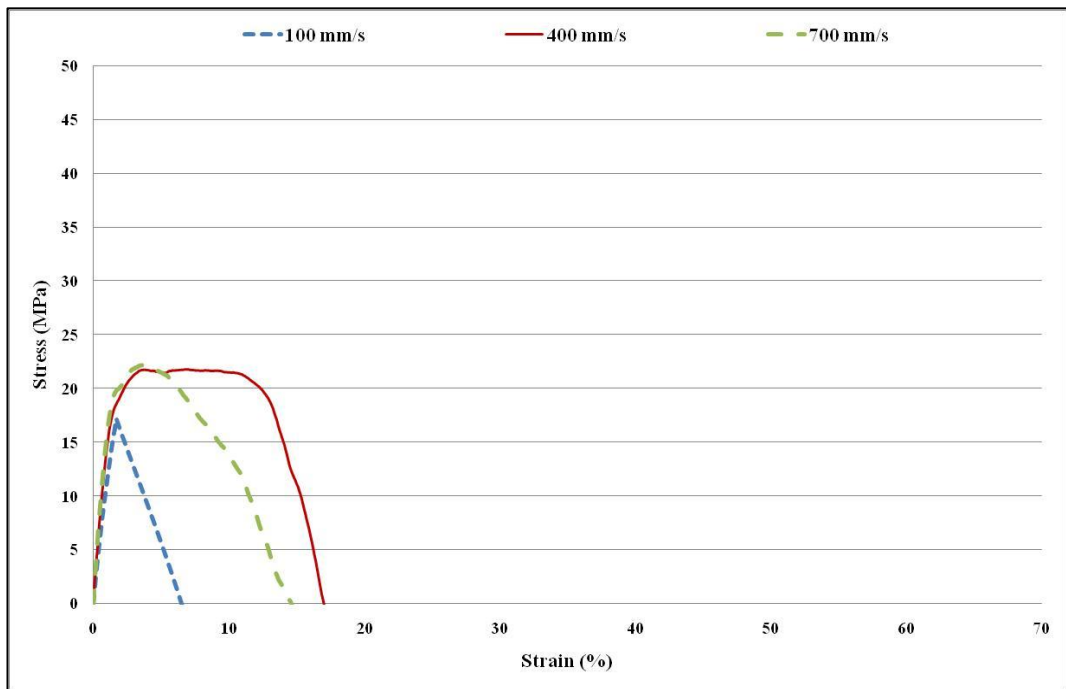


Figure 6.15 Stress-strain curve for PET/MAE (5 wt.%) micro size sample prepared at different injection speeds

Figures 6.14 and 6.15 show the stress-strain curves for PETNC at 3 and 5 wt.%. It is clear that the nanoclay increases the brittleness of the polymer nanocomposites. Although the difference with injection speeds exhibit a variety response to the tensile tests. Figures 6.12 to 6.15 represented random results of the tensile test from each PET/clay nanocomposites and the rest results have been plotted and listed in appendix 6 (see x6.13 to x6.18).

These results show that there appears to be an optimal injection speed and this observation in agreement with other studies' observations such as Ulcer et al. (1996) and Chan et al. (2002). It also show that the processing conditions such as injection speed are crucial factors affecting the mechanical properties of injection moulded products.

The normal phenomenon of micro-moulding skin/core structure for injection moulded samples may be expected to occur in our samples. As PET is a semi-crystalline polymer, it is expected for the molecular chains to orient in the flow direction and form shish-kebab crystalline structures in the skin layer due to the high injection speeds and rapid cooling as observed by Fujiyama et al. (1998) and Viana (2005). On the other hand, the chains of the PET molecules have less orientation and may present a mixture of shish-kebab and spherulite crystalline structure. In micro-size samples, as for thin wall mouldings the thickness is usually very small so the local cooling rates are very high which means the relaxation time is very short.

In the low injection speed samples (100 mm/s) the microstructure of the sample may consist of two thick skin layers surrounding a thin core layer so the orientation of the samples is very high in the skin layer and low in the core. In contrast the skin layer is very thin and the core thick in the case of samples injected at 700 mm/s.

It would be interesting to examine these layer sizes using Polarised Optical Microscopy (POM) but this was not achieved owing to time constraints.

The stress-strain curves results in presence of nanoclays are shown in figures 6.13 to 6.15 and show that the brittleness increases with increasing clay content. Furthermore the nanoplatelets may be expected to induce the orientation of the polymer matrix as a result of the effect of the shear amplification that occurs in the narrow gap between the close nanoplatelets in addition to the orientation created by the shear rate. The core of the moulded PETNC samples may be expected to have bit high orientation level due to the presence of nanoplatelets.

6.5 Conclusion

- The uniaxial tensile properties of un-filled PET and PET nanocomposites for films produced by cast extrusion and specimens produced from micro-moulding injection machine were tested.
- The objectives of this study were to investigate the effect of nanoclay on the tensile modulus of the PET product and the effect of nanoclay and the injection speed on the resultant stress-strain curves.
- The mechanical properties results of PET nanocomposite films correlated well to the TEM micrographs for the same films.
- At the lower speed film sample test (5 mm/min), Somasif MTE exhibits the greatest increase in the tensile modulus compared with the other nanoclays. Cloisite 25A (1 wt.%) reduced the tensile modulus prior to enhancement at 3 and 5 wt.% levels.
- The improvement in the tensile modulus when adding MAE or MTE can be attributed to many reasons such as the good dispersion of these clays within the PET matrix as the relevant TEM images show.
- The good compatibility between the PET chain and the MTE and MAE clays contributed to this improvement. The large inter-gallery spacing and greater aspect ratio of the MTE and MAE platelets when compared with Cloisite 25A increases the diffusion rate of the PET macromolecules into the inter-gallery space which enabled the Somasif clays to enhance the interfacial adhesion between the clay platelets and the PET matrix
- The drop in the tensile modulus of PET/Cloisite 25A (1 wt.%) may be attributed to agglomeration on the nanoclay within the PET matrix as shown in TEM images while the orientation of the PET chains reduces some of the failure

caused by the nanoclay by increasing the strength of the chain and aligning the nanoclay's platelets

- The failure to enhance the mechanical properties does not necessarily mean a reduction in other important properties.
- The tensile test results for the micro-moulded parts show that the processing conditions such as injection speed are crucial factors affecting the mechanical properties of polymer injection moulded products.
- The nanoplatelets counted as molecular chains orientation inducer when the PET molecules penetrate between the narrow gaps of the platelets at high speed.
- It was shown that a 'medium' injection speed (400mm/s) gave the best mechanical properties in terms of elongation to break as well as ultimate tensile strength.

Chapter seven

7. The permeability of PET nanocomposites

The main objective from this chapter is to study the effect of adding nanoclay on the barrier properties of PET film. The permeability of the PETNC films which produced via cast film extruder were measured. This chapter is divided into four sections: the first covers an introduction and a literature review on the barrier properties of PET nanocomposites, the second describes the barrier measurement procedure, the third covers the current barrier results and analysis, and the fourth is the conclusion.

7.1. Introduction

Traditionally materials such as glass and metal were the major materials for the packaging markets especially for food and beverages. Currently, polymeric materials such as PET have overtaken these materials owing to their lighter weight, flexibility and toughness.

Recent improvements in permeability properties for polymer products have further increased their advantages. Mark (2004) defined permeability as the steady state rate of mass transport or penetration of molecules through a polymer.

PET has good permeability properties. When PET is used in carbonated soft drink (CSD) packaging or oxygen-sensitive material packaging, it does not form a good barrier to carbon dioxide or oxygen. The diffusion of oxygen into the bottle and the loss of carbon dioxide or aroma from the bottle content depend on the barrier properties of the bottle wall, which is therefore an important factor in PET packaging production. Many applications require a long shelf life (e.g. carbonated soft drink (CSD), baby food and fruit juices) and PET cannot be a suitable material for these applications unless it

has good enough barrier properties. Therefore researchers driven by the needs of PET manufacturers have used different materials and techniques to enhance the barrier properties of PET for these applications. Using a polymer which has good barrier properties with PET (e.g. EVOH, PVDC or MXD6) to produce a multilayer structured product is one method that has been used to enhance the barrier properties of PET packaging without affecting other important properties such as transparency (see figure 7.1).

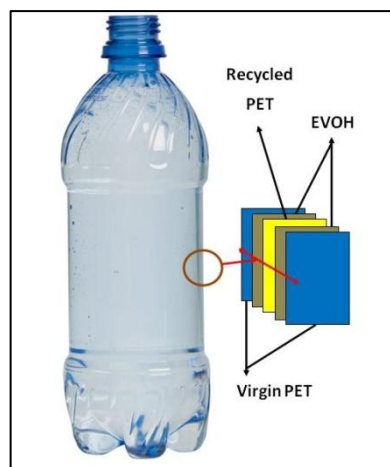


Figure 7.1 Schematic of 5-layer bottle.

This method gives a significant reduction in gas permeability. Its disadvantages are the difficulty of preform production using co-extrusion and co-injection technologies, operation and energy costs, lengthy processing time, and the difficulty of stretching and blowing the multilayer preforms. Another method of extending the shelf life of sensitive drinks is to apply an internal and external coating to the bottle using vacuum or plasma coating technology (figure 7.2), which sprays on a thin layer of barrier material. This thin layer can enhance the barrier properties of PET packages with regard to gases. The Sidel company uses a process called ACTICTM (Amorphous Carbon Treatment on Internal Surface) to enhance the barrier properties of PET packages. The US FDA (Food and Drug Administration) and TNO (Technische National Onderzoek) have issued no-

objection letters for the use of ACTIC™ in PET packages for food applications [Sidel (2010)].

The main problem with this method is its high energy consumption and the new equipment and skills required. Adding nanofillers to the PET matrix to produce PET nanocomposites is another important method used to achieve the same goal. PET can be compounded with the nanofiller at a low level (e.g. 5%) to produce a PET nanocomposite which has good enough barrier properties. The benefit of this method compared to the others is that the nanofiller usually enhances the polymer's physical and thermal properties as well as its barrier properties.

Increasing crystallinity improves the barrier properties of polymers, as Hedenqvist (1996) reported. Lasoski and Cobbs (1959) presented an equation that describes the relationship of water vapour permeability to the permeability of the un-oriented PET film (equation 7.1):

$$P = P_a X_a^2 \quad \text{Equation 7.1}$$

where P is the water vapour permeability, P_a is the permeability of the fully amorphous polymer and X_a is the volume fraction of the amorphous polymer. The equation shows that an increase in crystallinity (a decrease in X_a) leads to a decrease in the permeability of the water vapour. Frounchi and Dourbash (2009) reported that the permeability of oriented PET films is lower than that for un-oriented films.

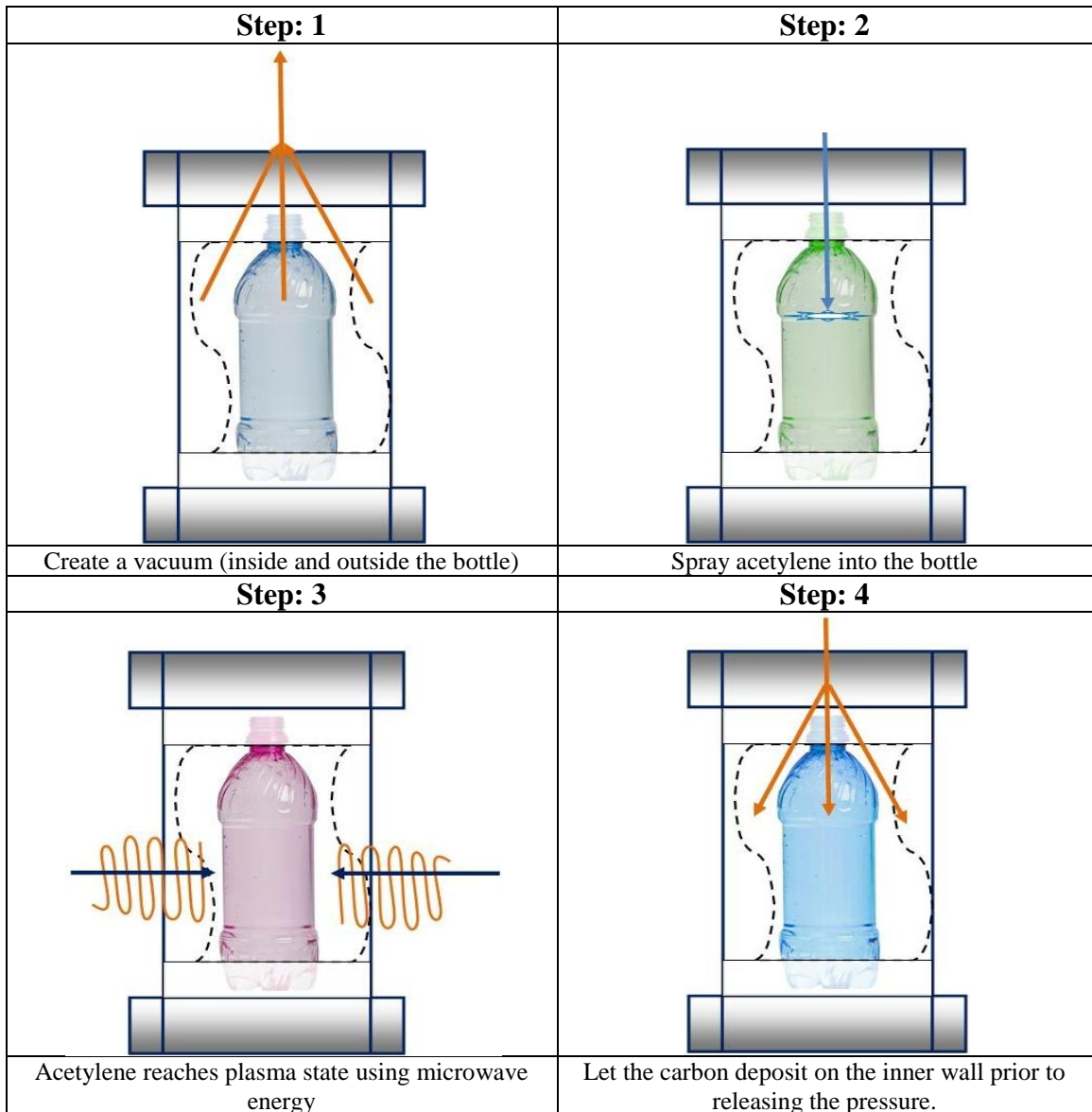


Figure 7.2 Plasma coating method. (e.g. Actic from Sidel)

According to Chanda and Roy (1993), “Diffusion occurs as a result of natural processes that tend to equalize the concentration gradient of a given species in a given environment”. Choudalakis and Gotsis (2009) reported that Fick’s law describes the diffusion mechanism within a polymer matrix. Fick’s Law can be stated as: “The net diffusion rate of a gas across a membrane is proportional to the difference in partial

pressure, proportional to the area of the membrane and inversely proportional to the thickness of the membrane” (equation 7.2) [Gooch (2007)].

$$dm = -D \frac{\partial c}{\partial x} A dt \quad \text{Equation 7.2}$$

where dm is the number of grams of the diffusing material crossing area A (cm^2) of the other material in time dt (sec.), D is the diffusion coefficient ($\text{cm}^2/\text{sec.}$) and $\frac{\partial c}{\partial x}$ is the concentration gradient [Chanda and Roy (1993)].

A regular arrangement of platelets in a parallel array is a simple permeability model (see figure 7.3) and this model has been proposed by Nielsen (1967). The Nielson model shows an approximation for estimating the effective ‘tortuosity’ of a matrix containing filler particles:

$$\tau = 1 + \left(\frac{L}{2t}\right) \phi \quad \text{Equation 7.3}$$

where: τ is tortuosity, L is length, ϕ is the volume fraction of the filler and t is the thickness of the plate. Increasing the volume fraction and the aspect ratio of the clay $\left(\frac{L}{2t}\right)$ leads to an increase in the tortuosity path which reduces the permeability of the film to the gas.

In general, the permeability of a nanocomposite is influenced by three factors: the orientation of the nanoplatelets relative to the diffusion direction, their volume fraction, and the aspect ratio of the nanoplatelets [Choudalakis and Gotsis (2009)].

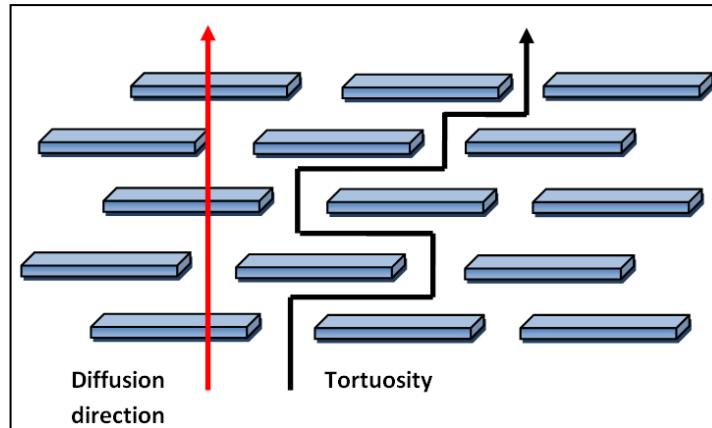


Figure 7.3 The regular arrangement of platelets in a parallel array.

Due to a more tortuous path, which is related to the shape and the degree of dispersion of the nanoplatelets, the decrease in diffusion coefficient is higher than the decrease in solubility coefficient, which is due to the reduction in the volume fraction of nanoplatelets, which is indeed low. This exfoliated dispersion of the nanoplatelets is a more effective way to enhance the barrier properties of the polymer because it produces higher values for the aspect ratio and the tortuosity factor compared with intercalated nanocomposites. Natu et al. (2005) studied the barrier properties of PET sheets and how morphology can affect the permeability of the sheet to oxygen. The authors found that tortuosity path of the gas through the sheet is affected by the size of the spherulites. Large spherulite size increases the tortuosity of the path more than does small spherulite size. It has also been observed that molecular orientation is an important factor controlling the gas permeability properties of a stretched PET sheet.

Furthermore, aggregation of silicate layers will decrease the aspect ratio of nanoparticles which means poor barrier property enhancement. This phenomenon is clear for high clay contents due to the difficulty of keeping a good degree of platelet dispersion. This phenomenon can be attributed to the agglomerates, which form large

scale pores in the matrix. These pores form a short pathway for gas diffusion within the polymer nanocomposites.

$$t_{active} = \frac{d_{film}^2}{D_{film}} \quad \text{Equation 7.4}$$

where t_{active} is working time, d_{film} is the thickness of the film and D_{film} is the diffusion coefficient [Choudalakis and Gotsis (2009)]. The working time can increase when the diffusion coefficient is reduced.

Frounchi and Dourbash (2009) studied the oxygen barrier properties of PET nanocomposite films. Two different Montmorillonite-based organoclays (Cloisite 15A and Nanolin DK2) were used to produce PET nanocomposite pellets using a co-rotating twin screw extruder. In order to produce the film the pellets were melted at 275°C for 5 min. in a compression moulding machine, and to avoid holes in the film this procedure was repeated a number of times prior to quenching the molten film at 15°C in a water bath. The PET nanocomposites showed a reduction in permeability for a 1 wt.% PET/Nanolin nanocomposite film which was about half that of the vPET. The same film showed the lowest permeability compared with 2 and 3 wt.% nanocomposites. The authors attributed this to an excellent dispersion of nanoclay at 1 wt.% (exfoliated) compared with 2 and 3 wt.% nanocomposites. The nanocomposites were exposed to harsh processing during the compounding process. The processing temperatures along the extruder were below the melting temperature of the PET and the screw speed was comparatively high, such that the nanocomposite pellets were exposed to a high temperature (275°C) many times in order to form the films. These two processes can degrade the polymer, destroy the silicate layers, and burn the surfactant of the nanoclay, which may explain why adding more nanoclay did not improve the barrier properties. The results also show that the Nanolin nanocomposites have lower permeability

compared with Cloisite nanocomposites, and the researchers attributed this to the better dispersion (exfoliation) of Nanolin with PET. The relatively poor affinity of Cloisite 15A with PET as discussed before (section 2.7) could be another reason.

Soon et al. (2009) characterised a PET/synthetic mica [MAE 3 wt.%] nanocomposite sheet and observed an improvement in the barrier to oxygen by 29%. This enhancement was attributed to good dispersion of the nanoclay in the PET.

Ke and et al. (2005) added modified MMT into PET resin by in situ polymerisation prior to using the nanocomposite material to produce bi-axial oriented film. The result showed a small enhancement in the barrier property of the film and permeability was reduced to half that of pure PET film when the clay content reached 3%.

Lewis and co-workers (2003) studied the solubility and diffusion of mixtures of two and three gases (oxygen, carbon dioxide and nitrogen) for PET film. In terms of oxygen diffusion, the results showed that the presence of carbon dioxide or nitrogen has a slight effect on oxygen diffusion and solubility. Usually, the oxygen is preferable to use in permeability tests because of the following features. Firstly, the O₂ diffusion coefficient is greater than that for CO₂ and N₂. Secondly, CO₂ solubility is greater than that of O₂ or N₂ which may affect the results by increasing the thickness of the film [Lewis et al. (2003)]. Choi et al. (2006) found that increases in clay content reduced the oxygen permeability of PET nanocomposite.

7.2. Experimental work

Un-filled PET (vPET) and PET nanocomposite PETNC films were tested. These films were produced via cast film extrusion (see section 3.2.4). The films were un-oriented and had a thickness of 0.11 ± 0.01 mm. A MOCON OX-TRAN (2/21 MH) barrier test instrument was used to test the permeability of these films. The description of the equipment and the test procedure were covered in section 3.5.6.

7.3 Results and discussion

The absolute permeability values of virgin PET (vPET), extruded vPET (Ext. vPET) and PET nanocomposites (PETNCs) are listed in Table 7.1. As expected, the nanoclay enhanced the barrier properties of the PET film. The enhancement in the permeability of PET film is apparent even at low nanoclay content (1 wt.%) as Table 7.1 and figure 7.4 show. When the content of the Cloisite 25A reached 5 wt.%, the gas permeability reduced to half that of the extruded vPET film (figure 7.4). The MTE and MAE showed a linear reduction in the permeability of oxygen on adding more clay (1, 3 and 5%) while Cloisite 25A (3%) did not show a significant reduction in permeability compared with 1% Cloisite 25A.

The improvement in the barrier properties of the PET films on adding nanoclays can be attributed to the good distribution of nanoclays within the PET matrix.

Film type	Permeability (cc/m²/day)	Barrier enhanced by (%)
vPET	25.77	-
Ext. vPET	29.51	-
PET/MAE (1%)	26.92	8.7
PET/MAE (3%)	23.82	19.3
PET/MAE (5%)	19.99	32.26
PET/MTE (1%)	25.46	13.7
PET/MTE (3%)	21.26	27.96
PET/MTE (5%)	17.29	41.41
PET/Cloisite 25A (1%)	25.08	15.0
PET/Cloisite 25A (3%)	23.78	19.42
PET/Cloisite 25A (5%)	14.76	49.98

Table 7.1 Permeability results for PET nanocomposite films

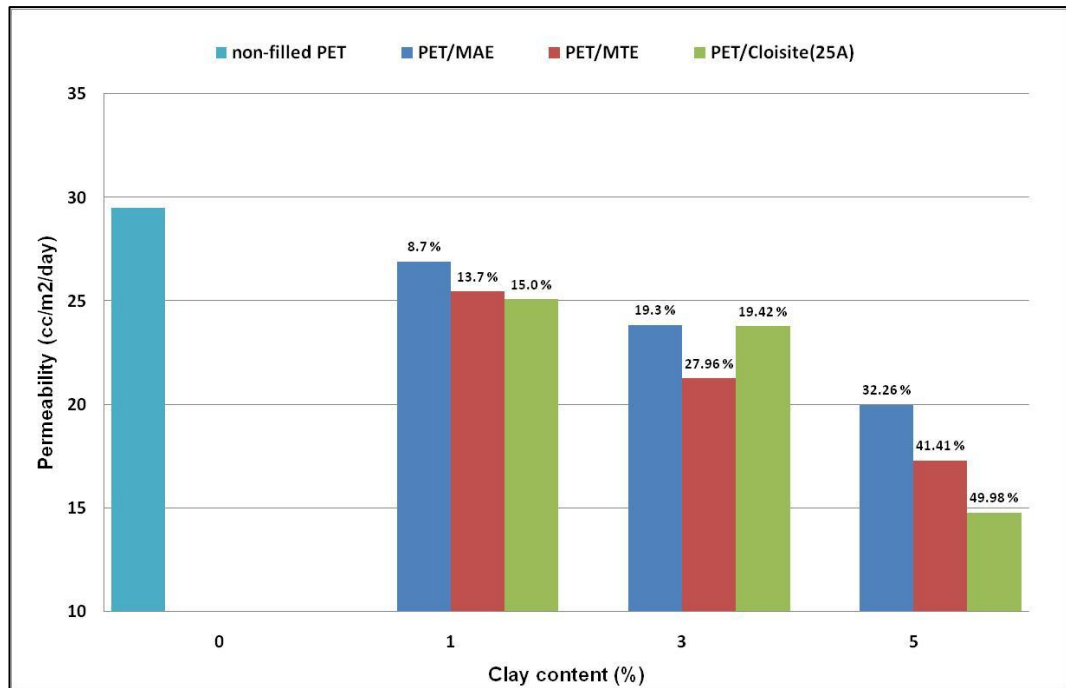


Figure 7.4 Reductions in PET film permeability on adding nanoclay.

Even when comparing vPET with PET nanocomposites, the nanocomposites show enhancements in the barrier properties of the film, as figure 7.5 shows. Producing the PET nanocomposite films directly from the twin screw extruder (compounding stage) may lead to further reductions in the permeability of the gas through the film wall. Good stability in oxygen permeability reduction (up to 8 hrs.) was observed with some PET nanocomposite films, as shown in figure 7.5.

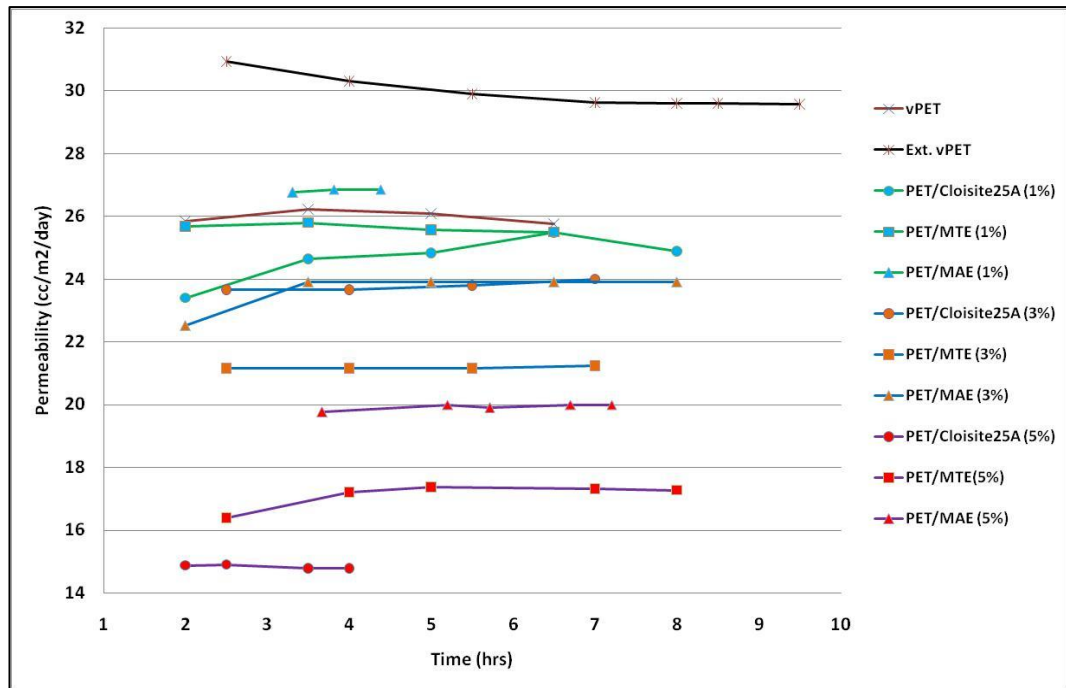


Figure 7.5 Reduction in the permeability of unfilled PET and PETNC films over a long period.

The excellent barrier property enhancement achieved by adding Cloisite 25A is counter to the relatively poor tensile modulus enhancement for the PET/Cloisite 25A NC films and more tactoids and few intercalation aspect for Cloisite 25A platelets as TEM images shown (discussed in section 6.4). There are many reasons for this phenomenon. The small aspect ratio of Cloisite 25A compared with Somasif clays leads to a small contact area between the clay platelets and the polymer matrix, which gives relatively poor reinforcement in addition to the tactoids aspect for PET/Cloisite25A samples. Another possible reason is that long aspect ratio clays take longer to align fully, which would give more resistance to the stress compared to small aspect ratio clays.

Figure 7.4 also shows a small change in barrier property enhancement for PET/Cloisite25A on adding 3 wt.% compared with 1 wt.%. On the other hand, the PET/Cloisite 25A (3 wt.%) film achieved greater enhancement in tensile modulus compared with the PET/Cloisite 25A (1 wt.%) film (discussed in section 6.4; see figure

6.3). This can be attributed to the relatively poor dispersion of the Cloisite 25A (3 wt.%) plates in the PET matrix, leading to clay agglomeration as TEM images show (see chapter 6).

Film transparency is an important property for end applications. Figure 7.6 shows some images for un-filled PET and PET nanocomposites. It is clear that the PET films produced by adding up to 3 wt.% nanoclay show acceptable transparency.

PET nanocomposites with (5 wt.%) films for MTE and Cloisite 25A are also acceptable. PET/MAE (5 wt.%) film has a slightly yellowish colour which means it could be used in coloured film applications, or that the melt processing needs to be reviewed. As mentioned before, these films were exposed to two melt processing operations (compounding then casting the film) so this may be one of the reasons for the discolouration.

While the aspect ratios of Somasif clays are higher than those of Cloisite 25A, the latter achieved good barrier property results compared with PET/Somasif NC films. This can be attributed to the fact that the effect of basal space (d space) is stronger than the effect of aspect ratio. Cloisite 25A has the smallest d spacing, followed by MTE and then MAE, and this sequence was observed in the gas permeability reduction.

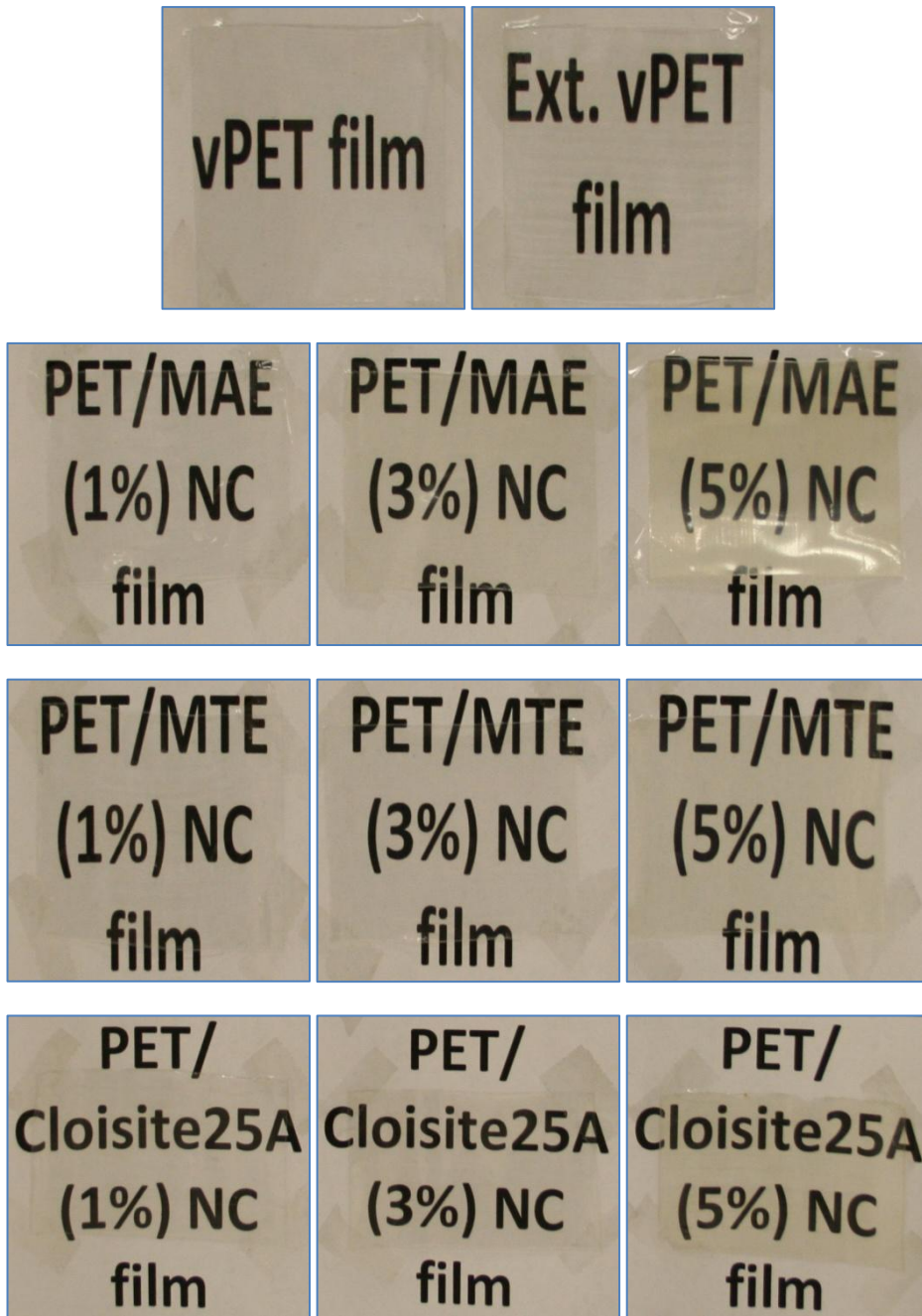


Figure 7.6 Transparency level of each film.

7.4 Conclusions

- Studying the effect of adding the nanoclay and the geometry of nanoclay on the barrier properties of PET films were the main objectives of this chapter.
- As expected, the nanoclay enhanced the barrier properties of the PET film. The enhancement in the permeability of PET film is apparent even at low nanoclay content (1 wt.%).
- When the content of the Cloisite 25A reached 5 wt.%, the gas permeability was reduced to approximately half that of the extruded vPET film.
- The MTE and MAE clays exhibited a linear reduction in the permeability of oxygen on adding more clay (1, 3 and 5%) while Cloisite 25A (3%) did not show a significant reduction in permeability compared with 1% Cloisite 25A.
- The improvement in the barrier properties of the PET films on adding nanoclays can be attributed to the good distribution of nanoclays within the PET matrix.
- Producing the PET nanocomposite films directly from the twin screw extruder (compounding stage) may lead to further reductions in the permeability of gas through the film wall.
- The excellent barrier property enhancement achieved by adding Cloisite 25A is counter to the relatively poor tensile modulus enhancement for the PET/Cloisite 25A NC films and more tactoids and few intercalation aspect for Cloisite 25A platelets. There are many reasons for this phenomenon. The small aspect ratio of Cloisite 25A compared with Somasif clays leads to a small contact area between the clay platelets and the polymer matrix, which gives relatively poor reinforcement for PET/Cloisite25A samples. Another possible reason is that long aspect ratio clays take longer to align fully, which would give more

resistance to the process imposed stress compared to the smaller aspect ratio clays.

Chapter eight

8. Degradation of PET nanocomposites

This chapter covers the degradation of PET and PET nanocomposites in detail. The types and mechanisms of PET degradation are covered in the first section and the second section covers PET nanocomposite degradation in particular, followed by experimental details, results and discussion. This chapter aims to study the thermal stability of PET nanocomposites and answer the following questions:

- a) Will the clay accelerate degradation?
- b) What is the effect of re-processing the nanocomposite materials on their viscosity and colour?
- c) What is the behaviour of the viscosity of the polymer nanocomposites over a long period of time?

8.1 PET degradation

8.1.1 Introduction

Understanding the degradation types and mechanisms of polyethylene terephthalate (PET) is essential to understand the melt processing of PET. The main challenge in any PET study is degradation. Most PET product failures are due to misunderstanding the sensitivity of PET to high temperatures, oxidative effects, long residence times and high screw speeds during the plastication stage, in addition to bad mechanical design.

The mechanisms of the degradation reactions have been described by two major schools and each school has its own opinion. Allan et al. (1957) and Goodings (1961) believe that the degradation mechanism is initiated at the ester link in the random chain scission, while Marshall and Todd (1953) argue that PET degradation is carried out at

chain ends. However there is evidence that both mechanisms occur in the PET degradation process [Brooks and Giles (2002)].

Gumther and Zachmann (1983) showed that in the presence of oxygen the thermal degradation rate is increased and the presence of even a very low quantity of moisture causes rapid hydrolytic degradation to occur above the melting temperature, which leads to a reduction in the polymer's molecular weight. Marshall and Todd (1953) studied thermal and hydrolytic degradation at high temperatures. Moisture was found to cause rapid hydrolytic degradation, which resulted in greatly reduced polymer molecular weight. Absorbed moisture is known to have significant effects on the thermal stability and physical properties of hygroscopic polymers. The glass temperature (T_g) of PET is sensitive to absorbed moisture and can be reduced significantly as a result of high moisture content.

Jabarin (1984) showed that the residence time and temperature of the melt during injection processing significantly affects the extent of degradation of PET. The amount of degradation was reduced by melting in an inert environment, or under vacuum, rather than in air. The drying conditions of the PET pellets also significantly affect the extent of degradation.

Brooks and Giles (2002) reported that when PET final products are left unprotected from the outside environment, the humidity, air and UV light can lead to significant reductions in the tensile properties. It is strongly recommended to coat the outdoor PET product (sheet or film) with a UV protective layer.

PET undergoes several types of degradation under different conditions during the plastication processes. The major degradation schemes are:

- Thermal degradation
- Thermal-oxidative degradation
- Hydrolytic degradation
- Chemical degradation
- Radiochemical degradation
- Photo-oxidative degradation

Thermal, thermal-oxidative and hydrolytic degradation are of the highest importance in injection moulding and extrusion processing of PET due to the absence of light, reactive ions and chemical reagents.

In the presence of heat, oxygen and water the degradation rate is increased due to the formation of additional end groups and thus a reduction in the molecular weight.

8.1.2 Degradation processes

Prior to presenting the types of degradation reactions, it is appropriate to introduce the chemical structure of the most important end groups as figure 8.1 shown.

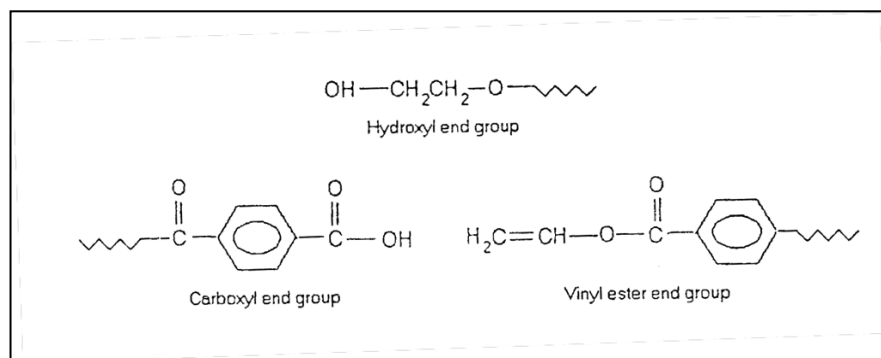


Figure 8.1 The chemical structures for some end groups [Jabarin (1996)]

A. Hydrolytic degradation

PET is a hydroscopic material which can rapidly absorb moisture from its environment. The chemical reaction of PET with water at high temperature results in the formation of hydroxyl and carboxyl end groups (Figure 8.2).

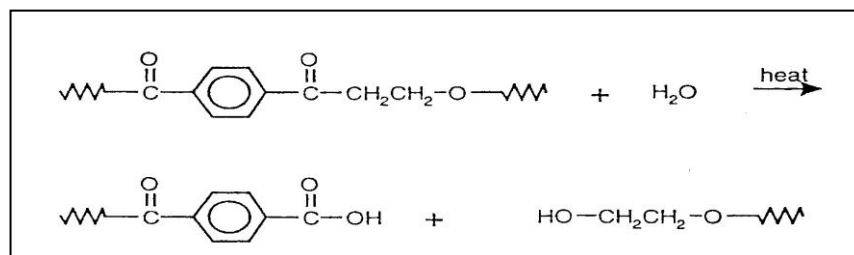


Figure 8.2 Hydrolytic degradation mechanism [Jabarin (1996)]

B. Thermal degradation

In the absence of air and under high processing temperatures, some chemical reactions occur that can lead to the breakdown of chemical bonds in the polymer. Thermal degradation is rarely considered as a main degradation reaction for PET downstream processing because it is carried out in the presence of air.

The main reaction in PET thermal degradation is ester elimination and the outputs of this reaction are vinyl ester and carboxylic acid groups, as shown in figure 8.3:

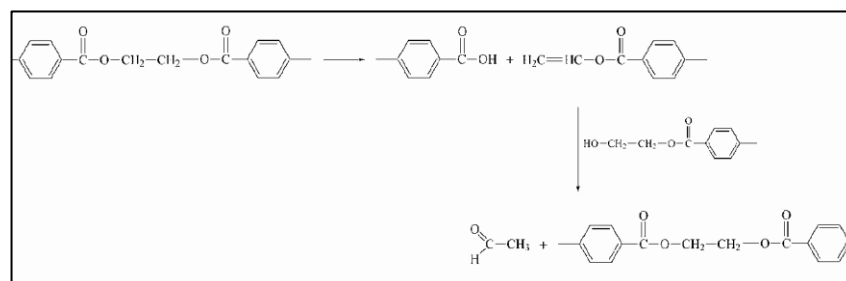


Figure 8.3 Thermal degradation reactions [Mark (2007)]

When thermal degradation starts, the vinyl ester groups form acetaldehyde. Khemani (2000) studied the thermal degradation of PET over long periods at high temperatures (280°C). It was found that the generated amount of Acetaldehyde at high temperature, gradually decrease with time. The thermal degradation mechanism suggested that the acetaldehyde may be generated via three different reactions. The first involves the vinyl group, the second mid-polymer chain scission and the third the hydroxyl end group.

Acetaldehyde can seriously affect the taste of mineral water packaged in PET, if excessive degradation has taken place. Acetaldehyde is a volatile material generated during polymerisation and degradation of PET. It has a sweet odour and is naturally present in many foods and beverages.

Acetaldehyde (AA) is also added as a flavouring to many other products so that the concentration of residual AA is of great importance to producers of containers destined for use with food and beverage products. In order to minimize the concentration of AA in finished containers, AA concentrations in the PET resin should be low and degradation should be limited during processing.

C. Thermal-oxidative degradation

Jabarin (1996) reported that thermal-oxidative degradation follows a free radical type reaction. The free radical reaction can lead to the formation of vinyl ester groups which can react with polymer chains containing hydroxyl end groups.

Marshall and Todd (1953), Goodings, (1961) and Spanniger (1974) reported that the reaction of oxygen with PET at high temperatures can lead to reduction in molecular weight and production of acetaldehyde in higher quantities than produced by purely thermal degradation. Also they showed that the reaction can lead to formation of

different functional groupings in the polymer, such as carboxyl end groups as well as discolouration of the polymer to produce yellowish products.

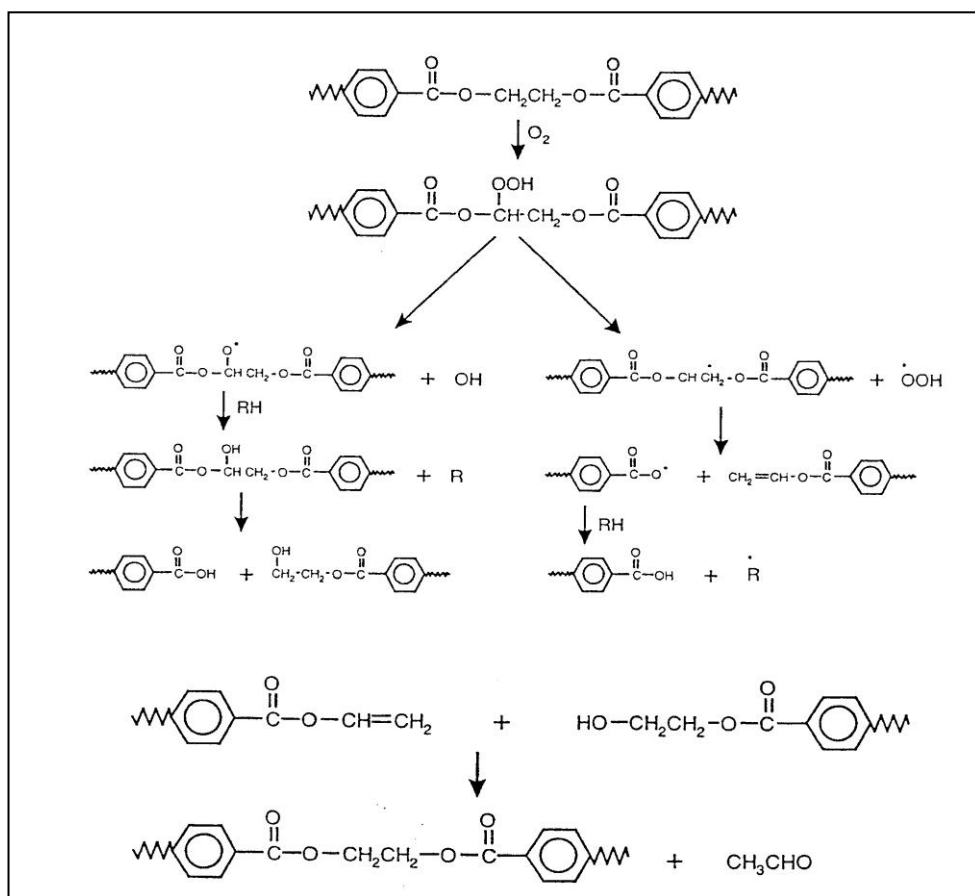


Figure 8.4 Thermal-oxidative degradation mechanisms [Jabarin (1996)]

8.2 PET nanocomposite degradation (literature review)

Preparing nanocomposites under high temperatures via melt extrusion or other methods can cause thermal degradation of the modified clay. The degradation in nanocomposites may occur because of unwanted reactions between surfactant decomposition and the polymer at high processing temperatures.

Qin et al. (2005) reported that the Bronsted acidic sites on the clay platelets cause polymer degradation. Xu et al. (2009) examined the factors affecting PET degradation. The chain extension reaction (PMDA) was used to control the thermal degradation of PET nanocomposites. It was found that the ammonium linkage on the clay and the amount of hydroxyl groups on the edge of clay platelets were the main factors in the polymer degradation. Xu et al. (2009) found similar results to those of Qin et al. (2005) when the hydroxyl groups on the edge and surfaces of the clay platelets acted as Bronsted acidic sites to accelerate the polymer degradation due to clay catalysis effects.

Wang and Gao et al. (2006) studied the thermal stability of PET nanocomposites. The authors observed that adding organo-Montmorillonite (DK2) enhanced the thermal stability of the PET. The peak degradation temperature and the onset degradation temperature of PET nanocomposites increased by 35°C and 12°C respectively when adding 1% of DK2. Utracki (2010) reported that at high temperatures, the ammonium-ion-intercalated organoclays degraded, leaving the surface of the clay which may lead to re-aggregation of the clay platelets.

Yoon et al. (2003, part 2) observed decreases in the I.V. of PC nanocomposites with increasing clay content. Similar observations have been reported by Fornes et al. (2003) in nylon-6 nanocomposites. The authors attributed this decrease to the instability of the organoclay under high shear rates and high processing temperatures. The authors

reported that the surfactant decomposition may produce unwanted side reactions with the polymer which may lead to a reduction in the I.V.

Yuan et al. (2008) studied the thermal properties of PET/Palygorskite (PT, a kind of fibrous clay) nanocomposites. Prior to preparing the nanocomposite via in situ polymerisation and in order to increase the thermal stability of the clay, PT was organically modified by water-soluble polyvinylpyrrolidone (PVP) due to the high thermal stability of the PVP. The thermal stability of the pure PET and PET nanocomposites were measured by TGA in an air and nitrogen atmosphere with various heating rates. The authors reported that the clay may release some metallic derivatives which may act as catalysts leading to a decrease in the thermal stability of nanocomposites. Meanwhile, the clay can enhance the thermal stability of nanocomposites when it acts as a thermal transport barrier in the PET matrix. The authors observed that at various heating rates in air, the oxidative thermal properties of PET nanocomposites were improved compared with the non-filled PET and this barrier effect is dominant. Conversely, the catalysis factor is dominant and the thermal stability of the nanocomposite decreases compared with non-filled PET at slow heating rates in nitrogen. Meanwhile, at high heating rates and in nitrogen, the thermal stability of the nanocomposites increases when compared to non-filled PET which suggested this is dominated by the barrier effect.

Xie et al. (2001) studied the degradation of six types of organically modified MMTs. The authors observed that the difference in surfactant type does not change the initial onset degradation temperature and this is in agreement with our reprocessing study results, which will be discussed later in this chapter. Soon et al. (2009) characterised PET/synthetic mica nanocomposites and correlated the decrease in the molecular weight

of the polymer matrix with increasing clay content to the degradation caused by the synthetic mica content. The surfactant of the synthetic mica interacted with the polymer matrix which catalysed degradation. The authors observed that the Somasif MAE clay reduced the molecular weight of the PET nanocomposites more than did Somasif MTE clay, and they refer this effect to the surfactant type. The authors also reported that even with the reduction in molecular weight, there were no significant reductions in mechanical performance.

8.3. Experiments

Three experiments were conducted to study the thermal stability of vPET and PET nanocomposites.

- 1- The thermal stability of nanoclays (Cloisite 25A, Somasif MAE and Somasif MTE) (as well as others) was investigated by Thermogravimetric Analysis (TGA) in nitrogen. The temperature was raised from 30 to 500°C and the heating rate was 10°C/min. The main focus of this investigation was on the PET melt processing temperature range (260-280°C).
- 2- The effect of re-passing the vPET and PET nanocomposites through the twin screw extruder was also studied. The vPET and PET nanocomposites produced in the compounding process stage were recycled again to investigate the effect of repeating the melt processing on the viscosity. Prior to feeding the pellets to the extruder, all pellets were re-crystallised in a vacuum oven for 20 hours at 150°C then immediately loaded to the hopper. The melt processing parameters which were used were similar to the processing parameters used in the compounding stage. All samples were then further re-crystallised before being analysed by shear rheometry.
- 3- The behaviour of vPET and PET nanocomposite viscosity at constant shear rates over a long period was studied. The viscosity of vPET and PET/MTE (1, 3 and 5 wt.%) nanocomposite pellets was tested by parallel plate rheometry at 260°C for 10 hours with strain amplitude 0.5%, frequency 10Hz and a 1mm gap. This method can investigate the effect of time on nanocomposite viscosity with increasing clay content.

8.4. Results and discussion

8.4.1 Thermogravimetric analysis (TGA) results for the nanoclays

The TGA results summarized in Table 8.1 and figure 8.5 show that the selected nanoclays in this project (Cloisite 25A, Somasif MTE and Somasif MAE) present the best thermal stability among the nanoclays tested. As the melting temperature of PET is around 250°C, the melt processing temperature is usually in the range 260°C to 280°C, depending on the output capacity, the residence time and the shear rate of the melt forming process.

Nanoclay	Degradation onset temperature (°C)	Weight loss at 260°C (%)	Weight loss at 280°C (%)
Cloisite 25A	206	5.09	6.97
Somasif MTE	205	5.80	8.81
Somasif MAE	200	6.69	11.00
Cloisite 30B	185	7.67	10.74
Cloisite 15A	198	7.76	11.56
Cloisite 10A	170	17.26	20.01

Table 8.1 Weight loss from each clay at 260 and 280°C and degradation onset temperature for different clays from TGA

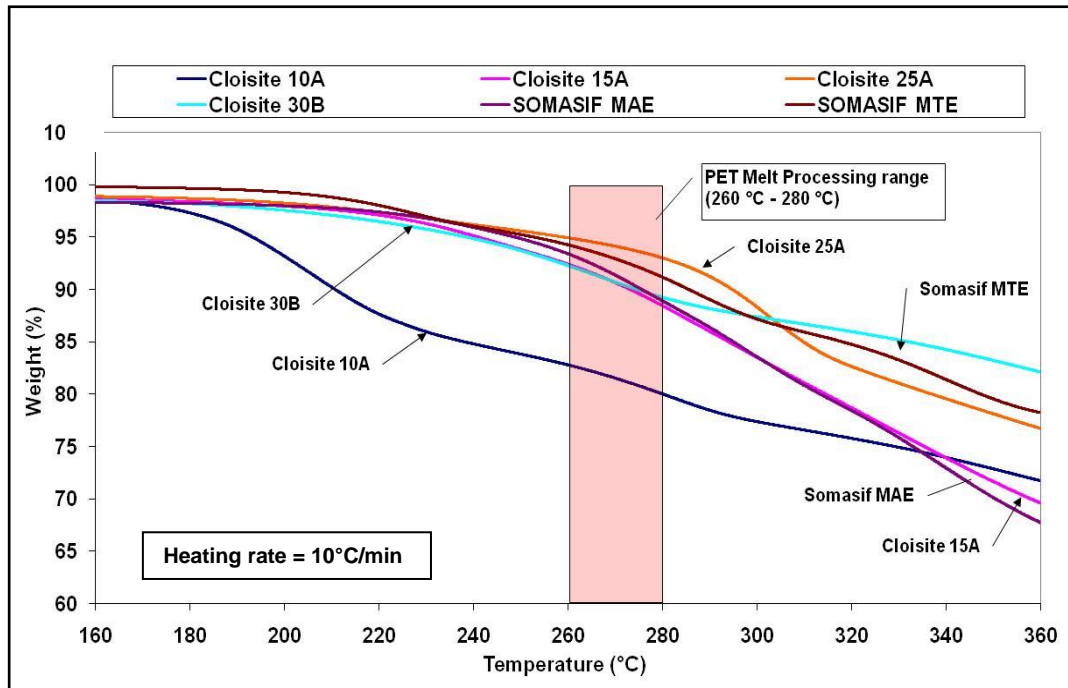


Figure 8.5 TGA curves for different nanoclays

The results from Table 8.1 and figure 8.5 assisted the choosing of nanoclays for this project. All three chosen nanoclays (Cloisite 25A, Somasif MTE and Somasif MAE) exhibit the highest weight loss onset temperatures and minimum weight loss between 260 and 280°C. For example, Cloisite 25A lost around 5% of its weight at 260°C while Cloisite 10A lost around 17% of its weight at the same temperature. If we focus on our three clays and how they behave during the melting process, we find that the Cloisite 25A and MTE curves do not drop significantly between 260 and 280°C, while the MAE curve decreases sharply (from 6.69% to 11.0%), showing MAE to be very sensitive to higher temperatures and thus requiring a process temperature of only around 260°C.

8.4.2 Re-processing the pellets through the twin screw extruder

The degradation of both the vPET and PET nanocomposites was expected during these recycling processes but the purpose of this study was to investigate the effect of the nanoclay on polymer viscosity and whether or not it accelerates degradation compared with the un-filled PET. As Table 8.2 (and Table x8.1) show, 29 samples were prepared and analysed for comparison purposes.

Sample	Description
vPET	Virgin PET
Ext. vPET	Extruded PET (non recycled)
Ext. vPET_1	Extruded PET (1 time recycled)
Ext. vPET_2	Extruded PET (2 times recycled)
Ext. vPET_3	Extruded PET (3 times recycled)
PET/MAE3%	PET/MAE_3% (non recycled)
PET/MAE3%_1	PET/MAE_3% (1 time recycled)
PET/MAE3%_2	PET/MAE_3% (2 times recycled)
PET/MAE3%_3	PET/MAE_3% (3 times recycled)
PET/MAE5%	PET/MAE_5% (non recycled)
PET/MAE5%_1	PET/MAE_5% (1 time recycled)
PET/MAE5%_2	PET/MAE_5% (2 times recycled)
PET/MAE5%_3	PET/MAE_5% (3 times recycled)

Table 8.2 Description of the re-passed samples

The following figures show the effect of recycling (re-extrusion) of the PET and PET/MAE (3 and 5 wt.%) nanocomposites. As mentioned before, all materials had a sufficient drying process to minimise the possibility of hydrolytic degradation so only the thermal oxidative and surfactant degradations could occur. It is obvious from all figures that the viscosity decreases with increasing passes.

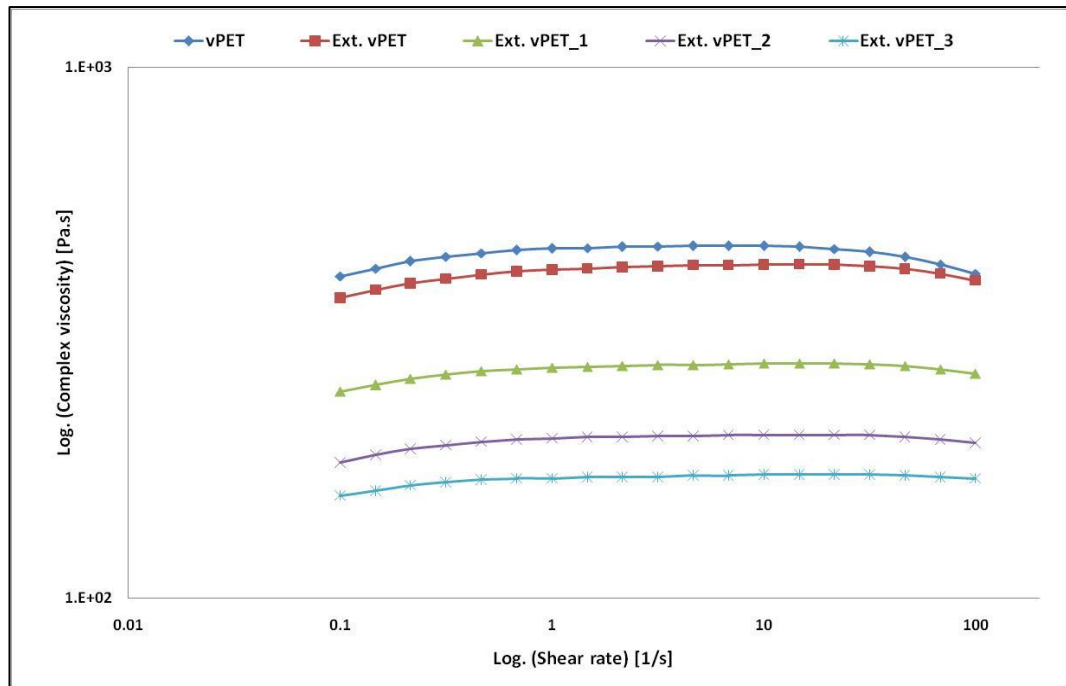


Figure 8.6 Viscosity of un-filled PET re-extruded up to four times

As shown in figure 8.6, the viscosity of un-filled PET kept its Newtonian behaviour even as the viscosity decreased. Figure 8.7 shows the corresponding colour of the un-filled amorphous pellets after each re-processing stage.

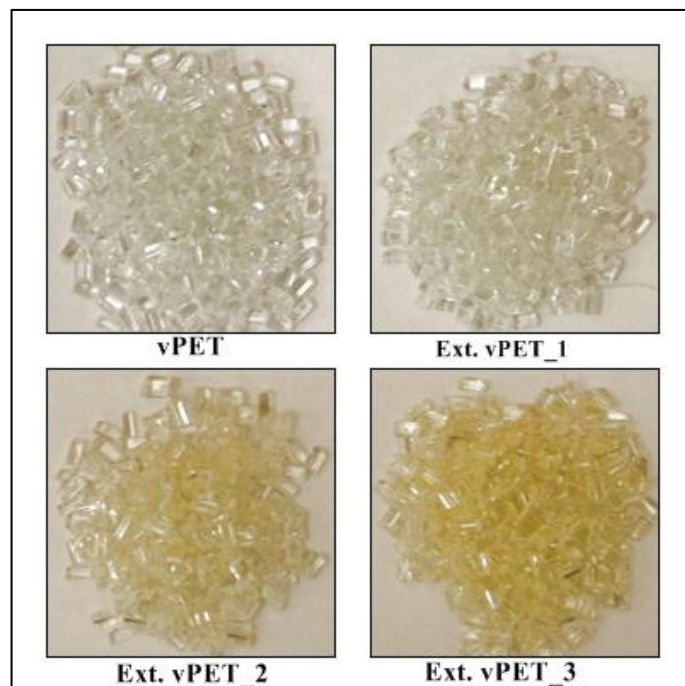


Figure 8.7 Colour of the amorphous vPET after re-pass stages

The reduction in the viscosity and discolouration of the pellets to a yellowish colour supports the hypothesis that thermal-oxidative degradation occurs in the polymer.

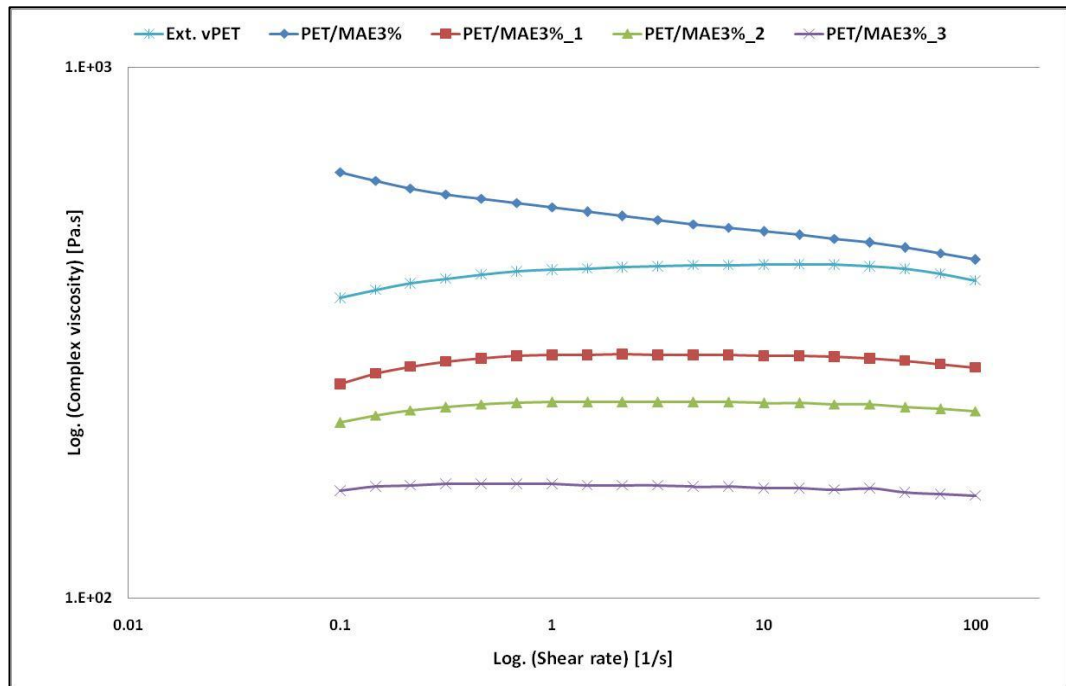


Figure 8.8 Viscosity vs. shear rate of PET/MAE (3 wt.%) nanocomposites re-extruded up to four times

While the viscosity of PET/MAE 3 wt.% is greater than the ext. vPET and slightly tends to non-Newtonian behaviour at low shear rates, the viscosity of re-passed samples reduces and clearly exhibits Newtonian behaviour (figure 8.8).

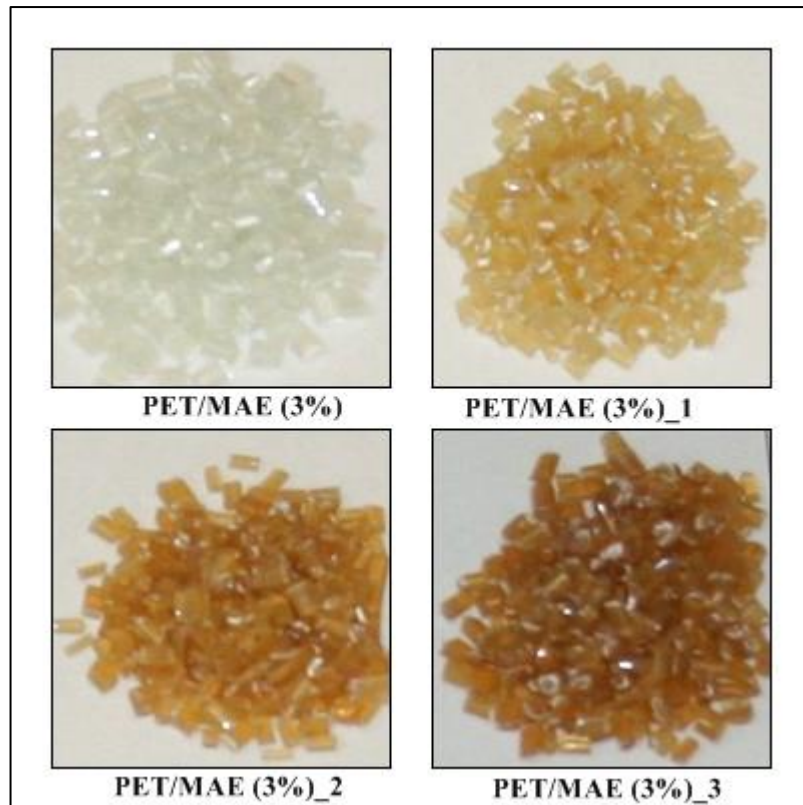


Figure 8.9 Colour of amorphous PET/MAE (3 wt.%) after re-pass stages

The pictures of the pellets after each re-passing stage for PET/MAE 3 wt.% (figure 8.9) indicate that the colour of the pellets immediately darkened during the first reprocessing. The change in colour of PET nanocomposites pellets occurs much more gradually which means the nanoclay additive (MAE) plays a strong role in the degradation process due to the existence of the surfactant.

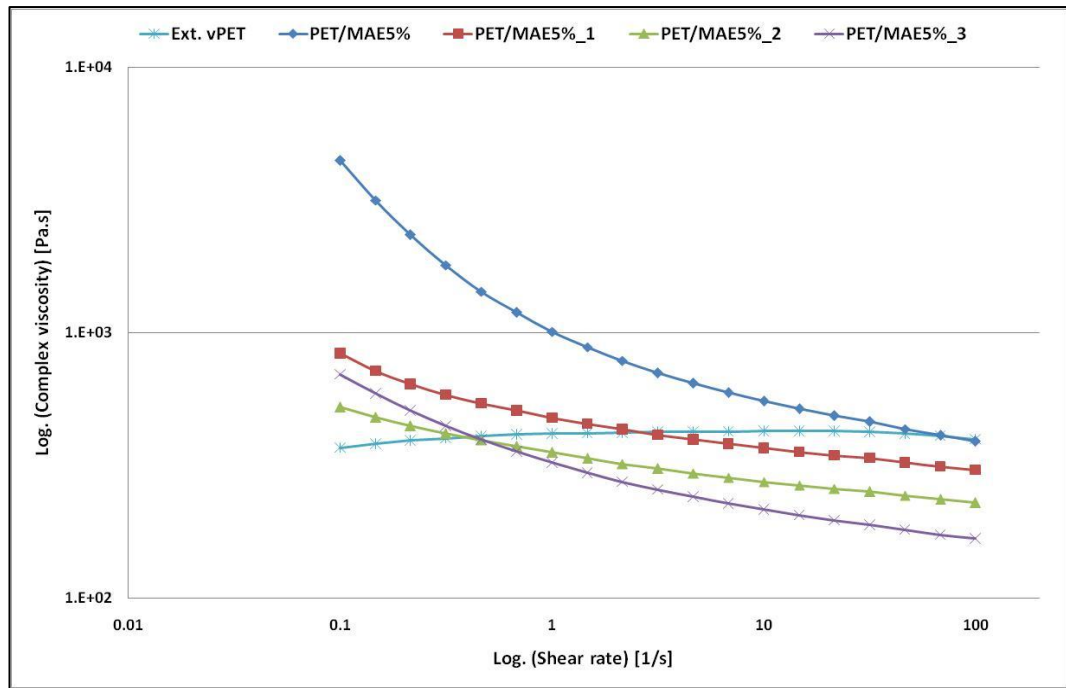


Figure 8.10 Viscosity vs. shear rate of PET/MAE (5 wt. %) nanocomposites re-extruded up to four times

Similar results occur for PET/MAE 5 wt.% as shown in figure 8.10. The viscosity dropped and the extent of the shear thinning tends to decrease with increasing passing times. The colour changed strongly to dark brownish as shown in figure 8.11.

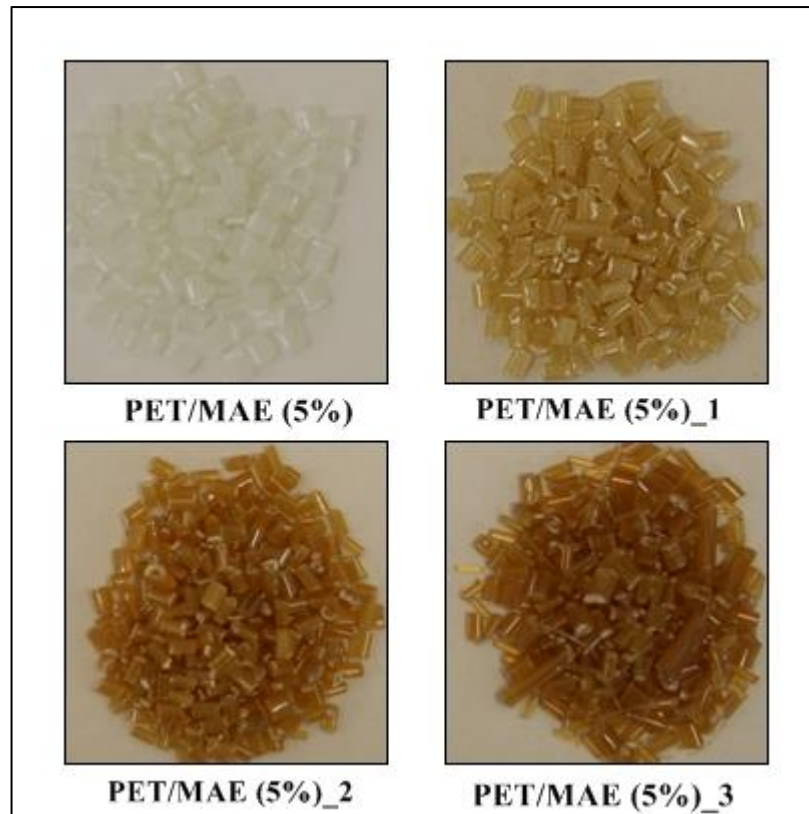


Figure 8.11 Colour of the amorphous PET/ MAE (5 wt.%) after re-pass stages

Similar observations and conclusions have been found from analysing the re-processed samples for PET/MTE (3 and 5 wt.%) and PET/Cloisite 25A (3 and 5 wt.%) with corresponding decreases in viscosity and optical clarity. These figures and pictures can be found in appendix x8 [figures x8.1 - x8.7].

8.4.3 Effect of time on viscosity

The aim of this study was to quantify nanoclay effects on the viscosity of PET nanocomposites with long processing times, under constant shear conditions.

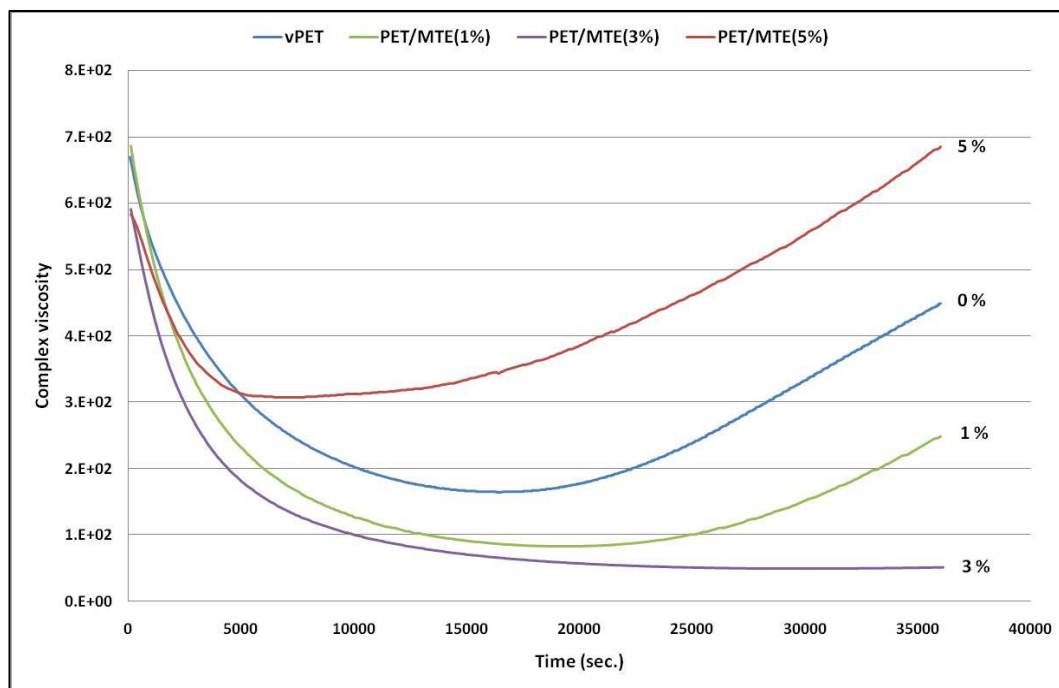


Figure 8.12 Viscosity behaviour of vPET and PET/MTE (1, 3 and 5 wt.%) over a long period (10 hrs)

As figure 8.12 shows, the viscosity of all samples started to decrease with increasing time prior each sample exhibiting different behaviour with increasing time. While the viscosity of the sample with 3 wt.% MTE content continued to decrease then stabilise after a long period, the other samples started to re-build in viscosity after set periods of time. The viscosity of vPET started to increase after approximately 4.5 hours, and as the sample was exposed to oxygen during the test (atmospheric environment) the increase in viscosity may be attributed to oxidative cross-links. The presence of oxygen catalyses the broken bonds to re-build and join again in a cross-linking reaction. Similar hypotheses can also be applied for PET/MTE (1 wt.%) but the presence of clay causes a

decrease in viscosity where the surfactant interacts with the polymer, which may catalyse the degradation and keep the clay particle aligned in the matrix. This decrease in viscosity reduces then the viscosity tend to increase due to the oxidative cross-link in the PET matrix, while the decrease in viscosity for PET/MTE (3 wt.%) hides or offsets the increases in viscosity due to sufficient amounts of surfactant in the clay. Following the same concept, the viscosity of PET/MTE 5 wt.% was expected to be lower than the viscosity of PET/MTE 3 wt.%, but its viscosity increased even more than the vPET. This phenomenon can be attributed to the fact that the most of the surfactant had already left the surface of the nanoclay, then the nanoclay re-aggregated, as Utracki (2010) reported, so the nanoclay dominates and catalyses the cross-link reaction in addition to the PET polymer.

8.5 Conclusions

- This chapter aims to study the thermal stability of PET nanocomposites and answer the following questions:
 - a) Will the clay accelerate degradation?
 - b) What is the effect of re-processing the nanocomposite materials on their viscosity and optical clarity?
 - c) What is the behaviour of the viscosity of the polymer nanocomposites over a long period of time?
- The TGA results show that the selected nanoclays in this project (Cloisite 25A, Somasif MTE and Somasif MAE) present the best thermal stability among the nanoclays tested.
- While the viscosity of PETNCs (3 wt.%) is greater than that for the ext. vPET and slightly tends to non-Newtonian behaviour at low shear rates, the viscosity of re-passed samples reduces and clearly exhibits Newtonian behaviour.
- The pictures of the pellets after each re-passing stage for PETNCs 3 and 5 wt.% indicate that the colour of the pellets immediately darkened during the first reprocessing. The change in colour of PET nanocomposites pellets occurs much more gradually which means the nanoclay additive plays a strong role in the degradation process due to the existence of the surfactant.
- The rheological behaviour of unfilled PET and PET/MTE nanocomposites over a long period of time (10 hrs) was investigated. During the first hours, the viscosity of all samples was reduced. Following this time, the samples show increasing viscosity except at loading 3 wt.% which exhibits Newtonian behaviour.

Chapter nine

9 General conclusion and future work

9.1 General conclusion

The objectives of this study have been successfully achieved. The PET/clay nanocomposites pellets which were produced can achieve the PET downstream manufacturers requirements by enhancing the rheological properties of the PET melt and the crystallisation of the PET final product, which reflect positively on the injection or/and extrusion processes. Moreover the requirements of PET bottles or packaging producers were achieved by enhancing the barrier properties of the final product as well as its mechanical properties and in the same time keeping the original distinguish feature of PET product (transparency) in reasonable levels.

The thesis started by giving a general introduction about PET (marketing, chemistry, manufacturing and application) then presented the fundamental concepts of nanocomposite materials in the belief that a good understanding of nanoparticles would act as a guide to understand the effect of nanoclay particles on the behaviour of the polymer. All raw materials, extrusion processes and characterisation techniques have been clarified and described.

Three nanoclays (Somasif MAE, Somasif MTE and Cloisite 25A) were compounded individually with Polyethylene Terephthalate (PET) pellets via twin screw extrusion to produce PETNC (20 wt.%) as a masterbatch and then diluted to produce PETNCs (1, 3 and 5 wt.%). Feeding the materials to the extruder's hopper was via dual motor feeders ensured a good distribution for the nanoparticles with the PET prior to melting. The intrinsic viscosity and thermal properties for these PETNC amorphous pellets were

studied. The rheological behaviour of the re-crystallised PETNCs was investigated over a wide range of shear rates. Films and micro-size tensile bars of PETNCs were produced via cast film extrusion and micromoulding injection respectively, from re-crystallised PETNCs pellets. Further tests have been applied to the PETNCs films such as uniaxial tensile test to study the effect of nanoclays at various concentration on the tensile modulus, biaxial tensile tests to study the effect of nanoclay on the thermal properties of biaxial stretched PET films; and barrier property tests to study the effect of nanoplatelets on the permeability of films; while only uniaxial tensile tests were applied to the micromoulding specimens to study the effect of different injection speeds on the end product tensile modulus.

In this project, many factors were taken into account to achieve well-processed materials required for this study such as care in choosing the nanoclay in order to achieve good dispersion in terms of compatibility and thermal stability. The second factor taken into account was the preparation of the material prior to compounding or analysis such as sufficient drying or re-crystallisation of the pellets. The third important factor was that the feeding of the material to the twin screw extruder should be simultaneously via dual motor feeders to avoid poor distribution of the nanoclay in the PET melt. A fourth factor was to try to avoid the long residence time, high processing temperatures and high screw speeds in order to decrease the possibility of potential thermal degradation of the melt.

Many points were observed from this study such as:

I. PETNC rheological behaviour:

- By studying the rheological behaviour of PET pellets under different state (dried, amorphous, re-crystallised), the importance of sufficient drying and re-crystallisation of the amorphous pellets prior to any melt processing seems clear.
- At high shear rates, it is clear that the absolute value of the melt viscosity of PETNC is significantly lower than for un-filled PET, and the extent of this reduction increases with adding more nano-filler at a given shear rate. This reduction follows the shear thinning behaviour which shows the dependence of the shear viscosity for the un-filled PET and PETNC on the shear rate.
- This shear thinning behaviour at high shear rates can be explained by two mechanisms which can occur simultaneously. When applying high shear rates, the level of entanglements is significantly reduced and the molecular chains tend to orient in the flow direction. The nanoparticles also align with the flow direction at high shear rate.
- At high shear rate, Somasif MAE clay exhibits the maximum reduction in the shear viscosity of PET compared with the other clays used. This observation may be attributed to either the fast alignment of MAE platelets with the flow direction due to the large gap (d-spacing) between the platelets when compared to the other nanoclays used, or to the higher degradation level of PETNC in the presence of MAE due to high surfactant content, or to both causes.
- At low shear rates, the magnitudes of the complex viscosity are dependent on the nanoclay concentrations and processing shear rate. The nanoclay leads to increases in complex viscosity with increases in the clay loading above 1 wt.%. The vPET, ext. vPET, and PET nanocomposites (1 wt.%) and PET/MTE (3 wt.%) exhibit Newtonian behaviour for low shear rate ranges. The complex

viscosity started to deviate from Newtonian behaviour and behaved in a shear thinning manner at a 3 wt.% concentration. Usually the formation of aggregates is responsible for an increase in complex viscosity.

- Storage and loss moduli for the PETNCs show a significantly diminished shear rate dependence and this becomes more obvious on increasing the clay content. The polymer transfers from fluid-like to solid-like behaviour at certain filler concentrations, this phenomenon being known as the percolation threshold. From the results presented it seems that the percolation threshold is reached approximately at 3 wt.% loading.
- PET/MTE exhibits the lowest storage modulus values among the PETNCs at the same concentration (3 wt.%) or, in other words the lowest percolation threshold, which can be attributed to an excellent exfoliation occurring in the MTE case. This observation is assisted by the observation of good dispersion for MTE into the PET matrix as shown by TEM images.
- Cole-Cole plots has been used to explore the influence of adding a nano-filler on the structure of a PET matrix at a fixed temperature. The change in the slope of the curves is an indication of increasing interaction between the PET matrix and the nanoclay platelets. The slope of the curve at 3 wt.% content is near unity which implies that the PETNC at this point is rheologically heterogeneous and further energy can be dissipated. Furthermore, some slopes of the curves at high shear rates are nearer 2 which indicates that the rheology is that of a homogenous system, and this can be attributed to the effect of a high shear rate on the network structure, or in other words, the high shear rate induces a collapse in some interactions.

- The relaxation time of the PETNCs increased with decreasing shear rate, this being attributed to the reduction in PET chain mobility at low shear rates. The physical interaction between the PET chains and nanoclay platelets can be broken with increases in the shear rate, which can lead to shorter relaxation times.
- The rheological results over a wide range of shear rates show that the Cox-Merz rule does not hold for PET nanocomposites or indeed for unfilled PET.
- The absolute value of intrinsic viscosity (I.V.) of PETNC reduced on increasing the clay concentration, and this reduction can be attributed to two reasons: first, the presence of clay platelets which align with the flow and increase the ‘flowability’ of the dissolved solution during the I.V. test, and second, the possibility of thermal-oxidative degradation of nanoclay during the compounding, which can increase the magnitude of this reduction.

II. PETNC thermal properties:

- It was observed that all three nanoclays used in this project (MAE, MTE and Cloisite 25A) act as effective nucleation agents for the crystallisation process by increasing the T_{mc} and decreasing the T_{gc} , while causing no consistent trends in the absolute crystallisation values.
- It can also be noticed that the change in the T_g and T_m in present of nanoclay was small.
- With increasing clay content, the peak of crystallisation temperature from the melt (T_{mc}) moves to the right (higher T_{mc} temperature) and gets sharper (decrease in the half-time $t^{1/2}$) which indicates the crystallization rate is increased.

- The thermal properties of un-filled PET and PET/MTE nanocomposite (1, 3 and 5 wt.%) films (oriented and un-oriented) were analysed and it was observed that stretching of the un-filled PET film decreased chain flexibility as is indicated by the increase in glass transition temperature (T_g). Stretching the film also accelerates the crystallisation temperature of the film from the solid phase (T_{gc}).
- Adding further MTE filler (e.g. 3 or 5 wt.%) leads to the MTE starting to build up crystallinity immediately after the glass transition temperature in the case of the stretched film. This confirms that the stretch process accelerates the formation of crystalline structures inside the PET matrix. It was also observed that the stretching accelerated T_{gc} and this acceleration increases in the presence of a nanoclay. The more rapid start in building the crystal structure in the presence of the nanoclay could be attributed to the stretching process expanding the gallery space (d-basal), which would give an increased contact surface area between the nanoclay platelets and the PET matrix, which may lead to an earlier nucleation process.
- Normally crystallised PET exhibits a single endotherm melting temperature (T_m) but the PET used in this project as received from the supplier (Tergal F9) exhibits a double endotherm T_m . It has been shown that with sufficient SSP processing through the SSP reactor, the double melting behaviour becomes a single melting peak.

III. PETNC end product properties:

- The mechanical properties of PETNCs films and micromoulding specimen were measured by uniaxial tensile testing these results correlated well to the TEM micrographs for the same films.

- The addition of all nanoclays to PET leads to significant increases in tensile modulus (up to 125% increase for PET/MTE at 5% concentration) indicative of good dispersion and strong interfacial interaction between the PET and the nanoclay (MTE > MAE > Cloisite 25A).
- The improvement in the tensile modulus when adding MAE or MTE can be attributed to many reasons including the good dispersion of these clays within the PET matrix as its TEM images show.
- The good compatibility between the PET chain and MTE or MAE clays contributed to this improvement. The large inter-gallery spacing and greater aspect ratio of the MTE and MAE platelets when compared with Cloisite 25A increases the diffusion rate of the PET macromolecules into the inter-gallery space which enabled the Somasif clays to enhance the interfacial adhesion between the clay platelets and the PET matrix
- The reduction in the tensile modulus of PET/Cloisite 25A (1 wt.%) may be attributed to agglomeration on the nanoclay within the PET matrix as shown in the relevant TEM images though the orientation of the PET chains can mitigate some of this decrease caused by the nanoclays by increasing the strength of the chain and also aligning the nanoclay's platelets. The failure of Cloisite 25A (at loading 1 wt.%) to enhance the mechanical properties and its relatively poor enhancement at loading 3 or 5 wt.% does not necessarily mean a reduction in performance in terms of other properties of the interest. The PET/Cloisite 25A exhibits excellent gas barrier improvements and act as nucleation agents as seen in the crystallisation temperature and rate results.
- The tensile test results for the micro-moulded samples shows that the processing conditions such as injection speed are crucial factors affecting the mechanical

properties of polymer injection moulded products. The nanoplatelets counted as molecular chains orientation inducer when the PET molecules penetrate between the narrow gaps of the platelets at high speed. It was shown that a ‘medium’ injection speed (400mm/s) gave the best mechanical properties in terms of elongation to break as well as ultimate tensile strength.

- Barrier properties of the films are significantly enhanced by addition of all three nanoclays. A 50% decrease in permeability has been achieved (Cloisite 25A > MTE > MAE).
- The reduction in the permeability of PET film is apparent even at low nanoclay contents (1 wt.%). When the content of the Cloisite 25A reached 5 wt.%, the gas permeability reduced to 50% that of the extruded vPET film.
- The MTE and MAE showed a linear reduction in the permeability of oxygen on addition of clay (1, 3 and 5%) while Cloisite 25A (3%) did not show a significant reduction in permeability compared with 1 wt.% Cloisite 25A.
- The improvement in the barrier properties of the PET films on adding nanoclays can be attributed to the good distribution of nanoclays within the PET matrix.
- The excellent barrier property enhancement achieved by adding Cloisite 25A is counter to the relatively poor tensile modulus enhancement for the PET/Cloisite 25A NC films and more tactoids and few intercalation aspects for Cloisite 25A platelets as TEM images shown. There are many reasons for this phenomenon. The small aspect ratio of Cloisite 25A compared with Somasif clays leads to a small contact area between the clay platelets and the polymer matrix, which gives relatively poor reinforcement for PET/Cloisite25A samples. Another possible reason is that long aspect ratio clays take longer to align fully, which would give more resistance to the stress compared to small aspect ratio clays.

- While the viscosity of PETNCs (3 wt.%) are greater than the ext. vPET and slightly tends to non-Newtonian behaviour at low shear rates, the viscosity of re-passed samples reduces and clearly exhibits Newtonian behaviour.
- The pictures of the pellets after each re-passing stage for PETNCs 3 and 5 wt.% indicate that the colour of the pellets immediately darkened during the first reprocessing. The change in colour of PET nanocomposites pellets occurs much more gradually which means the nanoclay additive plays a strong role in the degradation process due to the existence of the surfactant.
- The rheological behaviour of unfilled PET and PET/MTE nanocomposites over a long period of time (10 hrs) was investigated. During the first hours, the viscosity of all samples was reduced. Following this time, the samples show increasing viscosity except at loading 3 wt.% which exhibits Newtonian behaviour.

9.2 Future work

- There are many tests were performed and its data under analysis such as biaxial stretch film and wide/single angle x-ray scattering (WAXS/SAXS) for oriented and un-oriented PETNCs films.
- Modelling the barrier properties results is currently underway by Dr. J. Sweeney. AFM studies on PET nanocomposite films also underway with Dr. Colin Grant.
- Producing the PETNCs films directly from the twin screw extruder in the compounding process is highly recommended in order to study the tensile modulus and barrier properties and also to minimise the extrusion processes. The TEM technique could be used to support the thermal properties results for the

oriented film and to study the effect of biaxial stretch on the platelet distribution and alignments.

- The infrared (IR) wave use to heat up the preform in order to produce bottles or during the thermoforming processes. Some PET manufacturers add additive during the preforms or sheets production to work as scattering particles for the IR waves in order to increase the path of the wave in the final production stage (e.g. stretch blow moulding or thermoforming). The aim is to save the power by reducing the power consumption and increase the production capacity of the bottle by reducing the time of heating up stage. So short study can conducted on the PETNCs' films to investigate the effect of clay platelets on the IR.
- Needs to optimise behaviour of PETNCs so as to produce materials with excellent optical, barrier, mechanical, crystal and rheological behaviour in one material.

References

- Ajayan, P., Schadler, L. and Braun, P., "Nanocomposite science and technology", Wiley-VCH, (2003). ISBN: 9783527303595
- Allan, R., Iengar, H. and Ritchie, P., "Pyrolysis IX. Pyrolysis of the model systems 2-benzoyloxyethyl and 2-p-chlorobenzoyloxyethyl terephthalate and of poly(ethylene terephthalate)", *J. Chem. Soc.*, (London), p.2107, (1957).
- Ammala, A., Bell, C. and Dean, K., "Poly(ethylene terephthalate) clay nanocomposites: Improved dispersion based on an aqueous ionomer", *Compos. Sci. Tech.*, v.68, pp.1328–1337, (2008).
- Anderson, P., "Twin screw extrusion guidelines for compounding nanocomposites" *SPE ANTEC*, 48, (2002).
- Anoop, A., Agarwal, U., and Rani, J., "Carbon nanotubes-reinforced PET nanocomposite by melt-compounding", *Polymer*, v.47, pp.3976-3980, (2006).
- Anoop, A., Agarwal, U. S. and Joseph, R., "Carbon Nanotubes-Reinforced PET Nanocomposite by Melt Compounding", *J. Appl. Polym. Sci.*, v.104, pp.3090–3095, (2007).
- Antoniadis, G., Paraskevopoulos, K., Bikiaris, D. and Chrissafis, K., "Kinetics study of cold-crystallization of poly(ethylene terephthalate) nanocomposites with multi-walled carbon nanotubes", *Thermochimica Acta*, v.493, pp.68–75, (2009).
- Barber, G., Calhoun, B. and Moore, R., "Poly(ethylene terephthalate) ionomer based clay nanocomposites produced via melt extrusion", *Polymer*, v.46, pp.6706–6714 (2005).
- Bell, J. and Dumbleton, J., "Relation between melting behavior and physical structure in polymers" *J. Polym. Sci.*, Part A-2, pp.1033-1057, (1969).
- Bell, J. and Murayama, T., "Relations between dynamic mechanical properties and melting behavior of nylon 66 and poly(ethylene terephthalate)", *J. Polym. Sci.*, Part A-2, pp.1059-1073, (1969).
- Bhattacharya S., Gupta R. and Kamal, S., "Polymeric nanocomposites: theory and practice", (1st edition), Hanser Gardner Publications, (2008).
- Bhattacharya, S., Gupta, R. and Bhattacharya, S., "The rheology of polymeric nanocomposites", in *Polymer nanocomposites handbook*, Chapter 8, editors Gupta et al., CRC Press, (2010). ISBN: 9780849397776.
- Bizarria, M., Giraldi, A., Carvalho, C., Velasco, J., Avila, M. and Mei, L., "Morphology and thermomechanical properties of recycled PET–organoclay nanocomposites", *Polymer*, v.104, pp.1839–1844, (2007).

Blumstein, A., "Polymerization of adsorbed monolayers. II. Thermal degradation of the inserted polymer", *J. Polym. Sci., Part A: General Papers*, v.3, pp.2665–2672, (1965).

Booker, R. and Boysen, E., "Nanotechnology for dummies (1st edition)", Wiley Publishing Inc. (2005). ISBN: 9780764583681.

Brandao, L., Mendes, L., Medeiros, M., Sirelli, L. and Dias, M., "Thermal and mechanical properties of poly(ethylene terephthalate)/lamellar zirconium phosphate nanocomposites", *Polymer*, v.102, pp.3868–387, (2006).

Brink, A., "Thermoplastic polyester composites", Chapter15 in "Modern polyester (1st edition)", Scheirs J. and Long, T., John Wiley and Sons Inc., (2003). ISBN:0471498564.

British Plastic Federation (BPF), this link accessed on 3rd of March 2011. http://www.bpf.co.uk/sustainability/plastics_recycling.aspx

Brody, A. and Marsh, K., "The wiley encyclopedia of packaging technology (2nd edition)", Wiley-Interscience, (1997). ISBN: 0470087048.

Brooks, David W., Glies, Geoff A., "PET packaging technology (1st edition)", Sheffield Academic Press (2002). ISBN: 1841272221.

Brown, N. and Ward, I., "Load drop at the upper yield point of a polymer", *J. Polym. Sci. Part A-2: Polym. Phys.*, pp. 607-620, (1968).

Buzea, C., Pacheco, I. and Robbie, K. "Nanomaterials and nanoparticles: Sources and Toxicity", *Biointerphases*, vol. 2, pp. MR17-MR172, (2007).

Calcagno, C., Mariani, C., Teixeira, S. and Mauler, R., "The effect of organic modifier of the clay on morphology and crystallization properties of PET nanocomposites", *Polymer*, v.48, pp.966-974, (2007).

Carrado, K., "Polymer-clay nanocomposites", Chapter 10, p. 351, in "Advanced Polymeric Material Structure Property Relationships", edited by Shonaike, G. and Advani, S., CRC Press, (2003).

Cassagnau, P., "Melt rheology of organoclay and fumed silica nanocomposites", *Polymer*, v.49, pp.2183-2196, (2008).

Castle, L. "Migration of plastics into foods during microwave and conventional cooking and into bottled beverages", *J. Food protection*, v.52, pp.337-342, (1989).

Chae, D. and Kim, B., "Thermal and rheological properties of highly concentrated PET composites with ferrite nanoparticles", *Comp. Sci. Tech.*, v.67, pp.1348–1352, (2007).

Chan, C., Wu, J., Li, J. and Cheung, Y., "Polypropylene/calcium carbonate nanocomposites", *Polymer*, v.43, pp.2981-2992, (2002).

Chanda, M. and Roy, S., "Plastic Technology Handbook (2nd edition)", Marcel Dekker Inc. (1993). ISBN: 0849370396.

Chang, J., Kim, S., Joo, Y. and Im, S., "Poly(ethylene terephthalate) nanocomposites by in situ interlayer polymerization: the thermo-mechanical properties and morphology of the hybrid fibers", *Polymer*, v.45, pp.919–926, (2004).

Chang, J. and Mun, M., "Nanocomposite fibers of poly(ethylene terephthalate) with montmorillonite and mica: thermomechanical properties and morphology", *Polym. Int.*, v.56, pp.57–66, (2007).

Chatterjee, A., Price, F. and Newman, S., "Heterogeneous nucleation of crystallization of high polymers from the melt. III. Nucleation kinetics and interfacial energies", *J. Polym. Sci.: Polym. Phys. Ed.*, v.13, pp.2391–2400, (1975).

Chen, X., Li, C., Shao, W. and He, J., "Preparation and properties of poly(ethylene terephthalate)/ATO nanocomposites", *Appl. Polym. Sci.*, v.105, pp.2783–2790, (2007).

Cheremisinoff, N., "An introduction to polymer rheology and processing" CRC Press Inc, (1993). ISBN: 0849344026.

Cho, J. and Paul, R., "Nylon 6 nanocomposites by melt compounding", *Polymer*, v.42, pp.1083-1094, (2001).

Choi, W., Kim, H., Yoon, K., Kwon, O. and Hwang, C., "Preparation and barrier property of poly (ethylene terephthalate)/clay nanocomposite using clay-supported catalyst", *J. Appl. Polym. Sci.*, v.100, pp.4875-4879, (2006).

Choudalakis, G. and Gotsis, A., "Permeability of polymer/clay nanocomposites: A review", *Euro. Polym. J.*, v.45, pp.967–984, (2009).

Chung, J., Son, S., Chun, S., Kang, T. and Kwak, S., "Thermally stable exfoliated poly(ethylene terephthalate) (PET) nanocomposites as prepared by selective removal of organic modifiers of layered silicate", *Polym. Degrad. Stab.*, v.93, pp.252-259, (2008).

Chung, S., Hahm, W. and Im, S., "Poly(ethylene terephthalate)(PET) nanocomposites fumed silicas by melt compounding", *Macro. Res.*, v.10, pp.221-229, (2002).

Cogswell, F., "Polymer Melt Rheology (1st edition)", Woodhead Publishing Ltd., (1998). ISBN: 1855731983.

Costache, M., Heidecker, M., Manias, E. and Wilkie, C., "Preparation and characterization of poly(ethylene terephthalate)/clay nanocomposites by melt blending using thermally stable surfactants", *Polym. Adv. Tech.*, v.17, pp.764–771, (2006).

Culbert, B. and Christel, A., "Continuous solid-state polycondensation of polyester", Chapter 4 in "Modern polyester (1st edition)", Scheirs J. and Long, T., John Wiley and Sons Inc., (2003). ISBN:0471498564.

Daubeny, R., Bunn, C. and Brown, C., "The Crystal Structure of Polyethylene Terephthalate", *Proceedings of the Royal Society of London Ser. A*, v.226, pp. 531-542, (1954).

Dealy, J. and Saucier, P., "Rheology in plastics quality control", Hanser Gardner Publications, (2000). ISBN: 3446210695.

Dealy, J. and Wissbrun, K., "Melt Rheology and Its Role in Plastics Processing: Theory and Applications", Springer, (1990). ISBN: 0792358864.

Dennis, H., Hunter, D., Chang, D., Kim, S., White, J., Cho, J. and Paul, D., "Effect of melt processing conditions on extent of exfoliation on organoclay-based nanocomposites", *Polymer*, v.42, pp.9513-9522, (2001).

Drozdov, A., Jensen, E. and Christiansen, J., "Pseudo-solid-like behavior of nanocomposite melts", *Int. J Nanotech. App.*, v.2, pp.1-14, (2008).

Dupaix, R. and Boyce, M., "Finite strain behavior of poly(ethylene terephthalate) (PET) and poly(ethylene terephthalate)-glycol (PETG)", *Polymer*, v.46, pp.4827-4838, (2005).

Durmus, A., Woo, M. Ahmet Kasgoz, A., Macosko, C. and Tsapatsis, M., "Intercalated linear low density polyethylene (LLDPE)/clay nanocomposites prepared with oxidized polyethylene as a new type compatibilizer: Structural, mechanical and barrier properties", *Euro. Polym. J.*, v.43, pp.3737-3749, (2007).

Fasulo, P., Rodgers, W. and Ottaviani, R., "Extrusion processing of TPO nanocomposites", *Polym. Eng. and Sci.*, v.44, pp.1036-1045, (2004).

FDA's Center for Food Safety and Applied Nutrition. This link accessed on 2nd of January 2010. <http://www.cfsan.fda.gov/~dms/opa-indt.html>

Fornes, T., Yoon, P. and Paul, D., "Polymer matrix degradation and color formation in melt processed nylon 6/clay nanocomposites", *Polymer*, v.44, pp.7545-7556, (2003).

Fornes, T., Yoon, P., Keskkula, H. and Paul D., "Nylon 6 nanocomposites: the effect of matrix molecular weight", *Polymer*, v.42, pp.9929-9940, (2001).

Frounchi, M. and Dourbash, A., "Oxygen barrier properties of poly(ethylene terephthalate) nanocomposite films", *Macro. Mater. Eng.*, v.294, pp.68-74, (2009).

Fujiyama, M., Wakino, T. and Kawasaki, Y., "Structure of skin layer in injection-molded polypropylene", *J. Appl. Polym. Sci.*, v.35, pp.29-49, (1998).

Gabbott, P., "Principles and application of thermal Analysis (1st edition)", Wiley-Blackwell, (2007). ISBN: 9781405131711.

Giannelis, E., "Polymer-layered silicate nanocomposites: synthesis, properties and applications", *Appl. Organometal. Chem.*, v.12, pp.675-680, (1998).

- Giraldi, A., Bizarria, M., Silva, A., Velasco, J., d'Avila, M. and Mei, L., "Effects of extrusion conditions on the properties of recycled poly(ethylene terephthalate)/nanoclay nanocomposites prepared by a twin-screw extruder", *J. Appl. Polym. Sci.*, v.108, pp.2252–2259, (2008).
- Goltner, W., "Solid-state polycondensation of polyester resins: fundamentals and industrial production", chapter 5 in "Modern polyester (1st edition)", Scheirs J. and Long, T., John Wiley and Sons Inc., (2003). ISBN:0471498564.
- Gooch, J., "Encyclopedic dictionary of polymers", Springer, p.401, (2007). ISBN: 0387335021.
- Goodings E., "Thermal degradation of polymers", *SCI Monograph 13, Soci. Chemi. Ind., London*, pp.211–227, (1961).
- Guan, G., Li, G., Zhang, D., Yuan, X., Xiao, Y. and Liu, X., "New insight into the crystallization behavior of poly(ethylene terephthalate)/clay nanocomposites", *J. Polym. Sci.: Part B*, v.46, pp.2380–2394, (2008).
- Gumther, B. and Zachmann, H., "Influence of molar mass and catalysts on the kinetics of crystallization and on the orientation of poly(ethylene terephthalate)", *Polymer*, v.24, pp.1008-1014, (1983).
- Gupta, R. and Bhattacharya, S., "Polymer-clay nanocomposites: current status and challenges", *Indian Chemi. Eng.*, v.50, pp.242-267, (2008).
- Gurmendi, U., Eguiazabal, J. and Nazabal, J., "Structure and properties of nanocomposites with a poly(ethylene terephthalate) matrix", *Macro. Mater. Eng.*, v.292, pp.169 – 175, (2007).
- Han, C., "Rheology in polymer processing", Academic press, New York, (1976). ISBN: 0123224500.
- Han, J., Choi-Feng, C., Li, D. and Han, C., "Effect of flow geometry on the rheology of dispersed two-phase blends of polystyrene and poly(methyl methacrylate)", *Polymer*, v.36, pp.2451-2462, (1995).
- Han, K. and Yu, M., "Study of the preparation and properties of UV-blocking fabrics of a PET/TiO₂ nanocomposite prepared by in situ polycondensation" *J. Appl. Polym. Sci.*, v.100, pp.1588–1593, (2006).
- Hatakeyama, T. "Handbook of thermal analysis", John Wiley & Sons, Inc. (1998). ISBN: 0471983632.
- Hedenqvist, M. and Gedde, U. W., "Diffusion of small-molecule penetrates in semicrystalline polymers", *Prog. Polym. Sci.*, v.21, pp.299-333, (1996).
- Holdsworth P. and Turner-Jones, A., "The melting behaviour of heat crystallized poly(ethylene terephthalate)" *Polymer*, v.12, pp.195-208, (1971).

Hsiung, C. and Cakmak, M., "Detailed investigations of structural layering phenomena in injection molded thermotropic liquid crystalline polymers", *Int. Polym. Process*, issue 3, pp.255–270, (1993).

Hsiung, C., Tian, J. and Cakmak, M., "Detailed investigations of structural Layering phenomena in injection molded thermotropic LCP", *Int. Polym. Process*, issue 2, pp. 164–177, (1993)

Imai, Y., Nishimura,S., Abe,E., Tateyama,H. Abiko,A., Yamaguchi,A., Aoyama, T. and Taguchi, H., "High-modulus poly(ethylene terephthalate)/expandable fluorine mica nanocomposites with a novel reactive compatibilizer", *Chemi. Mater.*, v.17, pp.477-479, (2002).

Jabarin, S. and Lofgren, E., "Solid state polymerization of poly(ethylene terephthalate): Kinetic and property parameters". *J. Appl. Polym. Sci.*, v.32, pp. 5315-5335, (1986).

Jabarin, S., "Orientation studies of poly(ethylene terephthalate)", *Polym. Eng. Sci.*, v. 24, pp.376-384, (1984).

Jabarin, S., "Poly(ethylene terephthalate): chemistry and preparation" in, *Polymeric materials encyclopedia*, Salamone, J., editor, CRC Press, Boca Raton, FL, pp. 6079–6085, (1996). ISBN-10: 084932470X.

Jeol, S., Fenouillot, F., Rousseau, a., Masenelli-Varlot, k., Gauthier, C. and Briois, J., "Drastic modification of the dispersion state of submicron silica during biaxial deformation of poly(ethylene terephthalate)", *Macro.*, v.40, pp.3229-3237, (2007).

Jin, S., Young-Bin Park, Y. and Yoon, K., "Rheological and mechanical properties of surface modified multi-walled carbon nanotube-filled PET composite", *Compos. Sci. Tech.*, v.67, pp.3434–3441, (2007).

Jones, K., "PET materials and application", Chapter 3, p. 36, in "PET Packaging Technology", edited by Brooks, D. and Giles, G., Wiley-Blackwell, (2002). ISBN: 1841272221.

Karagiannidis, P., Stergiou, A. and George P. Karayannidis, G., "Study of crystallinity and thermomechanical analysis of annealed poly(ethylene terephthalate) films", *Euro. Polym. J.*, v.44, pp.1475–1486, (2008)

Kattan, M., Dargent, E., Ledru, J. and Grenet, J., "Strain-induced crystallization in uniaxially drawn PETG plates", *J. Appl. Polym. Sci.*, v.81, pp.3405–3412, (2001).

Ke, Z. and Yongping, B., "Improve the gas barrier property of PET film with montmorillonite by in situ interlayer polymerization", *Mater. lett.*, v.59, pp. 3348-3351, (2005).

Ke, Y, Yang, Z. and Zhu, C., "Investigation of properties, nanostructure, and distribution in controlled polyester polymerization with layered silicate", *J. Appl. Polym. Sci.* , v.85, pp.2677-2691, (2002).

Ke, Y., Long, C. and Qi, Z., "Crystallization, properties, and crystal and nanoscale morphology of PET–clay nanocomposites", *J. Appl. Polym. Sci.*, v.71, pp.1139–1146 (1999).

Ke, Y., Wu, T. and Xia, Y., "The nucleation, crystallization and dispersion behavior of PET-monomodisperse SiO₂ composites", *Polymer*, v.48, pp.3324–3336, (2007).

Kelly, A., Gough, T., Whiteside, B. and Coates, P., "High shear strain rate rheometry of polymer melts", *J. Appl. Polym. Sci.*, v.114, pp.864–873, (2009).

Khan, A., Bhaumik, D. and Dutta-Roy, B., "Charge trapping by solitons-a possible transport mechanism in macromolecular systems", *Bulletin of Mathematical Biology*, v.49, pp.729–735, (1987).

Khemani, K., "A novel approach for studying the thermal degradation, and for estimating the rate of acetaldehyde generation by the chain scission mechanism in ethylene glycol based polyesters and copolyesters", *Polym. Degrad. Stab.*, v.67, pp.91–99, (2000).

Kim, D., Lee, J., Barry, C. and Mead, J., "Evaluation and prediction of the effects of melt-processing conditions on the degree of mixing in Alumina/Poly(ethylene terephthalate) nanocomposites", *J. Appl. Polym. Sci.*, v.109, pp.2924–2934, (2008).

Kim, H., Bang, Y., Chou, S. and Yoo, K., "Morphology and mechanical properties of PET by incorporation of amine-polyhedral oligomeric silsesquioxane", *Compos. Sci. Tech.*, v.68, pp.2739–2747, (2008).

Kim, J., "The effect of carbon nanotube on the physical properties of poly(butylene terephthalate) nanocomposite by simple melt blending", *J. Appl. Polym. Sci.*, v.112, pp.2589–2600, (2009).

Kim, J., Choi, H., Kang, C. and Kim, S., "Influence of modified carbon nanotube on physical properties and crystallization behavior of poly(ethylene terephthalate) nanocomposite", *Polym. Comps.*, (2009).

Kim, J., Park, H. and Seong, H., "Multiwall-carbon-nanotube-reinforced poly(ethylene terephthalate) nanocomposites by melt compounding", *J. Appl. Polym. Sci.*, v.103, pp.1450–1457, (2007).

Kim, T. and Jabarin, S., "Solid-state polymerization of poly(ethylene terephthalate). II. modeling study of the reaction kinetics and properties", *J. Appl. Polym. Sci.*, v.89, pp.213–227, (2003).

Kim, T. and Jabarin, S., "Solid-state polymerization of poly(ethylene terephthalate). III. Thermal stabilities in terms of the vinyl ester end group and acetaldehyde", *J. Appl. Polym. Sci.*, v.89, pp.228–237, (2003).

Kim, T., Lofgren, E. and Jabarin, S., "Solid-state polymerization of poly(ethylene terephthalate). I. Experimental study of the reaction kinetics and properties", *J. Appl. Polym. Sci.*, v.89, pp.197–212, (2003).

Kong, Y. and Hay, J., “Multiple melting behaviour of poly(ethylene terephthalate)”, *Polymer*, v.44, pp.623–633, (2003).

Koo, J. “Polymer nanocomposites: processing, characterization and applications (1st edition)”, McGraw-Hill, New York, (2006). ISBN-10: 0071458212.

Kracalik, M., Mikesova, J., Thomann, R., Friedrich, C. and Puffr, R., “Effect of 3D structures on recycled PET/organoclay nanocomposites”, *Polym. Bul.*, v.58, pp.313–319, (2007).

Kracalik, M., Studenovský, M., Mikesova, J., Kovarova, J., Sikora, A., Thomann, R. and Friedrich, C., “Recycled PET-organoclay nanocomposites with enhanced processing properties and thermal stability”, *J. Appl. Polym. Sci.*, v.106, pp.2092–2100, (2007).

Kracalik, M., Studenovský, M., Mikesova, J., Sikora, A., Thomann, R., Friedrich, C., Fortelny, I. and Simonik, J., “Recycled PET nanocomposites improved by silanization of organoclays”, *J. Appl. Polym. Sci.*, v.106, pp.926–937, (2007).

Krikorian, V. and Pochan, D., “Poly (L-Lactic acid)/layered silicate nanocomposite: fabrication, characterization, and properties”, *Chemi. Mater.*, v.15, pp.4317–4324, (2003).

Krishnamoorti, R. and Yurekli, K., “Rheology of polymer layered silicate nanocomposites”, *J. Chem. Phys.*, v.114, pp.4968-4973, (2001).

Lange, J. and Wyser Y., “Recent innovations in barrier technologies for plastic packaging – a review”, *Pack. Tech. Sci.*, v.16, pp.149–158, (2003).

Larson, R., “The structure and rheology of complex fluids”, New York: Oxford University Press; (1999). ISBN: 9780195121971.

Lasoski, S. W. and Cobbs, W. H., “Moisture permeability of polymers. I. Role of crystallinity and orientation”, *J. Polym. Sci.*, v.36, pp.21-33, (1959).

LeBaron, P., Wang, Z. and Pinnavaia, T., “Polymer-layered silicate nanocomposites: an overview”, *Appl. Clay Sci.*, v.15, pp.11–29, (1999).

Lee, W. and Im, S., “Thermomechanical properties and crystallization behavior of layered double hydroxide/poly(ethylene terephthalate) nanocomposites prepared by in-situ polymerization”, *J. Polym. Sci. Part B*, v.45, pp.28–40, (2007).

Lewis, E., Duckett, R., Ward, I., Fairclough, J. and Ryan, A., “The barrier properties of polyethylene terephthalate to mixtures of oxygen, carbon dioxide and nitrogen”, *Polymer*, v.44, p.1631-1640, (2003).

Li, Z., Luo, G., Wei, F. and Huang, Y., “Microstructure of carbon nanotubes/PET conductive composites fibers and their properties”, *Comp. Sci. Tech.*, v.66, pp.1022-1029, (2006).

- Li, X, Kang, T, Cho, W., Lee, J. and Ha, C., “Preparation and characterization of poly(butylene terephthalate)/organoclay nanocomposites”, *Macro. Rapid Commun.*, v.22, pp.1306-1312, (2001).
- Liu, Q. and Chen, D., “Viscoelastic behaviors of poly(ϵ -caprolactone)/attapulgite nanocomposites” *Euro. Polym. J.*, v.44, pp.2046-2050, (2008).
- Liu, W., Tian, X., Cui, P., Li, Y., Zheng, K. and Yang, Y., “Preparation and characterization of PET/silica nanocomposites”, *J. Appl. Polym. Sci.*, v.9, pp.1229–1232, (2004).
- Lu, H., Wang, H., Zheng, A. and Xiao, H., “Hybrid poly(ethylene terephthalate)/silica nanocomposites prepared by in-situ polymerization”, *Polym. Compos.*, v.28, pp. 42-46 (2007).
- Mark, H., “Encyclopedia of polymer science and technology (3rd edition)”, Wiley-Interscience (2004). ISBN: 0471275077.
- Mark, J., “Physical properties of polymers handbook (2nd edition)”, Springer, chapter 23, (2007). ISBN: 0387312358.
- Marshall, I. and Todd, A., “The thermal degradation of polyethylene terephthalate”, *Trans. Faraday Soc.*, v.49, pp.67-78, (1953).
- Matayabas, J. and Turner, S., “Nanocomposite technology for enhancing the gas barrier of polyethylene terephthalate”, in *Polymer-Clay. Nanocomposites*, edited by Pinnavaia, T. and Beall, G., Wiley, England, Chapter 11, (2001). ISBN: 0471637009.
- McConnell, D., Hornsby, P., Lew, C. and Qua, E., “Structure-property relationships in PET nanocomposite fibres” “, *SPE ANTEC Tech. Papers* pp. 387-392 (2006).
- McIntyre, E., “The historical development of polyesters”, chapter 1 in “Modern polyester (1st edition)”, Scheirs J. and Long, T., John Wiley and Sons Inc., (2003). ISBN: 0471498564.
- Medellin-Rodriguez, F., Phillips, P., Lin, J. and Campos, R., “The Triple Melting Behavior of Poly(ethylene terephthalate): Molecular Weight Effects”, *J. Polym. Sci. Part B*, v.35, pp.1757-1774, (1997).
- Medellin-Rodriguez, F., Phillips, P., Lin, J., “Melting behavior of high-Temperature polymers”, *Macro.*, v.29, p.7491, (1996).
- Mehta A, Gaur U, Wunderlich B., “Equilibrium melting parameters of poly(ethylene terephthalate)”, *J. Polym. Sci.: Polym. Phys. Ed.*, v.16, pp.289-296, (1978).
- Menczel, J. and Prime, R., “Thermal analysis of polymers: fundamentals and applications”, Wiley-Blackwell, chapter 3, p.241, (2009). ISBN: 9780471769170
- Mezger T., “The rheology handbook (2nd edition)”, Vincentz Network GmbH & Co. (2006). ISBN: 3878701748.

MOCON, (2010). This link has been accessed on 17th of May 2010, s [http://www.mocon.com/pdfperm/OX221%20Brochure%20Pages.pdf]

Mucha, M., Marszalek, J. and Fidrych, A., “Crystallization of isotactic polypropylene containing carbon black as a filler”, *Polymer*, v.41, p.4137-4142, (2000).

Muksing, N., Nithitanakul, M., Grady, B. and Magaraphan, R., “Melt rheology and extrudate swell of organobentonite-filled polypropylene nanocomposites”, *Polym. Test.*, v.27, pp. 470–479, (2008).

Mulhaupt, R., “Hermann Staudinger and the origin of macromolecular chemistry”, *Angewandte Chemie Int. Ed.*, v.43, pp.1054–1063, (2004).

Nakajima N., Bowerman H., Collins W., “Nonlinear viscoelastic behavior of butadiene-acrylonitrile copolymers filled with carbon black”, *J. Appl. Polym. Sci.*, v.21, p.3063, (1977).

Natarajan, K. and Wu, S., “Polyester compositions with improved crystallization rate”, *United States Patent 5344892*, (1994).

Natu, A, Lofgren, E. And Jabarin, S., “Effect of morphology on barrier properties of poly (ethylene terephthalate)”, *Polym. Eng. Sci.*, p. 400-409, (2005).

Nielsen L., “Models for the permeability of filled polymer system”. *J. Macro. Sci. (Chemi.) A1* (5), pp.929–942, (1967).

Odian, G., “Principles of polymerization (edition 4)”, John Wiley and Sons, (2004). ISBN: 0471274003.

Okada, A. and Usuki, A., “The chemistry of polymer-clay hybrids”, *Mater. Sci. Eng.: C* 3, pp. 109-I 15, (1995).

Ou, C., Ho, M. and Lin, J., “Synthesis and characterization of poly(ethylene terephthalate) nanocomposites with organoclay”, *J. Appl. Polym. Sci.*, v.91, pp.140–145, (2004).

Packaging Materials: 1- Polyethylene Terephthalate (PET) for Food Packaging Applications. international life sciences institute, 2000, Washington, DC, p.11.

Papaspyrides, C. and Vouyiouka, S., “Fundamentals of solid state polymerization”, chapter1 in “Solid state polymerization (1st edition)”, Papaspyrides, C. and Vouyiouka, S., John Wiley and Sons Inc., (2009). ISBN: 9780470084182.

Pavlidou, S. and Papaspyrides, C., “A review on polymer-layered silicate nanocomposites”, *Progress in polymer science*, v.33, pp.1119–1198, (2008).

Pees, B., Marc, A., Maliha, K. and Helen, E., “Process for production of (Co) polyamide nanocomposite materials”, *United States Patent Application 20080293883*, (2008).

Pegoretti, A., Kolarik, J., Peroni, C. and Migliaresi, C., “Recycled poly(ethylene terephthalate)/layered silicate nanocomposites: morphology and tensile mechanical properties”, *Polymer*, v.45, p.2751-2759, (2004).

Potschke, P., Fornes, T. and Paul, D., “Rheological behavior of multiwalled carbon nanotube/polycarbonate composites”, *Polymer*, v.43, p.3247, (2002).

Qin, H., Zhang, S., Liu, H., Xie, S., Yang, M. and Shen, D., “Photo-oxidative degradation of polypropylene/montmorillonite nanocomposites”, *Polymer*, v.46, pp.3149–3156, (2005).

Rajeev, R., Harkin-Jones, E., Soon, K., McNally, T., Menary, G., Armstrong, C. and Martin, P., “Studies on the effect of equi-biaxial stretching on the exfoliation of nanoclays in polyethylene terephthalate”, *Euro. Polym. J.*, v.45, pp.332–340, (2009).

Ratner, M. and Ratner, D., “Nanotechnology: a gentle introduction to the next big idea (1st edition)”, Prentice Hall (2003). ISBN: 0131014005.

Ray, S. and Okamoto, M., “Polymer/layered silicate nanocomposites: a review from preparation to processing”, *Prog. Polym. Sci.*, v.28, pp.1539–1641 (2003).

Ray, S., “Rheology of polymer/layered silicate nanocomposites”, *J. Ind. Eng. Chem.*, v.12, pp.811-842, (2006).

Ray, S., Bousmina, M. and Okamoto, K., “Structure and properties of nanocomposites based on poly(butylene succinate-co-adipate) and organically modified montmorillonite”, *Macro. Mater. Eng.*, v.290, p.759-768, (2005).

Reinking M. and Rufener P., “Shear modification of HDPE-clay nanocomposites” patent no. US6884834B2 (2005).

Rieckmann, T. and Volker, S., “Poly(ethylene Terephthalate) Polymerization—Mechanism, Catalysis, Kinetics, Mass Transfer and Reactor Design”, Chapter2 in “Modern polyester (1st edition)”, Scheirs J. and Long, T., John Wiley and Sons Inc., (2003). ISBN: 0471498564.

Roberts R., “Poly(ethylene terephthalate) II—Morphological changes on annealing”, *Polymer*, v. 10, pp. 117-125, (1969).

Rubin, I., “Handbook of plastic materials and technology”, Wiley-Blackwell, (1990). ISBN: 0471096342.

Sanches, N., Dias, M. and Pachecom, E., “Comparative techniques for molecular weight evaluation of poly (ethylene terephthalate) (PET)”, *Polym. Test.*, v.24, pp.688–693, (2005).

Sanchez-Solis, A. Garcia-Rejon, A. and Manero, O., “Production of nanocomposites of PET-Montmorillonite clay by an extrusion process”, *Macro. Symp*, v. 192, pp. 281-292 (2003).

Sanchez-Solis, A., Romero-Ibarra, I., Estrada, M., Calderas, F. and Manero, O., “Mechanical and rheological studies on polyethylene terephthalate-montmorillonite nanocomposites”, *Polym. Eng. Sci.*, v.44, pp.1094-1102, (2004).

Schiraldi, D., “New poly(ethylene terephthalate) copolymers”, chapter6 in “Modern polyester (1st edition)”, Scheirs J. and Long, T., John Wiley and Sons Inc., (2003). ISBN: 0471498564.

Sharples, A., “Introduction to polymer crystallisation”, Edward Arnold (Publishers), Ltd. London, (1966).

Shen, S., Lin, Y., Du, Q., Zhong, W. and Yang, Y., “Preparation and rheology of polyamide-6/attapulgite nanocomposites and studies on their percolated structure”, *Polymer*, v.46, pp.5758–5766, (2005).

Sidel, “Actis™ barrier process”, this link has been accessed on 5th of Jan. 2011. http://www.sidel.com/en/content/download/168/762/version/3/file/Actis_EN.pdf

Soon, K., Harkin-Jones, E., Rajeev, R., Menary, G., McNally, T., Martin, P. and Armstrong, C., “Characterisation of melt-processed poly(ethylene terephthalate)/synthetic mica nanocomposite sheet and its biaxial deformation behavior”, *Polym. Int.*, v.58, pp.1134-1141, (2009).

Spanninger, P., “Thermoxidative degradation leading to gel in poly(ethylene terephthalate)”, *J Polym Sci*, v.12, pp.709-717, (1974).

Sperling, L., “Introduction to physical polymer science (4th edition)”, John Wiley and Sons, (2006). ISBN: 047170606X.

Svoboda, P., Zeng, C., Wang, H., Lee, L. and Tomasko, D., “Morphology and mechanical properties of polypropylene/organoclay nanocomposites”, *J. Appl. Polym. Sci.*, v.85 pp. 1562–1570 (2002).

Tadmor, Z. and Gogos, G., “Principle of polymer processing (2nd edition)”, A John Wiley & Sons Inc., Publication (2006). ISBN: 0471843202.

Tang, Y., Yang, C., Gao, P., Ye, L., Zhao, C. and Lin, W., “Rheological study on high-density polyethylene/ organoclay composites”, *Polym. Eng. Sci.*, v.51, pp.133–142, (2011).

Tarverdi, K. and Sontikaew, S., “Experimental study of extrusion and surface of treatment of organo clay with PET nanocomposites”, ANTEC, (2008).

Theng B., “Formation and properties of clay-polymer complexes”, Elsevier Science Ltd. (1979). ISBN: 0444417060.

Tzavalas, S., Mouzakis, D., Drakonakis, V., Gregoriou, V., “Polyethylene terephthalate–multiwall nanotubes nanocomposites: Effect of nanotubes on the conformations, crystallinity and crystallization behavior of PET”, *J. Polym. Sci. Part B*, v.46, pp.668–676 (2008).

Ulcer, Y., Cakmak, M., Miao, J. and Hsiunc, C., “Structural gradients developed in injection-molded syndiotactic polystyrene (sPS)”, *J. Appl. Polym. Sci.*, v.60, pp.669-691 (1996).

Usuki, A., Kawasumi, M., Kojima, Y., Okada, A., Kurauchi, T. and Kamigaito, O., “Swelling behavior of montmorillonite cation exchanged for ω -amino acids by ϵ -caprolactam”, *J. Mater. Res.*, v.8, pp.1174-1178, (1993).

Usuki, A., Koiwai, A., Kojima, Y., Kawasumi, M., Okada, A., Kurauchi, T. and Kamigaito, O., “Interaction of nylon 6-clay surface and mechanical properties of nylon 6-clay hybrid”, *J. Appl. Polym. Sci.*, v.55, pp.119–123, (1995).

Utracki, L., “Clay-containing polymeric nanocomposites (1st edition, v.1)”, Rapra Technology Limited (2004). ISBN: 1859574378.

Utracki, L., “Mechanical properties of clay-containing polymeric nanocomposites”, chapter 13, p.341, in “Polymer Nanocomposites Handbook”, edited by Gupta, R., Kennel, E. and Kim, K., CRC Press, (2010). ISBN: 9780849397776.

Utracki, L., Sepehr, M. and Boccaleri, E., “Synthetic, layered nanoparticles for polymeric nanocomposites (PNCs)”, *Polym. Adv. Tech.*, v.18, pp.1–37, (2007).

Vassiliou, A., Chrissafis, K. and Bikiaris, D., “In situ prepared PET nanocomposites: Effect of organically modified montmorillonite and fumed silica nanoparticles on PET physical properties and thermal degradation kinetics”, *Thermochimica Acta*, v.500, pp.21–29, (2010).

Viana, J. “Structural interpretation of the strain-rate, temperature and morphology dependence of the yield stress of injection molded semicrystalline polymers”, *Polymer*, v.46, pp.11773–11785, (2005).

Wadekar, S., Agarwal, U., Boon, W. and Nadkarni, V., “Recent developments in solid state polymerization of poly(ethylene terephthalate)”, chapter 8 in “solid state polymerization (1st edition)”, Papaspyrides, C. and Vouyiouka, S., John Wiley and Sons Inc., (2009). ISBN: 9780470084182.

Wang, K., Liang, S., Du, R., Zhang, Q. and Fu, Q., “The interplay of thermodynamics and shear on the dispersion of polymer nanocomposite”, *Polymer*, v.45, pp.7953–7960, (2004).

Wang, Y., Gao, J., Ma, Y. and Agarwal, U., “Study on mechanical properties, thermal stability and crystallization behavior of PET/MMT nanocomposites”, *Composites: Part B*, v.37, pp.399–407, (2006).

Wang, Z., Xie, G., Wang, X., Li, G., and Zhang, Z., “Rheology enhancement of polycarbonate/calcium carbonate nanocomposites prepared by melt-compounding”, *Mater Lett*, v.60, pp.1035–1038, (2006).

Ward, I. and Sweeney, J., “An introduction to the mechanical properties of solid polymers (2nd edition)”, Wiley-Blackwell, (2004). ISBN: 047149626X.

Whelan, A., "Polymer Technology Dictionary", Springer, (1994). ISBN: 9780412581809.

Whitney, W. and Andrews, R., "Yielding of Glassy Polymers", *J. Polym. Sci. C*, v.16, pp.2981-2989, (1967).

Wu, D., Zhou, C. and Zhang, M., "Rheology of isothermally crystallized poly(butylene terephthalate) nanocomposites with clay loadings under the percolation threshold", *J. Polym. Sci.: Part B: Polym. Phys.*, v.45, pp.229-238, (2007).

Wu, D., Zhou, C., Hong, Z., Mao, D. and Bian, Z., "Study on rheological behaviour of poly(butylene terephthalate)/montmorillonite nanocomposites", *Euro. Polym. J.*, v.41, pp.2199-2207, (2005).

Xanthos, M., Baltzis, B. and Hsu, P., "Effects of carbonate salts on crystallization kinetics and properties of recycled poly(ethylene terephthalate)", *J. Appl. Polym. Sci.*, v.64, pp.1423-1435, (1997).

Xanthos, M., Yilmazer, U., Dey, S. and Quintans, J., "Melt viscoelasticity of polyethylene terephthalate resins for low density extrusion foaming", *Polym. Eng. Sci.*, v.40, pp.554-566, (2000).

Xie, W., Gao, Z., Pan, W., Hunter, D., Singh, A. and Vaia, R., "Thermal degradation chemistry of alkyl quaternary ammonium montmorillonite", *Chem. Mater.*, v.13, pp.2979-2990, (2001)

Xu, X., Ding, Y., Qian, Z., Wang, F., Wen, B., Zhou, H., Zhang, S. and Yang, M., "Degradation of poly(ethylene terephthalate)/clay nanocomposites during melt extrusion: Effect of clay catalysis and chain extension", *Polym. Degrad. Stab.*, v.94, pp.113-123, (2009).

Xue, Y., Hara, M., "Novel blends made of ionic naphthalene thermotropic polymer and poly(ethylene terephthalate)", *Polymer*, v.47, pp.6710-6717, (2006).

Yalcin, B., Valladares, D. and Cakmak, M., "Amplification effect of platelet type nanoparticles on the orientation behavior of injection molded nylon 6 composites", *Polymer*, v.44, pp.6913-6925, (2003).

Yao, X., Tian, X., Xie, D., Zhang, X., Zheng, K., Xu, J., Zhang, G. and Cui, P., "Interface structure of poly(ethylene terephthalate)/silica nanocomposites", *Polymer*, v.50, pp. 1251-1256, (2009).

Yoon, P., Hunter, D. and Paul, D., "Polycarbonate nanocomposites. Part 1. Effect of organoclay structure on morphology and properties", *Polymer*, v.44, pp.5323-5339, (2003).

Yoon, P., Hunter, D. and Paul, D., "Polycarbonate nanocomposites: Part 2. Degradation and color formation", *Polymer*, v.44, pp.5341-5354, (2003).

Yuan, X., Li, C., Guan, G., Xiao, Y. and Zhang, D., “Thermal degradation investigation of poly(ethylene terephthalate)/ fibrous silicate nanocomposites”, *Polym. Degrad. and Stab.*, v.93, pp.466-475, (2008).

Zaroulis, J. and Boyce, M., “Temperature, strain rate, and strain state dependence of the evolution in mechanical behaviour and structure of poly(ethylene terephthalate) with finite strain deformation”, *Polymer*, v.38, pp.1303-1315, (1997).


Zhao, J., Mayes, R., Chen, G., Chan, P. and Xiong, Z., “Polymer micromould design and micromoulding process”, *Plast. Rub. Compos.*, v.32, pp.240-247, (2003).

Zhong, G., Li, L., Mendes, E., Byelov, D., Fu, Q. and Li, Z., “Suppression of skin core structure in injection-molded polymer parts by in situ incorporation of a microfibrillar network”, *Macro.*, v.39, pp.6771-6775, (2006).

Zhou, C. and Clough, S., “Multiple melting endotherms of poly(ethylene terephthalate)”, *Polym. Eng. Sci.*, v.28, pp.65-68, (1988).

Appendix x3.1 Raw material data sheet

I PET pellets



POLYESTER POLYMER

T74F9 0.80 / Item code PF00040

CAS: N° 25038-59-9

CHARACTERISTICS:

- ⇒ Product description..... White granulates
- ⇒ Melt point..... Approx 252 °C
- ⇒ Bulk density..... Approx 0, 83 g/cm³
- ⇒ Density..... Approx 1, 40 g/cm³

SPECIFICATIONS		METHODS
⇒ INTRINSIC VISCOSITY (dl/g)	0.80 ± 0.02	05 - Poly. 3K - 310
⇒ COLOR	L*..... ≥ 81	05 - Poly. 3K - 250
⇒	a*..... -2 ≤ a ≤ 0	05 - Poly. 3K - 250
⇒	b*..... b < 1	05 - Poly. 3K - 250
⇒ ACETALDEHYDE (ppm)	≤ 1	05 - Poly. 3K - 230
⇒ Carboxylic End Groups (moeq/t)	≤ 60	05 - Poly. 3K - 140
⇒ Diethylene Glycol (%)	≤ 2	05 - Poly. 3K - 280
⇒ Weight of 100 chips	1, 4 g ± 0, 1	05 - Poly. 3K - 300

CONDITIONING AND TRANSPORT

STOCKHOLDING ⇒ Big Bags of 1100kg or road-tanker

USES ⇒ Keep stock protected from humidity

HYGIENE AND SAFETY ⇒ Bottles, films, yarns, fibres

TRANSPORT REGULATIONS ⇒ This product presents no particular toxic features

PRODUCTION SITE ⇒ Not applicable

PRODUCTION SITE ⇒ 02 430 GAUCHY / FRANCE

The information contained in this notice is based on the state of our knowledge of the product concerned at the issue date of the notice. The information is given in good faith and does not constitute a guarantee on our part. It is only offered as an indication, except for the actual specifications. It ought not, in any case, to be a substitute for evaluation trials which the user should out to verify, on each situation, its acceptability for the intended end use.

Our services are at your disposal to give you all additional information and offer you our documentation. We reserve the right to carry out technical modifications to the product.

II Cloisite 25A Data Sheet

SOUTHERN CLAY PRODUCTS / A SUBSIDIARY OF ROCKWOOD SPECIALTIES, INC.

PRODUCT BULLETIN/Cloisite®



Southern Clay Products, Inc.
1212 Church Street
Gonzales, TX 78629
Phone: 800-324-2891
Fax: 830-672-1903
www.scprod.com

Cloisite® 25A

Typical Physical Properties Bulletin

Description:

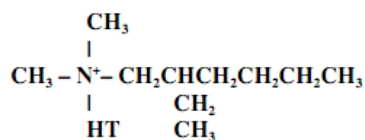
Cloisite® 25A is a natural montmorillonite modified with a quaternary ammonium salt.

Designed Used:

Cloisite® 25A is an additive for plastics to improve various plastic physical properties, such as reinforcement, HDT, CLTE and barrier.

Typical Properties:

<u>Treatment/Properties:</u>	Organic Modifier (1)	Modifier Concentration	% Moisture	% Weight Loss on Ignition
Cloisite® 25A	2MHTL8	95 meq/100g clay	< 2%	34%



Where HT is Hydrogenated Tallow (~65% C18; ~30% C16; ~5% C14)

Anion: methyl sulfate

(1) 2MHTL8: dimethyl, dehydrogenated tallow, 2-ethylhexyl quaternary ammonium

Typical Dry Particle Sizes: (microns, by volume)

10% less than:	50% less than:	90% less than:
2 μ m	6 μ m	13 μ m

Color: Off White

Density:

Loose Bulk, lbs/ft ³	Packed Bulk, lbs/ft ³	Density, g/cc
12.08	20.48	1.87

X Ray Results: $d_{001} = 18.6\text{\AA}$

For additional information or technical assistance contact Southern Clay Products, Inc.
toll free at 800-324-2891.

SYNTHETIC MICA

MICROMICA



SOMASIF

CO-OP CHEMICAL CO.,LTD.

Introduction

Synthetic Micas are tetrasilicic fluoromicas, which have excellent qualities. They are mainly formed by an intercalation reaction of alkali ion into the interlayer site of talc.

These products are divided into two categories according to their chemical and physical properties, that is, SOMASIF and MICROMICA.

SOMASIF is synthesized by heating

talc and Na_2SiF_6 for several hours in an electric furnace. It readily expands when water molecules or moisture is incorporated into the phyllosilicate at room temperature.

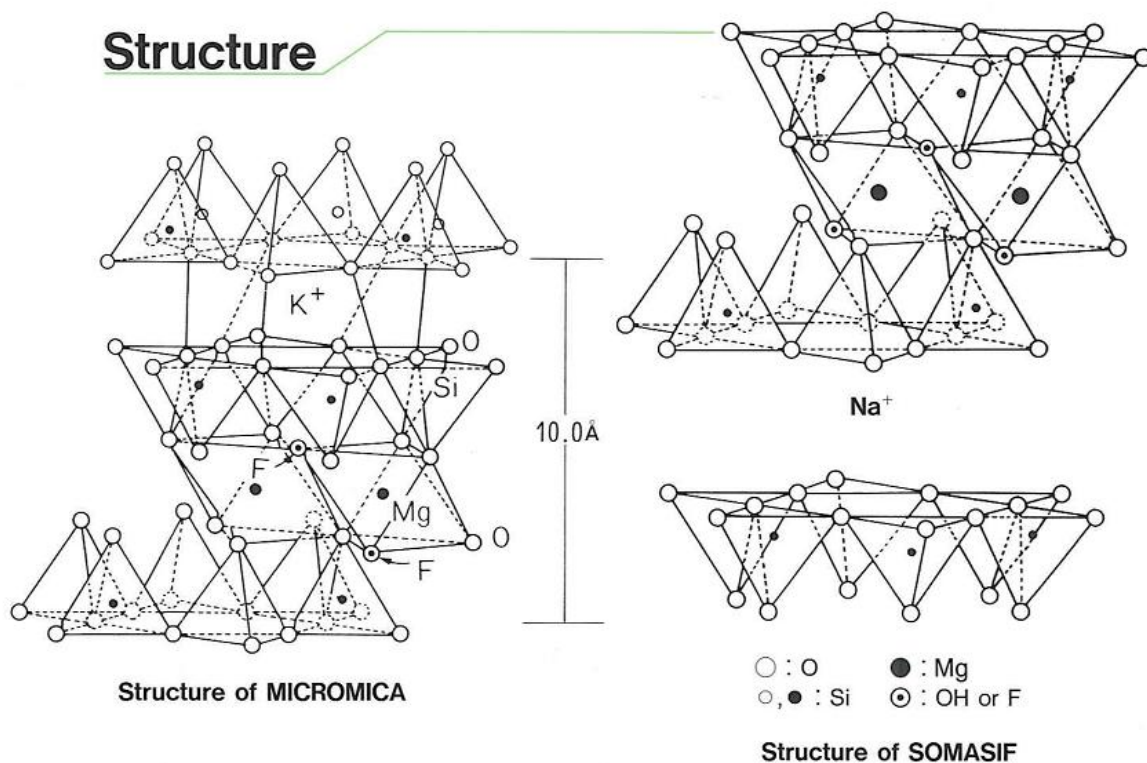
On the other hand, when K_2SiF_6 instead of Na_2SiF_6 is used as a starting material, a nonswellable fluorine mica (MICROMICA) is easily obtained.

Characteristics

1. Synthetic Mica contains a very small amount of impurities, the result of omitting process of crushing this product.
2. The particles size of talc and alkali silicofluoride can be selected in order to reflect a desirable size of the Mica, generally with an average size being about $2\mu\text{m}$ or less.
3. A prominent weight loss of Mica on heating can not be observed until $800\sim 900^\circ\text{C}$, indicating a high thermal resistance.
4. Synthetic Mica is colorless and transparent, with brightness comparable to that of the naturally occurring one. Therefore it can be utilized widely as fillers, pigments and other various uses.
5. SOMASIF can be swelled in water, resulting in the formation of transparent and thixotropic gels.
6. The aspect ratio of MICROMICA is $20\sim 40$ and furthermore the quality can be increased by lamination and refinement.
7. Several compounds can be intercalated in the cation-exchangeable site of SOMASIF, to form organic and inorganic interlayer complexes.

We welcome inquiries of special type micas even of different compositions, particle sizes or applications mentioned in this catalogue.

Structure



Characteristics

Trade name	MICROMICA			SOMASIF
Trade No.	MK100	MK200	MK300	ME100
Average particle size [D50, μ]	3~5	5~8	10~20	5~7
Brightness [%]	95>	95>	95>	90>
Density [-]	2.7	2.7	2.7	2.6
Specific gravity [g/cm ³]	0.1	0.1	0.3	0.2
Aspect ratio [-]	20~30	20~30	20~30	-
Thermal resistance [°C]	900	900	900	800
Specific surface area [m ² /g]	3	2	1	9
pH [-]	7~8	7~8	7~8	9~10
CEC [mep/100g]	-	-	-	120
Apparent viscosity [mPa·s]				
6rpm	-	-	-	4,000~8,000
60rpm	-	-	-	800~1,600
Thixotropy [-]	-	-	-	≒5

- pH, Viscosity measured at 7% dispersion
- Viscosity measured at Brookfield viscometer

Dispersion property of SOMASIF

ME-100 : Hydrophilic swellable mica

MAE, MTE, MEE, MPE : Organophilic swellable mica

Group	Solvent	SOMASIF									
		ME-100		MAE		MTE		MEE		MPE	
stationary time (after dispersion)		1h	12h	1h	12h	1h	12h	1h	12h	1h	12h
Water		○	○	-	-	-	-	-	-	-	-
Aromatic hydrocarbon	Benzene			○	○	△	△	○	△	○	△
	Toluene			△	△	△	△	○	△	○	△
	Xylene			○	△	△	△	○	○	○	△
Ether	Ethyl ether			△	△	△	×	△	△	△	△
	Tetrahydrofuran			△	△	△	△	○	△	○	○
Ketone	Acetone			△	△	△	×	△	△	○	△
Aliphatic hydrocarbon	n-Pentane			△	△	×	×	×	×	×	×
Alcohol	Methanol			△	△	△	×	△	×	○	△
	Ethanol			△	×	×	×	△	×	○	△
	Propanol			△	△	×	×	△	×	○	△
	Isopropanol			△	△	×	×	△	×	○	△
Halogenated hydrocarbon	Chloroform			○	○	○	○	○	○	○	○
	Methylene chloride			○	○	○	△	○	○	○	△
Others	Ethyl acetate			△	△	△	△	△	△	○	△
	Methyl methacrylate			△	△	△	△	△	△	○	△
	Diocetyl phthalate			×	×	○	△	○	○	○	○
	Dimethyl formamide			×	×	○	△	○	○	○	△
	Methyl cellosolve			△	△	△	△	○	△	○	△

Concentration of dispersion : 10wt%

Dispersion test

- : Well dispersion
 - △ : Dispersion, but partially precipitated
 - ×
- × : Form to precipitate

Composition

(wt%)

Trade name	MICROMICA			SOMASIF
Trade No.	MK100series	MK200series	MK300series	ME100series
Si	26.7	25.7	27.9	26.5
Mg	16.5	16.2	15.4	15.6
Al	0.1	0.1	0.2	0.2
Na	-	-	-	4.1
K	6.2	6.3	6.1	-
Fe	0.1	0.1	0.0	0.1
F	8.6	8.4	8.1	8.8

Characteristics and applications of synthetic micas

	MICROMICA(MK)						SOMASIF(ME)						
	Brightness	Processing	Heat resistance	Vibration repressor	Electric insulation	Reinforcement	Heat resistance	Film forming	Viscosity	Adsorbability	Dispersion	Thixotropy	Intercalation
Paint	○	○	○	○	○	○	○	⊙	○	○	○	○	⊙
Cosmetics	⊙						○	○	○	⊙	○	○	
Catalysis						○			○				⊙
Electronics		○	○	⊙		○	○	○		○	○		
Mica sheet	○	⊙		⊙	○	○	⊙	○			○		⊙
Film		○	⊙	⊙	○	○	○		○	○	○		
Paper	○	○		○		⊙	○		⊙	○	○		⊙
Plastics	○	⊙	○	⊙	⊙	○		○	○		○		⊙
Gum		○		○	⊙	○			○				○
Construction		○	⊙	○	○	○	○						⊙

Appendix x3.2**Density results**

vPET (Tergal F9)	Density (g/cc)
1	1.39959
2	1.3996
3	1.3995
4	1.3993
5	1.3992
Average	1.4

Figure x3.2.1 Density of vPET

Somasif MAE	Density (g/cc)
1	1.5482
2	1.5468
3	1.5478
4	1.5485
5	1.5464
Average	1.55

Figure x3.2.2 Density of Somasif MAE

Somasif MTE	Density (g/cc)
1	1.7257
2	1.7278
3	1.7253
4	1.7251
5	1.7256
Average	1.73

Figure x3.2.3 Density of Somasif MTE

Cloisite 25A	Density (g/cc)
1	1.764
2	1.7643
3	1.7641
4	1.7641
5	1.7635
Average	1.76

Figure x3.2.4 Density of Cloisite 25A

x3.3 XRD results for all nanoclays used in this project.

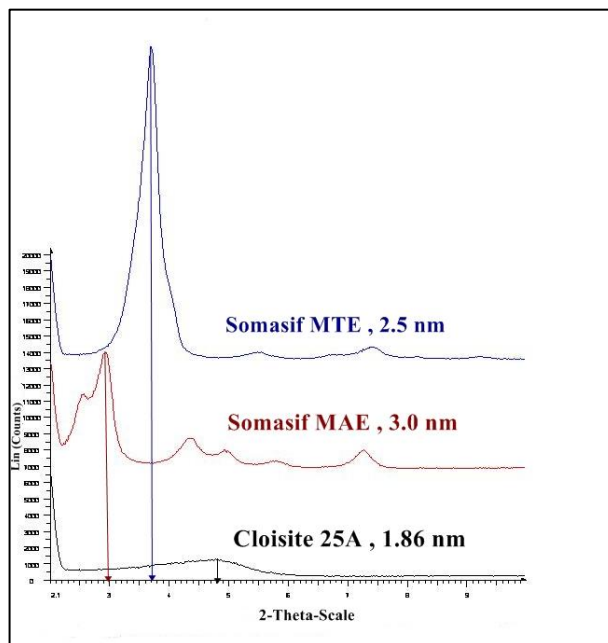


Figure x3.3.1 XRD results for the nanoclays

Appendix chapter four (x4)

x4.1 Cox-Merz rule

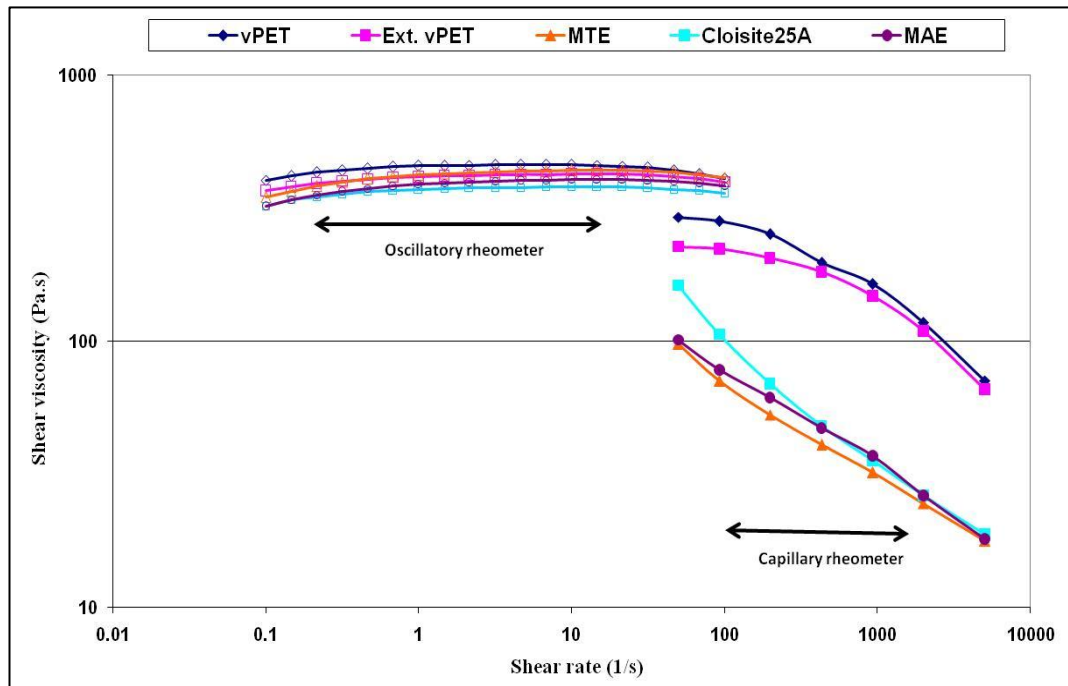


Figure x4.1 Plots of shear rate vs. shear viscosity for PET nanocomposites at 1 wt.% nano-filler concentrations.

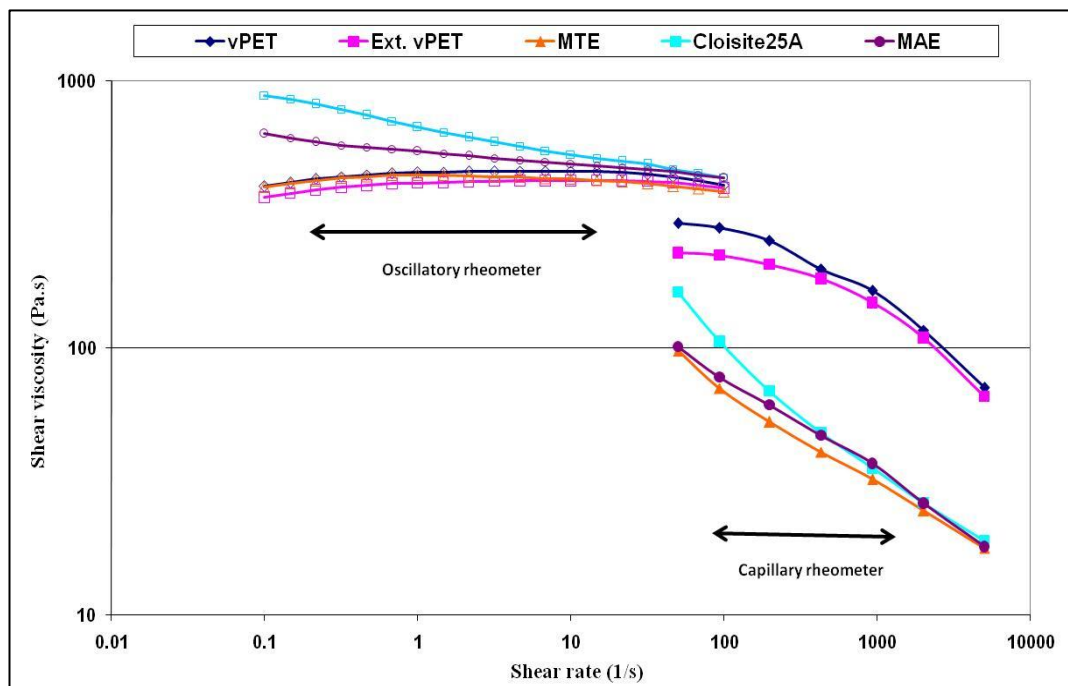


Figure x4.2 Plots of shear rate vs. shear viscosity for PET nanocomposites at 3 wt.% nano-filler concentrations.

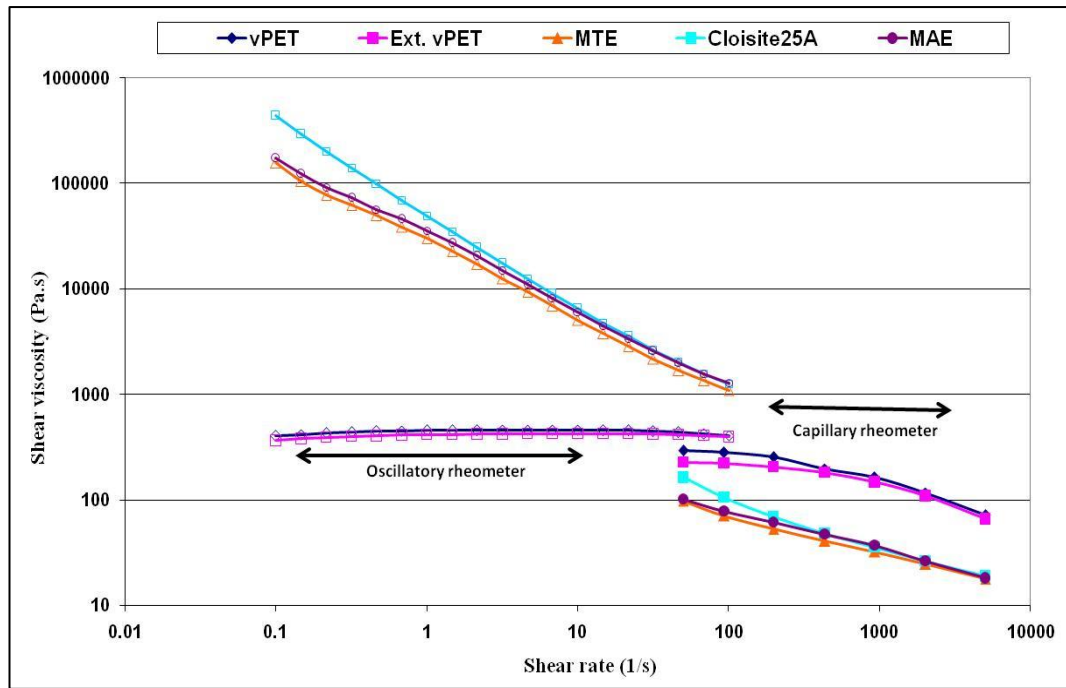


Figure x4.3 Plots of shear rate vs. shear viscosity for PET nanocomposites at 20 wt.% nano-filler concentrations.

x4.2 Loss modulus vs. shear rate for different PETNCs at various concentrations

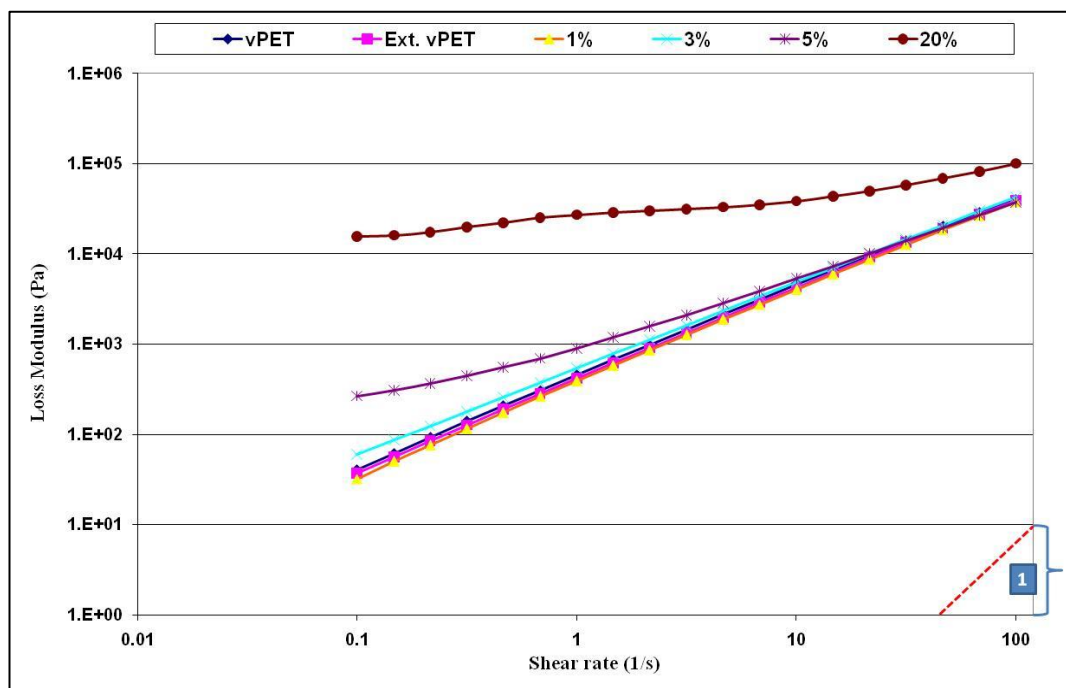


Figure x4.4 Loss modulus behaviour for PET/MAE NC at different clay concentrations with low shear rate.

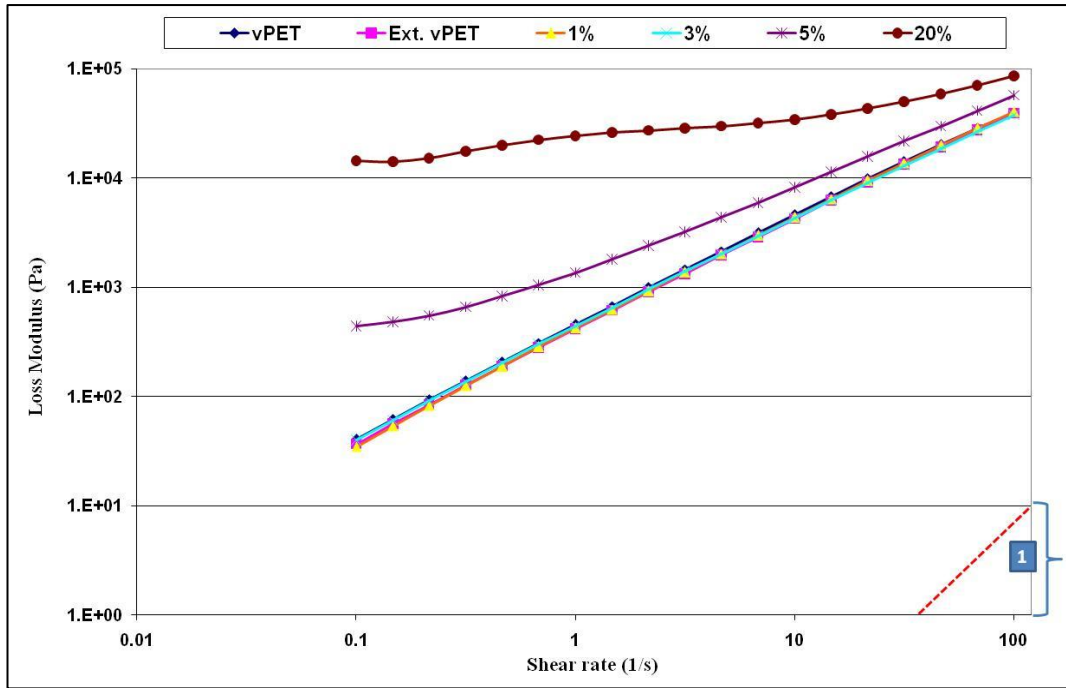


Figure x4.5 Loss modulus behaviour for PET/MTE NC at different clay concentrations with low shear rate.

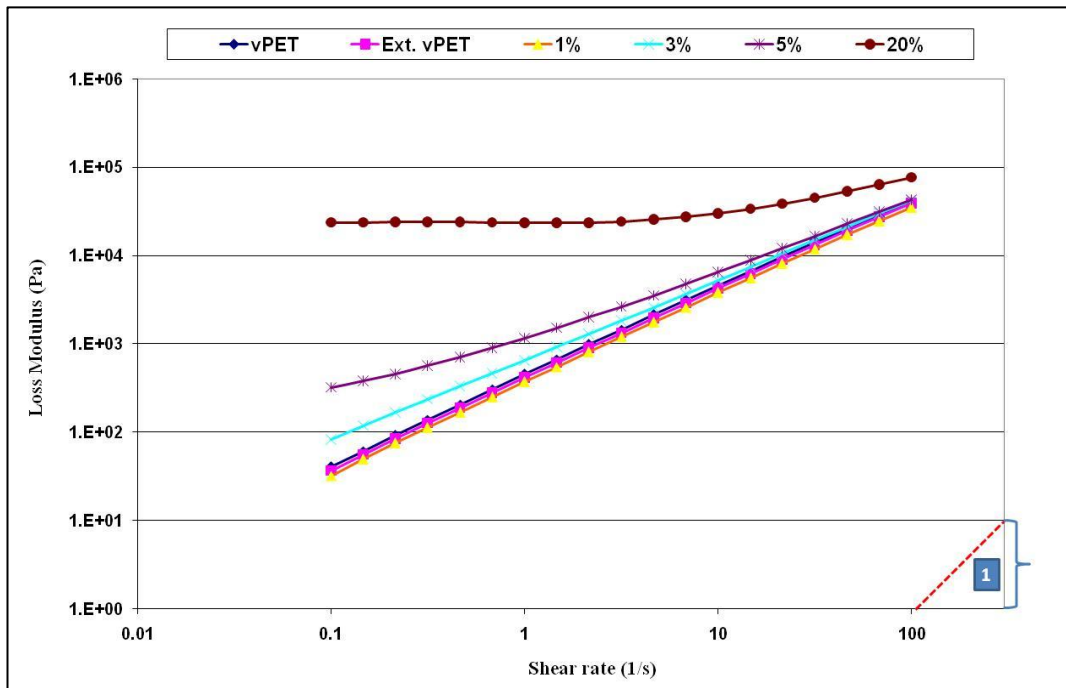


Figure x4.6 Loss modulus behaviour for PET/Cloisite 25A NC at different clay concentrations with low shear rate.

x4.3 Storage modulus as a function of shear rate for different nano-fillers at certain loading %.

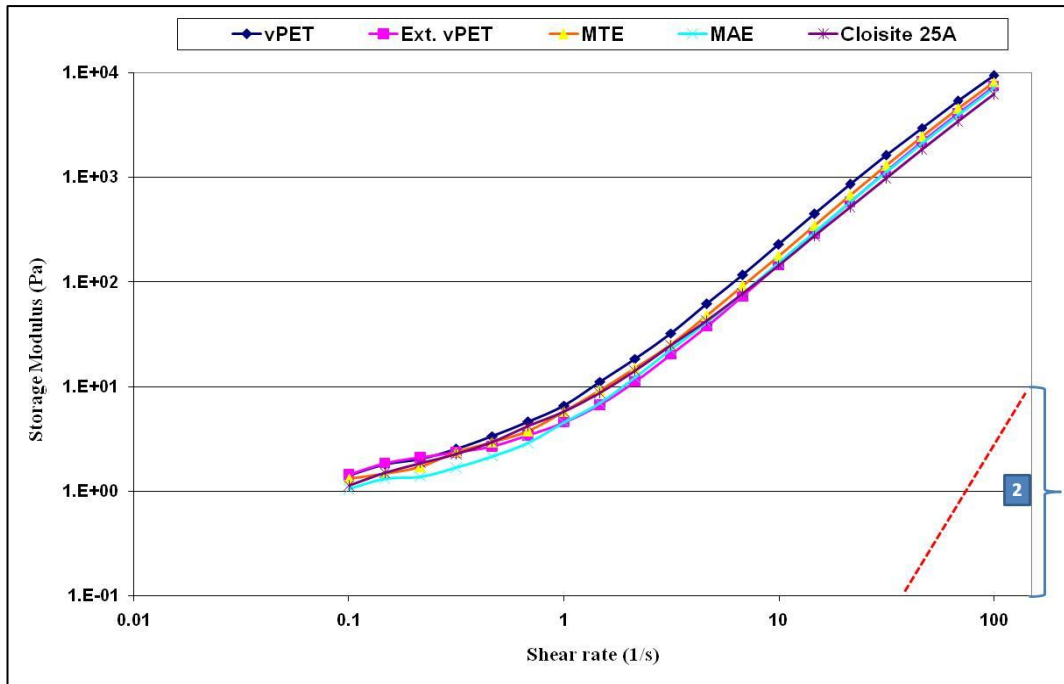


Figure x4.7 Storage modulus behaviour for PETNCs at 1wt.% loading with low shear rate.

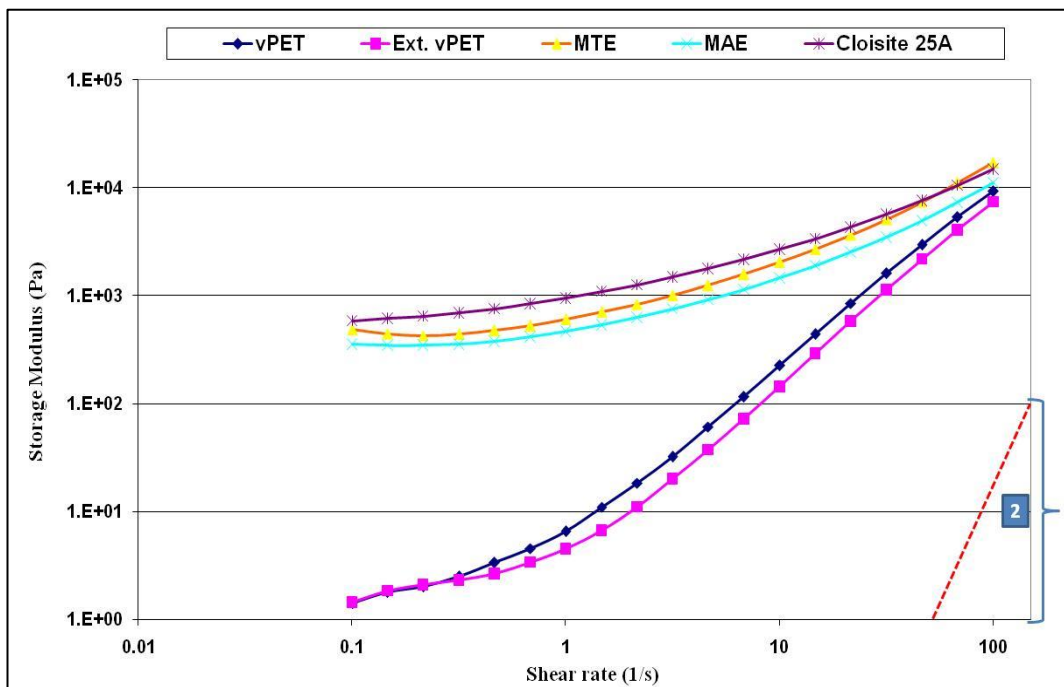


Figure x4.8 Storage modulus behaviour for PETNCs at 5wt.% loading with low shear rate.

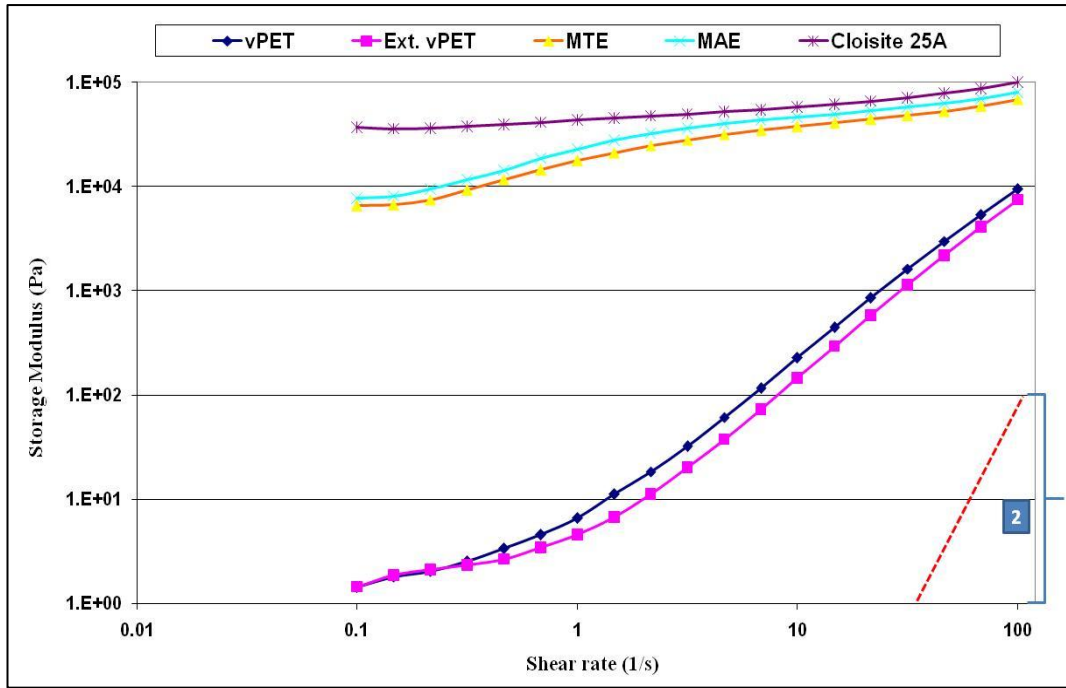


Figure x4.9 Storage modulus behaviour for PETNCs at 20wt.% loading with low shear rate.

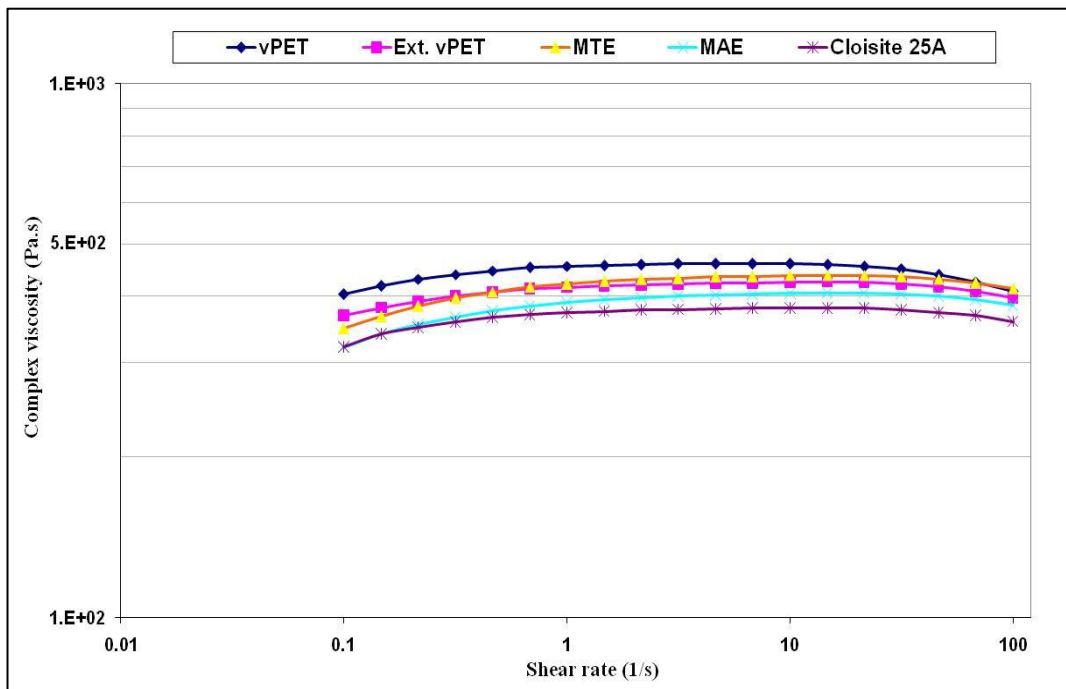


Figure x4.10 Complex viscosity variation of PET nanocomposites at the same concentration (1 wt.%) with low shear rate.

x4.5 Shear rate (s^{-1}) vs. complex viscosity (Pa.s) for different types of PET nanocomposites with the same nano-filler content

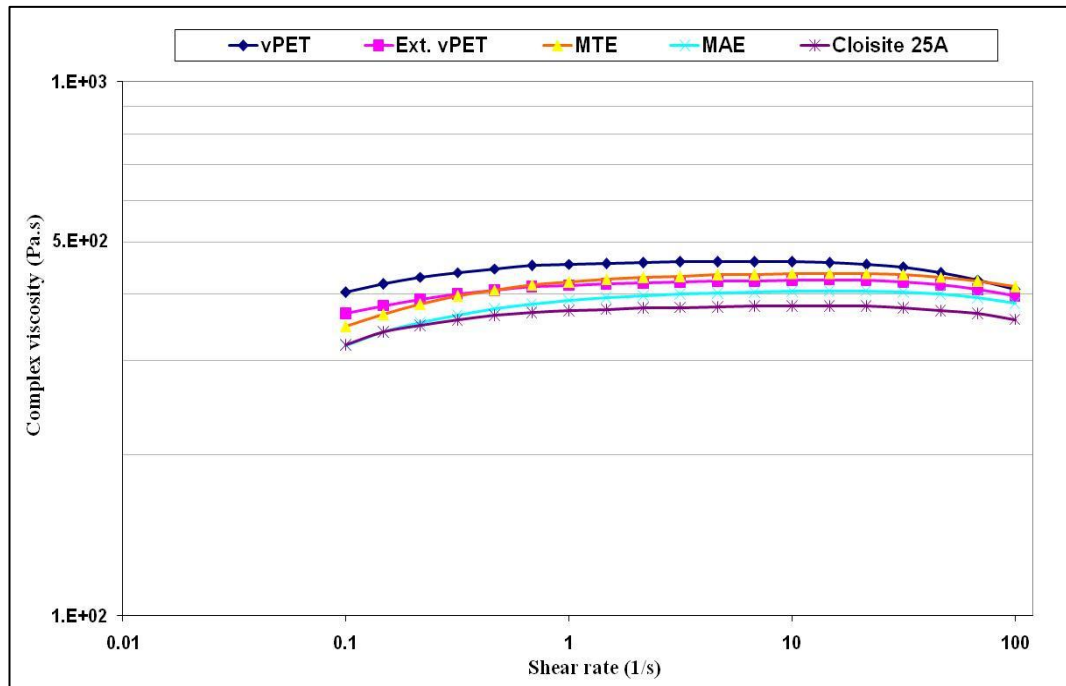


Figure x4. 2 Complex viscosity variation of PET nanocomposites at the same concentration (1 wt.%) with low shear rate

Appendix chapter 5 (x5)

x5-1 Additional results for sections 5.4.2, 5.4.3 and 5.4.4

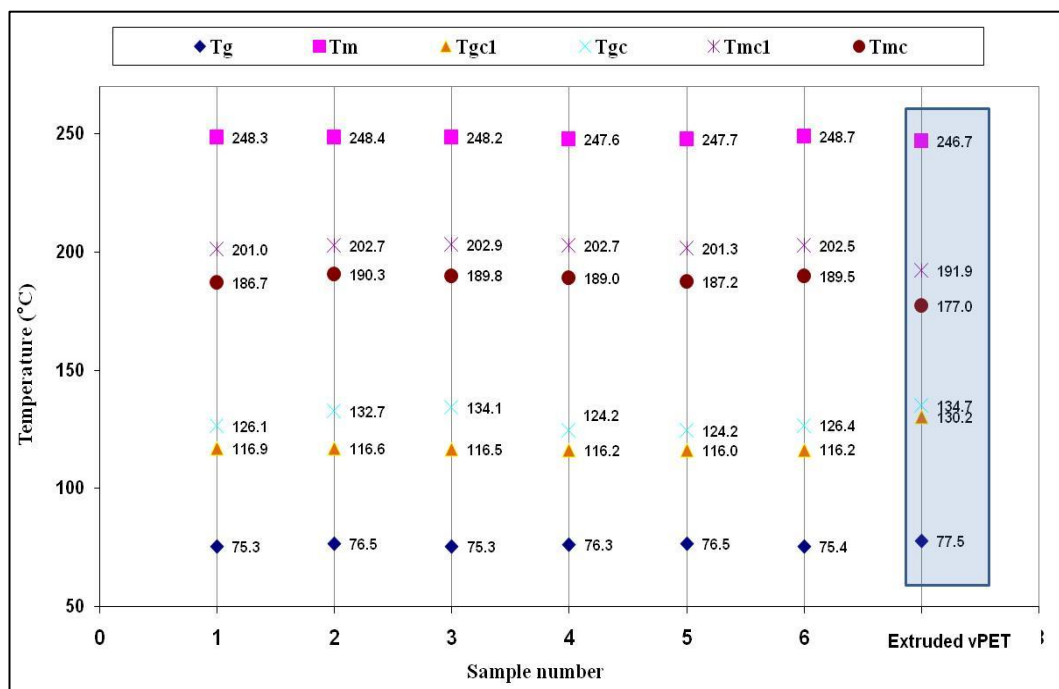


Figure x5.1 DSC results for 6 samples from same run to produce PET/MAE 3 wt.%.

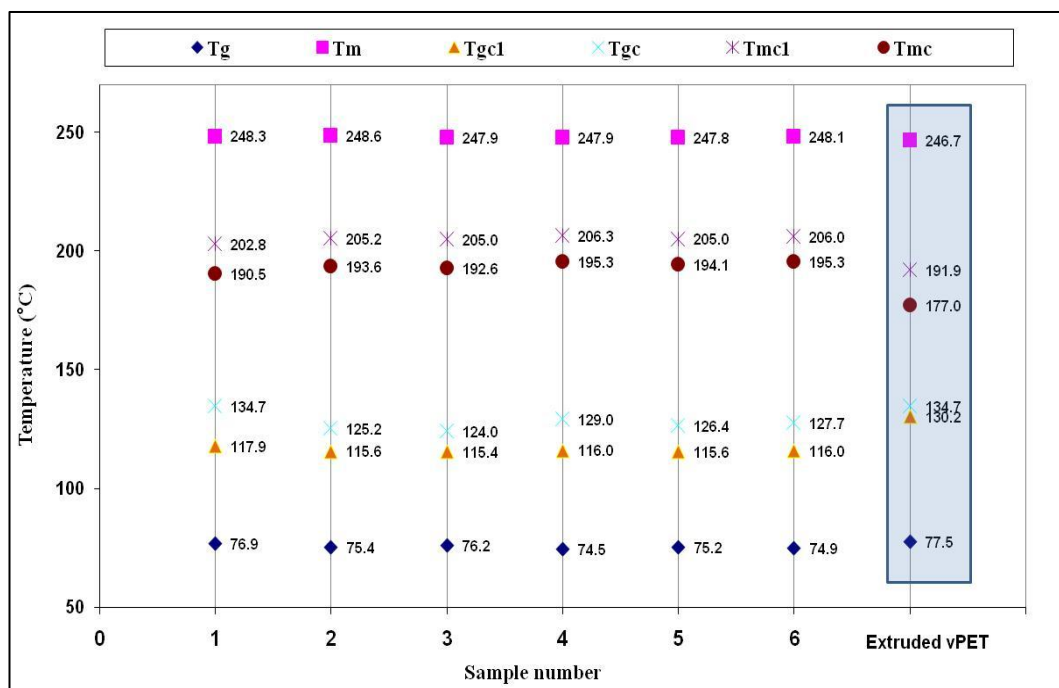


Figure x5.2 DSC results for 6 samples from same run to produce PET/MAE 5 wt.%.

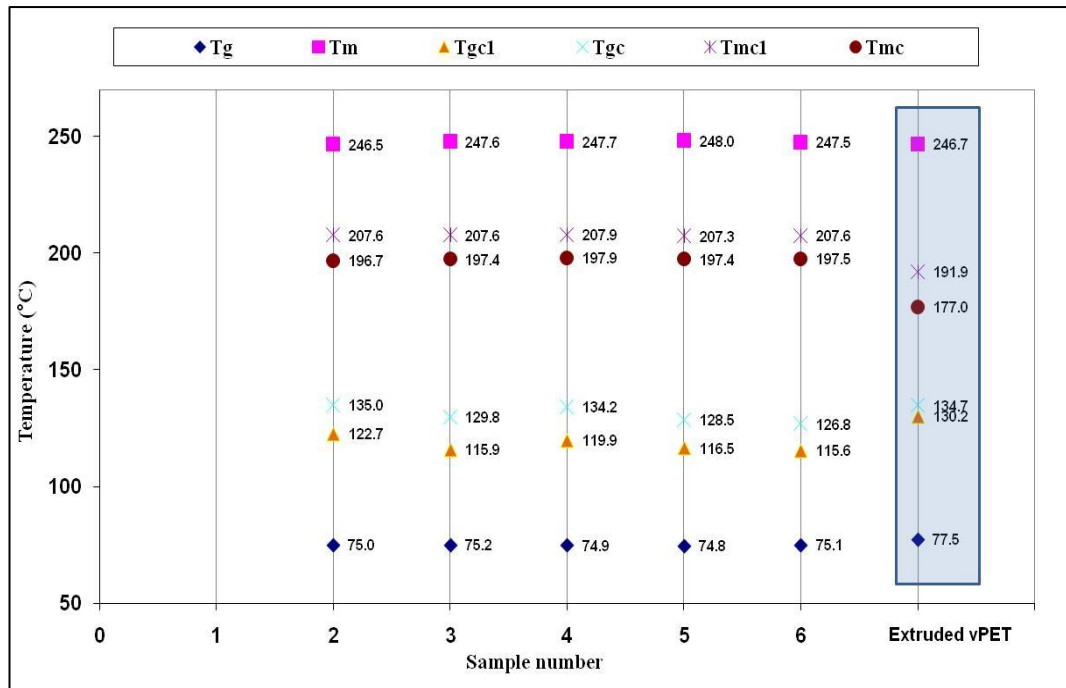


Figure x5.3 DSC results for 6 samples from same run to produce PET/MAE 20 wt.%.

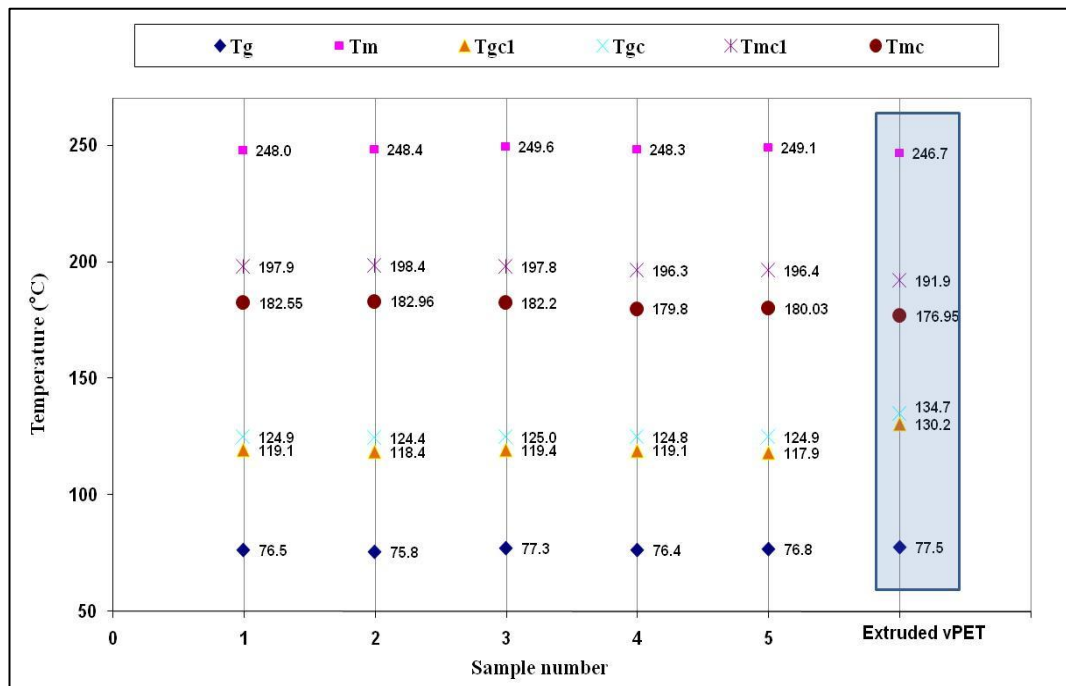


Figure x5.4 DSC results for 6 samples from same run to produce PET/MTE 1 wt.%.

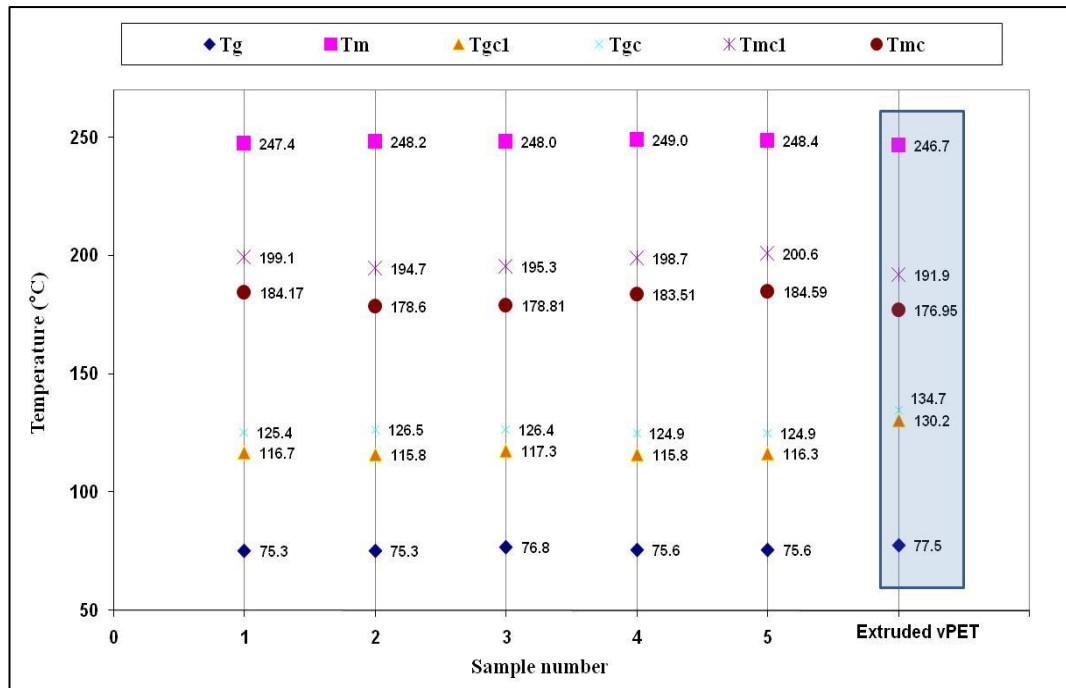


Figure x5.5 DSC results for 6 samples from same run to produce PET/MTE 3 wt.%.

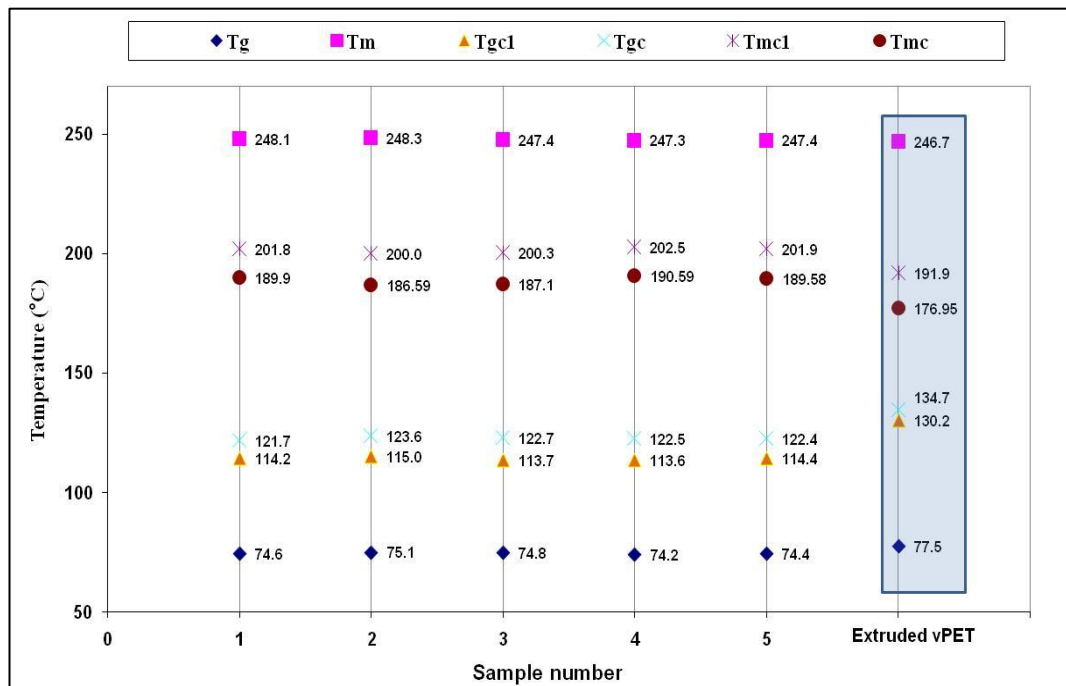


Figure x5.6 DSC results for 6 samples from same run to produce PET/MTE 5 wt.%.

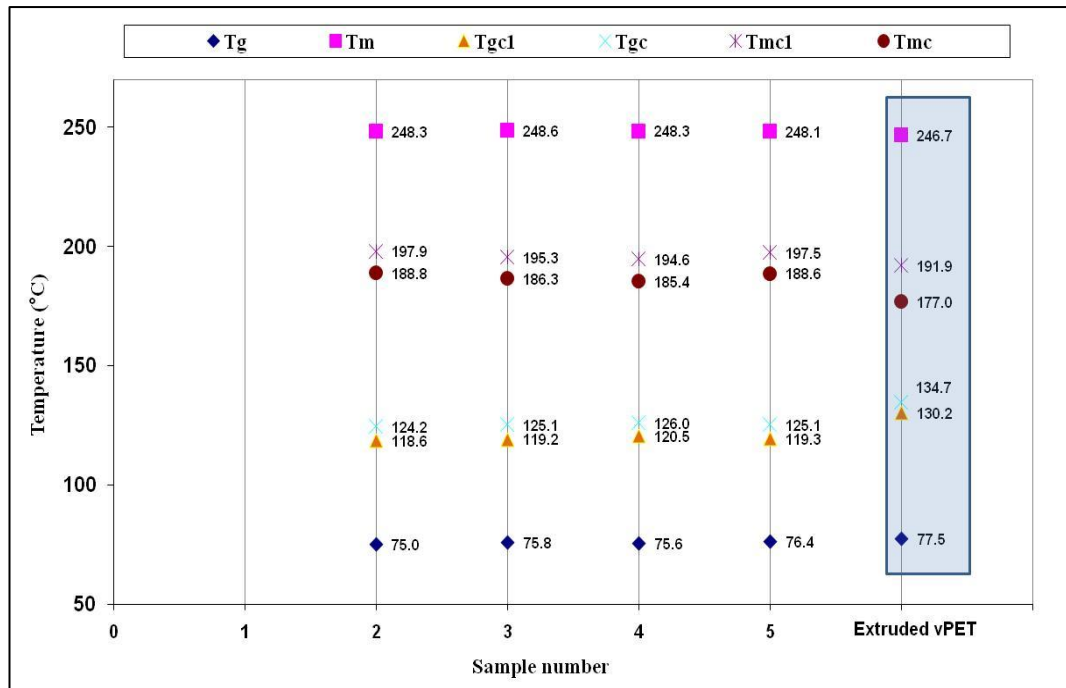


Figure x5.7 DSC results for 4 samples from same run to produce PET/Cloisite 25A 1 wt.%.

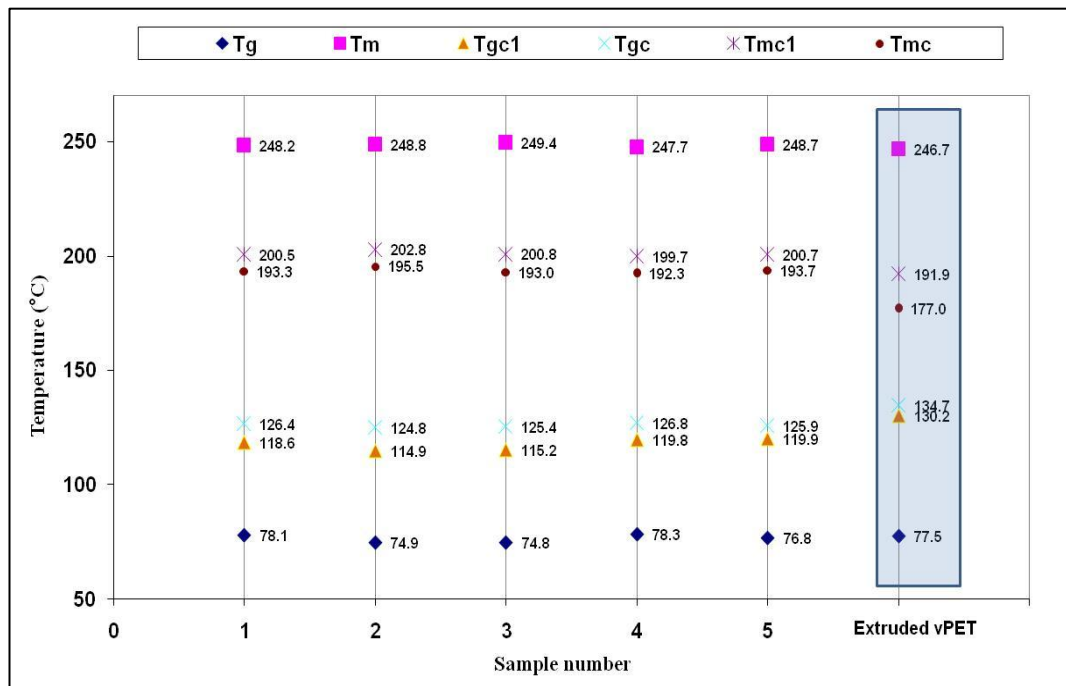


Figure x5.8 DSC results for 5 samples from same run to produce PET/Cloisite 25A 5 wt.%.

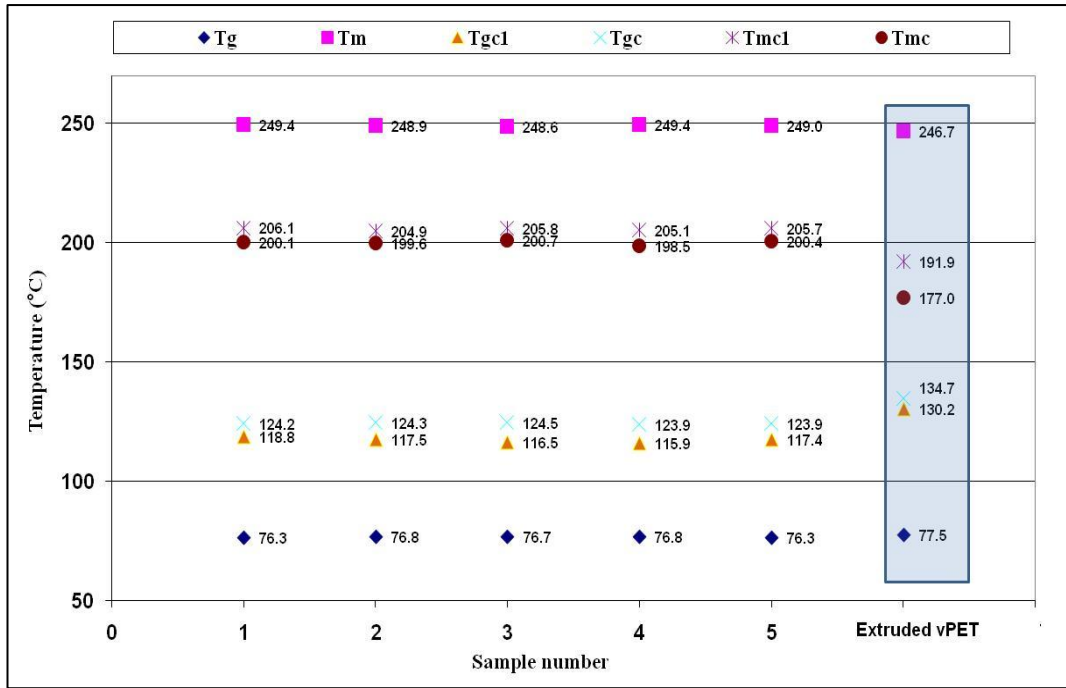


Figure x5.9 DSC results for 4 samples from same run to produce PET/Cloisite 25A 20 wt.%.

x5-2 Additional results for section 5.4.6

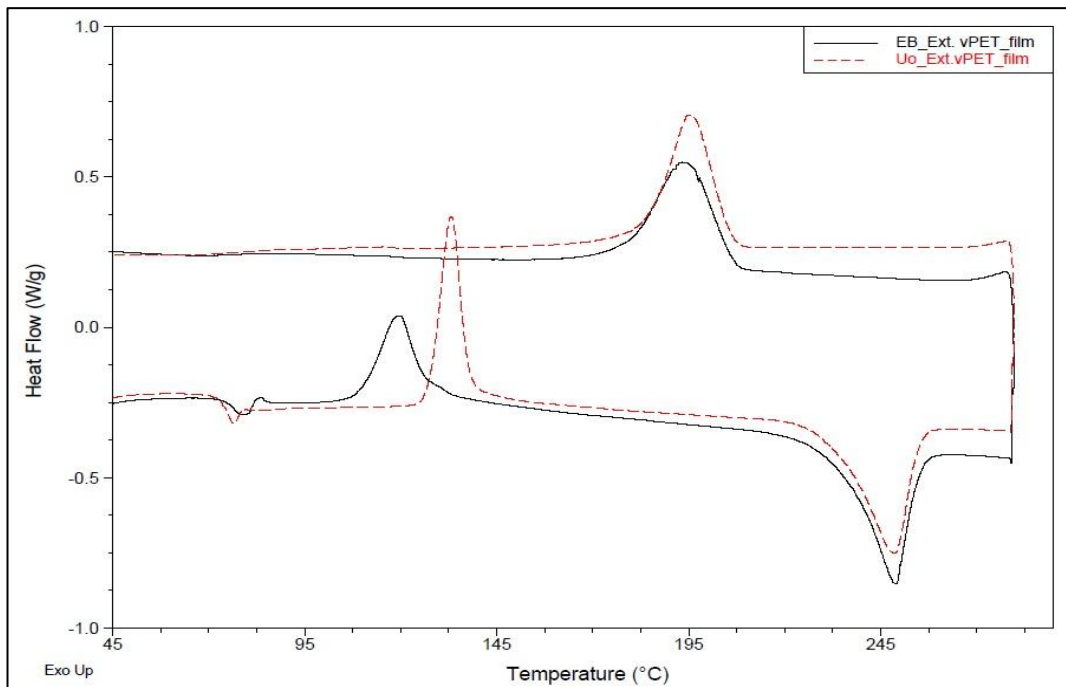


Figure x5.10 DSC curve for ext. vPET film (un-oriented and equal-biaxial stretch).

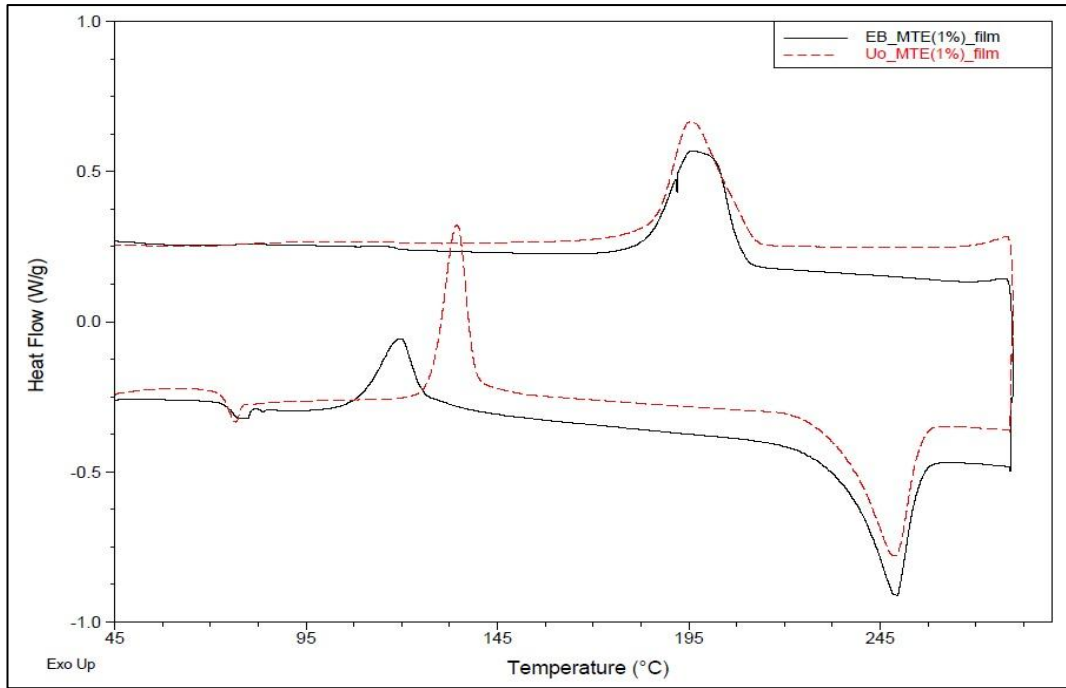


Figure x5.11 DSC curve for ext. PET/MTE 1 wt.% film (un-oriented and equal-biaxial stretch).

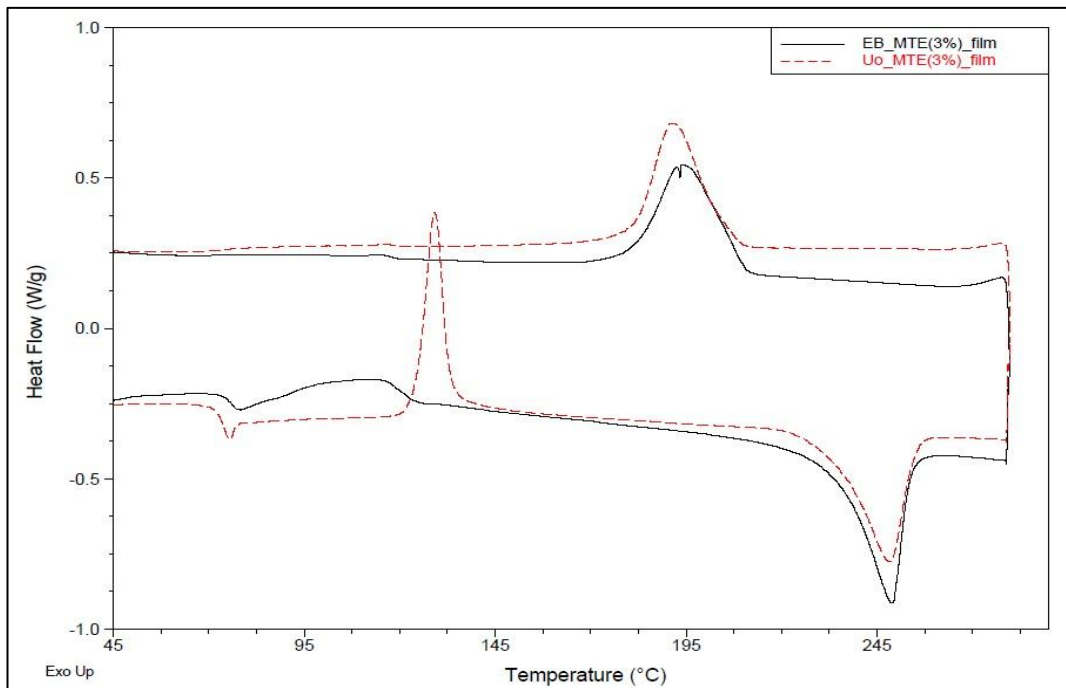


Figure x5.12 DSC curve for ext. PET/MTE 3 wt.% film (unoriented and equal-biaxial stretch).

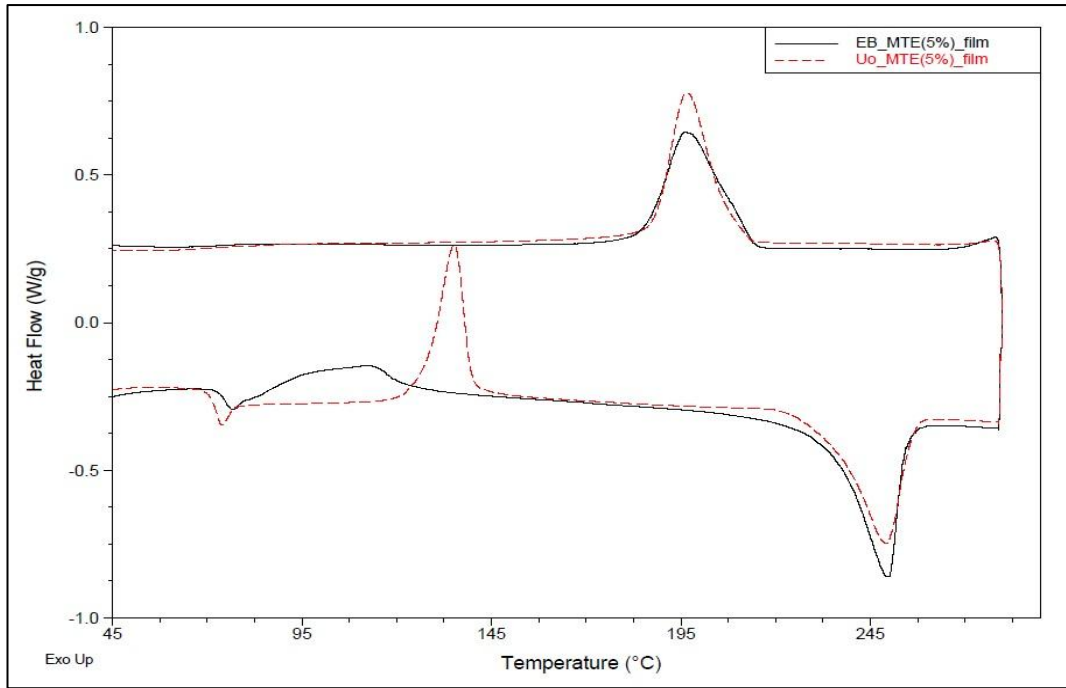


Figure x5.13 DSC curve for ext. PET/MTE 5 wt.% film (un-oriented and equal-biaxial stretch).

x5-3 Additional results for section 5.4.5

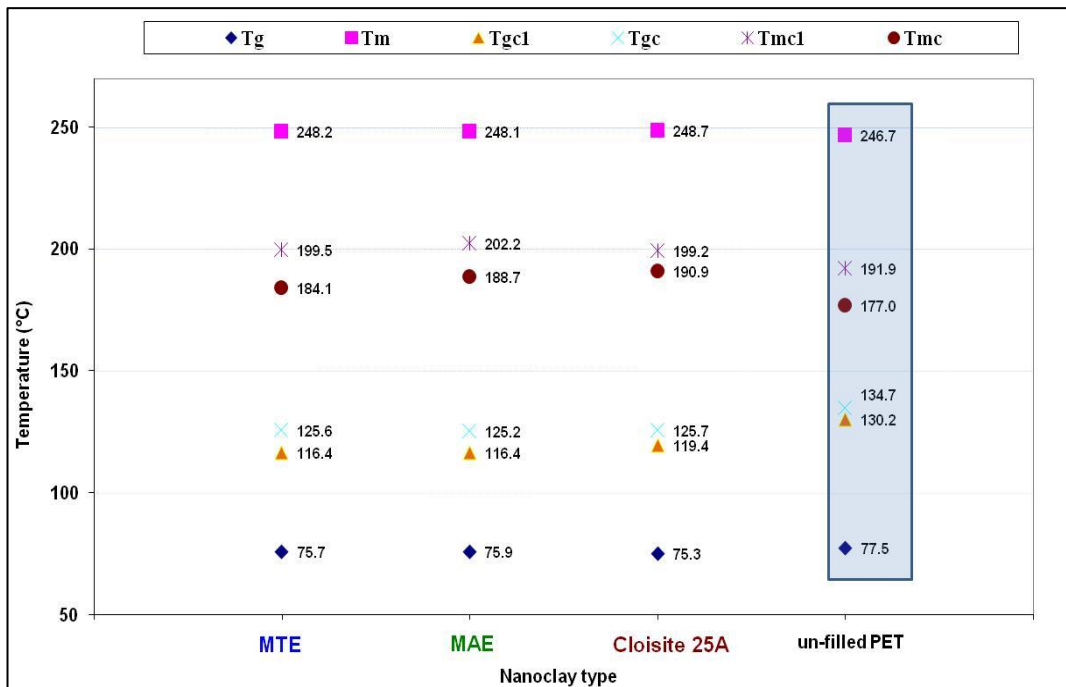


Figure x5.14 DSC results for PET nanocomposites at 3 wt.% for all nanoclay types.

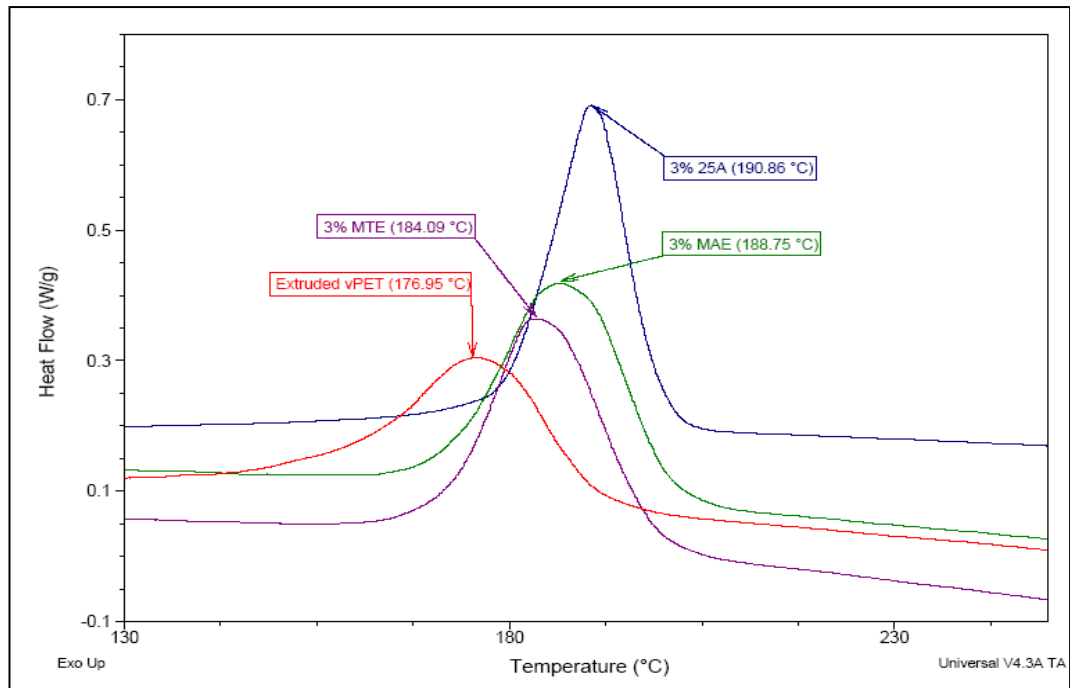


Figure x5.15 Tmc curves obtained from the DSC for all clays at 3 wt.%.

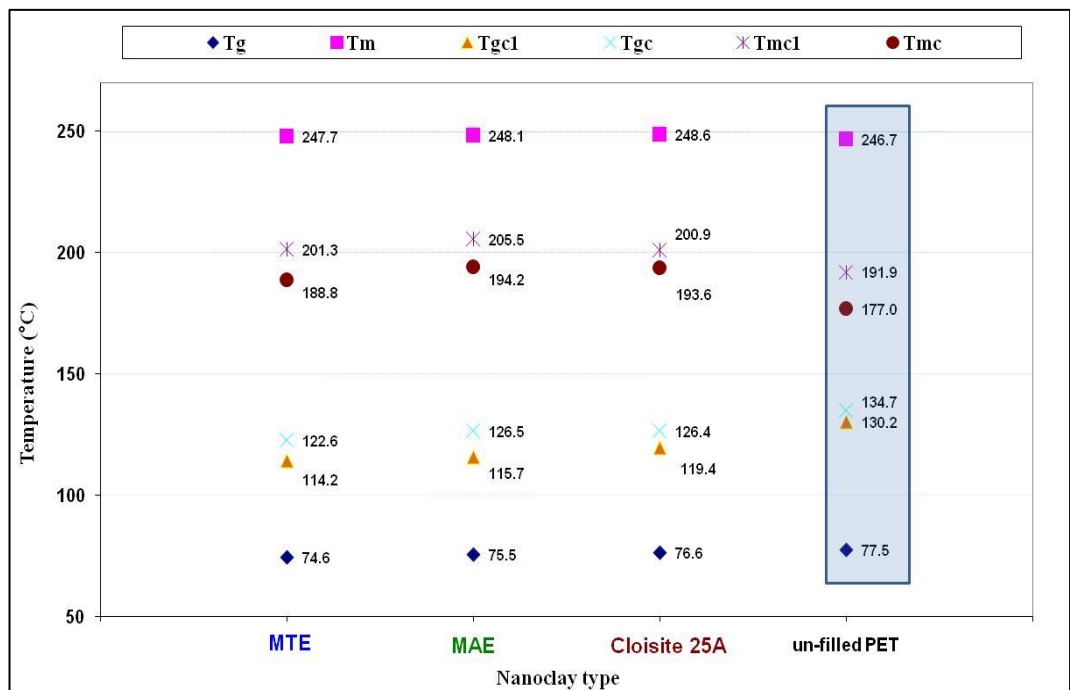


Figure x5.16 DSC results of PET nanocomposites at 5 wt.% for all nanoclay types.

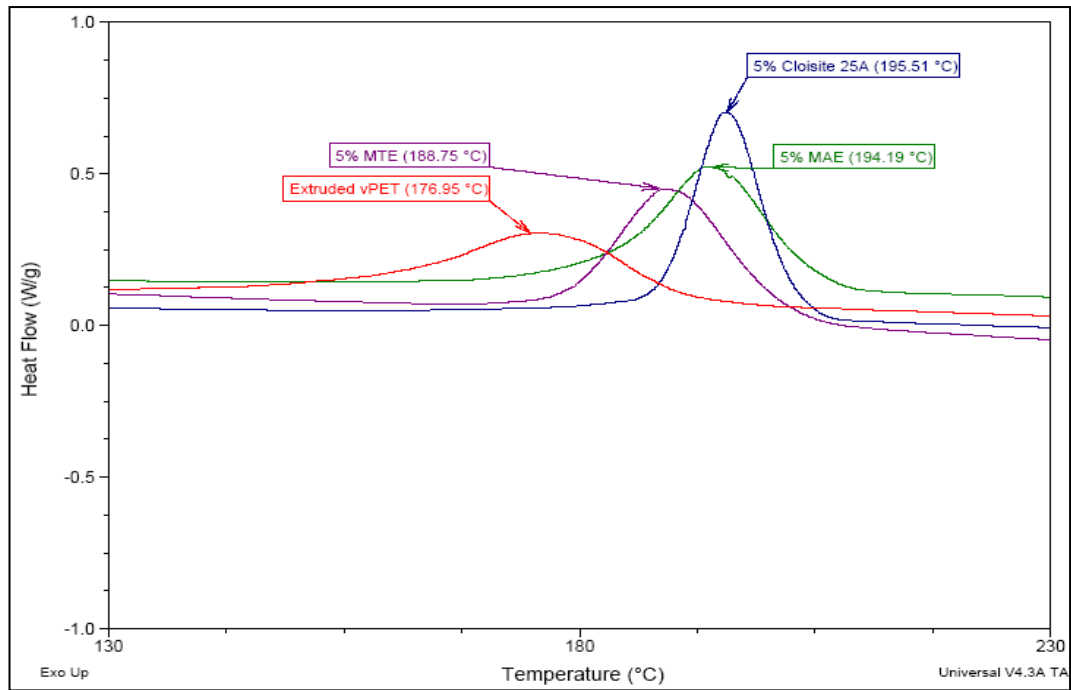


Figure x5.17 Tmc curves obtained from the DSC for all clays at 5 wt.%.

x5.4 Preliminary study

x5.4.1 Introduction

A preliminary study was conducted on some PET nanocomposite sheets obtained from Queens University, Belfast. These sheets were prepared under the EPSRC QBOX project by blending PET pellets (Tergal F9) with nanoclays (Somasif MAE and MTE).

This study was initiated to study the effect of different cooling rates (when analysing the thermal properties of the samples using Differential Scanning Calorimetry, DSC) on the crystallisation properties, and also to compare thermal properties such as glass transition temperature (T_g), melting temperature (T_m), and crystallization temperature from solid (T_{gc}) and from melting (T_{mc}), obtained from PET nanocomposite sheets (QBOX project) with PET nanocomposites prepared in IRC (Bradford).

x5.4.2 PET nanocomposite sheets

The preliminary study was based on analysing PET sheets (seven samples) received from Queens University, Belfast. The virgin PET pellets were blended with two varieties of organoclay and at different concentrations as shown in Table x5.4-1.

Sample No.	Type of sheet
1	Virgin PET
2	PET + 1% MAE
3	PET + 2% MAE
4	PET + 5% MAE
5	PET + 1% MTE
6	PET + 2% MTE
7	PET + 5% MTE

Table x5.4-1 Sheet types.

x5.4.3 Differential scanning calorimetry (DSC) results and discussion

In this section, all DSC results (T_g , T_{gc} , T_{mc} and T_m) are plotted in order to show the effect of nanoclay type (MAE and MTE) and concentration (1, 2 and 5 wt.%) on thermal properties, and also to study the effect of cooling rate on T_{mc} .

The DSC experiment scenario was as follows:

- Heat the sample from 30 to 300°C with heat rate 10°C/min to obtain glass transition temperature (T_g), crystallisation temperature from solid (T_{gc}) and melting temperature T_m ;
- Cool from 300 to 30°C with cooling rates 5, 20 and 35°C/min to obtain crystallisation temperatures from melt (T_{mc}).

21 samples were analysed and the results are summarized in Table x5.4-2 below:

Run No.	Sample PET+	Cooling rate °C/min	Tg °C	Tgc °C	Tmc °C	Tm °C
1	Unfilled	5	73.53	128.92	197.9	250.74
2	1%MAE	5	72.36	127.61	202.16	250.46
3	2%MAE	5	72.61	126.67	203.30	251.49
4	5%MAE	5	72.48	125.15	208.60	251.17
5	1%MTE	5	72.63	127.17	203.63	250.68
6	2%MTE	5	72.84	124.40	204.22	250.19
7	5%MTE	5	71.96	125.66	206.04	250.6
8	Virgin	20	73.81	128.75	178.08	249.75
9	1%MAE	20	73.31	128.00	182.92	250.06
10	2%MAE	20	73.23	126.25	184.55	250.22
11	5%MAE	20	72.47	125.60	187.54	250.27
12	1%MTE	20	73.33	127.76	181.94	250.48
13	2%MTE	20	73.73	126.77	185.08	250.67
14	5%MTE	20	72.31	125.39	184.12	250.13
15	Virgin	35	72.94	129.62	166.56	250.58
16	1%MAE	35	72.77	127.88	175.76	250.07
17	2%MAE	35	73.13	126.84	174.84	250.66
18	5%MAE	35	71.78	123.58	178.34	250.69
19	1%MTE	35	73.01	127.63	175.10	250.6
20	2%MTE	35	72.98	127.00	176.83	250.17
21	5%MTE	35	71.95	124.57	170.78	251.27

Table x5.4-2 Thermal temperature results for all sheet types

Table x5.4-2 shows some of the results obtained from the DSC curves which illustrate the glass transition temperature (Tg), melting temperature Tm, crystallisation temperature from solid (Tgc) and crystallisation temperature from melt state (Tmc) for PET/(MAE and MTE) nanocomposite sheets.

Sample No.	Type of sheet	T _g (°C) (average over 3 heating runs)
1	Virgin PET	73.43
2	PET + 1% MAE	72.81
3	PET + 2% MAE	73.00
4	PET + 5% MAE	72.30
5	PET + 1% MTE	73.00
6	PET + 2% MTE	73.18
7	PET + 5% MTE	72.07

Table x5.4-3 T_g (average results) for vPET and PET NC sheets.

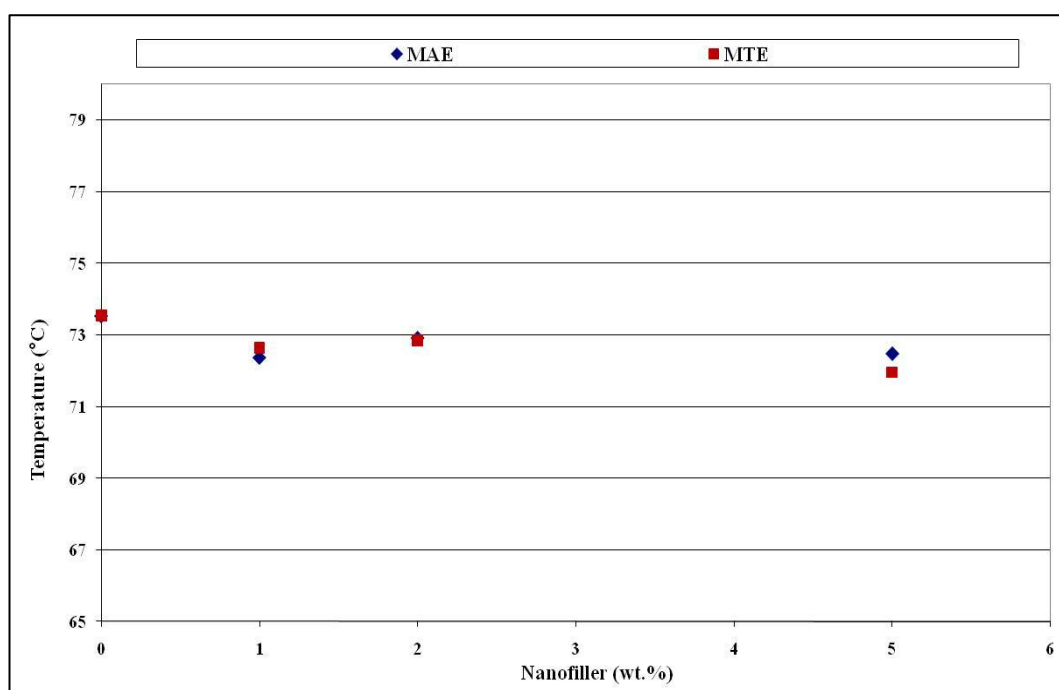


Figure x5.4.1 Effect of nanofillers (MAE and MTE) at different content levels (1, 2 and 5 wt.%) on T_g.

Glass transition temperatures (T_g) for vPET sheets and PET NC sheets are summarized in Table x5.4.3 and Figure x5.4.1. It is apparent that the differences between the results are small.

Sample No.	Type of sheet	T _m (°C)
		(average over 3 heating runs)
1	Virgin PET	250.36
2	PET + 1% MAE	250.2
3	PET + 2% MAE	250.79
4	PET + 5% MAE	250.71
5	PET + 1% MTE	250.62
6	PET + 2% MTE	250.34
7	PET + 5% MTE	250.67

Table x5.4.4 T_m (average results) for vPET and PET NC sheets.

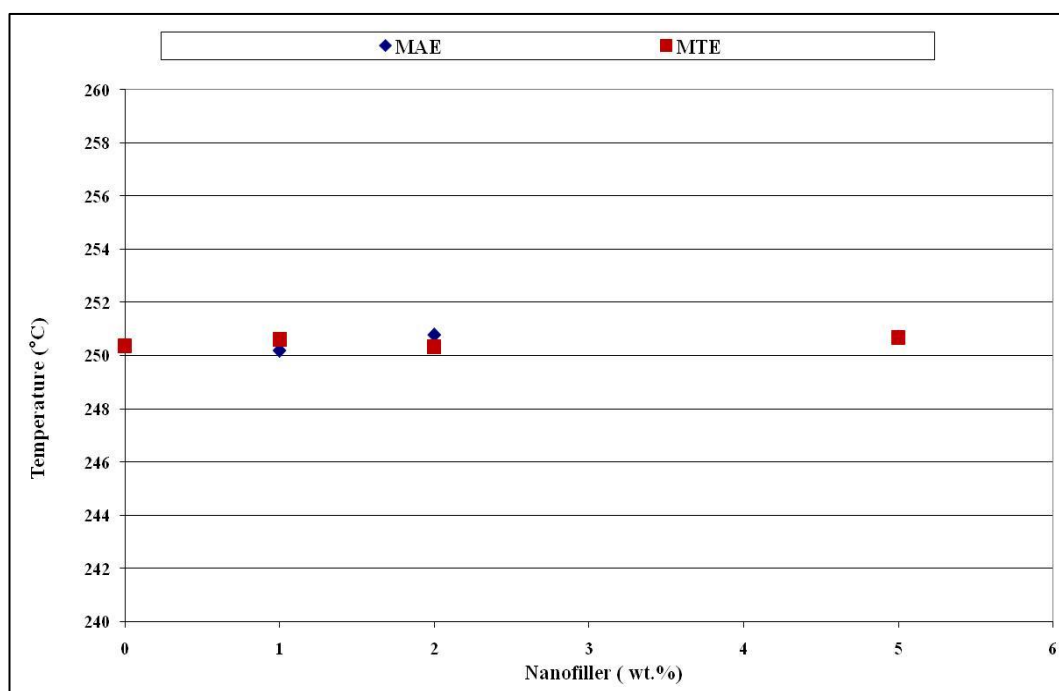


Figure x5.4.2 Effect of nano-fillers (MAE and MTE) at different contents (1, 2 and 5 wt.%) on T_m.

The effect of adding nanofillers (MAE and MTE) at different content levels (1, 2 and 5 wt.%) is shown in Table x5.4.4 and Figure x5.4.2. Since the PET melt processing temperature is more than 260°C, the effect of the nanofillers is small.

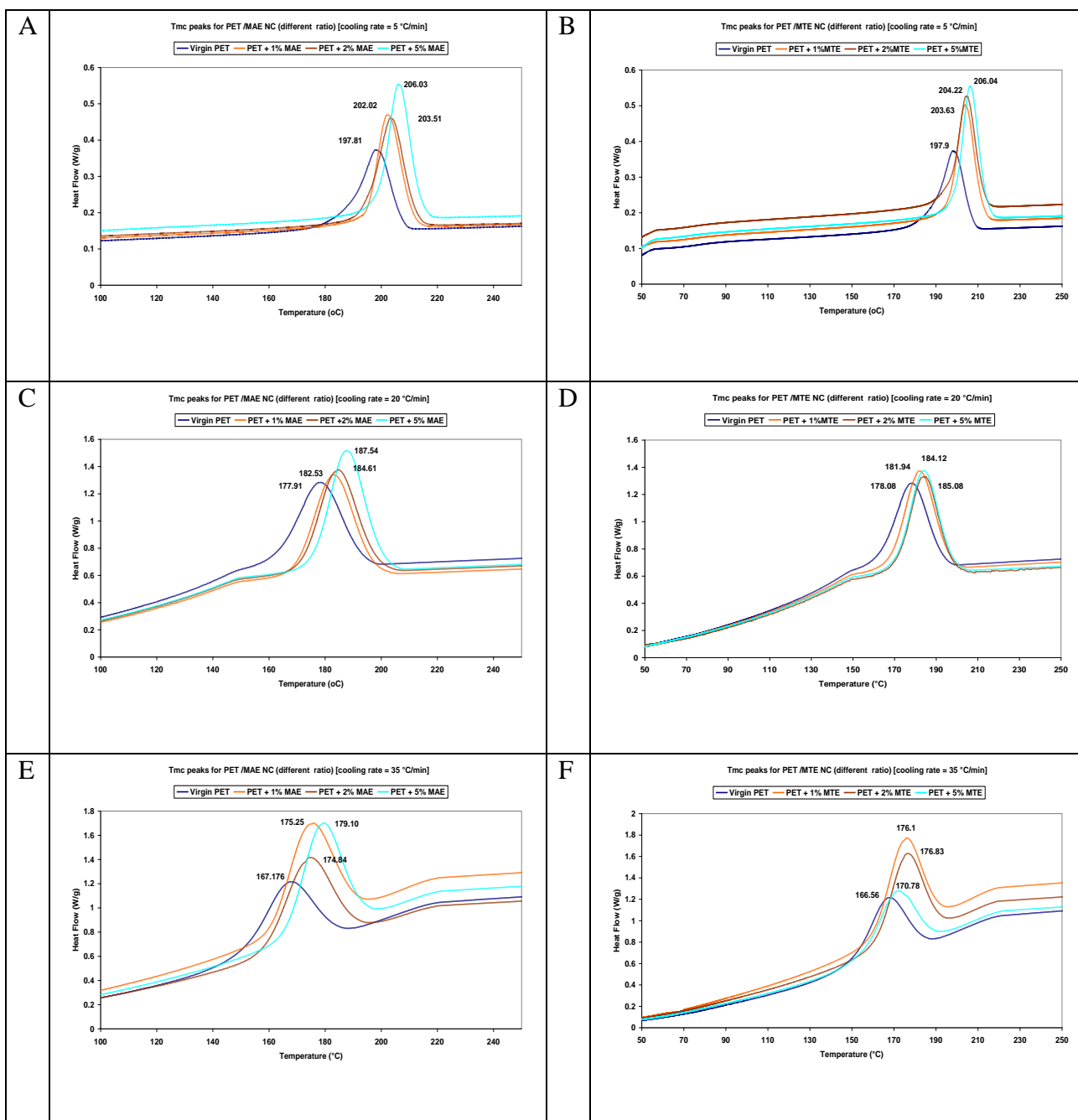


Figure x5.4.5 (A-F) Relationship between Tmc and nanofillers (MAE and MTE) at different nanoclay contents (1, 2 and 5 wt.%).

Generally, figures x5.4.5 (A-F) show that on increasing MAE or MTE concentration the value of Tmc increases, the crystallization peaks tend to be sharper, and the half peak decreases, which indicates that the rate of crystallization is increased.

There are many possible reasons for this phenomenon. The structure of the nanofillers (MAE and MTE) can help the PET molecules accumulate on each other to grow into

crystallites, which enhances the crystallization rate. A further possible reason is that the nanofiller can act as an effective heterogeneous nucleating agent. In this case, in the molten state the segments of the PET molecules can easily interact with the surface of the nanofiller, developing crystallization nuclei.

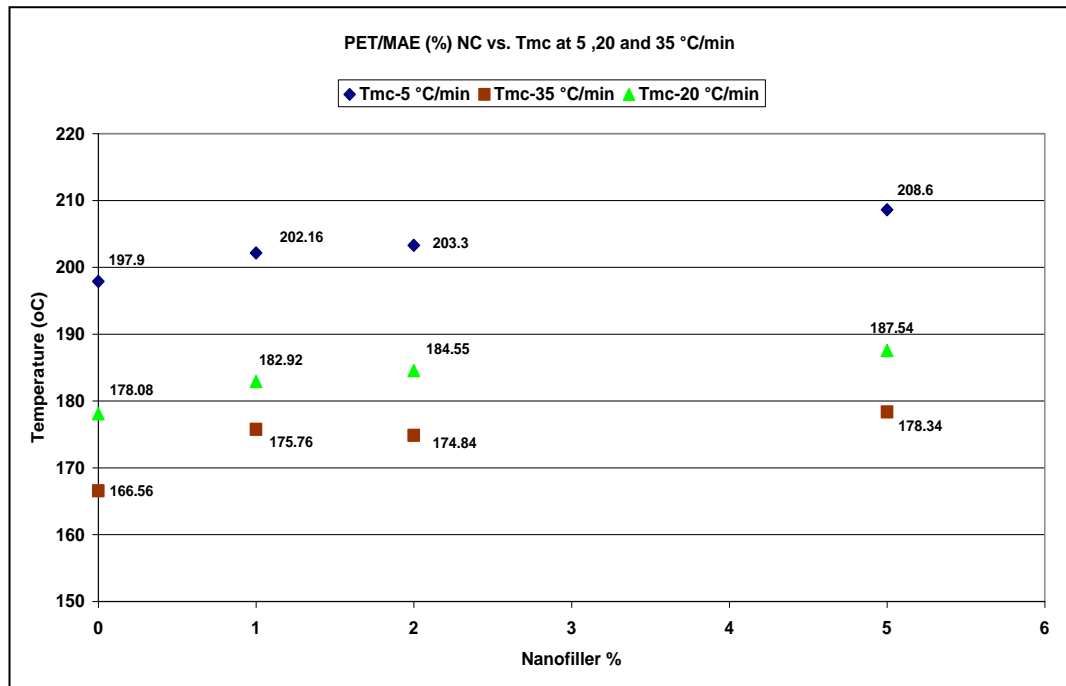


Figure x5.4.6 Relationship between Tmc and MAE (1, 2 and 5 wt.% concentrations) at different cooling rates (5, 20 and 35°C).

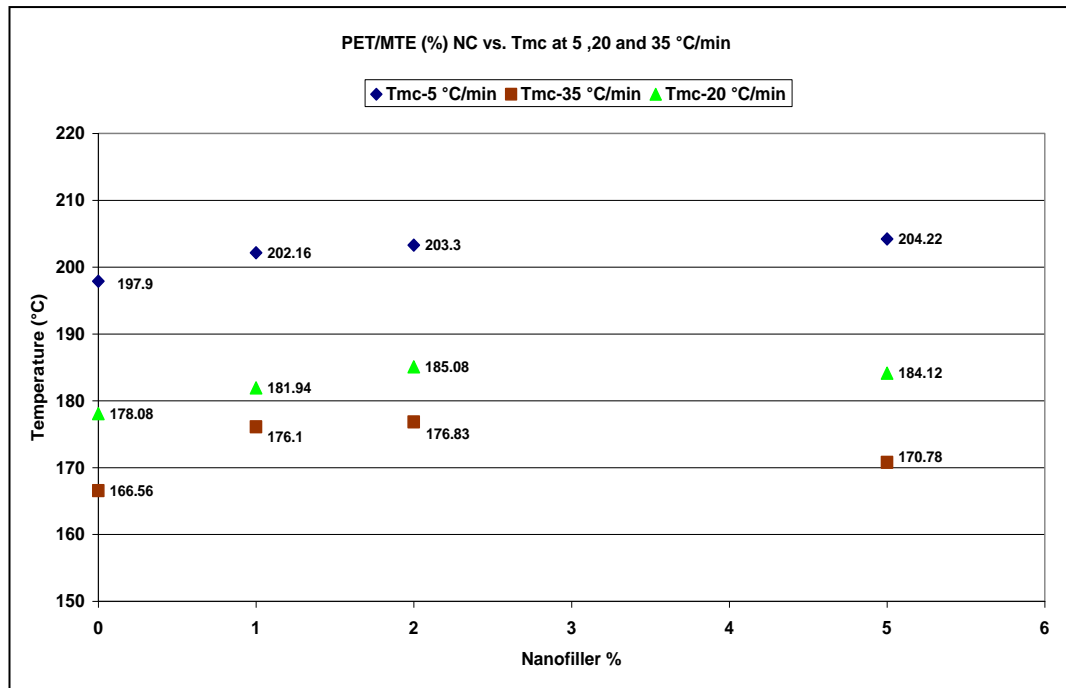
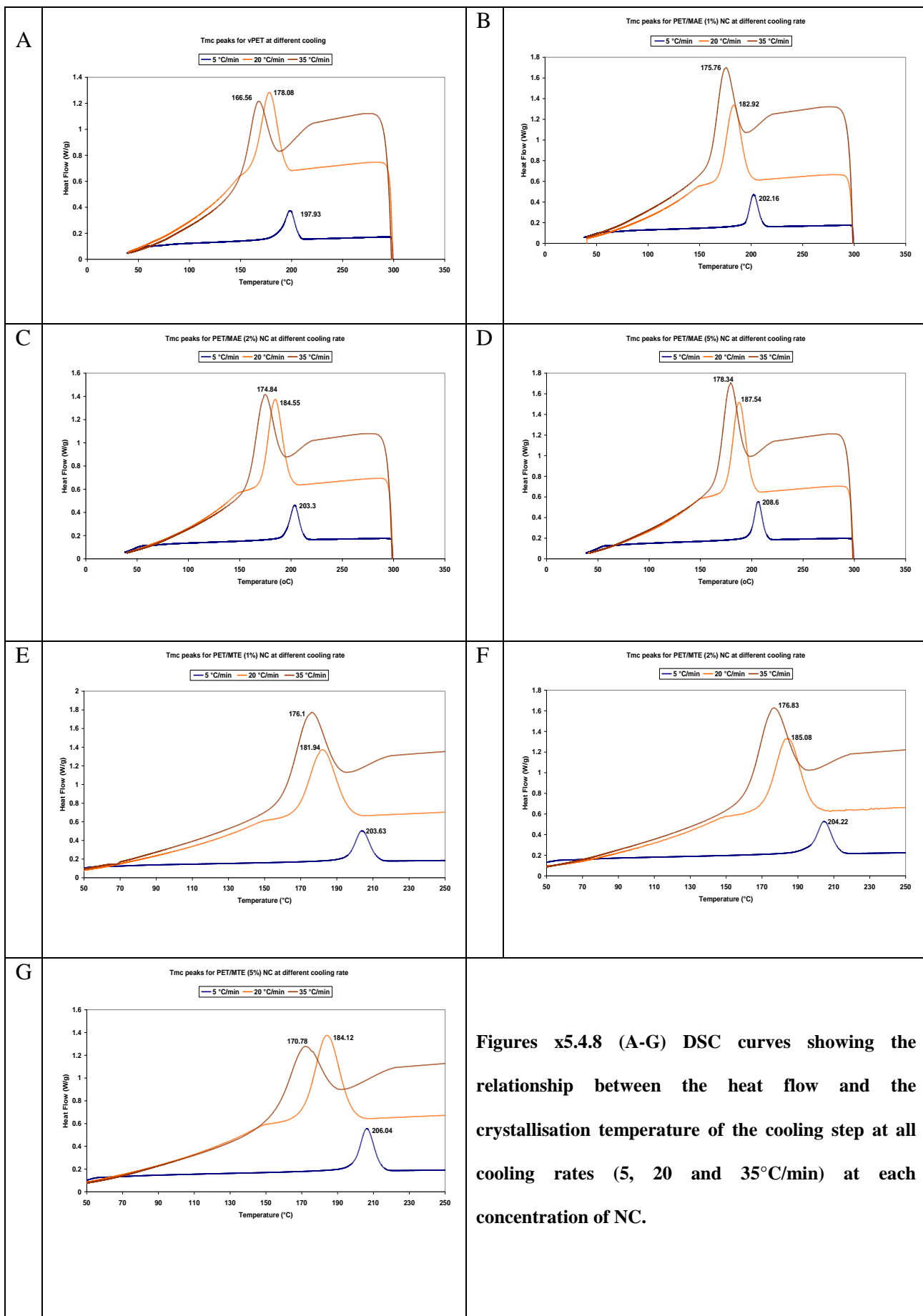


Figure x5.4.7 Relationship between Tmc and MTE (1, 2 and 5 wt.% concentrations) at different cooling rates (5, 20 and 35 °C).

Figures x5.4.6 and x5.4.7 illustrate the relationship between the crystallization temperature from the melt (Tmc) and the nanofiller concentration (0, 1, 2 and 5 wt.%) under different cooling rates (5, 20 and 35°C/min). It is apparent that Tmc increases with increasing filler concentration. Also the higher the cooling rate, the lower the Tmc at the same filler and concentration.



Figures x5.4.8 (A-G) DSC curves showing the relationship between the heat flow and the crystallisation temperature of the cooling step at all cooling rates (5, 20 and 35°C/min) at each concentration of NC.

In figures x5.4.8 (A-G) it was expected that T_{mc} would decrease on increasing the cooling rate. For instance, for PET/MAE (1 wt.%) NC, T_{mc} with a slow cooling rate (5°C/min) was higher than T_{mc} with a fast cooling rate (35°C/min), which indicates that the lower cooling rate gives enough time for the molecular chains to pack into a unit cell forming the nuclei, and also that the time for the nanocomposite to finish crystallisation was much shorter than for vPET. On the other hand at high cooling rates a small heat flow peak was seen for vPET sheets compared with PET/(MAE or MTE) NC sheets, which showed large heat flow peaks, indicating the addition of nanofiller (MAE or MTE) increased both the crystallinity and crystallisation rate of the NC sheets when compared with virgin PET.

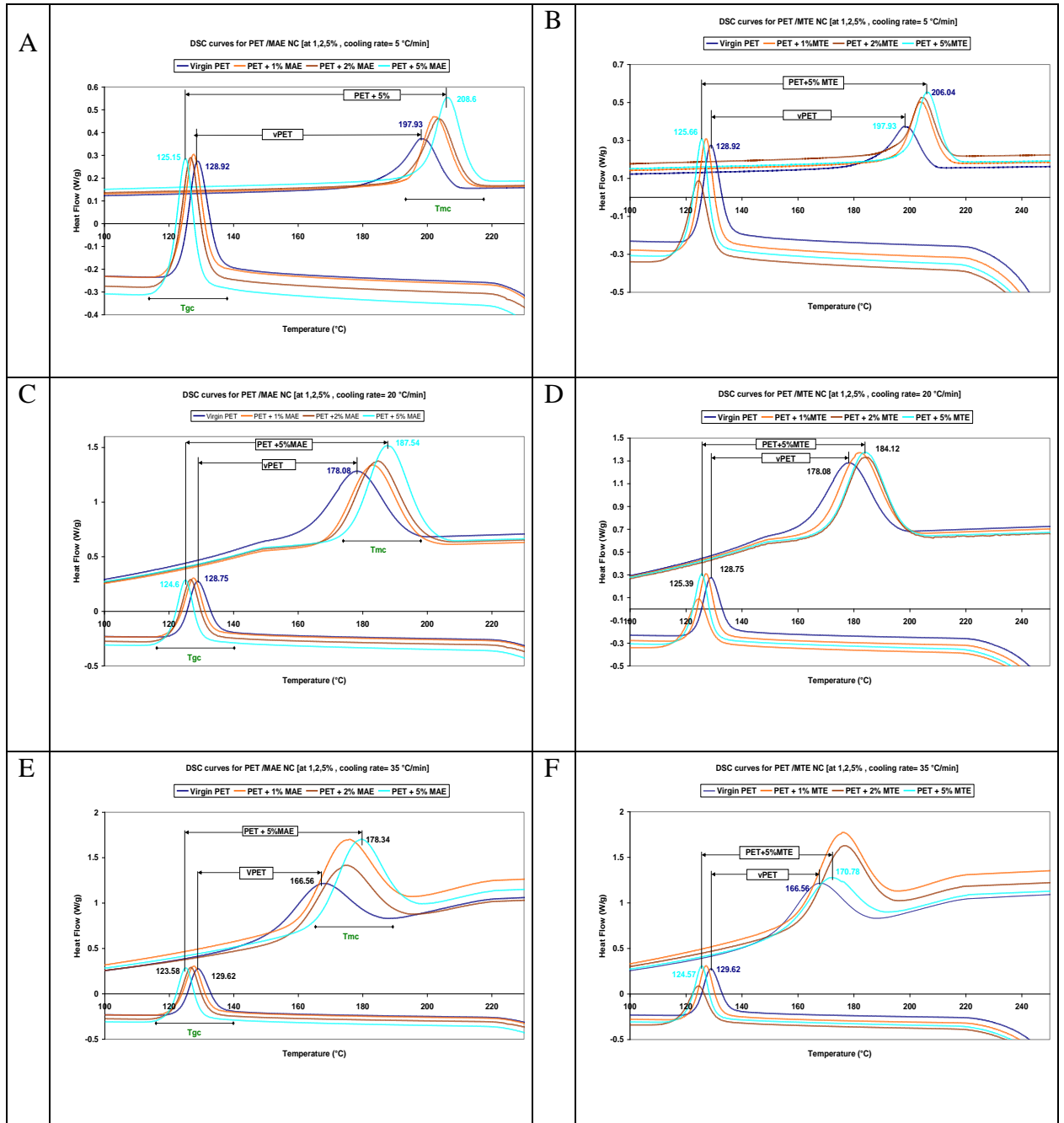


Figure x5.4.9 (A-F) DSC curves for PET nanocomposites showing the Tmc and Tgc peaks.

The crystallization from melt state (Tmc) and crystallization from solid state (Tgc) peaks of vPET sheets and PET NC sheets (at different nanofiller ratios and different cooling rates) are shown in figures x5.4.9 (A-F).

It is apparent that the T_{gc} peaks shift to lower temperatures on increasing the nanofiller content. In contrast, the T_{mc} peaks shift to higher temperatures on increasing the nanofiller content. This indicates that the PET crystallizes at a higher temperature from the melt and crystallizes at a lower temperature from the solid state indicating that the nanofiller acts as an effective nucleation agent in the PET crystallization process.

x5.4.4 Comparison of the samples analysed in the preliminary and main studies

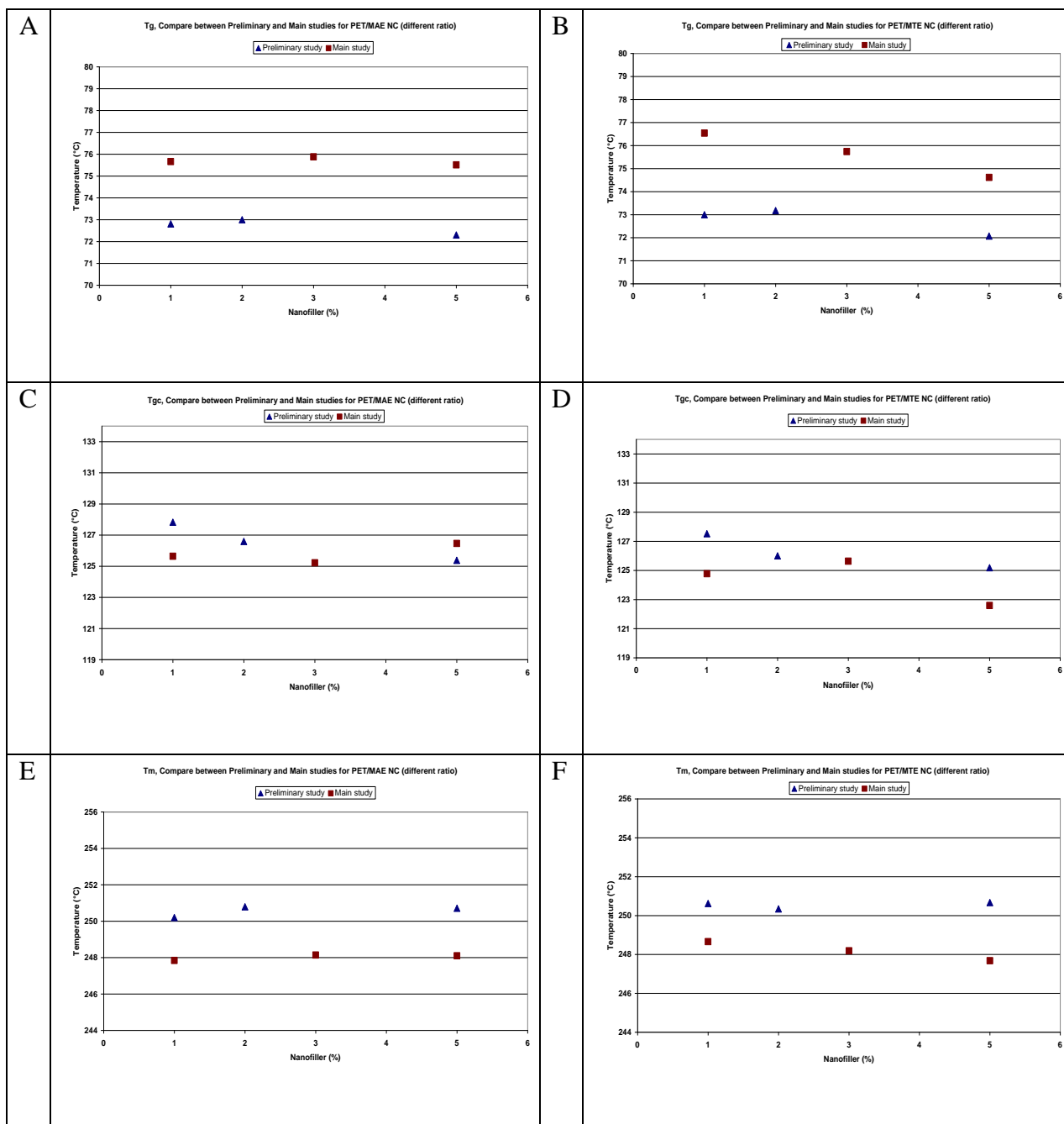


Figure x5.4.10 (A-F) Thermal analyses (Tg, Tgc and Tm) for PET/(MAE, MTE) NC at different clay concentrations [comparing the preliminary study and main study].

Figure x5.4.10 summarises the thermal analyses for PET/(MAE and MTE) NC at different clay concentrations in the preliminary study and the main study.

A big difference in T_g between the samples analysed in the preliminary and the main study is shown in Figure x5.4.10 A and B; the difference is about 3°C . The samples analysed in the main study show a small decrease in T_g compared to the samples in the preliminary study, which indicates good melt processing and a sufficient drying process for the PET pellets and clays prior to the mixing process in the main study. Figure x5.4.10 C and D show a small difference in T_{gc} between the samples analysed in both studies. The nanofiller in the main study decreased the T_{gc} more than in the preliminary study, which indicates that the nanofiller in the main study showed a better performance than the same nanofiller in the preliminary study. That can also be attributed to the difference in the nature of the samples, which were amorphous pellets in the main study and sheets in the preliminary study. The sheets were pulled uniaxially by the chill rolls which can induce crystallinity in the sheet. In general, the good drying procedure and the mixing method that applied in the main study may be made the differences in the thermal results compare to the preliminary study.

Appendix x6

x6.1 Tensile modulus of PET nanocomposites films vs. clay content at tensile test speed of 5 and 50 mm/min

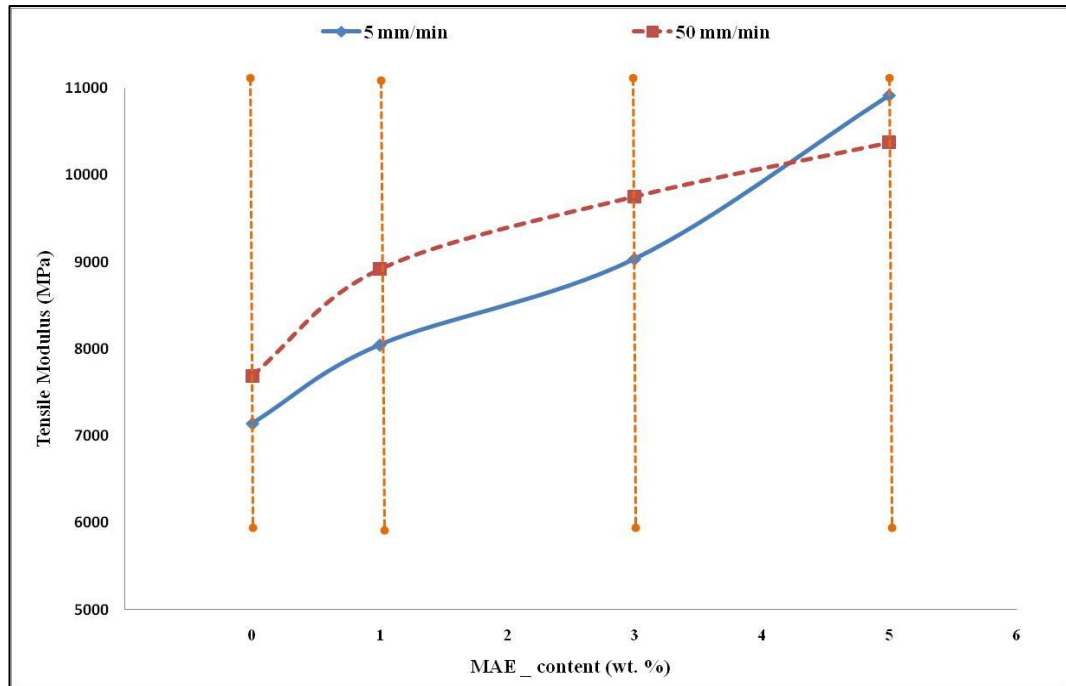


Figure x6.1 Tensile modulus of PET/MAE nanocomposites films vs. clay contents at tensile test speed of 5 and 50 mm/min

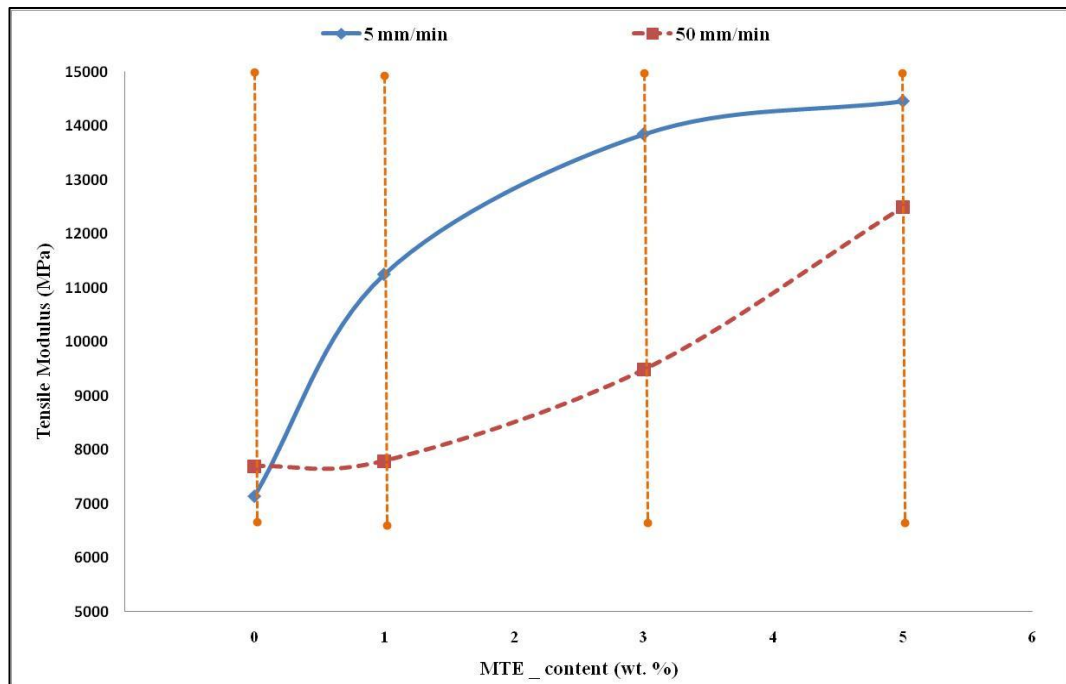


Figure x6.2 Tensile modulus of PET/MTE nanocomposites films vs. clay contents at tensile test speed = 5 and 50 mm/min

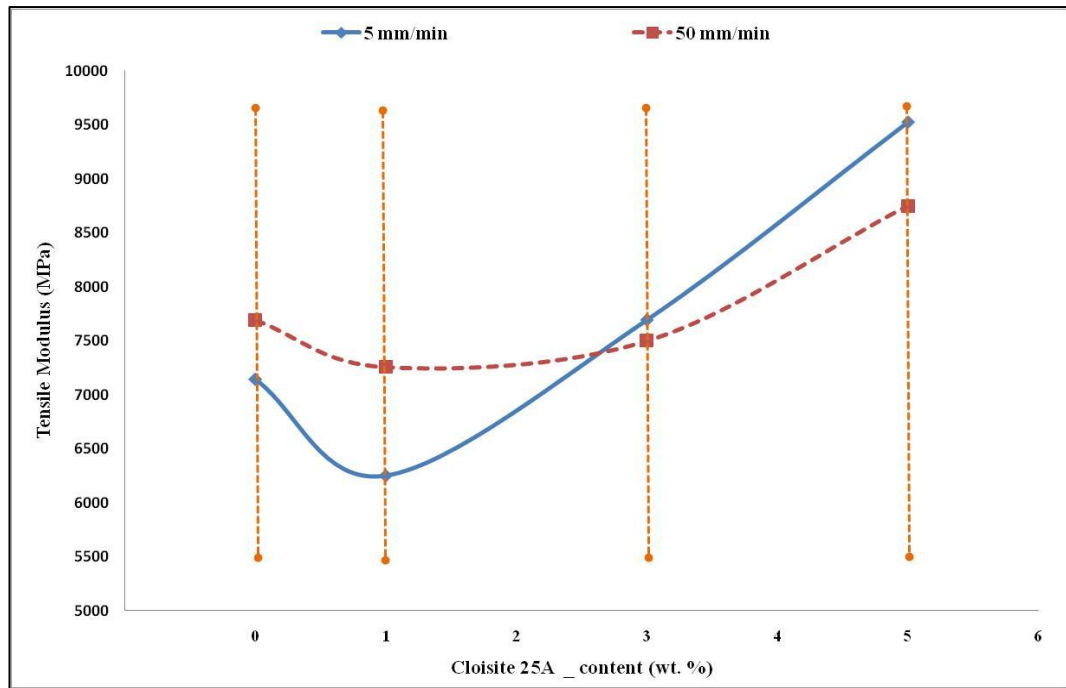


Figure x6.3 Tensile modulus of PET/Cloisite 25A nanocomposites films vs. clay contents at tensile test speed = 5 and 50 mm/min

X6.2 TEM micrographs for PET nanocomposites films

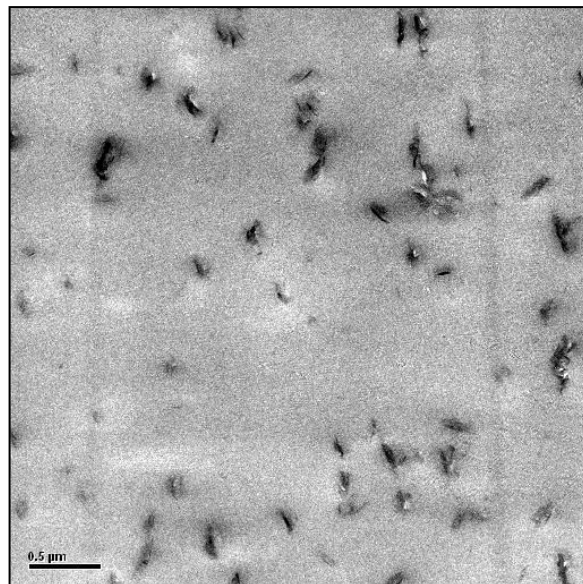


Figure x6.4 TEM micrographs for PET/MAE (1 wt.%) nanocomposites films

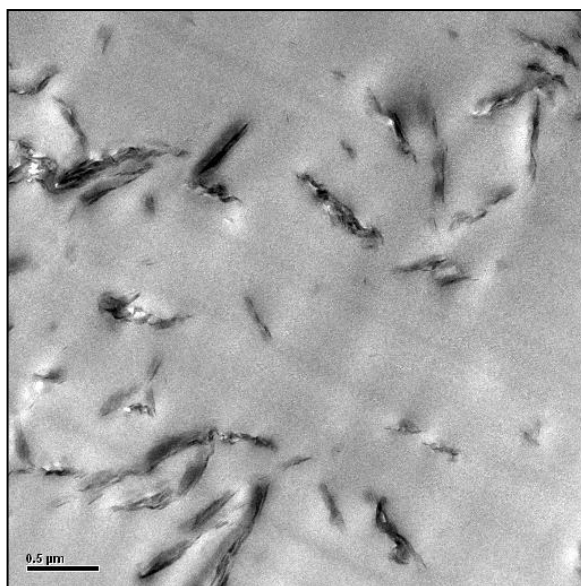


Figure x6.5 TEM micrographs for PET/MAE (3 wt.%) nanocomposites films

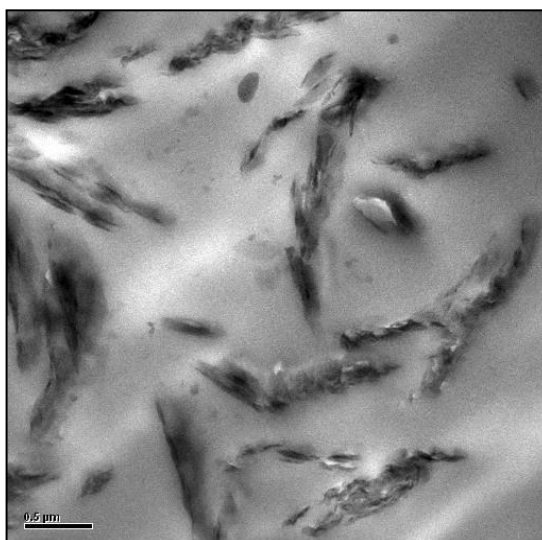


Figure x6.6 TEM micrographs for PET/MAE (5 wt.%) nanocomposites films

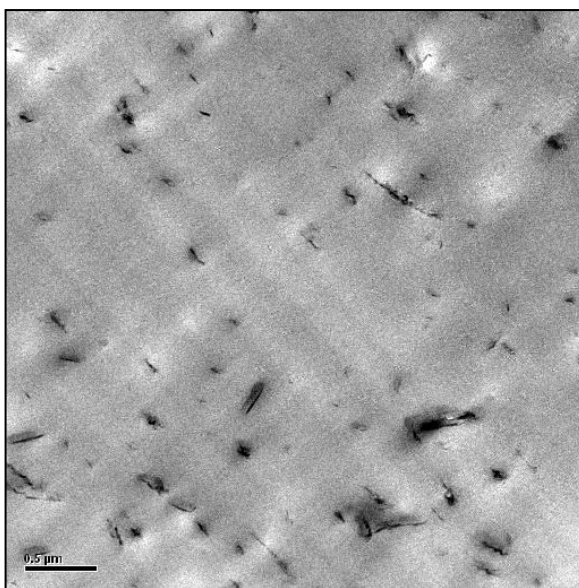


Figure x6.7 TEM micrographs for PET/MTE (1 wt.%) nanocomposites films

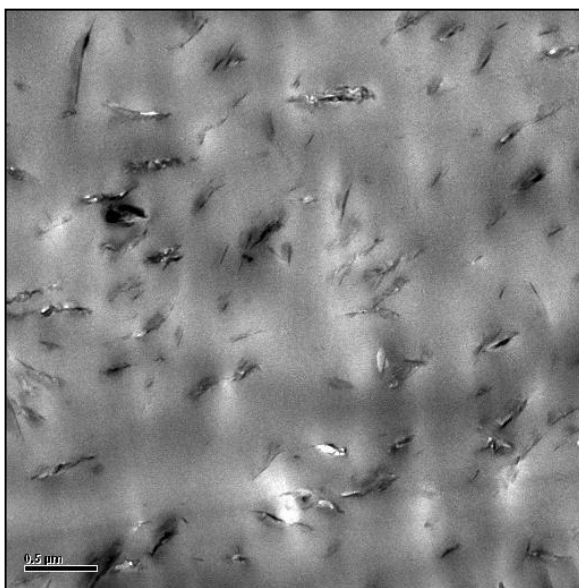


Figure x6.8 TEM micrographs for PET/MTE (3 wt.%) nanocomposites films

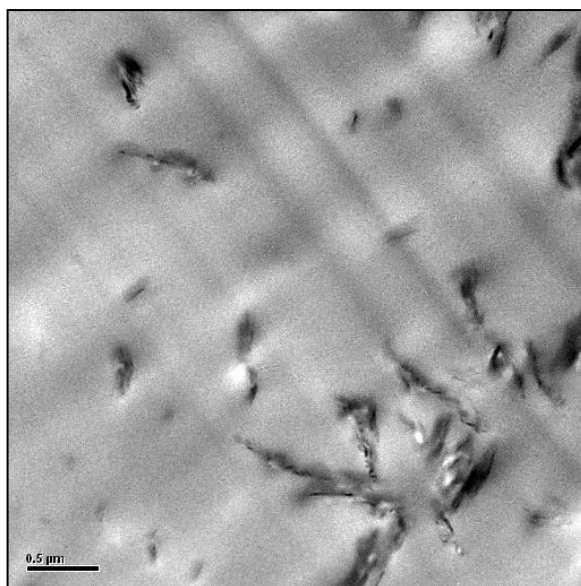


Figure x6.9 TEM micrographs for PET/MTE (5 wt.%) nanocomposites films

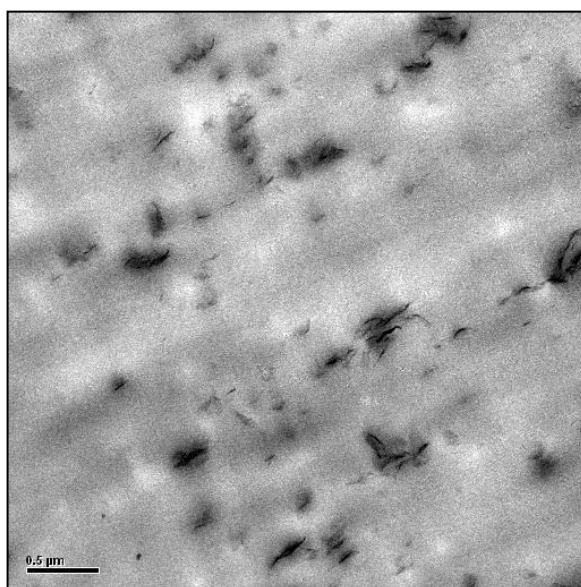


Figure x6.10 TEM micrographs for PET/Cloisite 25A (1 wt.%) nanocomposites films

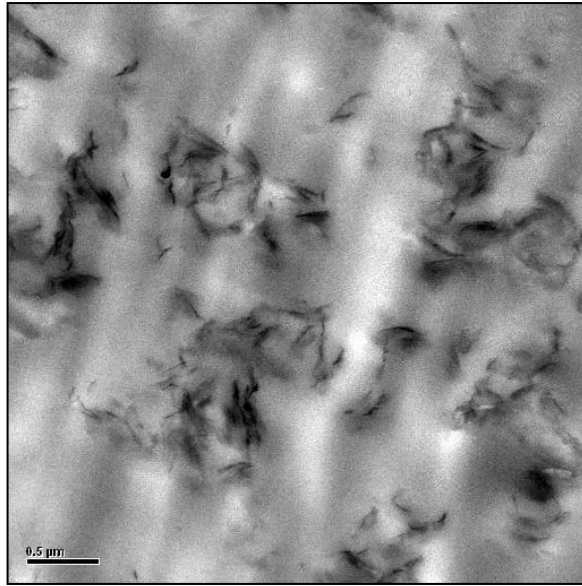


Figure x6.11 TEM micrographs for PET/Cloisite 25A (3 wt.%) nanocomposites films

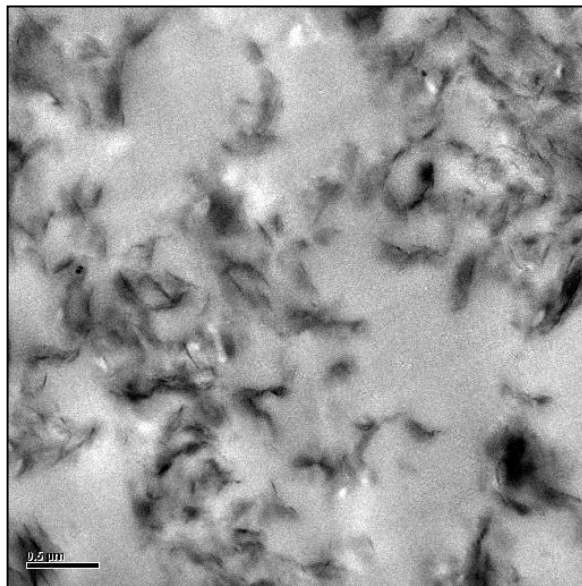


Figure x6.12 TEM micrographs for PET/Cloisite 25A (5 wt.%) nanocomposites films

x6.3 Stress-strain curve for PET nanocomposites micro size sample prepared at different injection speeds

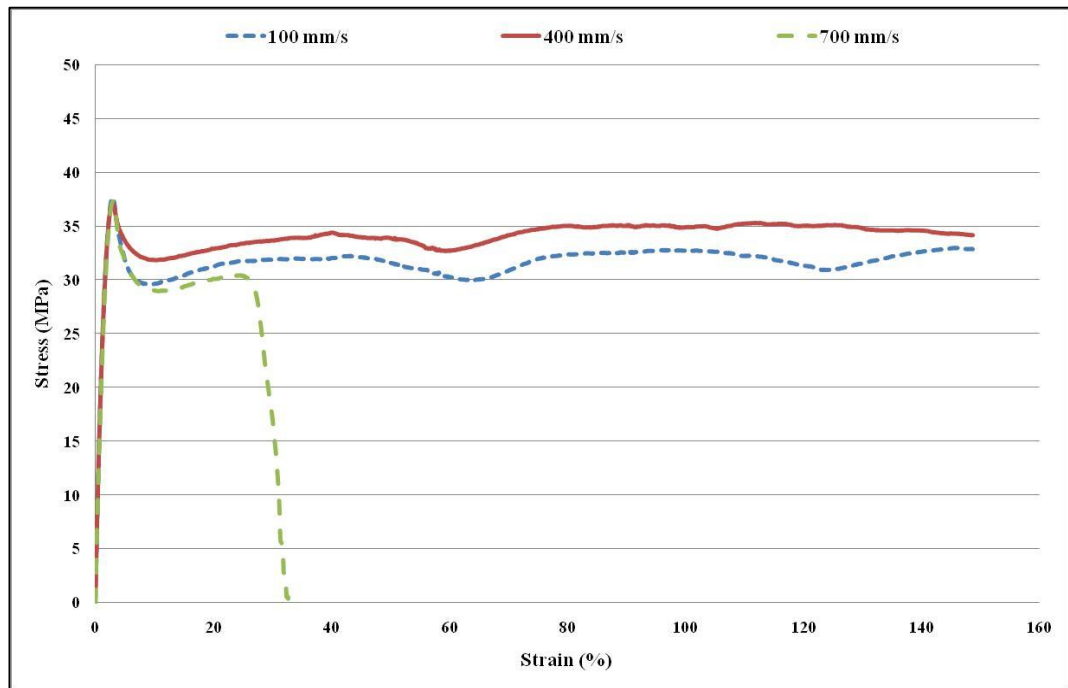


Figure x6.13 Stress-strain curve for PET/MTE (3 wt.%) micro size sample prepared at different injection speeds

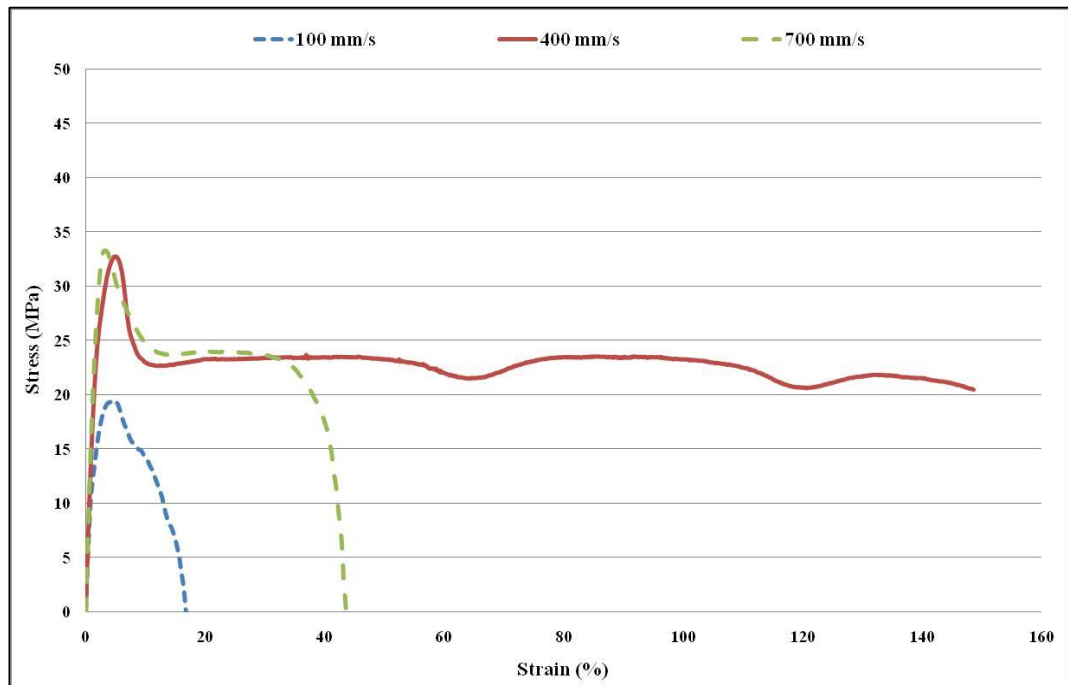


Figure x6.14 Stress-strain curve for PET/MTE (5 wt.%) micro size sample prepared at different injection speeds

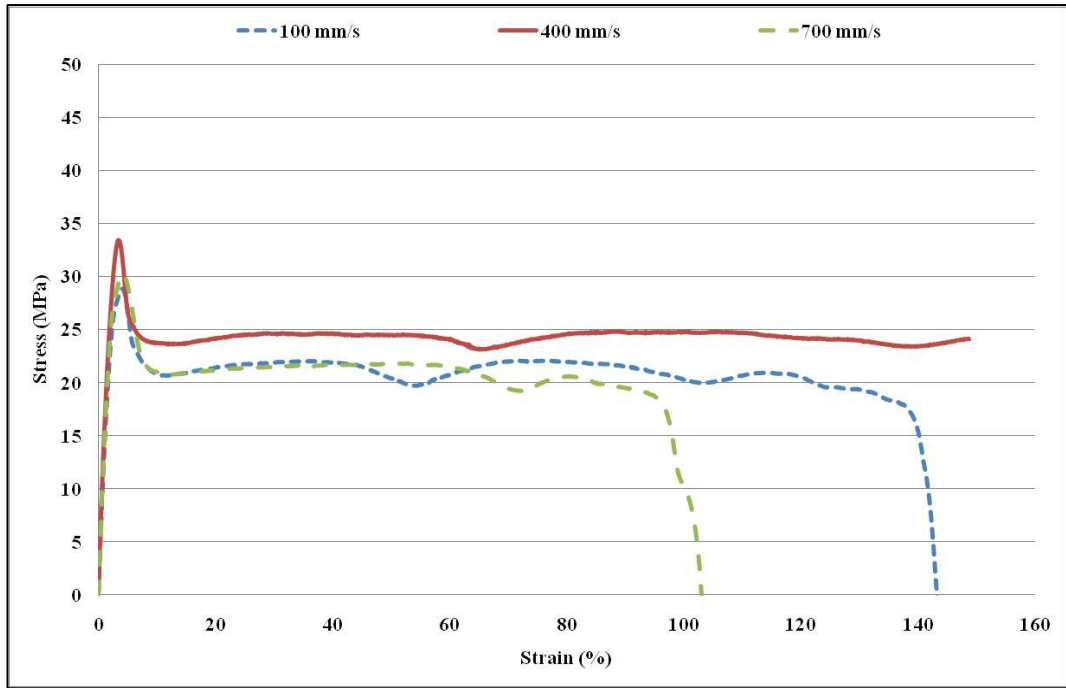


Figure x6.15 Stress-strain curve for PET/Cloisite 25A (1 wt.%) micro size sample prepared at different injection speeds

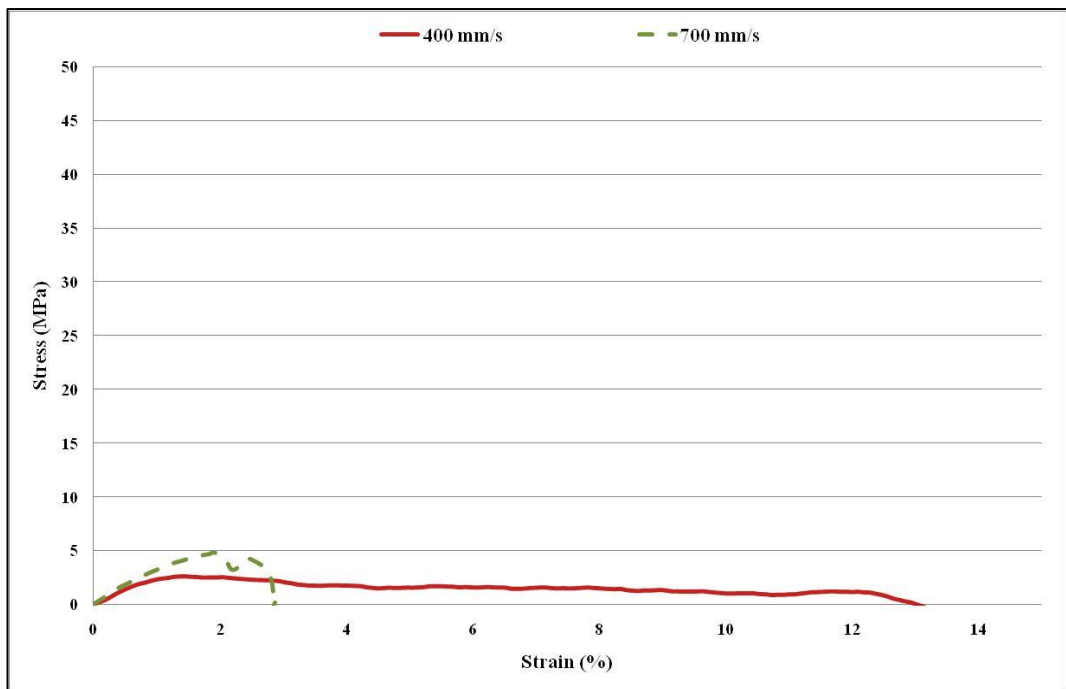


Figure x6.16 Stress-strain curve for PET/Cloisite 25A (5 wt.%) micro size sample prepared at different injection speeds

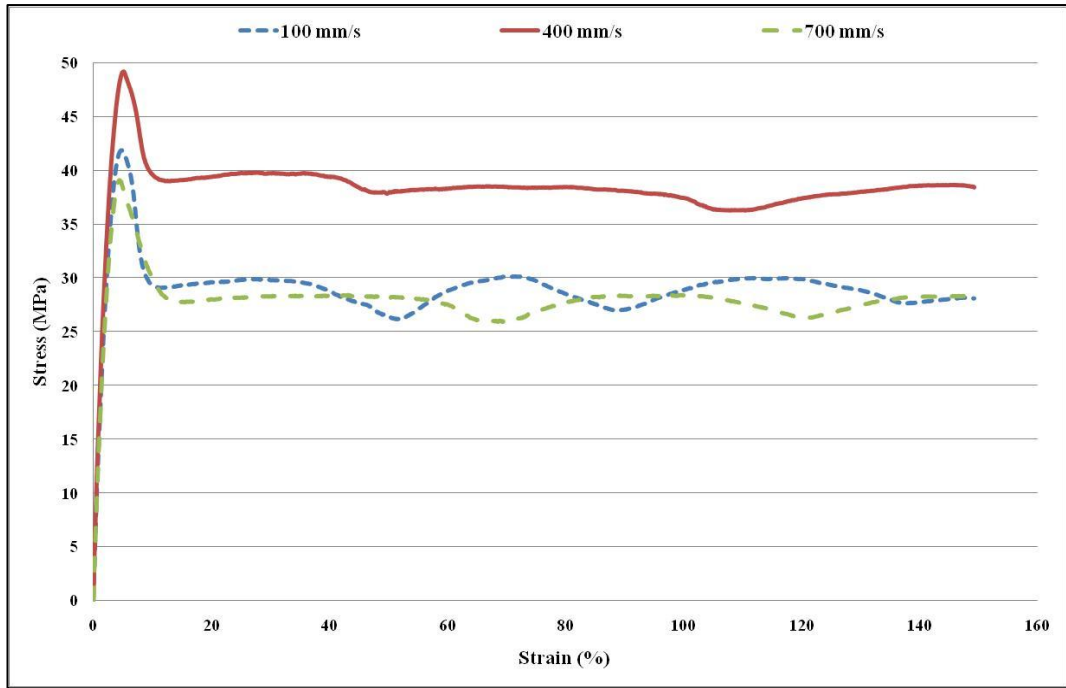


Figure x6.17 Stress-strain curve for PET/MAE (1 wt.%) micro size sample prepared at different injection speeds

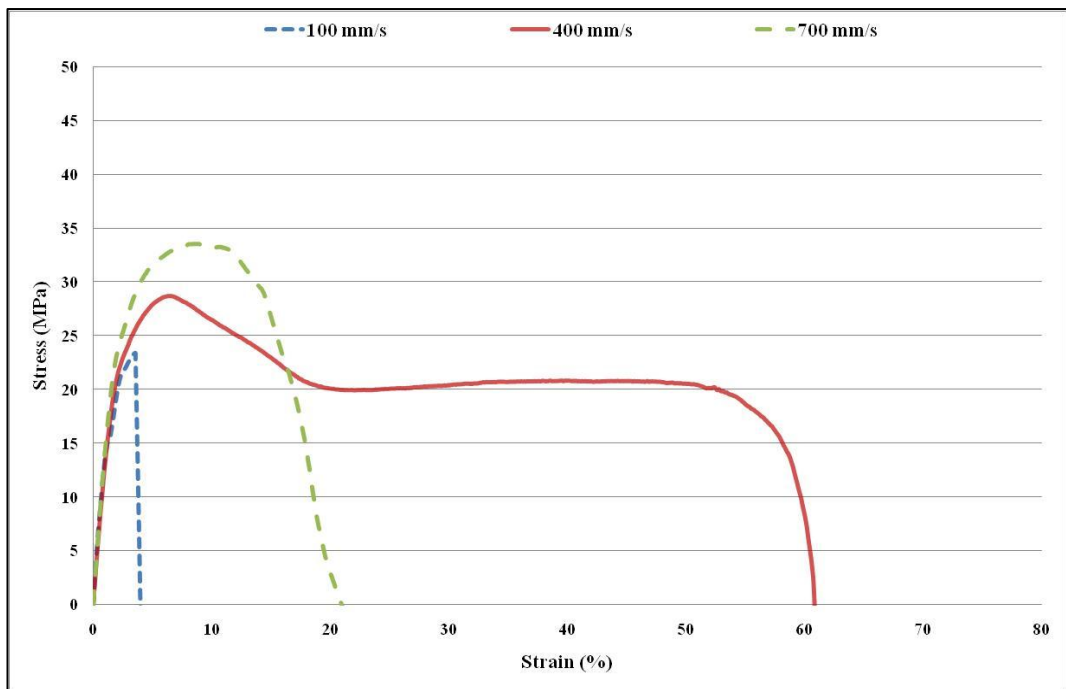


Figure x6.18 Stress-strain curve for PET/MAE (5 wt.%) micro size sample prepared at different injection speeds

Appendix x8 (Chapter 8)

x8.1 Samples description

Sample	Description
Ext. vPET	Extruded PET (non recycled)
PET/MTE3%	PET/MTE_3% (non recycled)
PET/MTE3%_1	PET/MTE_3% (1 time recycled)
PET/MTE3%_2	PET/MTE_3% (2 times recycled)
PET/MTE3%_3	PET/MTE_3% (3 times recycled)
PET/MTE5%	PET/MTE_5% (non recycled)
PET/MTE5%_1	PET/MTE_5% (1 time recycled)
PET/MTE5%_2	PET/MTE_5% (2 times recycled)
PET/MTE5%_3	PET/MTE_5% (3 times recycled)
PET/Cloisite25A_3%	PET/ Cloisite25A _3% (non recycled)
PET/Cloisite25A_3%_1	PET/ Cloisite25A _3% (1 time recycled)
PET/Cloisite25A_3%_2	PET/ Cloisite25A _3% (2 times recycled)
PET/Cloisite25A_3%_3	PET/ Cloisite25A _3% (3 times recycled)
PET/Cloisite25A_5%	PET/ Cloisite25A _5% (non recycled)
PET/Cloisite25A_5%_1	PET/ Cloisite25A _5% (1 time recycled)
PET/Cloisite25A_5%_2	PET/ Cloisite25A _5% (2 times recycled)
PET/Cloisite25A_5%_3	PET/ Cloisite25A _5% (3 times recycled)

Table x8.1 Description of the re-passed samples.

x8.2 viscosity vs. shear rate of PET nanocomposites re-extruded number of times and the pellets pictures.

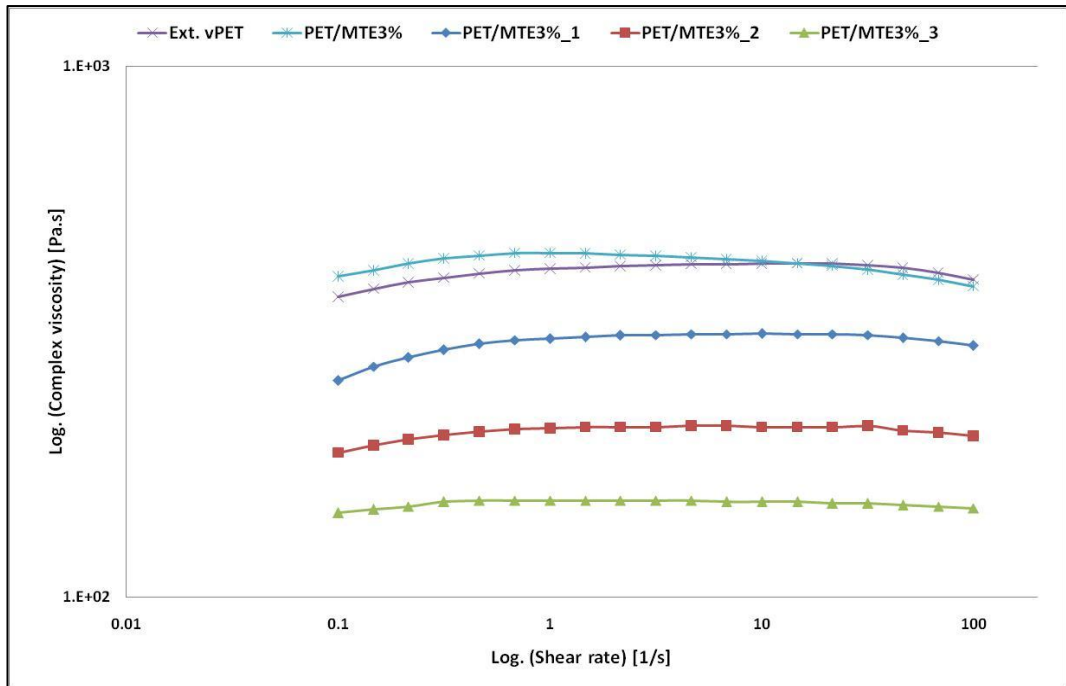


Figure x8.1 Viscosity vs. shear rate of PET/MTE (3 wt.%) nanocomposites re-extruded a number of times.

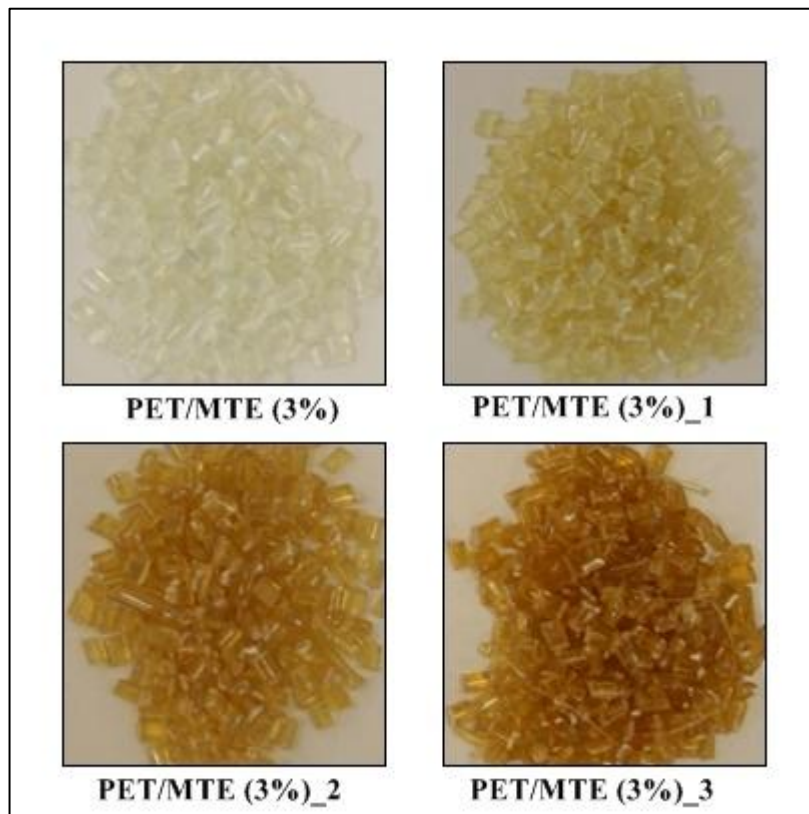


Figure x8.2 Colour of the amorphous PET/MTE (3 wt.%) after re-pass stages.

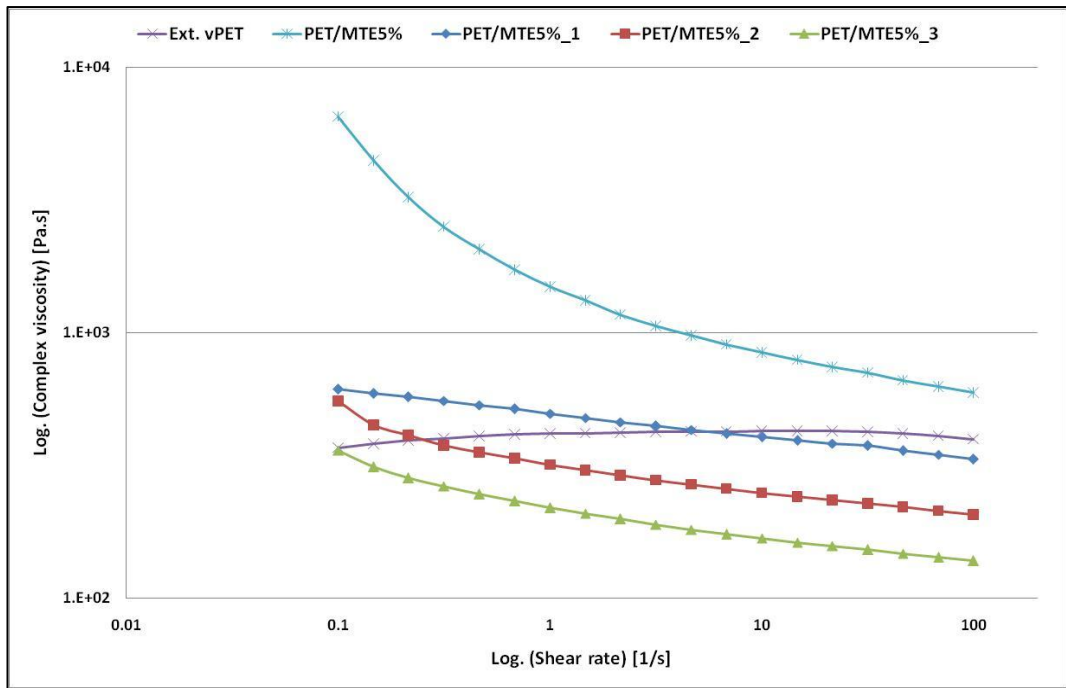


Figure x8.3 Viscosity vs. shear rate of PET/MTE (5 wt.%) nanocomposites re-extruded a number of times.

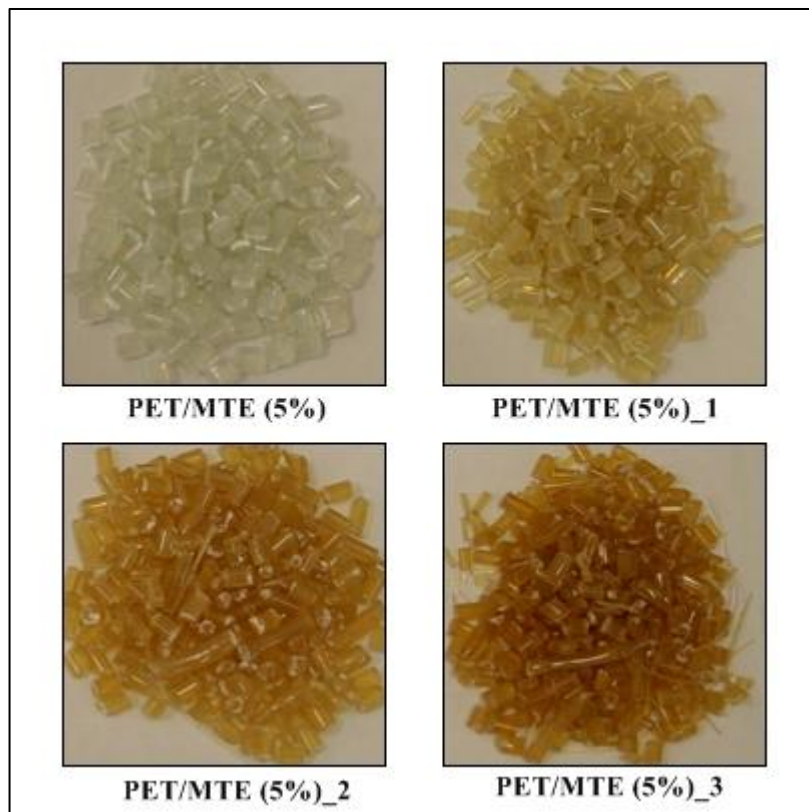


Figure x8.4 Colour of the amorphous PET/ MTE (5 wt.%) after re-pass stages.

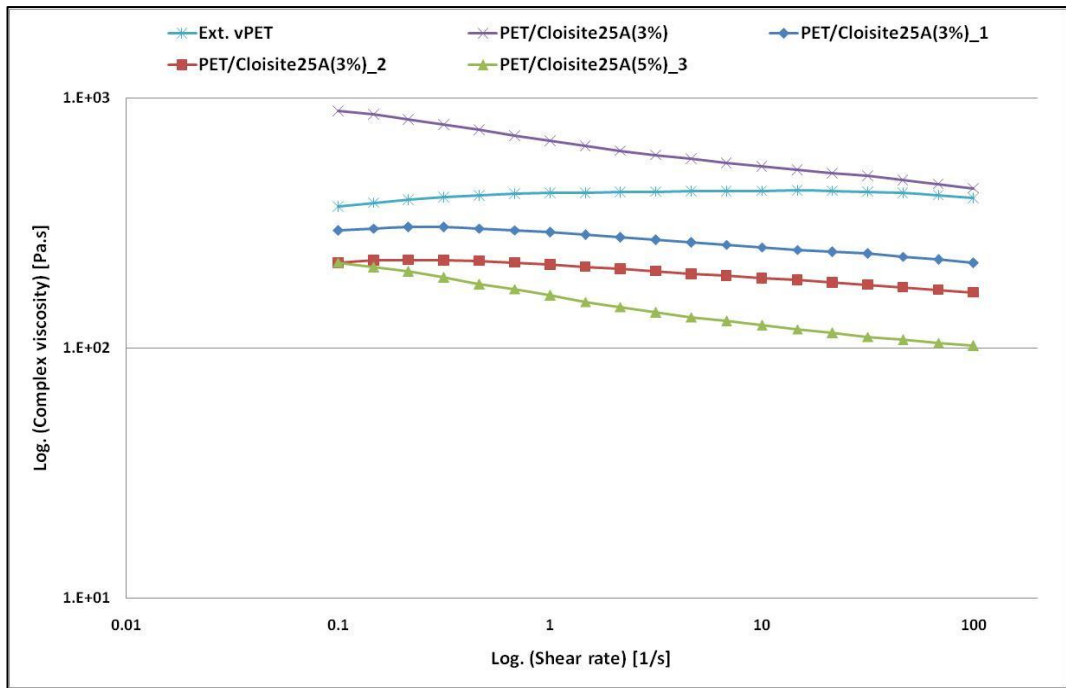


Figure x8.5 Viscosity vs. shear rate of PET/Cloisite 25A (3 wt.%) nanocomposites re-extruded a number of times.

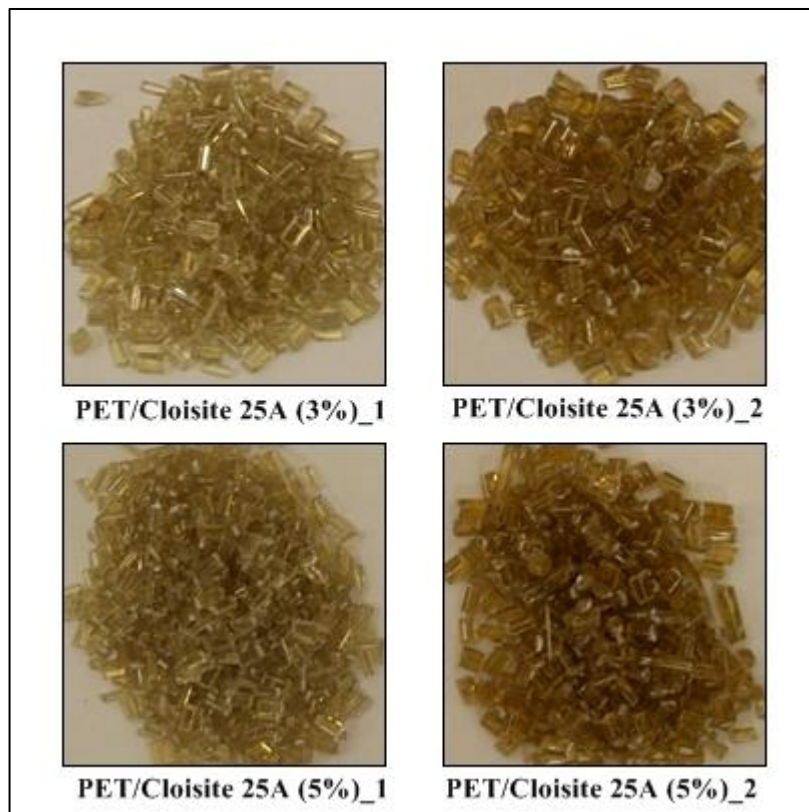


Figure x8.6 Colour of the amorphous PET/ Cloisite25A (3 and 5 wt. %) after re-pass stages.

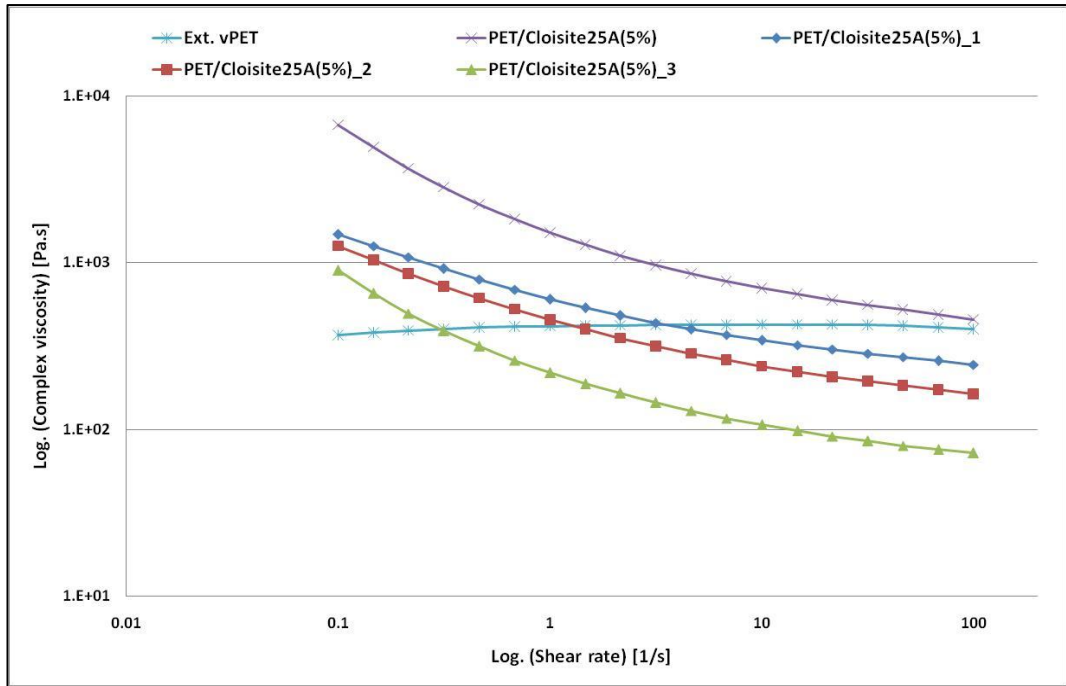


Figure x8.7 Viscosity vs. shear rate of PET/Cloisite 25A (5 wt.%) nanocomposites re-extruded a number of times.